The spatial and temporal distribution of pipe and pockmark formation

Jennifer Leigh Moss

PhD Thesis, Cardiff University

December 2010

ProQuest LLC
789 East Eisenhower Parkway
P.O. Box 1346
Ann Arbor, MI 48106-1346

DECLARATION

This work has not previously been accepted in substance for any degree and is not concurrently submitted in candidature for any degree

Signed..... (candidate) Date..14/12/10.

STATEMENT 1

This thesis is being submitted in partial fulfilment of the requirements for the degree of PhD.

Signed..... (candidate) Date..14/12/10.

STATEMENT 2

This thesis is the result of my own independent work/investigation, except where otherwise stated. Other sources are acknowledged by explicit references.

Signed..... (candidate) Date..14/12/10.

STATEMENT 3

I hereby give consent for my thesis, if accepted, to be available for photocopying and for inter-library loan, and for the title and summary to be made available to outside organisations.

Signed..... (candidate) Date..14/12/10..

STATEMENT 4

I hereby give consent for my thesis, if accepted, to be available for photocopying and for inter-library loans after expiry of a bar on access previously approved by the Graduate Development Committee.

Signed..... (candidate) Date..14/12/10...

Contents

Chapter 5

Chapter 6

List of Figures

Appendix Figures

List of Tables

Appendix Tables

List of Spatial Statistics Equations

Abstract

Pockmarks and pipes are found globally. They represent loci for overpressure generation and seal breach and are therefore of significant importance for basin analysis and modelling, the modelling of overpressure development and analysing seal integrity.

This research concentrates on two study areas. A family of blowout pipes from North Namibia imaged in 3D seismic data; and a group of large buried pockmarks and a field of small seabed pockmarks from the Western Nile Deep Sea Fan (NDSF) imaged in ultra high resolution 2D seismic data. The general themes of this research are pipe and pockmark morphology and formation process, their spatial and temporal distribution and the magnitude and frequency of fluid flux through the conduit.

A family of blowout pipes from Namibia exhibit a variety of seismic characteristics, with the largest pipes containing a blowout crater and evidence of possible stacked palaeo-pockmarks. Formation of the Namibian blow out pipes is attributed to overpressure induced hydrofracturing of the seal, hydrofracture propagation towards the seabed and blow out. Blow out is accompanied by crater formation and collapse of the overburden resulting from volume loss at the base of the pipe due to fluidization. Fluidization and the migration of fluid and some sediment through the pipe are interpreted from localised reflection thickening at the top of the pipe, in a depositional pattern similar to channel levees.

Namibian pipe formation is shown to be intermittent and persistent throughout the Neogene. The fluid source for the family of pipes is unknown, however inferences based on the spatial position of pipes in relation to significant unit boundaries (Post Rift 1 and the Syn Rift) suggest the likely source is at depth (> 1 km). A close association between the size and location of the pipes, the development of hydrate (as identified by a Bottom Simulating Reflector) in Post Rift 3, and the Syn Rift, a proven hydrocarbon source region in South Namibian basins, is noted. If the Namibian pipes are source from the Syn Rift, these pipes are potentially sourced direct from a hydrocarbon kitchen and would have maximum pipe heights in excess

of 5 km. To the authors knowledge these would be the tallest recorded pipes in the literature and the first to be sourced from a kitchen. A conceptual model is developed in which the spatial position of pipes adheres to both basinal and local controls.

A group of large buried pockmarks on the NDSF are interpreted to have formed between 15,000 yrs BP and 100,000 yrs BP, the majority of which are believed to have formed at the same time c. 50,000-80,000 yrs BP. These buried pockmarks show evidence for highly focused, episodic fluid flow following burial of the pockmark. The longevity of post formation fluid migration is estimated to be ~15;000-100,000 yrs.

A field of > 13,800 small seabed pockmarks (Nile Deep Sea Fan) are interpreted to have formed within the last 6,500 yrs. Spatial statistics identified an exclusion zone or "drainage cell" surrounding each pockmark which is not penetrated by the formation of any other pockmark. A conceptual model for a drainage cell is proposed whereby pockmark formation dissipates a radius/area of fluid and overpressure, thereby preventing the formation of another pockmark within that cell.

The overall conclusions of this thesis suggest that pipes form episodically over multi-million year timescales in response to both local and basinal conditions. It is suggested that the formation of pipes and pockmarks is, to a certain degree, governed by the location of surrounding pipes / pockmarks and their associated drainage [over]pressure cells. Post formation fluid migration through these conduits can potentially continue > 100,000 yrs, although this fluid migration may be of a higher frequency and lower magnitude compared to the initial formative flux.

This thesis has contributed to the knowledge and understanding of focused fluid flow by demonstrating the spatio-temporal characteristics of a group of pipes and pockmarks. This thesis concurrently tackles questions of fluid migration timing with the spatial location of seal breach, and considers the re-use of the fluid migration conduit with time and space and the magnitude and frequency of that fluid flux. To the author's knowledge, this is the first spatio-temporal analysis of its kind.

Chapter 1

1 INTRODUCTION

1.1 Rationale

Pockmarks are "[conical] features which record the existence of [fluid] seepages in at least some types of seabed sediment" (Hovland and Judd, 1988 pp 1). Pipes focus the migration of fluid to the seabed.

Pipes and pockmarks are found globally in both deep and shallow water settings (Hovland and Judd, 1988; Judd and Hovland, 2007). They have been identified on active and passive continental margins (Suess et al., 1998; Berndt, 2005), and in marine and freshwater settings in sea, coastal, estuary, fjord and lake environments (Paull et al., 2002; Van Rensbergen et al., 2002; Ussler III et al., 2003; Cartwright et al., 2004; Naudts et al., 2006; Rogers et al., 2006; Webb et al., 2009).

Since their discovery on the Scotian Shelf (King and MacLean, 1970), pockmarks have been the focus of significant academic and industrial interest. Interest in pockmarks concerns 1) their role in reservoir seal failure (Cartwright et al., 2007), 2) as potential habitats for fish and chemosynthetic communities (Olu-Le Roy et al., 2007; Judd and Hovland, 2008), 3) potential links between pockmarks and fluid induced seabed slope instability (Bünz and Mienert, 2004; Chapron et al., 2004; Lastras et al., 2004), 4) potential hazards to drilling and seabed installations (Judd, 1981; Haskell et al., 1999; Hovland et al., 2002; García-García et al., 2004; Heggland, 2004; Judd and Hovland, 2007), 5) potential geological indicators of tectonic movement e.g. precursors to earthquakes (Hasiotis et al., 1996) and 6) as potential contributors to oceanic methane and gas hydrates (Gorman et al., 2002; Haacke et al., 2009).

This research falls primarily within the broad category of reservoir seal failure. Pipes and pockmarks represent the focused migration of fluids from a reservoir, and

identification of such features within a petroleum producing basin can have both a positive and negative impact on play assessment. On the one hand the presence of pipes and pockmarks is used to identify reservoir targets; on the other hand they represent localised trap failure and a breakdown in seal integrity. This conundrum highlights why pockmarks and pipes are significant components of basin analysis and modelling, and the modelling of overpressure development.

Pipes are reservoir "pressure valves", balancing the system inputs and outputs. They are a complex interaction of some of the most fundamental components in hydrocarbon exploration, namely, the reservoir, the seal, fluid migration (primary and secondary) and pressure. Beyond the hydrocarbon industry, the global propensity of pipes/pockmarks ensures that they are likely to be present in many basins, whether directly or indirectly linked to a main hydrocarbon fluid reserve. It is this propensity which provides the fundamental reason for pipe and pockmark analysis; it implies there is a scale invariant baseline component/process to fluid migration which must hold true globally.

The overall objectives of this research are to further understand this baseline component in terms of its morphology and process, spatial and temporal variation and frequency and magnitude of flux.

1.2 Aims of study

The overall aims of this research are to describe the spatio-temporal characteristics of pipe and pockmark formation. The research presented in this thesis is based on two case study areas; 1) deep (seabed to basement) 3D seismic data from offshore Namibia permitting analysis of large scale, basin wide features; and 2) a shallow ultra high resolution 2D seismic survey from the Western Nile Deep Sea Fan permitting analysis of small scale features. This research is focused around 6 central themes; morphology and process, spatial and temporal distribution, and frequency

and magnitude (Fig. 1.5.). The methodology utilises spatial statistics tools not previously used in pockmark investigations to further develop pockmark analytical capabilities and explore new avenues for interpretation e.g. spatio-temporal analysis.

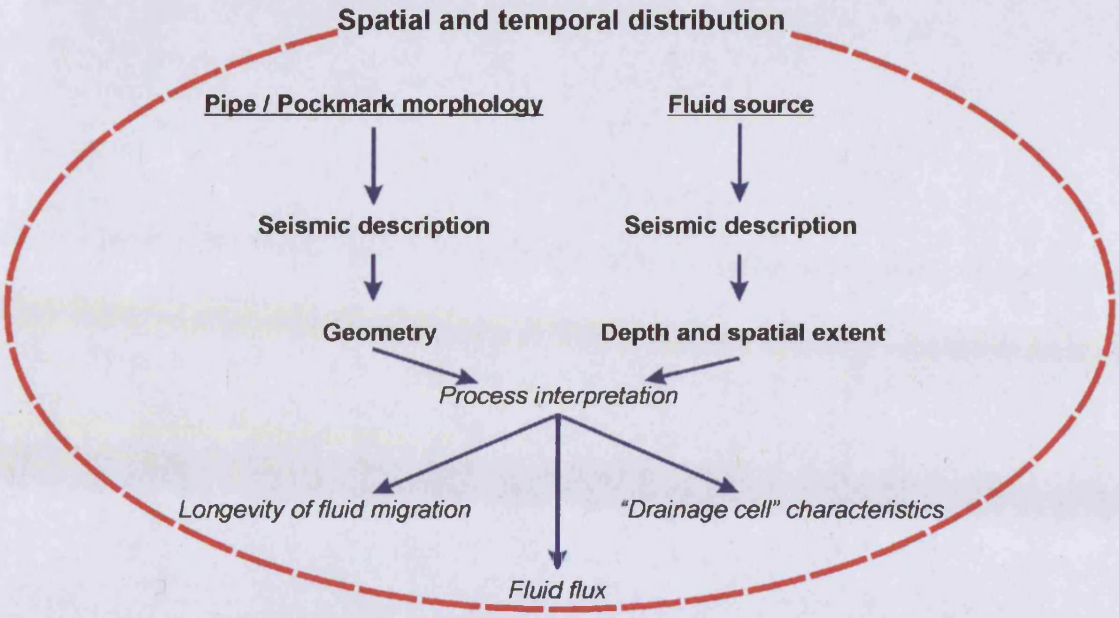

Figure 1.1 Research concept. Capturing the main themes of this research, morphology and process, spatial and temporal distribution, and magnitude and frequency

An outline of the main aims and objectives of this research, and the chapter to which they relate, are detailed below;

1. To extend the general descriptive base of blowout pipes in 3D
    - Describe a previously unknown group of blowout pipes from offshore Namibia (Chapter 4)
2. To investigate the spatial distribution of pipes and pockmarks
    - To analyse the spatial distribution of a family of blowout pipes (using 3D data) (Chapter 5)
    - To investigate the spatial distribution of pockmarks within a pockmark field using a case study from the Nile Deep Sea Fan (NDSF) (Chapter 7)
3. To investigate the temporal distribution of pipes and pockmarks
    - To analyse the sequential temporal distribution of blowout pipe formation in the Namib Basin, Namibia (Chapter 5)
    - To analyse the temporal formation pattern of buried pockmarks from the Rosetta Region of the NDSF and relate formation timings to any potential triggering mechanisms (Chapter 6)
4. To investigate the longevity of post-formation fluid migration and make inferences about the frequency and magnitude of flux
    - To analyse and interpret "stacked pockmarks" (Chapters 4 and 6)
    - To identify and interpret seismic reflection characteristics which typify post formation fluid migration (Chapters 4 and 6).
5. To determine whether spatial statistical techniques are a valuable tool for analysing pipe and pockmark distributions (Chapters 2, 5, 6, 7 and 8)

1.3 Overview

The aims of this chapter are 1) to introduce pipes and pockmarks within the context of reservoir seal failure; 2) to describes the conceptualised fluid flow system; 3) to summarize the role of pipes in seal by-pass; 4) to illustrate the contrasting seismic expression of pipes; 5) provide an overview of the current theory on pipe and

pockmark formation; and 6) to outline the current state of knowledge concerning the spatial and temporal distribution of pipes and pockmarks.

1.3.1 Fluid flow system

Fluid flow system is a generic term used to describe the lateral and vertical suite of processes involved in fluid migration from the accumulation of fluid in a trap, to trap breach and fluid escape (Fig. 1.1). The fluid flow system composition is highly variable and unique to each basin. The system comprises a vertically hierarchical arrangement of isolated reservoir bodies of different sizes, positioned at varying depths within the stratal sequence. These reservoir bodies are connected by vertical or sub-vertical migration pathways, connected laterally by carrier beds or units of high relative permeability, which permit the vertical movement of fluid from one body to another. These migration pathways can be any structural or stratigraphic feature which promotes fluid migration, e.g. pipe or fault. Once in the reservoir body, fluid may migrate laterally before re-migrating. Fluid can enter the system either through primary migration or in situ fluid generation, and exits the system at the seabed e.g. via a pipe and pockmark. The isolated reservoir bodies are inter-connected by members of the Seal By-Pass family (Cartwright et al., 2007).

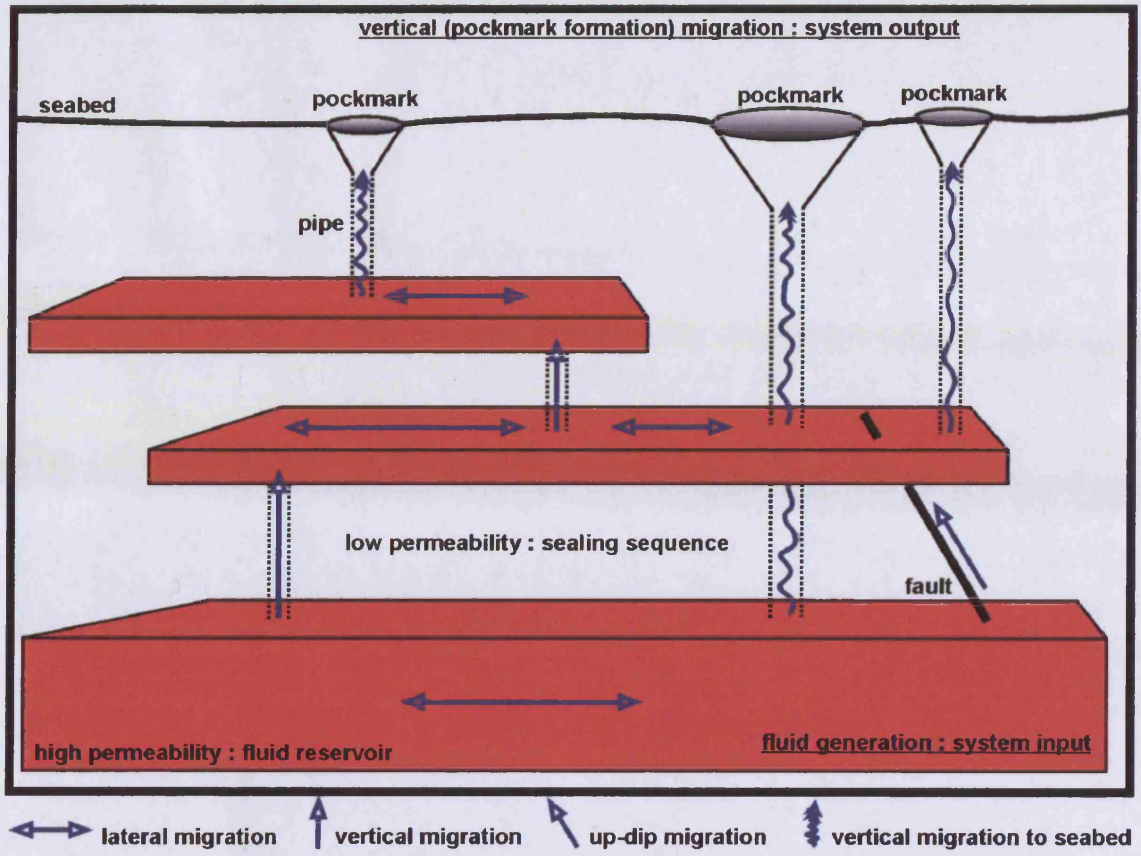

Figure 1.2 Schematic of the fluid flow system. Vertically hierarchical suite of reservoir bodies connected by vertical or sub-vertical migration pathways (SBS). Pipes and faults are shown but any member of the seal by-pass family could fulfil this role.

1.3.2 Pipes : a member of the Seal By-pass System

Pipes are members of the seal by-pass family (Cartwright et al., 2007). A Seal By-pass System (SBS) is defined as "large-scale (seismically resolvable) geological features embedded within sealing sequences that promote cross-stratal fluid migration and allow fluids to bypass the pore network." (Cartwright et al., 2007 pp1143). Seal By-pass Systems incorporate fault (trap defining and supratrap), intrusive (sandstone, igneous, salt/mud diapirs and diatremes) and pipe (dissolution, hydrothermal, blowout and seepage) by-pass (Cartwright et al., 2007). Pipes permit fluids to by-pass an assemblage of generally low-permeability lithofacies that halt or retard the flow of fluids (oil, gas, water) toward the seabed (Cartwright et al., 2007).

Pipes are defined as vertical to subvertical columnar zones of disturbed seismic reflections that may or may not be associated with subvertically stacked amplitude anomalies. Pipes range in height from tens of metres to several kilometres and are commonly circular to subcircular in planview (<25 m to >1000 m diameter), but their vertical and cross sectional geometry is often marred by seismic artefacts such as migration anomalies, scattering artefacts, lateral velocity anomalies and attenuation artefacts related to shallow diffractors (Løseth et al., 2001; Davies, 2003; Løseth et al., 2003; Cartwright et al., 2007).

Pipes are commonly differentiated from seismic artefacts (e.g. push downs, migration anomalies, defractors), by considering their geologic context (Fig. 1.2). Pipes are commonly seen to emanate from 1) crestal regions, e.g. structural crests i.e. tilted fault block crests or fold crests (e.g. Niger Delta) (Keller et al., 2007; Van Rensbergen et al., 2007; Cobbold et al., 2009); 2) fault tips (e.g. Fram Straight, NW Svalbard) (Cobbold et al., 2009; Hustoft et al., 2009a); 3) depositional or constructional crests i.e. diapiric crests (e.g. Central Adriatic Sea), sand bodies, turbidic crests or channel-levees with positive topography (e.g. Lower Congo Basin) (Gay et al., 2003; Gay et al., 2006a; Gay et al., 2007a; Geletti et al., 2008; León et al., 2010) or 4) fluid crests i.e. up dip limit of gas hydrates (e.g. Hydrate Ridge) or diagenetic boundaries i.e. the conversion of biogenic silica (opal-A) to opal-CT (cristobalite and tridymite) in biosiliceous sediment causes increased rates of water

expulsion due to the reduction in sediment porosity and dehydration of the amorphous opal-A phase resulting in pipe formation (e.g. Faeroe Shetland Basin) (Cowley and O'Brien, 2000; Tréhu et al., 2004; Davies et al., 2008) (Fig. 1.2). Nevertheless, many pipes are also documented from flat-lying units or synclinal regions, albeit with some focusing element at depth.

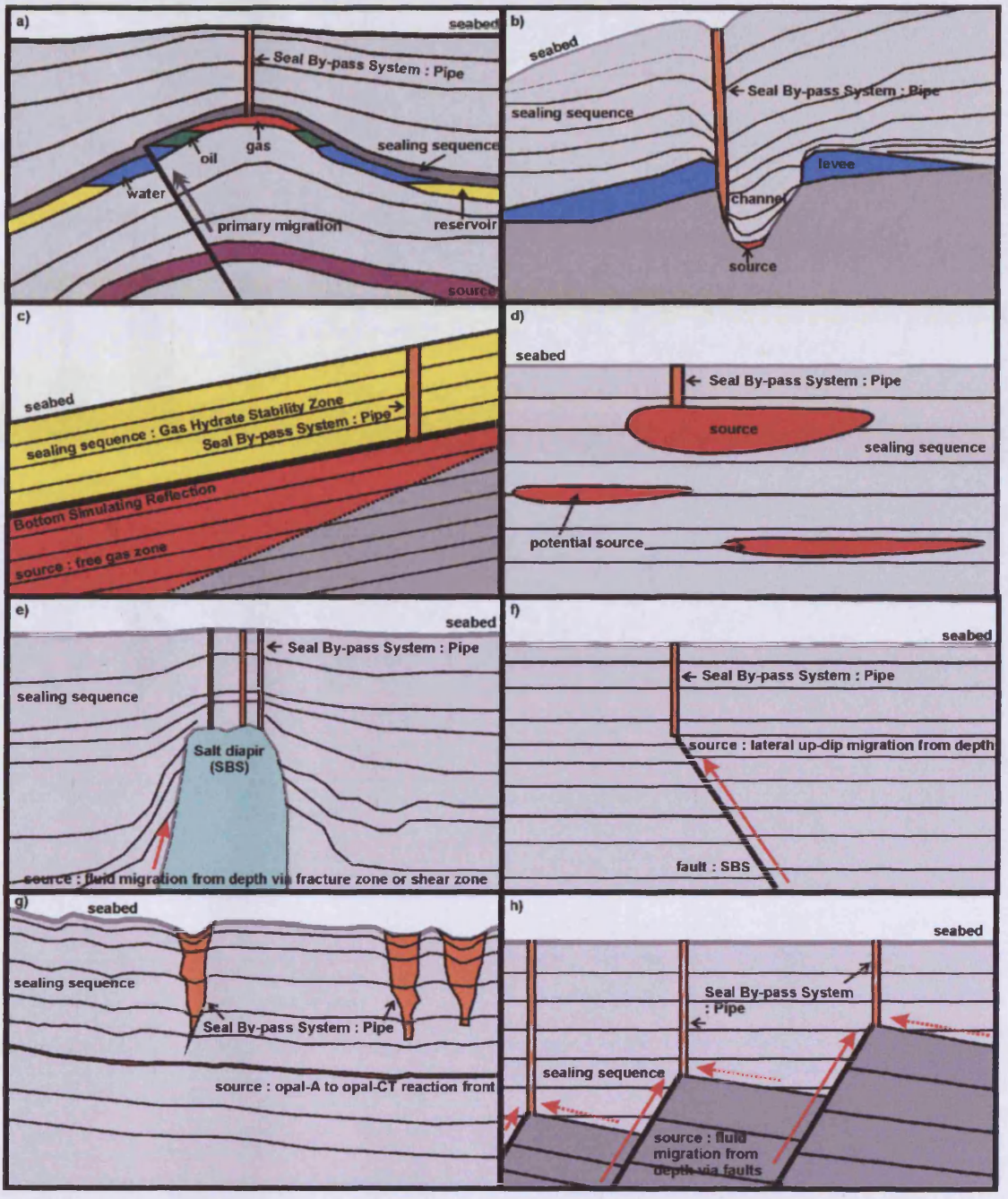

Figure 1.3 Geological context of pipes. a) generalised anticlinal trap b) buried channel-levee complex (Gay et al., 2003)), c) pipe emanating from the base of the gas hydrate stability field (Tréhu et al., 2004; Tréhu et al., 2004)), d) isolated shallow gas pockets, e) pipes forming at the crest of a salt diapir. Pipes have also been observed above mud volcanoes, f) pipe bleeding from the top of a fault (also observed above polygonal faults), g) pipes forming due to dewatering associated with the opal-A to opal C-T reaction front (Davies et al., 2008), h) pipes forming up-dip of structures e.g. tilted fault blocks

Cartwright et al. (2007) based their subdivision of pipe by-pass on the pipe's contextual setting. Dissolution pipes develop in areas of evaporite or carbonate karst and form by the dissolution of rock units at depth, creating subsurface cavities that promote instability in the overburden leading to collapse (Stanton, 1966; Cooper, 1986; Bertoni and Cartwright, 2005; Michaud et al., 2005). Hydrothermal pipes are found in sequences breached by igneous intrusions, and form by the release of a high flux of hydrothermal fluids associated with mafic sills, laccoliths and other kinds of igneous intrusions (Davies et al., 2002; Svensen et al., 2003; Trude et al., 2003).

Blowout pipes were first described by Løseth et al 2001 from the Nigerian continental margin. Similar to the other pipe families, they are typically seen on seismic data as a columnar zone of disturbed reflections or vertically stacked localized amplitude anomalies, often reaching the seabed and terminating in a pockmark or crater. Blowout pipe genesis is believed to result from the enigmatic and catastrophic breaching of top seals on shallow gas reservoirs (Løseth et al., 2001). The diagnostic link between blowout pipes and pockmarks is the main argument to support the concept that these pipes represent a discrete blowout event, instead of a longer term, slower flux process or seepage (Løseth et al., 2001; Cartwright et al., 2007). Blowout pipes are not linked to igneous intrusions or karstified units thereby differentiating them from dissolution and hydrothermal pipes. Seepage pipes have similar seismic characteristics to blowout pipes but lack the blowout crater (Cartwright et al., 2007).

1.3.3 Acoustic expression of blowout and seepage pipes

The basic description and definition of a pipe given above is simplistic. Complexities in the seismic expression of pipes have lead to a multitude of definitions and seismic examples in the literature. Specific literature examples have been chosen to illustrate this point (Berndt et al., 2003; Løseth et al., 2003; Morley, 2003; Xie et al., 2003; Trincardi et al., 2004; Gay et al., 2007a; Hustoft et al., 2007; Paull et al., 2008; Pinet et al., 2008; Plaza-Faverola et al., 2010).

At least five different terminological phrases are currently interchanged within the literature to describe what is broadly classified as a "pipe" i.e. a vertical columnar zone of seismic disturbance. The terminology often includes the terms "pipe" or "chimney", for example;

- Pipe (Berndt et al., 2003)
- Chimney structures (Paull et al., 2008)
- Seismic chimney (Pinet et al., 2008)
- Blowout pipe (Løseth et al., 2001; Trincardi et al., 2004)
- Gas chimneys (Løseth et al., 2003; Morley, 2003)
- Gas chimneys / plumes (Xie et al., 2003)
- Pipe / seismic chimney (Gay et al., 2007a)
- Acoustic pipe structure (Hustoft et al., 2007)
- Vertical fluid migration feature (Plaza-Faverola et al., 2010)

The multiplicity of terms for the seismic expression of the columnar structures, hereafter simply referred to as pipes, may reflect a degree of uncertainty in interpreting these features due to their seismic complexity and propensity for being shrouded in seismic artefacts. The seismic expression of pipes can be broadly classified into four groups; 1) up-bending convex reflections, 2) down-bending concave reflections, 3) distortion or chaotic loss of acoustic signal and 4) a combination of types. Examples of different pipe structures are shown in Figure 1.3; a brief description of each example is given in Table 1.1.

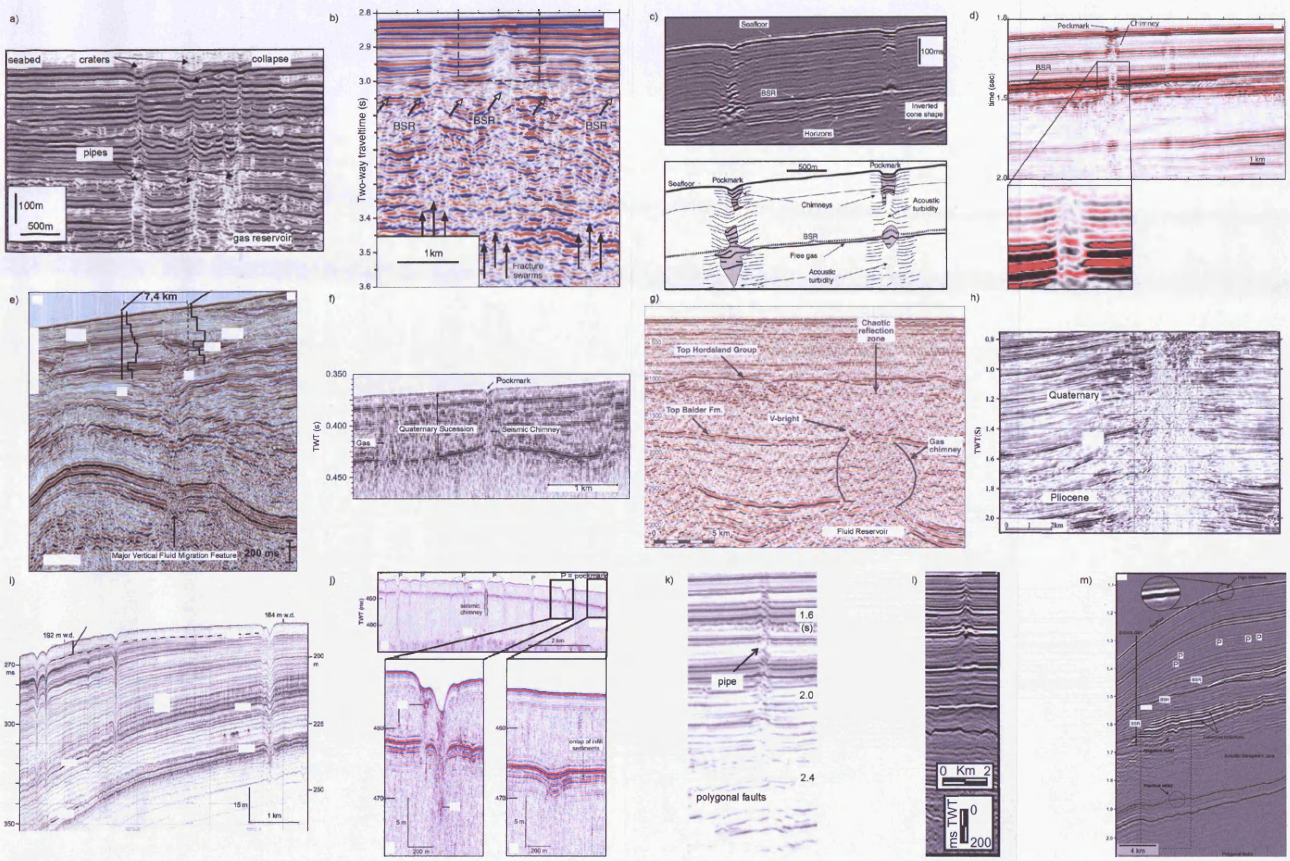

Figure 1.4 Variable acoustic expression of pipes (adapted from Løsethe et al 2001, Haacke et al 2009, Gay et al 2007, Paull et al 2008, Plaza-Faverola et al 2010, Pinet et al 2008, Løseth et al 2003, Xie 2003, Trincardi et al 2004, Pinet et al 2009, Berndt et al 2003, Gay and Berndt 2007 and Hustoft et al 2007)

Table 1.1 Basic pipe description (based on Figure 1.3)

Terminology	Basic description	Dimensions	Amplitude	Reflection geometry
Blowout pipes	Combination type : the lower section of the pipe is defined by clear breaks in reflection continuity in contrast with an upper section of upward bending continuous reflections	Height : ~ 1 km Width : < 100 m	Similar to background strata	Discontinuous at pipe top (down-turn) and bottom (upturn), continuous in the middle
Hydrate choked chimneys	Combination type : lower sections of the pipe are indistinguishable from the highly fractured background strata. The upper section of the pipe is characterised by reduced amplitude and loss of coherent acoustic expression	Height : ~ 100 ms Width : ~ 100 m	Less than background values	Discontinuous and a tendency towards up-turn reflections
Pipe / Seismic chimney	Combination type : seismic attributes differ between those above and below the BSR. Beneath the BSR the deep anomaly is an inverted cone shape in cross section and marked by lower amplitude reflectors and acoustic turbidity. Above the BSR reflections are up-bending, down-bending and discontinuous. The shallowest section of pipe is ovoid in shape with depressed high amplitude reflectors	Height : > 200 ms Width : ~ 250 m	Isolated reflections showing above background amplitudes	Near continuous up-turn and down-turn reflections asymmetric in shape
Chimney structures	Combination type : identified in seismic reflection profiles as local disturbances in the continuity of seismic reflections that are similar in width to the pockmark. Authors conclude this may be structural or a velocity effect	Height : > 300 ms Width : < 1km	Lower amplitude than the BSR but slightly higher than the background strata	Discontinuous with localised up-turn and down-turn reflections
Vertical fluid migration feature	Distortion : recognised by push-down and loss of frequency	Height : > 1 s Width : < 3km	Similar to background strata	Discontinuous, chaotic, wavy
Seismic chimneys	Distortion : Vertical zones of disturbance in the seismic data where amplitudes of reflectors are distorted	Height : ~ 100 ms Width : < 200m	Similar to background strata with isolated higher amplitudes	Highly discontinuous with localised reflection concavity towards the pipe top
Gas chimneys	Distortion : noise zones or noise filled seismic data with occasional high amplitude V-shaped brights clustered above the noise zone	Height : < 1 s Width : < 5 km	Similar to background strata	Discontinuous, chaotic, occasionally wavy

Terminology	Basic description	Dimensions	Amplitude	Reflection geometry
Gas chimneys / plumes	Distortion : low-middle seismic amplitudes and intermittently chaotic and blank reflecting seismic facies	Height : > 1 s Width : ~ 2 km	Generally lower than background values with isolated higher amplitude reflections	Discontinuous, chaotic, some acoustic blanking
Blowout pipes	Concave : stacked v-shaped continuous reflections	Height : < 100 ms Width : < 300 m	Similar to background strata with isolated higher amplitudes	Stacked v-shaped continuous reflections
Seismic chimneys	Concave / distortion: occasional concave reflections within a vertical wipe-out zone where the seismic signal is deteriorated and reflections are absent	Height : < 50 ms Width : < 200 m	Above background levels	Chaotic and discontinuous but showing evidence for continuous concavity where reflections permit
Pipe	Convex : circular zones of up bending, low amplitude reflections	Height : < 500 ms Width : < 500 m	Similar to background strata with isolated higher amplitudes	Discontinuous stacked convex reflections
Chimney / pipe	Convex : The upper part is ovoid in shape with high amplitude reflectors deflected upward directly beneath the pockmark depression. The deeper part is marked by a decrease in reflection amplitudes towards the centre	Height : > 300 ms Width : < 1 km	Similar to background strata with isolated higher amplitudes	Near continuous stacked inverted v-shaped reflections
Acoustic pipe structures	Convex : narrow vertical zones of acoustic wipe-out with upward bending marginal reflections	Height : > 500 ms Width : < 500 m	Similar to background strata	Continuous stacked inverted v-shaped reflections

The seismic expression of pipes also shares some common elements with sedimentary diatremes and small mud volcanoes/diapirs (Brown, 1990; Løseth et al., 2001; Cartwright and Huuse, 2005; Cartwright et al., 2007; Judd and Hovland, 2007). Elements such as 1) columnar, vertical acoustic distortions; 2) deviation in amplitude from background values; 3) concave, convex, discontinuous and/or chaotic reflections; and 4) similar geometrical attributes. These similarities are noted but not dealt with here.

From this small selection of pipe examples, it is clear that the same terminology has been given to pipes with very different seismic expressions and conversely, pipes with a similar seismic expression have different terms. For example, blowout pipes described by Løseth et al (2001) and Trincardi et al (2004) and stacked inverted v-shaped reflections by Hustoft et al (2007) and Gay and Berndt (2007).

For the purposes of this thesis I refer to a chimney as an amorphous acoustic distortion resulting from the presence of gas, seeping through the sedimentary column. Pipes represent distinct, clearly definable, columnar structures formed by the migration of fluid (pore water, gas) and some sediment, to the extent that it disrupts the sedimentary layering. I suggest that pipes which entrain (fluidized) material can be distinguished from pipes which only permit the migration of fluids by recognition of deposited (transported) material on the (palaeo)seabed. Pockmarks are small (< 1 km diameter) circular seabed depressions formed by the expulsion of fluid.

The variation in seismic expression is difficult to explain, and as yet, has not been tackled in the published literature. A discussion on the variations in observed seismic expressions of pipes is beyond the scope of this thesis and the limited information supplied in some articles on the data collection methods etc is insufficient to make clear comparative conclusions. I tentatively suggest that the variation in seismic expression may be the result of;

- Seismic data collection, processing, migration etc
- Acoustic anomalies and amplitude anomalies
- Differences in the host stratigraphy

- Variation in the fluid type and content (% gas in pore water) of the pipe
- Variation in how the pipe was formed i.e. blowout vs seepage
- Process e.g. collapse vs the upward movement of fluidized material

1.3.4 Pipe and pockmark formation

This section gives a brief introduction to the basics of pipe and pockmark formation. It is not a comprehensive account of the processes involved nor does it discuss any of the research in this thesis.

The formation of blowout pipes is poorly understood at present because only a few seismic examples have been described, and none have been calibrated by drilling (Cartwright et al., 2007). The only known published onshore example of a blowout pipe is from the Greek Island of Rhodes and consists of concentric rings of clasts in a muddy matrix surrounded by a halo of heavily fractured country rock ((Hanken et al., 1999) reported in Judd and Hovland 2007). The identification of hydraulically fractured rock is of paramount importance to blowout pipe formation. Hydraulic fractures enable vertical gas escape, violent enough to erode the seabed and create a void. This void is subsequently filled by clasts of the overlying rock as they fall back into the newly created blowout crater (Hanken et al., 1999; Løvlie and Hanken, 2002). It remains unclear whether this onshore example represents a blowout pipe or some other form of fluid migration or dissolution pipe given its limited exposure, however, this example does provide a good example of a collection of columnar hydrofractured structures. The description of Namibian blowout pipes in Chapter 4 is intended to extend this descriptive base.

Conversely, pockmarks have received a greater amount of attention (Hovland and Judd, 1988; Judd and Hovland, 2007; Pilcher and Argent, 2007; Sahling et al., 2008). Pockmarks are conical seabed depressions which range from <100 m to >1000 m

diameter and <1 to >20 m deep*. Their morphology is generally characterised as standard circular and/or elliptical, composite, asymmetric, unit, giant, pockmark strings and elongated pockmarks and troughs (Judd and Hovland, 2007). Formation involves seal breach at (shallow) depth instigating vertical fluid migration. Accumulations of gas in near seabed sediments result in increased pore pressures and produce doming of seabed and subseabed reflections. The dome is in tension and small fractures develop on the crest and flanks, through which gas establishes a route to the seabed forming unit pockmarks (diameter <5 m). A hydraulic connection is established, gas expands as it rises through the fractures and results in a violent burst of escaping fluid at the seabed forming a normal pockmark (diameter >100 m) (Judd and Hovland, 2007). Any fluidised sediments or entrained material is conveyed into the water column and dispersed by bottom currents. Unit pockmarks (~5 m to < 20 m diameter) continue to develop on the seabed around the newly formed pockmark and coalesce to form a composite pockmark. Site specific variations of this model of pockmark formation are present within the literature but not discussed here (Pilcher and Argent, 2007; Sahling et al., 2008).

Recently, numerical models have been utilised to further elucidate pockmark formation (Jain and Juanes, 2009; Cathles et al., 2010; Su et al., 2010). Cathles et al (2010) produced a "gas-piston-water-drive" numerical simulation of pockmark formation based on a capillary seal. A capillary seal is formed when capillary forces "attract" pore water into fine sediment pores, displacing gas into larger pores. Without sufficient pressure gas bubbles are unable to enter the finer pores preventing pore water and gas bubbles from migrating. It is essential that both pore water and gas are present for a capillary seal to be operational. In the Cathles et al (2010) model a single interface capillary seal traps gas until sufficient pressure has built up and the gas invades the seal. The seal fails completely (a unique aspect of capillary seals) releasing gas into an upward-propagating pipe, displacing water "like a piston" as it rises, liquefying the sediments (Cathles et al., 2010).

* see Appendix A1 for a database of pockmark geometries extracted from published articles. Please note, the database is not an exhaustive account of pockmark geometries and is only designed to illuminate the range in observed geometries

In the Cathles' et al (2010) model, a subsurface pipe can start to deform overlying sediments when the pipe height equals half the distance between the base of the source reservoir and seabed, pushing water up at increasingly higher velocities as the pipe approaches the seabed (Su et al., 2010). This suggests that where the sediment permeability is uniform, it is the buoyancy force of the rising gas column which pushes water out of the sediments above causing fluidisation and pockmark formation; permeability is not a consideration (Hovland et al., 2010). The rate of pipe growth depends on permeability and the ratio between the depth to the fluid source and the thickness of the fluid source (Cathles et al., 2010).
Jain and Juanes' (2009) discrete element model simulates pockmark formation at the grain scale. A fundamental outcome of the Jain and Juanes model is that grain size is the main factor controlling the mode of gas transport in sediment. Capillary invasion (where the gas/water interface invades the sediment pore throat if the capillary pressure [difference between gas pressure and water pressure] is larger than the capillary entry pressure) is preferential in coarse grained sediments (>1 μm) and hydraulic fracture in fine grained sediments (< 1 μm) (Jain and Juanes, 2009).

Slight, yet significant differences exist between the conceptual and numerical models. The Cathles et al model uses a uniform permeability of unstipulated grain size and advocates seal breach by seepage, analogous to the capillary invasion proposed by Jain and Juanes (2009), as the sole method of pockmark formation. The conceptual model proposed by Judd and Hovland (2007) implies fluid migration will utilise all available permeability pathways including fractures, a realistic compromise not integrated into the Jain and Juanes (2009) model which is also based on vertical permeability homogeneity.

The models presented here assume a vertical root system beneath the pockmark, constant fluid density and uniform vertical permeability. The models fail to incorporate heterogeneities in the flow pathways caused by permeability changes or diagenetic processes e.g. the formation of Methane Derived Authigenic Carbonates (MDAC) (a similar process is referred to as Hydrocarbon-related diagenetic zones (HRDZs) by Cowley and O'Brien (2000)). Studies of onshore fossil seeps have shown branching tubular networks of carbonate cemented chimneys attesting to the possible small scale dendritic nature of fluid migration at seep sites (Aiello, 2005; De

Boever et al., 2006b, a; De Boever et al., 2009a; De Boever et al., 2009b; Nyman et al., 2009). The numerical models also fail to incorporate the possibility of pathway "re-use" over time. The models clearly describe the first generation pockmark but fail to capture the effects of re-migration through existing conduits or that the formation of unit pockmarks may amalgamate into larger pockmarks as suggested by the conceptual model of Judd and Hovland (2007). The possibility of conduit re-use and the lateral components of fluid migration are discussed in more detail in Chapters 6 and 7.

Gaps still remain in our understanding of the process of pockmark formation. The next section summaries recent work on formation with a focus on the spatial and temporal distribution of pipe and pockmark formation, and the frequency and magnitude of flux; the key themes of this research.

1.3.4.1 Spatial and temporal distribution of pipe and pockmark formation

Incorporating spatial and temporal distribution analysis into discussions of pipe and pockmark formation is a relatively recent approach adopted within pockmark studies. Previous studies have analysed the distribution of fluid migration relative to focus points e.g. the up dip limit of structures, but to this author's knowledge, the work presented here is the first published spatio-temporal research of its kind. Recent published studies have started to incorporate elements of spatial and temporal analysis, and that work is reviewed here.

Analysis of pockmark formation in space and time requires detailed 3D mapping of pockmarked horizons within a stratigraphic sequence. A large proportion of pockmark studies focus on seabed pockmarks or seeps thus rendering their time of formation difficult to determine, especially if the seafloor is diachronous and/or has such low sedimentation rates that pockmarks of different ages become superimposed. Consequently, previous research has discussed the spatial aspects of pockmark formation and when they formed as separate issues. The research presented here (Chapters 4, 5, 6 and 7) combines this analysis into a holistic evolutionary model.

1.3.4.1.1 Spatial

Traditionally, the spatial analysis of seabed pockmarks has only extended to density as a basic spatial descriptor (Kelley et al., 1994; Rise et al., 1999; García-Gil et al., 2002; Paull et al., 2002; Bünz et al., 2003; Naudts et al., 2006; Rogers et al., 2006; Gay et al., 2007a; Van Rensbergen et al., 2007; Andresen et al., 2008; Jané et al., 2010), however more recent studies have incorporated more advanced statistics. Principle Component Analysis (PCA) and Variance have been used to describe the distribution of seep ecology within and surrounding pockmarks (Li et al., 2007; Olu-Le Roy et al., 2007; Galéron et al., 2009), Variogram analysis has been used on analogue onshore fossil seep studies (De Boever et al., 2009b), Nearest Neighbour analysis and Delaunay Triangulation were used to describe pockmark distributions from the Inner Oslofjord, Norway and Iberian Peninsula (Webb et al., 2009; Jané et al., 2010) and the Blade method was tested on pockmark distributions as a new statistical method for detecting point alignments (Hammer, 2009). To the author's knowledge, these are the only studies which incorporate advanced spatial statistics. With the exception of Nearest Neighbour analysis and Delaunay Triangulation, none of the spatial statistics utilised in this research have previously been applied to pockmark distributions.

1.3.4.1.2 Temporal

The temporal distribution of pockmark formation is often poorly documented (Gay et al., 2007b). Research which has considered the timing of pockmark formation can be subdivided into three categories; those which use chronostratigraphic dating techniques on pockmark cores (Paull et al., 2008; Webb et al., 2009), those which date the seismic stratigraphic unit containing the pockmark (Long, 1992; Kelley et al., 1994; Cole et al., 2000; Hansen, 2006; Gay et al., 2007b; Hjelstuen et al., 2009; Andresen and Huuse, 2010) and those which date the source layer feeding the pockmark (Heggland, 1998; Duck and Herbert, 2006; Gay and Berndt, 2007; Van Rensbergen et al., 2007; Pinet et al., 2008; Hustoft et al., 2010). The range of dates for the timing of pockmark formation can range from an accuracy of tens of years (chronostratigraphic dating) to geological time periods (dating the stratigraphic or source unit).

Few studies have considered the timing of pockmark formation, and none to the author's knowledge, have documented a series of pipes forming in sequence (as presented in Chapter 5). Possible reasons for this are 1) chronostratigraphically dating pockmarks is expensive and unrealistic considering the number of pockmarks within a basin or field, 2) arbitrarily chronostratigraphically dating pockmarks (methodology presented here, Chapter 5) is only applicable in uniform, continuous, well layered seismic stratigraphic sequences, 3) unlike buried pockmarks, it can be difficult to tie surface pockmarks to broad stratigraphic units of known geological age i.e. tied to wells and dated.

1.3.4.2 Frequency and magnitude of flux through pockmarks and pipes

Allied with the timing of pipe formation is the analysis of formation and/or recurrent flux through the conduit. Flux is the amount of fluid that migrates through a pipe and pockmark with time. Pipe and pockmark flux is a highly debated, complex and convoluted topic. It is a difficult topic to tackle simply because as yet there is no robust way to measure it. For example, calculating the volume of a cylinder based on pipe height and diameter as a proxy for minimum flux is insufficient because it is unlikely that a pipe has a large open core (Cartwright et al., 2007). It is tentatively suggested that measurements of flow and/or flux could be estimated from pockmark sediment fluidization deposition, if the evacuated sediment from a pockmark was deposited (and preserved) around a pockmark (repeat surveys would be required). Relative indications of sediment porosity could also be established if this material was sampled. This methodology is in its infancy and as yet untested.

To simplify discussions of fluid flux within this research, flux is discussed in terms of frequency and magnitude of fluid migration instead of volume. The concept of frequency and magnitude is shown diagrammatically in Figure 1.4. For the purposes of the research presented here, frequency relates to how often fluid is inferred to migrate through the pipe/pockmark and magnitude to the inferred "severity" of seabed eruption as documented by resultant pockmark geometry. This is further discussed in Chapter 8.

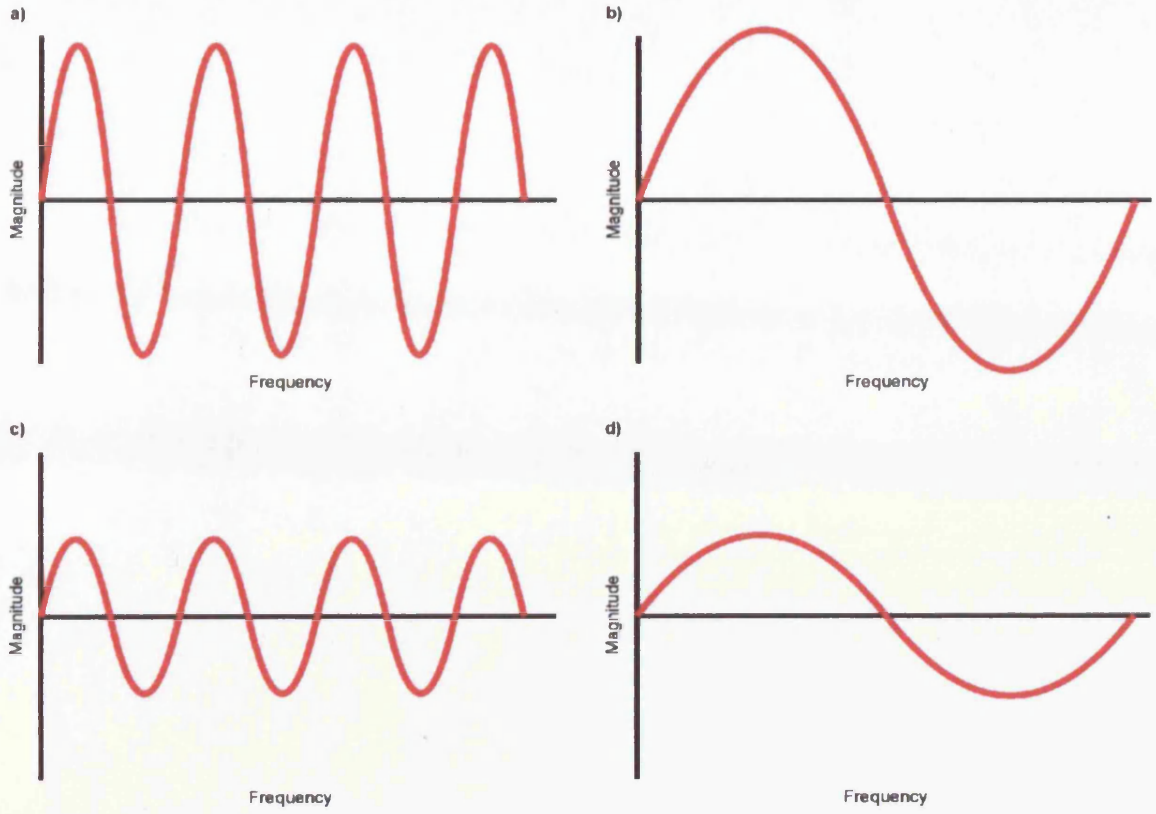

Figure 1.5 Frequency and Magnitude schematic. a) High frequency, high magnitude; b) Low frequency, high magnitude; c) High frequency, low magnitude; d) Low frequency, low magnitude

The frequency and magnitude of flux is difficult to assess. Several categories of fluid migration need to be considered. Firstly, pockmark flux can range from explosive blowout to a gentle egress of fluid at the seabed. Secondly, pockmark conduit re-use and recurrent flux may range from fluid venting as a one-off episode to continuous fluid seepage. Finally, fluid venting may occur frequently or episodically e.g. once a year or once every hundred thousand years.

Only modest research has been done on fluid flux and discussions are often qualitative and site specific. Exceptions to this are studies from onshore analogues and ROV (Remotely Operated Vehicle) seep studies. For example, studies of onshore mud volcano systems from NW Italy have demonstrated a prolonged period of intermittent fluid flow through conduits involving both a degassing phase of slow seepage permitting carbonate cementation and the growth of chemosymbiotic communities, and violent eruptive phases documented by the extrusion of soft mud breccias and dyke formation (Clari et al., 2004; Clari et al., 2009). Onshore fossil seep studies from Bulgaria identified variable seepage rates of a single hydrocarbon-charged fluid source at depth. Slow seepage allowed methane to oxidize within the sediment depleting δ13 C ratios. Increasing seepage rates caused calcite cemented conduits to form and even higher-energy fluid flow formed "whirled up" sediment cemented "pisoid" nodules within the conduits (De Boever et al., 2006a, b; De Boever et al., 2009a). Remotely Operated Vehicle (ROV) studies of submarine seep sites measuring flow rates and bubble sizes have reported variations in flux over short periods of time (~20 mins). Observations ranged from violent outbursts, each lasting 1 minute over a three minute interval which displaced and resuspended sediment grains forming small depressions (maximum 50 cm diameter and 15 cm depth) to constant bubble release giving a flow rate of 0.018-2.424 l/min (Naudts et al., 2010).

Fluid flux has been implied from offshore seismic interpretation studies of pockmarks (Paull et al., 2002; Hovland et al., 2005; Hustoft et al., 2009a). Collating information gathered from various studies of pockmarks offshore Norway, Hovland et al (2010) concluded that small unit-pockmarks likely manifest cyclic pore-water seepage and larger normal-pockmarks reflect periodic or intermittent gas eruptions, with extended intervening periods of slow, diffusive, and cyclic pore-water seepage.

Methane Derived Authigenic Carbonate formation within pockmarks is cited as evidence for long term seepage through these features (Hovland et al., 2010).

Gaps still remain in our understanding of fluid flux associated with pipe and pockmark formation and continuity/episodicity of fluid migration. Recent studies have recognised the possibility of conduit re-use by possible episodic fluid migration, however these studies have failed to suggest a timeline or period i.e. 1000 yrs for continued migration. It also remains unclear how often these conduits are re-used during this period. Chapters 5 and 6 aim to address these issues.

1.4 Thesis layout

An introduction and overview of the research topics covered in thesis has been presented in the preceding sections of Chapter 1. Seismic interpretation and spatial statistical methodologies common to all results chapters are presented in Chapter 2. Methodologies unique to particular research elements can be found in their related chapters. The geological setting of Namibia and the Nile Deep Sea Fan (NDSF) are presented in Chapter 3. The research presented in Chapters 4, 5, 6, 7 and Appendix A7 form the main results chapters of this thesis. Chapters 4 and 5 are based on the Namibian data and are in print. Chapters 6, 7 and Appendix A7 are based on the NDSF and are due for submission in October (Appendix A7 is in review). Appendix A7 represents ancillary research to Chapter 7. Appendix A7 utilises two datasets, the NDSF (same data as Chapter 7) and bathymetric data from Big Sur, California. This paper further develops the methodologies described in Chapters 2 and 7. The data collection, mapping, geometrical analysis / morphometrics and some statistical components of the research presented in Appendix A7 for both the NDSF and Big Sur datasets are the work of the author [JLM]. The remainder of the paper in Appendix A7 is the work of the lead paper author [AC] and is therefore placed in the appendix. An over-arching summary and discussions / implications are presented in Chapter 8 and conclusions drawn in Chapter 9.

Chapter 2

2 METHODOLOGY

2.1 Introduction

The results presented in this thesis are based on the interpretation of 3D exploration seismic data, 2D Ultra High Resolution (UHR) seismic data, Chirp profiler and side scan sonar data. The aims of this chapter are 1) to outline the datasets used in this thesis; 2) provide a brief overview of the seismic method; 3) describe the seismic survey parameters; 4) outline the seismic interpretation and Geographic Information System techniques applied; and 5) describe the spatial statistics used in this thesis.

2.2 Seismic data

The Namibian research is based on a single exploration 3D cube. The Nile Deep Sea Fan research is based on an exploration 3D seismic, 2D UHR data and AUV (Autonomous Underwater Vehicle) collected Chirp profiler, side scan sonar with backscatter data. A 3D volume of the NDSF was used to provide the structural framework for the shallow data. Data from a single shallow geotechnical borehole was made available for the study area in Chapter 7. Chronostratigraphic dates for specific horizons were made available for Chapter 6 however this data is not available for publication.

2.2.1 2D and 3D seismic data

The two-way travel time (TWTT) of compressional waves (P-waves) is used in the construction of seismic reflection data. In a typical offshore situation, P-waves

originating from an airgun seismic source are reflected from geological boundaries between different rock lithologies (subsurface impedance contrasts) to a series of geophones towed behind a survey vessel (Evans, 1997). The strength of the impedance contrast is a function of the rock density and wave velocity contrasts. The seismic velocity of a rock varies according to factors such as composition, texture, porosity, fluid content, elastic modulus and density (Kearey et al., 2002).

According to common convention, seismic data in this thesis is displayed in zero phase SEG (Society of Exploration Geophysicists) normal polarity. The convention of SEG normal polarity is that an increase in acoustic impedance corresponds with a peak in the seismic wavelet and the wavelet is symmetrical with the peak corresponding to the zone of maximum energy (Fig. 2.1) (Evans, 1997; Brown, 2004).

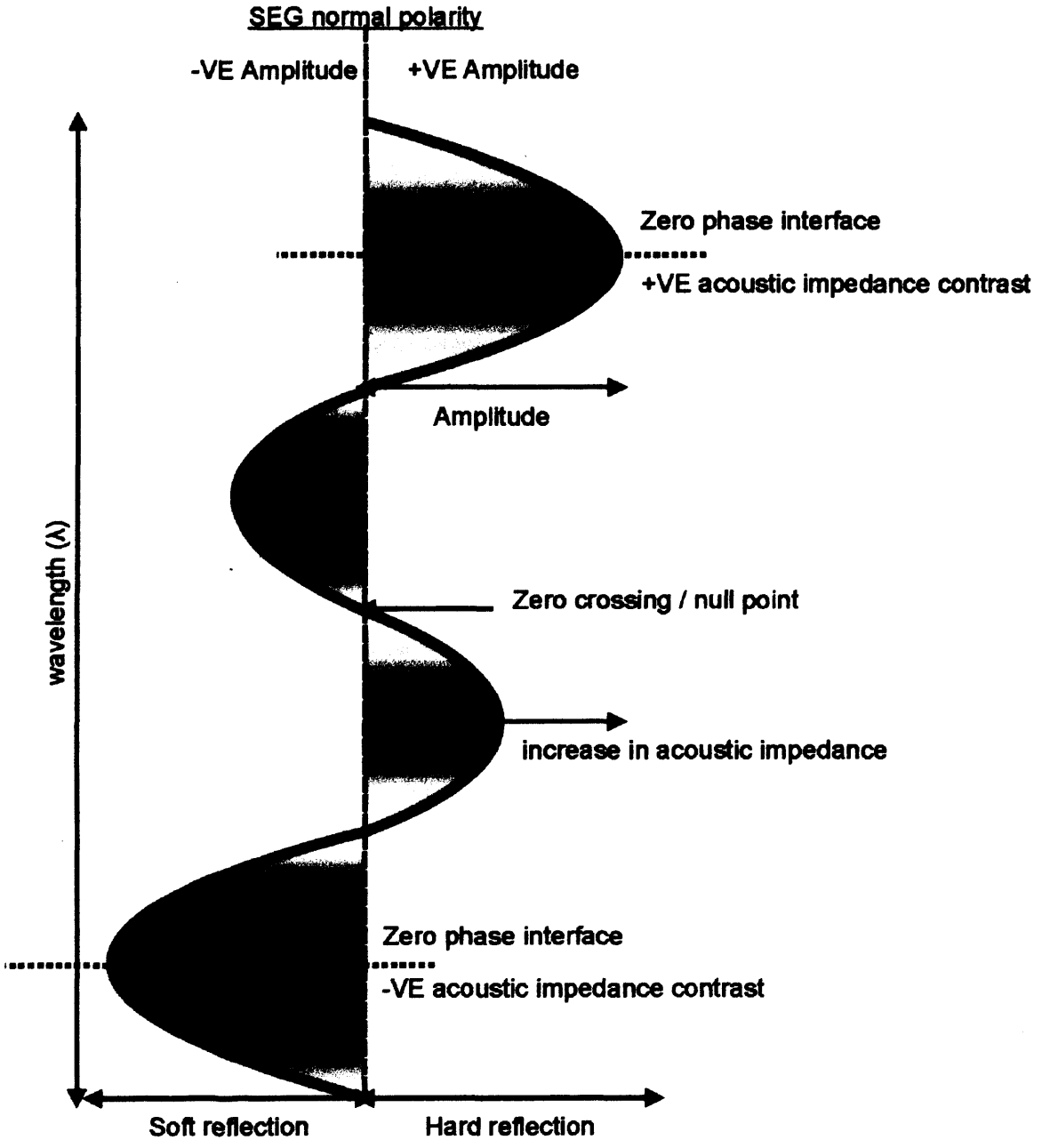

Figure 2.1 Seismic wave schematic illustrating the conventions of SEG normal polarity. Two wavelengths are shown. Wave colours relate to the 3D seismic lines used in this research (adapted from Hart, 1999)

Compressional waves (P-waves) which are reflected from an interface showing positive downwards impedance contrast will be correlated with a peak on the wavelet whereas P-waves reflected from a surface showing negative downwards impedance contrast will be correlated with a trough (Fig. 2.1). Wave amplitude (height of the peak or trough) corresponds to the magnitude of impedance contrast.

The resolution of the seismic data varies both vertically and horizontally, and generally decreases with depth. Seismic velocities increase with depth as the rocks become older and more compact. Predominant frequencies decrease with depth as the high frequencies in the seismic signal are more quickly attenuated (lost by adsorption) resulting in an increasing wavelength and a poorer resolution (Brown, 2004). Vertical resolution is ¼ of the dominant wavelength (λ) of the seismic pulse (limit of separability) (Fig. 2.2). The limit of visibility is reached when the bed thickness is less than the tuning thickness and the reflection signal becomes obscured by background noise (depends on acoustic impedance contrast and noise level) (Fig. 2.2). The tuning effect is a phenomenon of constructive or destructive interference of waves from closely spaced reflections. At a spacing of less than ¼λ, reflections undergo constructive interference and produce a single reflection of high amplitude. At spacing greater than that, the reflection begins to be resolvable as two separate reflections. The tuning thickness is the bed thickness at which two events become indistinguishable in time.

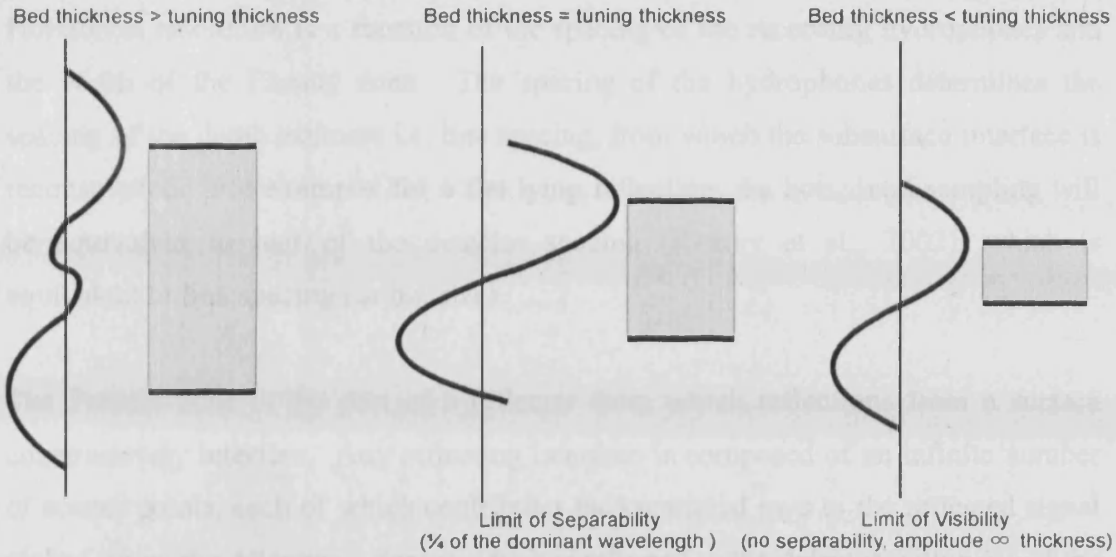

Figure 2.2 Vertical resolution and tuning thickness. Resolution of the reflections from the top and bottom of a bed is dependant on the interaction of closely spaced wavelets (adapted from Brown, 2004)

Horizontal resolution is a function of the spacing of the recording hydrophones and the width of the Fresnel zone. The spacing of the hydrophones determines the spacing of the depth estimate i.e. line spacing, from which the subsurface interface is reconstructed. For example, for a flat lying reflection, the horizontal sampling will be equivalent to half of the detector spacing (Kearey et al., 2002), which is equivalent to line spacing (or bin size).

The Fresnel zone is the part of a reflector from which reflections from a surface constructively interfere. Any reflecting interface is composed of an infinite number of scatter points, each of which contributes backscattered rays to the reflected signal picked up by the detectors. Energy which is returned to the detector within ½λ of the initial reflected arrival interferes constructively (Sheriff and Geldart, 1995; Kearey et al., 2002). The (first) Fresnel zone is the part of the interface from which this energy is returned (Fig. 2.3). All features (on buried horizons) with a lateral extent exceeding the Fresnel zone will be visible. Migration of the seismic data focuses the energy spread in the Fresnel zone, re-arranges reflections misplaced due to dip and removes reflection patterns from points and edges (Brown, 2004). This improves the horizontal resolution to about ¼ wavelength.

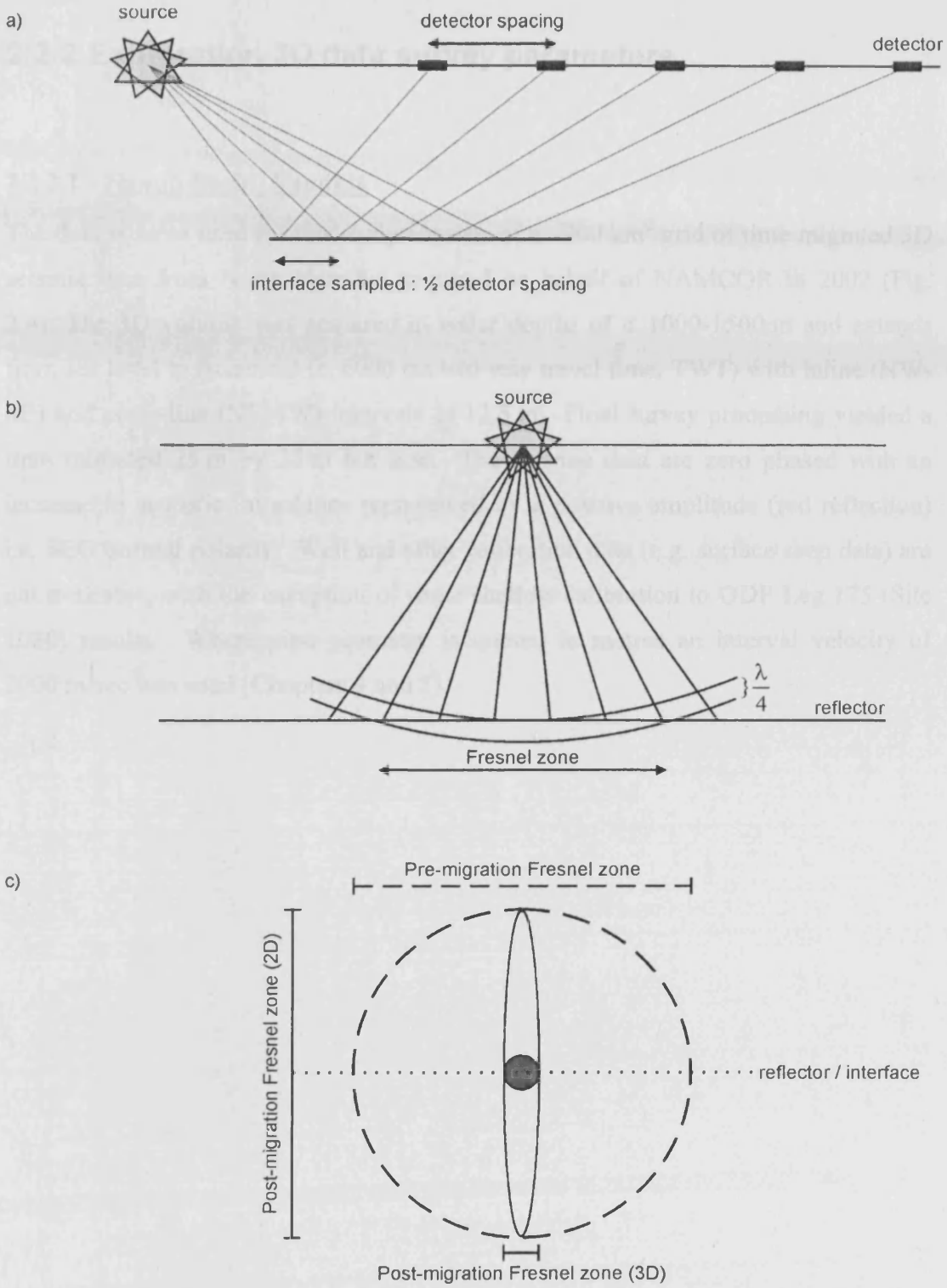

Figure 2.3 Horizontal resolution. a) horizontal sampling of a seismic reflection is half the detector spacing. b) energy is returned to the source from all points of a reflector. The region that produces the reflection (Fresnel Zone) has a minimum vertical resolution of a quarter of a wavelength. c) effect of migration on the Fresnel zone (adapted from Kearey et al (2002)).

2.2.2 Exploration 3D data survey parameters

2.2.2.1 Namib Basin, Namibia

The data volume used for this study consists of a ~900 km^2 grid of time migrated 3D seismic data from North Namibia acquired on behalf of NAMCOR in 2002 (Fig. 2.4). The 3D volume was acquired in water depths of c. 1000-1500 m and extends from sea level to basement (c. 6000 ms two way travel time, TWT) with inline (NW-SE) and cross-line (NE-SW) intervals of 12.5 m. Final survey processing yielded a time migrated 25 m by 25 m bin size. The seismic data are zero phased with an increase in acoustic impedance represented by a positive amplitude (red reflection) i.e. SEG normal polarity. Well and other calibration data (e.g. surface seep data) are not available, with the exception of some shallow calibration to ODP Leg 175 (Site 1080) results. Where pipe geometry is quoted in metres an interval velocity of 2000 m/sec was used (Chapters 4 and 5).

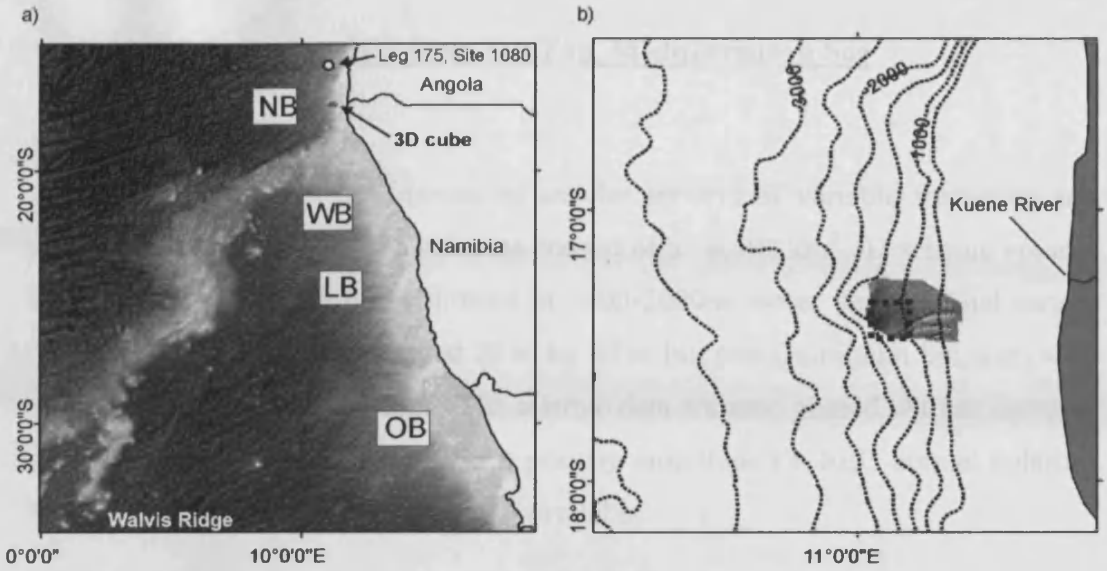

Figure 2.4 Location map. a) Gross structure map of the South Atlantic showing the location of the 3D cube on the Namibian continental margin and the location of the Walvis Ridge, NB, Namib Basin; WB, Walvis Basin; LB, Luderitz Basin; OB, Orange Basin. White circle represents the location of ODP Leg 175, Site 1080.; b) bathymetric map showing the location of the 3D cube (depth contour intervals are in metres). Kuene River marks the Angolan : Namibian border. Black box denotes an area containing isolated zones of Bottom Simulating Reflections (BSR).

2.2.2.2 Rosetta Region, Nile Deep Sea Fan, Mediterranean Sea

2.2.2.2.1 3D survey

The 3D seismic dataset is a mosaic of smaller surveys of variable frequency and resolution (Fig. 2.5). The data volumes consist of a ~6,400 km^2 3D seismic volume clipped at the Messinian (4s) collected in ~100-2000 m water depth. Final survey processing yielded a time migrated 25 m by 25 m bin size (minimum bin size) with N-S in-lines and E-W cross-lines. The seismic data are zero phased with an increase in acoustic impedance represented by a positive amplitude i.e. SEG normal polarity. Well and other calibration data were not available.

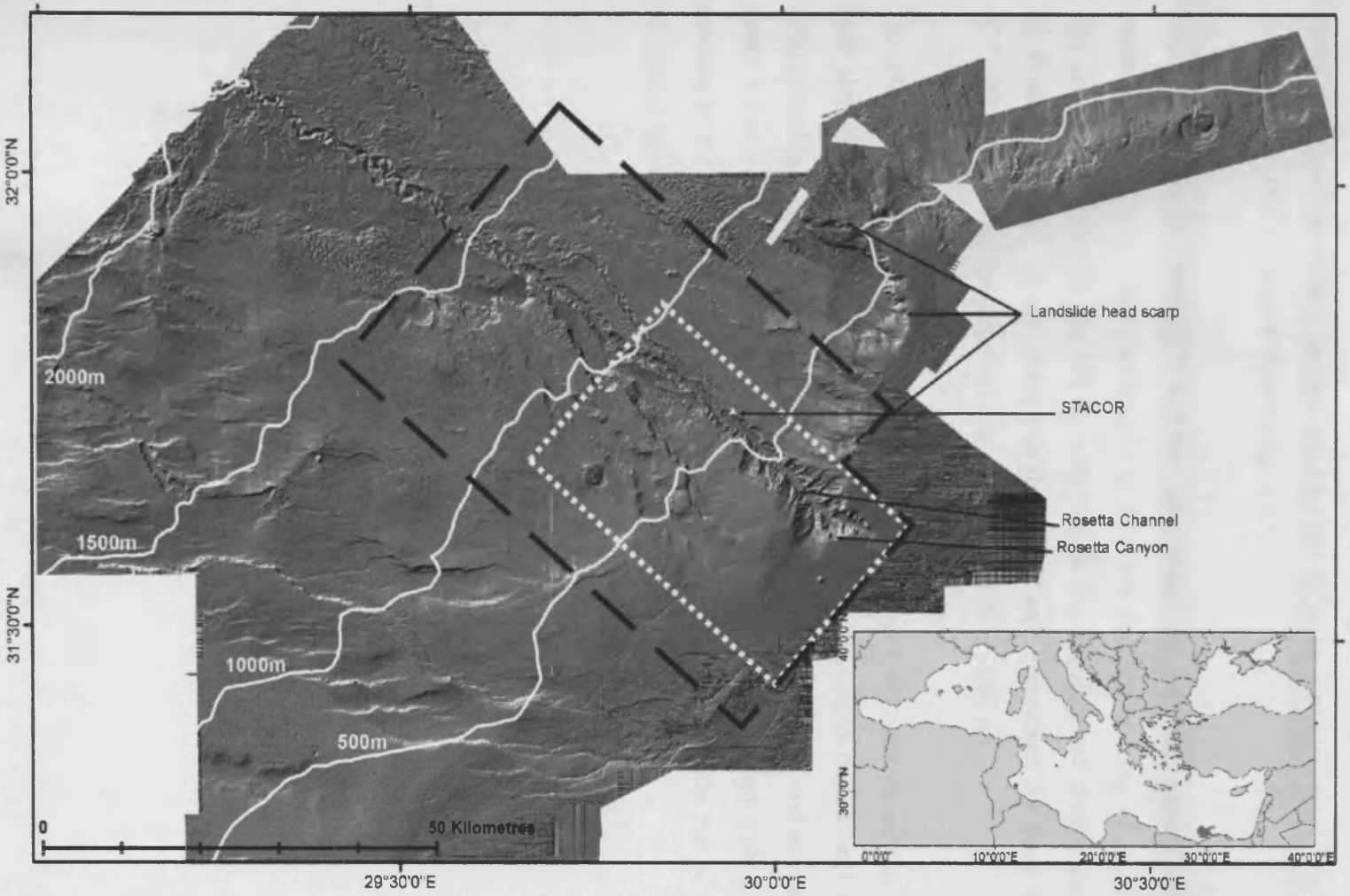

Figure 2.5 Nile Deep Sea Fan location map. Dip map of 3D seismic seabed pick is shown. White box, AUV survey; Black box, UHR survey; white triangle, STACOR location. Bathymetric contours are in metres. Note the prominent landslide head scarps east of the Rosetta Channel. Location of 3D volume on the Mediterranean Sea inset map is to scale

2.2.2.2.2 2D Ultra High Resolution data survey parameters

A combined survey of Autonomous Underwater Vehicle (AUV) and 2D Ultra High Resolution (UHR) seismic data were collected by Fugro Survey, on behalf of BP, in 2004 and 2005 in water depths of 16-1089 m with survey vessels M/V Geo Prospector and M/V Western Shore (Fig 2.6).

The UHR survey, totalling 4,536 km, comprised 99 primary lines (3,239 km), oriented 132 ° / 312 °, with line lengths of 3-71 km and line spacing of 250-2000 m. The general line spacing is 1000 m, with tighter line spacing and shorter lines over the Rosetta Region. Cross lines, totalling 1,297 km, comprised 59 lines oriented 42 ° / 222 °, with line lengths 7-41 km and spaced every 2000 m.

The 2D UHR digital seismic data were acquired with a 60 channel airgun, 6.25 m shot and group intervals, 2.0-2.7 second record length (depth dependant) and 0.5 millisecond sampling rate. Source tow depth was 1.0 m +/- 0.5 m and streamer tow depth 1.5 m +/- 0.5 m. The digital UHR seismic data were migrated with a vertical resolution < 5 m. High frequency and short wavelengths provide better vertical resolution when compared with the NDSF 3D data.

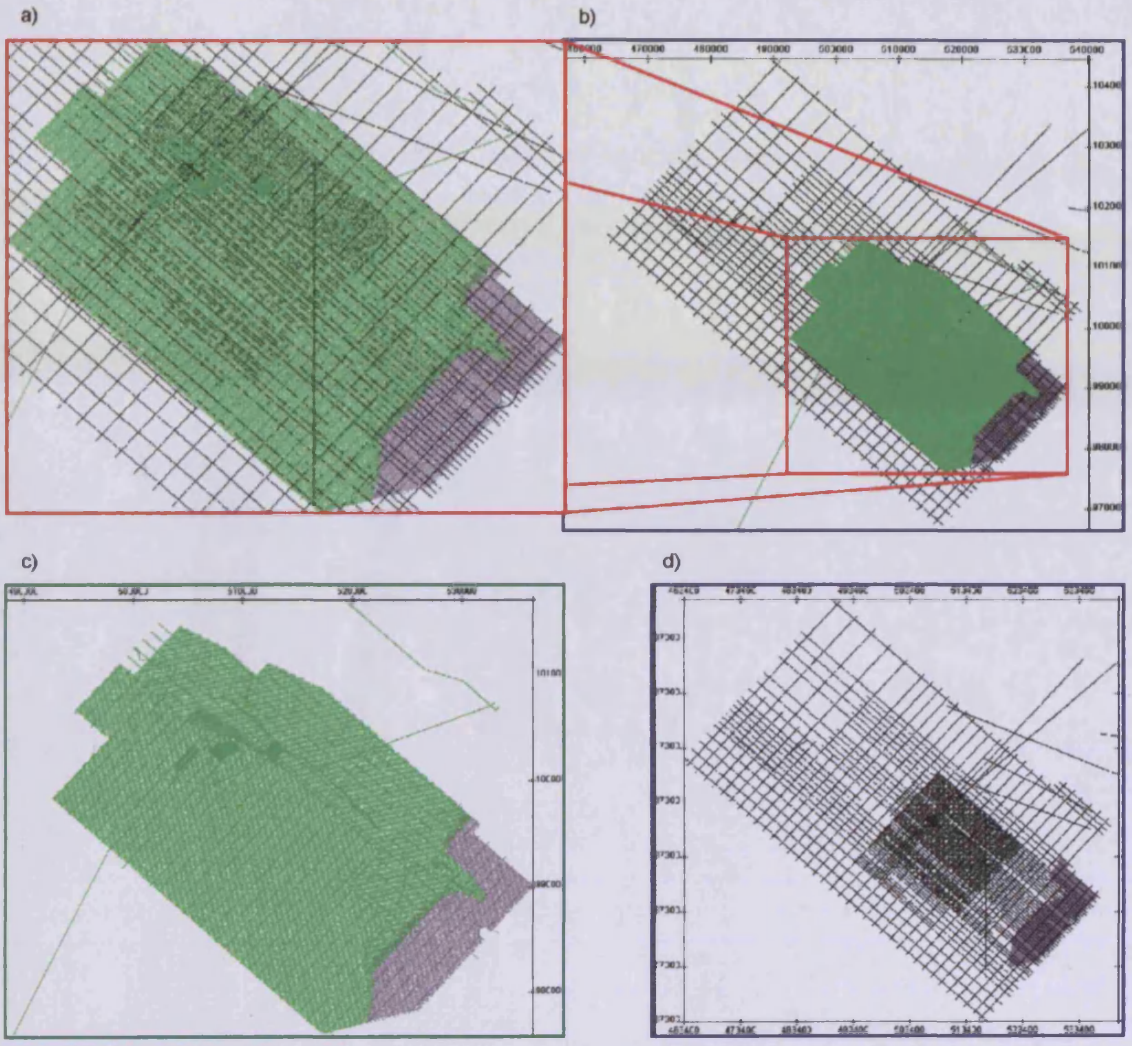

Figure 2.6 Nile Deep Sea Fan 2D survey. a) Rosetta Region UHR (black lines) and AUV (green lines). b) Entire coverage AUV and UHR seismic. c) AUV 2D survey lines. d) UHR survey lines

2.2.2.2.3 Autonomous Underwater Vehicle data survey parameters

The AUV data was acquired with the Hugin 3000 AUV S/V Echo Surveyor using a Simrad EM2000 multibeam echo sounder, Edgetech side scan sonar and Edgetech sub-bottom profiler. The survey comprised >800 survey lines, totalling 6750 km of AUV data. The line spacing was 150 m (NE-SW) with orthogonal tie-lines at 1000 m intervals, additional tie-lines were also run within the survey area (Fig. 2.6). The AUV typically operated at a height of 30-35 m above the seabed at a speed of 3.6 knots continually acquiring data from all its onboard sensors.

The multibeam echo sounder operated with 111 beams at a frequency of 200 k Hz with a ping rate of up to 10 Hz. Beam width was 1.5 ° along and 3.5 ° across with an angular coverage of up to 150 °. Chirp profiler penetration is to 100 ms, with a vertical resolution of ~0.5 m. Time : depth conversion of the seafloor achieved assuming average seismic velocities of 1519 m/s. The full spectrum chirp dual frequency DW-120 /410 side scan sonar system was operated at 120 k Hz with a nominal range of 200 m (bathymetry and backscatter data). The Edgetech DW-216 chirp profiler system operated at frequencies between 2 and 10 kHz with a firing rate of 250 ms and a nominal record length of 210 ms. No smoothing / sub-sampling were applied to the data and the final bin size for the bathymetry data was 3 m^2.

2.2.3 Seismic interpretation techniques and integration with Geographic Information Systems (GIS)

The results presented in this thesis are derived from mapping of 2D and 3D seismic data using Kingdom Suite (PC) and Schlumberger GeoFrame 4.0.2 (UNIX) software respectively. This section focuses on the methods generally applicable to all 2D and 3D seismic studies (Chapters 3–7 and Appendix A7). Individual results chapters will provide further details of procedures used where necessary.

Mapping is the basic process by which 2D and 3D surfaces of both structural and stratigraphic features are created. Within the interpretational software package the

horizon of interest is tracked (manually or automatically) on a series of lines oriented perpendicular to one another (2D survey lines, or 3D in-line / cross-line) providing a basic grid coverage of the area of interest. Grid density should be appropriate for the data resolution. Additional arbitrary lines are included as necessary. The tracked horizons provide seed points for automated tracking algorithms which propagate the interpretation according to the picking constraints and seismic volume constraints provided, converting lines into a surface coverage.

Once computed, various attribute information can be extracted from the surfaces including grid-based (dip), seismic trace (amplitude) and seismic volume (coherence) attributes. Seismic attributes utilised in this research are as follows;

- **Dip**: Dip is a measurement of changes in gradient. Dip maps are used here to highlight surface morphology.
- **Amplitude**: Seismic amplitude is the difference between the maximum displacement of a wave and the point of no displacement (null point) and is measured at the crest of the reflection (Fig. 2.1). Amplitude variations on a single horizon are commonly due to changes in acoustic impedance caused by variations in lithology, bedding continuity, gross porosity or fluid content (Brown, 2004). Fluid content is recognised by acoustic turbidity, acoustic blanking, enhanced reflections, pull-ups, push-downs, bright spots and flat spots (Judd and Hovland, 2007), all of which may be modified by variations in amplitude when compared to background strata.
- **Root Mean Squared (RMS) Amplitude**: RMS amplitude squares amplitude values over a specified time window and then averages the results. Consequently high amplitudes are more noticeable in surface maps. Care should be taken when interpreting average amplitude values, especially above pipes, because RMS windows can cross stratigraphic boundaries and gas pockets possibly introducing unwanted values into the calculation.
- **Coherence**: Time slices (or horizon slices/extractions) can be used to visualize coherency data with the aim of highlighting discontinuities in the reflections and is often free from interpretational bias i.e. the utilization of mapped horizons is not a requirement (Brown, 2004). Coherence uses a set of mathematical calculations similar to correlation to compare adjacent waveforms and return a

value which represents the similarity of the waveforms (cf. Brown, 2004). Coherence is excellent for mapping and identifying the three dimensional nature of faults (including throw) and therefore has strong applications for pipe/pockmark interpretation.

2.2.3.1 Quantitative measurements derived from seismic data

In order to substantiate some of the qualitative observation made about the seismic data, quantitative measurements were taken. The methodological details of how these measurements were taken are given in the relevant chapters. These measurements were all taken from seismic sections and are accurate to < 5 ms TWT (Two Way Travel Time) and 25 m and 5 m for the Namibian and NDSF data respectfully. Time / depth conversions are given above.

2.2.3.2 GIS

Seismically derived data were imported into ArcInfo 9.2 Geographic Information System (GIS). Seabed and horizon picks and amplitude maps were exported out of the seismic interpretation software as x,y,z files. These files were interpolated to surfaces within the GIS. Coherency slices were imported into the GIS and georectified.

Seismically derived data such as horizons and maps were exported into a GIS environment. Breaks of slope, slope angle, faults and planform geometry were identified from azimuth and dip maps, and coherency slices.

Once the raw seabed/horizon data were interpolated within the GIS, surface functions could be performed on the data. These included;

- Depth maps and contours: Depth topographic surfaces (ms or m)
- Hillshade: Shaded relief map generated using light source altitude and azimuth specifications (produces a similar result to dip)
- Slope: The slope of the surface (degrees < 90)

- Azimuth: The direction the slope is facing i.e. N, S, E, W (degrees < 360)
- Surface calculations e.g. isochron maps: Any mathematical function between two surfaces e.g. subtracting surface depth values to calculate unit thicknesses

GIS attribute databases were created which contained pipe/pockmark coordinates and additional quantitative, geometrical or qualitative information gained from the seismic data e.g. pipe height (top pipe depth – base pipe depth), pipe/pockmark width, depth (converted to metres where necessary), fluid source (levee, shallow gas pocket, unknown). This data has been collated in the appendix*.

2.3 Spatial statistics

Most of the spatial statistics were performed using the analysis packages built within the GIS. Minimal Spanning Tree, Self Organised Criticality and Hardcore simulations are the exception. These statistical models were run by Annabel Cartwright (AC) using specialist statistical software (Appendix A7). Point distributions are based on the centre of the pipe/pockmark as defined by a 4-way dip structure. Surface coordinates are taken for all pockmarks. Pipe coordinates are based on the top most reflection of the column.

Commonly associated with computing, engineering, physics, astronomy and mathematics, the spatial statistics used here are also widely used in biological and environmental sciences to analyse point distributions. For example the spatial distribution of plant and animal species (Asuka et al., 2004; Rozas et al., 2009), viruses (Siede and Büchler, 2006), water quality samples (Choi et al., 2007), earthquake hypocentre distributions (Nicholson et al., 2000) and tephra deposition (Bonadonna and Houghton, 2005).

The spatial statistical significance of pipe and pockmark distributions where analysed using univariate spatial autocorrelation statistics; Nearest Neighbour Analysis (*Rn*),

* For attribute information see Appendix A2.

Anselin Local Moran's I cluster and outlier analysis (*I*), Ripley's K multidistance cluster analysis (*Ld*), in addition to Density, Minimal Spanning Tree and Voronoi polygons (Dirichlet, 1850; Voronoi, 1907; Voronoi, 1908; Clark and Barber, 1954; Anselin, 1995a; Bailey and Gatrell, 1995; Cartwright and Whitworth, 2004).

2.3.1 Nearest Neighbour Index

The nearest neighbour index (*Rn*) measures the ratio of the observed mean distance to the expected mean distance for a hypothetical random distribution to determine whether the points are clustered (Clark and Evans, 1954; Mitchell, 2005). The *Rn* value was calculated with the formula;

(1)

$$Rn = \frac{\bar{D}(Obs)}{0.5\sqrt{\frac{a}{n}}}$$

Where *D(Obs)* is the mean observed nearest neighbour distance, (*n*) is the number of pipes and (*a*) is the aerial extent of pipe coverage in the study area.

A ratio of 1 is a random distribution and a ratio of < 1 is clustered, the nearer to 0 the more clustered the distribution. A ratio > 1 is a regular distribution. In order to reject the null hypothesis that there is no pattern to pipe distribution (pipes are randomly distributed), the Z score is calculated. The Z score (*Z*) is a test of statistical significance which evaluates for a normal distribution of the nearest neighbour distances (*Rn*). Very high or a very low Z scores are found in the tails of the normal distribution and this indicates it is very unlikely that the observed pattern is there by chance. Z scores are measures of standard deviation away from the mean.

(2)

$$Z = \frac{\bar{D}(Obs) - 0.5\sqrt{\frac{a}{n}}}{SE}$$

Where

(3)

$$SE = \frac{0.26136}{\sqrt{n^2 / A}}$$

Where SE is the standard error and A is the aerial extent of pipe coverage in the study area (Ebdon, 1985). Z scores are given to all spatial statistics used here.

This equation is tailored to Moran's I and Ripley's K statistic by substituting the Rn component in equation (2) with that of other spatial statistics.

2.3.2 Nearest neighbour distances and exclusion zone

Nearest neighbour distance is the distance (in metres) between a pockmark and its nearest neighbour (*nn*). Exclusion zone is defined as half the nearest neighbour distance (see Chapter 7). The exclusion zone is a fixed, non-overlapping distance (or area) which is unique to each pockmark.

2.3.3 Moran's I

Cluster and outlier analysis (Anselin Local Moran's I) (Anselin, 1995b) uses a set of weighted data points to identify those clusters of points with values similar in magnitude and those clusters of points with very heterogeneous values. It is used in Chapter 5 to measure the spatial autocorrelation of both pipe locations and age (TP1) values simultaneously. Moran's I emphasizes how individual pipe TP1 values differ from the values in the study area as a whole by comparing the TP1 value of each pipe in a pair to the mean TP1 value for all pipes in the study area i.e. the statistic concentrates on local variation.

Moran's I (*Ii*) calculates the mean TP1 value for the data points and calculates the difference from the mean for each neighbour and multiples it by the weight (*wij*) for that neighbour. Then the product is summed, and the sum is multiplied by the ratio of the difference from the mean for the original data points, divided by the variance (Mitchell, 2005).

(4)

$$Ii = \frac{n\sum_i\sum_j w_{ij}\left(x_i - \bar{x}\right)\left(x_j - \bar{x}\right)}{\sum_i\sum_j w_{ij}\sum_i\left(x_i - \bar{x}\right)^2}$$

where n is the number of pipes indexed by i and j; x is the variable of interest or TP1; $\bar{x}$ is the mean of x; and *wij* is a matrix of spatial weights.

A positive value for *Ii* indicates that the pipe is surrounded by pipes with similar TP1 values. Such a pipe is part of a cluster. A negative value for *Ii* indicates that the pipe is surrounded by pipes with dissimilar TP1 values. Such a pipe is an outlier. *Ii* value *Z* scores are calculated (see above) and the null hypothesis that there is no spatial clustering of TP1 values is rejected at the 95% level for all pipes with a *Ii z* score < 2 or > 2.

2.3.4 Ripley's K

Ripley's K (Ripley, 1976, 1977, 1979) is a second order statistic. The K function is similar to the Nearest Neighbour Index, however the K function includes all neighbours occurring within a given distance, rather than the distance to each point's single nearest neighbour. Ripley's K formula is given by

(5)

$$K(d) = \frac{A}{n^2} \sum_{i \neq} \sum_{j} I_{ij} d_{ij}$$

The value of the *K* statistic at distance *d* (*K(d)*) is the measured distance (*d*) between points (*i, j*), the weight for the pair (I_{ij}), the area (*A*) and the number of points (*n*).

The weight (*I*) is either 1, if the neighbouring point is within the distance of the target point or 0 if it is not.

The K value is transformed using a variation of the K function (*L(d)*) to reduce the size of the K value as distance increases (Mitchell, 2005). The transformation is given by

(6)

$$L(d) = \sqrt{\frac{A \sum_{i \neq} \sum_{j} I_{ij} d_{ij}}{\pi n(n-1)}}$$

The *L(d)* method states that the expected value for any distance, given a random distribution of points, is the distance (*d*) itself (Mitchell, 2005). At any given distance, if the observed *L(d)* values are above that for the expected values, the distribution is more clustered than expected for a random distribution. Lower and upper confidence envelopes for a random distribution are generated to indicate a statistically significant clustered pattern at any given distance.

2.3.5 Voronoi polygons

Voronoi tessellations proportionally divide a point distribution into cells or Voronoi polygons (Dirichlet, 1850; Voronoi, 1907; Voronoi, 1908; Okabe et al., 2000). Similar to a honeycomb structure, the area around the pipe/pockmark is divided into polygons which have the unique property that each polygon contains only one

pipe/pockmark, and any location within the polygon is closer to its associated pipe/pockmark than to the pipe/pockmark of any other polygon. Voronoi polygons are used in proximity analysis to determine "spheres of influence" around input data points.

2.3.6 Density

Circular neighbourhoods are defined around each pockmark, and the number of pockmarks that fall within the neighbourhood is totalled and divided by the area of the neighbourhood (Mitchell, 2005). Neighbourhood areas were 1 km^2 for the Plateau and Rosetta Region and 500 m^2 for the pockmark field respectively (refer to Chapters 6 and 7). Utilising a 1 km^2 neighbourhood provides a more generalised density calculation than those resulting from smaller neighbourhoods.

2.3.7 Minimal Spanning Tree (MST)

The Minimal Spanning Tree (MST) is a unique network of straight lines joining a set of points, such that the total length of all the lines (edges) in the network is minimised and there are no closed loops (Gower and Ross, 1969). Starting at any point, an edge is created joining that point to its nearest neighbour. The tree is then extended by always constructing the shortest link between one of its nodes and an unconnected point, until all the points have been connected (refer to Chapter 7 and Appendix A7 for more information).

The mean edge length ($\bar{m}$) of the MST is used as a measure of close range clustering within an array of data points (Cartwright and Whitworth, 2004). Short values ($\bar{m}$) indicate clustering, whilst maximum values ($\bar{m}$) and the smallest variance $\sigma(m)$ indicate a perfect lattice (Dussert et al., 1986; Dussert et al., 1987). The advantage of MST statistics is that it completely describes the layout and space-filling

characteristics of the points and is powerful in bringing out patterns which cannot be revealed by a simple visual examination (Dussert et al., 1988; Dussert et al., 1989). Minimal Spanning Tree requires no compensation for edge effects because the analysed data is compared with random datasets occupying the same spatial domain.

2.3.8 Self Organised Criticality (SOC)

Self Organised Criticality (SOC) is considered to be a universal theory of complex behaviour (Ball, 2004). First described by Bak et al. (1987) the concept was illustrated by describing the evolution of a Sand Pile Model whereby the maintenance of a sand pile with critical slope is a scale-free power-law distribution of avalanche size. The theory states that a spatially distributed system gradually accumulates energy which is suddenly released at a particular location when a critical state is reached. The extent of the local energy release is variable and highly non-linear, i.e. it depends on the spatial interconnectedness of events (pockmarks, as applied in Chapter 7), the surrounding topography (surface and subsurface) and rate of energy dissipation with space and time. The defining characteristic of a system exhibiting SOC would be self-similarity in the magnitude of the pockmark events (see Chapter 8 for further discussion).

In this study a simple SOC simulation was used to generate a series of coordinates of avalanche collapses. A plane with 1000 x 1000 incremented cells was triggered to collapse whenever a cell's contents exceeded a threshold value. The collapse emptied not only that cell but also the neighbouring cells which exceeded some lesser critical threshold value. The simulation settled into a self-organising state, and the coordinates of collapses occurring in the middle 100 x 100 zone were recorded.

2.3.9 Hardcore Distribution

The Hardcore, or Diggle model (Diggle, 1983, 2002) produces an anticlustered distribution, with each coordinate pair having a defined exclusion radius of diameter (*d*) within which no other point is permitted. For a given area (*A*) containing *n* points, there is a theoretical maximum value of *d* which corresponds with a perfect grid of points, where $d^2 = A / n$.

Hardcore distribution was created by generating pairs of independent coordinates using random numbers, *Rx* and *Ry*, which were discarded if they were within a distance (*d*) of a previously generated point (Diggle, 2002). The larger the value of *d*, the more regular and lattice-like the distribution of points.

2.3.10 Complete Spatial Randomness (CSR)

Random datasets were created using random number generators to create *n* independent pairs *Rx* and *Ry* of x and y coordinates in the appropriate ranges (including identical spatial extents and number of coordinate pairs). Random datasets were also created using in-built GIS algorithms.

2.4 Potential errors and limitations

All qualitative and quantitative measurements and observations are given based on a full appreciation of the resolution and potential errors of the data. General considerations are given here with specific errors discussed in the relevant chapters.

Within the seismic data acoustic and amplitude anomalies associated with the presence of gas are prevalent, this however is neither surprising nor can be avoided given the context of this research. Phenomenon of relative seismic velocities e.g.

push downs (shallow layer/feature with a low seismic velocity (e.g., gas chimneys, hydrocarbon indicators) surrounded by rock with a higher seismic velocity causes what appears to be a structural low beneath it) are common. It is anticipated that seismic migration will reduce the magnitude of this effect but degrees of pull up / push down will still be present (Brown, 2004). Acoustic distortion or wipeout is common in the presence of gas and will mask the true geometry of a feature. This is an error inherent with the utilisation of P-wave data for pipe analysis (Hustoft et al., 2007). Potential errors associated with 3D seismic imaging of pipes is further discussed in Chapter 4.

All GIS models are subject to a maximum spatial positioning error of half a bin size i.e. Namibia 25 m ±12.5 m and NDSF 3 m ±1.5 m. This is due to the interpolation algorithm used to construct the surfaces. Spatial statistics are highly susceptible to the precision of the coordinates in the point dataset, the sample size and the mathematical boundary area imposed on the spatial analysis. Sample sizes used in this research are considered sufficient for statistical analysis (Mitchell, 2005). The pipe coordinates (Namibia) were collected from coherence, dip and seismic profiles in the seismic interpretation software package. Limitations associated with 3D data resolution have been mentioned above. The centre of each NDSF unit pockmark (x,y,z), described by a 4-way dip structure, was determined at a scale of 1:1,000 using an aspect (°), slope (°), depth (m) and hillshade model within the GIS and subject to the limitations of data resolution as mentioned above. The mathematical boundary area imposed on the spatial analysis was a minimum enclosing rectangle. Where possible, the boundary area was kept constant to permit comparison between statistical results from a single test. Deviation from a constant boundary area, simulation of edge effects and comparison to random populations are discussed separately in the relevant chapters (Chapters 5 and 7).

Chapter 3

3 GEOLOGICAL SETTING

3.1 Introduction

The aims of this chapter are 1) to describe the regional geology and tectonic setting of the Namibian continental margin (Chapters 4 and 5); 2) describe the seismic stratigraphy of the Namib Basin (Chapters 4 and 5); and 3) describe the regional geology and tectonic setting of the Nile Deep Sea Fan (Chapters 6 and 7). STACOR (geotechnical core) information is available in Chapter 7.

3.2 Namibe Basin, Namibia

3.2.1 Regional geology and tectonic setting of the Namibian continental margin

The West African passive continental margin was initiated during the opening of the South Atlantic Ocean during the Early Cretaceous (Rabinowitz and Labrecque, 1979; Austin Jr and Uchupi, 1982; Nürnberg and Müller, 1991; Guiraud and Maurin, 1992; Karner et al., 2003; Goudie, 2005). Initial Gondwanaland break-up along this margin is related to lithospheric extension (Maslanyj et al., 1992) coupled to magmatic weakening and the extrusion of a major flood basalt province (the Parana-Etendeka) (Gladczenko et al., 1998). Progressive northwards propagation of the South Atlantic rift during the Mesozoic created important differences in the timing of rifting (Summerfield, 1991; Maslanyj et al., 1992) and volcanic activity in the areas north and south of the Walvis Ridge.

The gross structure of the Namibian margin comprises an eastern inner half-graben, separated from the shallow basement of the almost unextended coastal zone by a prominent hinge line. The Namibian margin comprises four major depocentres, the Orange, Luderitz, Walvis and Namibe Basins (Fig. 2.4). The gross stratigraphy of the Namibian continental margin is known from c. 10 exploration wells drilled in the last 25 years (Aizawa et al., 2000; Bluck et al., 2007; Cartwright et al., 2008). It consists 3-5 km thick, mainly clastic, post-rift sediments overlying a rifted continental basement (Aizawa et al., 2000). In conjunction with previous authors (Light et al., 1992; Maslanyj et al., 1992; Light et al., 1993; Bagguley and Prosser, 1999; Aizawa et al., 2000) the seismic sequence stratigraphy interpretation described and interpreted here broadly correlates with the mega sequences described by Light et al (1993).

3.3 Seismic sequence stratigraphy in the Namibe Basin

The stratigraphy of the Namibe Basin is not directly calibrated by deep drilling results, and my understanding is currently based entirely on (1) seismic-stratigraphic interpretation (Light et al., 1993; Clemson et al., 1997; Hopkins, 2006), (2) long-range correlations to the Walvis Basin and (3) limited shallow drilling during ODP leg 175 "Benguela Current" site 1080 (Berger et al., 2002). For mapping purposes, I have divided the basin fill into 6 seismic units (Syn-Rift, Transitional/Post Rift, Post-Rift 1, Post-Rift 2 and Post-Rift 3 which has been further subdivided into Post-Rift 3a, b, c and d). The seismic stratigraphy is described with reference to a representative seismic profile across the basin (Fig. 3.1).

The deepest part of the basin is characterized by rotated and eroded fault blocks with probable terrestrial sediments infilling the half-graben. By analogy with the equivalent rift sequences further south, these half-graben fills may include gas-prone source rock intervals. The syn-rift sequence seen throughout the study area is likely to consist of Late Jurassic to Early Cretaceous siliclastic and volcanic rocks

(Clemson et al., 1997; Clemson et al., 1999; Aizawa et al., 2000). Reflections are transparent to low amplitude, broken, discontinuous, non parallel and chaotic in places, consistent with the likely mixed terrestrial depositional system that is inferred here (Fig. 3.1).

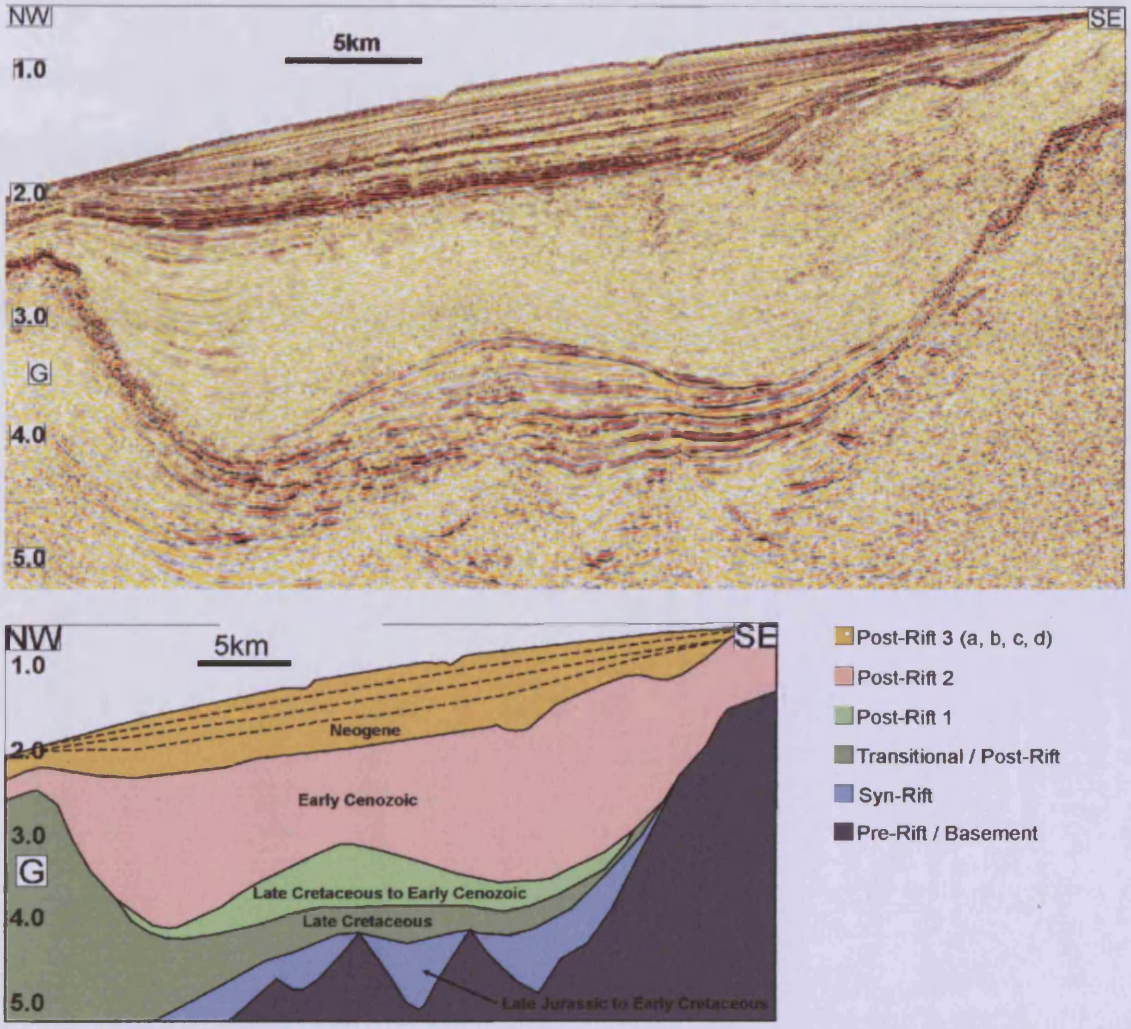

Figure 3.1 Seismic stratigraphy of the study area is divided into 6 units after Light et al. (1993). The Syn-Rift is likely to consist of Late Jurassic to Early Cretaceous siliclastic and volcanic sediments. Transitional/Post Rift is likely to consist of volcaniclastic material of probable Late Cretaceous age, possibly associated with the guyot (G) and the formation of the Walvis Ridge. Possible hydrocarbon indicators have been interpreted in this unit and deeper. Post Rift 1 is a lensoid body likely to consist of mixed claystone and biogenic components of probable Late Cretaceous to Early Cenozoic age. Post Rift 2 has a drape geometry and is likely to consist of Early Cenozic claystone with coarser facies in the channelized units and overbank deposits. Post Rift 3 is likely to consist of fine grained material of probable Neogene in age with the base being of Miocene age. Polygonal faults and pipes dominate this unit. Seismic scale is in seconds TWT.

The transitional sequence is probably of Late Cretaceous age. It is likely that this sequence includes a significant fraction of volcaniclastic material, and this may explain the high amplitudes and discontinuous seismic facies in the western part of the basin, closer to the origin of known volcanic complexes (Clemson et al., 1997) (Fig. 3.1).

The remainder of the stratigraphy is divided into three main seismic stratigraphic units, Post Rift 1-3. This succession was deposited during a major relative sea level rise due to thermal subsidence (Light et al., 1993). Post Rift 1 is probably of Late Cretaceous to Early Cenozoic age. It comprises a lensoid sedimentary body whose maximum thickness of c. 600 m is developed along the basin axis. The body appears to exhibit the internal and external geometry of a large constructional body, with a convex upwards top, and a concordant base. The margins of the body are marked by depositional thinning, onlap, and some erosional truncation. It is interpreted as a large sediment drift (Hopkins, 2006). The internal reflections exhibit high lateral continuity, high to moderate amplitude and probably consist of mixed claystone and biogenic components (Fig. 3.1).

Post Rift 2 is probably largely Early Cenozoic in age. It varies in thickness from c. 500 m in the upper slope region to over 2000 m thick in the base of slope position. This unit is largely developed in a drape geometry with concordant relationships to Post-Rift 1 and a more irregular complex stratification to Post-Rift 3 where numerous channels have developed in the upper part of the slope. The reflection amplitude is very low in the base of the sequence, but towards the upper third, becomes more variable, especially in the channelized part of the interval. The dominant lithofacies is expected to be claystone, but with coarser facies in the channelized units and respective overbank deposits.

Post Rift 3 is composed entirely of laterally continuous stratal reflections, with medium to high amplitude that are correlatable throughout the study area (this is highly significant for the methodology outlined in Chapter 5). The sequence has a maximum thickness of c. 800 m in the basin axis, and thins upslope and downslope, by a combination of onlap (upslope) and stratal condensation (downslope). The sequence pinches out almost entirely by the shelf break, and the shelf is a condensed

interval suggesting an efficient bypass was occurring throughout this period. The sequence is likely to be Neogene in age, with the base being of Miocene age. Polygonal faults are widely developed in the lower part of this interval, suggesting that a large part of this sequence is very fine grained (Cartwright and Dewhurst, 1998). The pipes transect all or part of this sequence, with the larger pipes extending down into post Rift 2 (Fig. 3.1). There is no evidence of major channelling in these slope sediments, and the depositional system seems to be dominantly one of a passive slope drape, under probable strong bottom current influences.

A prominent bottom simulating reflection (BSR) is developed within the sediments of Post Rift 3 on the southern edge of the dataset (Fig. 2.4). The presence of the BSR marks the location of the base of the gas hydrate stability field (BGHSZ) (Mienert and Posewang, 1999; Riedel et al., 2006). This indicates that adequate concentrations of gas exist at the base of the gas hydrate stability zone to saturate the pore water within the underlying sediments with methane and suggest that conditions suitable for the occurrence of gas hydrate exist in the sediments overlying the BSR (Paull et al., 2008). Numerous laterally extensive amplitude anomalies are seen within the highly reflective units of Post Rift 3, and these coincide at their upper limits with the BSR, supporting the notion that they result from free gas trapped beneath the hydrate layer. A few smaller, isolated zones of less prominent BSR are observed in the centre-west of the study area.

The occurrence of seismically detectable BSR covers more than 1500 km^2 and extends beyond the limits of the study area (Swart, 2009). The BSR is observable in isolated regions and shows a reverse polarity to that of the sea floor. Numerous lensoid high amplitude bodies are evident at various depths throughout Post-Rift 3, these may represent palaeo-BSRs but this assertion must remain highly speculative. The thickness of the transparent blanking layer above the BSR is typically 250-350 ms TWT, placing the BSR within the theoretical depth of the base of the gas hydrate stability field, c. 300-800 m (given typical temperatures and pressures) (Pecher et al., 2001). A clear indication of the volume of hydrate is difficult to determine at present (Swart, 2009). Seabed sampling of the Namibe Basin was undertaken by TDI-Brooks on behalf of NAMCOR in 2004. No sampling of hydrates was planned but hydrate was recovered from the bottom of a 5m drop core

in the study area (Swart, 2009). No age data for the sediments are available. Heat flow measured in the basin was in the range 43.0 - 45.9 m W/m^2 and sea bottom temperature varied from 4.4 - 4.6 °C (Swart, 2009). Sampling undertaken during a previous ODP Leg (Leg 175) at sites north and south of the Namibe Basin showed no evidence of hydrates (Berger et al., 2002; Swart, 2009).

Post Rift 3 may have been calibrated to some extent by site 1080 of ODP leg 175, located some 100 km northwest of the Namibian study site (Berger et al., 2002). Berger et al (2002) reported that continuity of core recovery was affected by the strong development of gas pressure from abundant methane and carbon dioxide within the sediments which produced sediment expansion, created voids and cracks and retarded sediment compaction. Problems encountered at the Namibe Basin site 1080 resulted in only 52 m of core recovery. The core contained clay to silty clay which equates to 1.25 Myr (water depth 2777 m) but because of the stratigraphic problems age models for site 1080 were not considered (Berger et al., 2002), and detailed calibration with the study area is not possible. Average sedimentation rates of the biogenic claystones found in the Pleistocene in ODP leg 175, site 1080 are c. 40 m/Ma (Berger et al 2002).

3.3.1 Nile Deep Sea Fan, Mediterranean Sea

3.3.2 Regional geology and tectonic setting of the NDSF

The Nile Deep Sea Fan (NDSF) is a large (c. 100,000 km^2) sedimentary wedge constructed since the Late Miocene largely by terrigenous sediment delivered by the Nile River (Salem, 1976). The NDSF extends northward to the Mediterranean Ridge and northeastward to the Eratosthenes Seamount (Ross and Uchupi, 1977; Ryan, 1978) (Fig. 3.2). The NDSF lies in a multifaceted geodynamic setting characterised by a complex pattern of active thick skinned crustal tectonics resulting from various plate and microplate interactions (McKenzie, 1970; Courtillot et al., 1987; Le Pichon et al., 1995; Mascle et al., 2000; McClusky et al., 2000).

The Egyptian margin, commonly considered as a passive margin, has been subject to a complex structural evolution. In the distal regions of the margin, it was influenced by the subduction / collision of Africa beneath Aegea–Anatolia along the eastern Hellenic and Cyprus arcs (Ducassou et al., 2007). To the East and North-East, the active transcurrent motion of the Arabian plate relative to Africa led to significant basement faulting (Le Pichon et al., 1995; McClusky et al., 2000) and similarly to the South-East the margin was deformed by the very slow, almost aborted, rifting within the Suez Rift area (Mascle et al., 2000; Loncke et al., 2002; Loncke and Mascle, 2004) (Fig. 3.2). Significant alignments of earthquake epicentres are associated with the plate boundaries and rifts (McKenzie, 1970; El-Sayed et al., 1994; Elenean et al., 2010). Two major fault trends characterize the offshore Nile, the Temsah trend which runs NW–SE, and the Rosetta trend running NE–SW to ENE–WSW (Abdel Aal et al., 2001).

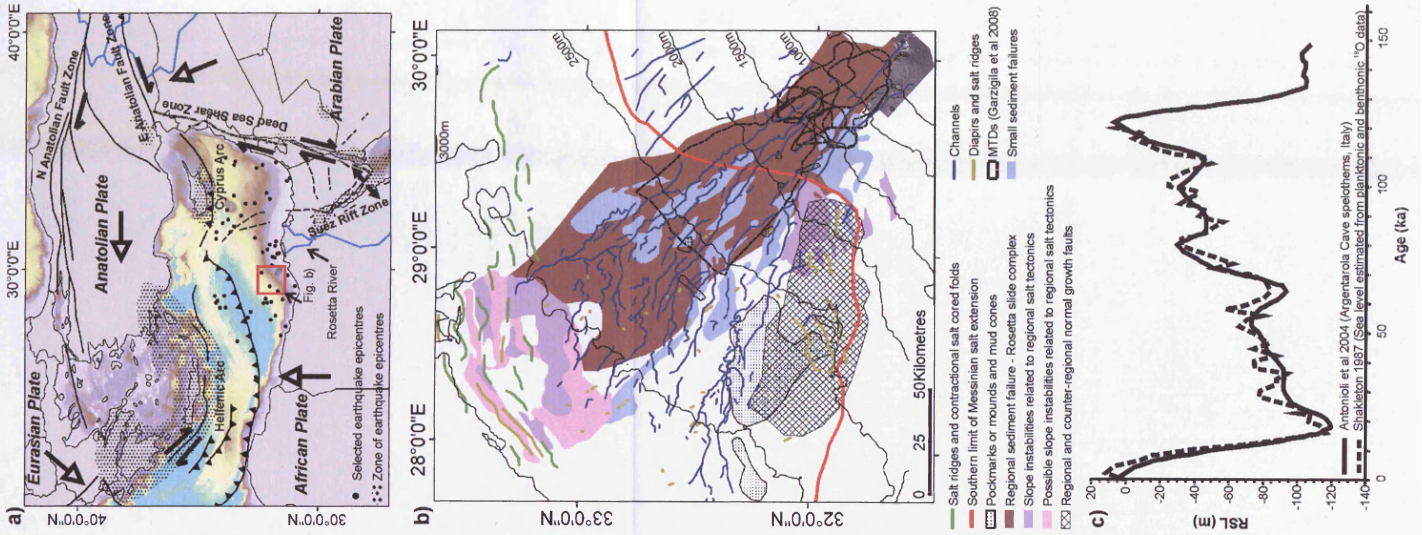

Figure 3.2 Regional geological setting. A) Tectonic framework of the Eastern Mediterranean (adapted from (McKenzie, 1970; Mascle et al., 2000; Loncke et al., 2006; Elenean et al., 2010)). Earthquake zones and selected offshore epicentres close to the NDSF are >3 magnitude earthquakes. B) Regional geology of the Western NDSF (adapted from (Loncke et al., 2006; Garziglia et al., 2008; Loncke et al., 2009)). C) Eustatic sea level change. Relative sea level change (m) since the Pleistocene (adapted from (Shackleton, 1987; Antonioli et al., 2004)).

The Mediterranean Sea was initiated by the opening of the Tethys Ocean in the Early / Late Triassic (Morelli, 1978; Hirsch et al., 1995). The progressive closure of the Tethys Ocean caused by the convergence of the African and Eurasian plates isolated the Mediterranean Sea from the Atlantic Ocean in the Late Miocene. Isolation of the Mediterranean Sea caused a drastic decrease in sea level resulting in major evaporation, the deposition of evaporites in the deeper basins (Messinian Salinity Crisis) and large-scale canyon incision (Ryan, 1978).

Sea level rise and subsequent fall in the Plio-Pleistocene (Fig. 3.2) permitted progradation of the modern Nile Delta (Dupré et al., 2007). The total sedimentary thickness of the Egyptian margin is believed to exceed 9–10 km (Abdel Aal et al., 2001). Overburden thicknesses in the Plio-Pleistocene are in excess of 3 km in many regions and rapid deposition of clay-dominated sequences provided ideal conditions for the development of significant overpressures in the more deeply buried sediments as evidenced by considerable sediment remobilisation (Frey-Martínez et al., 2006).

In addition to thick skinned crustal-scale tectonics, the NDSF is further modified by thin-skinned, gravity-driven deformation of Messinian evaporites and overlying sediments (Gaullier et al., 2000; Loncke et al., 2006; Cartwright and Jackson, 2008). Thin skinned syn-sedimentary deformation relating to salt tectonics and downslope gravity spreading or gliding of the evaporites and sedimentary overburden strongly affects the middle and lower Nile fan, especially in the western and eastern provinces where mass transport complexes (MTC), growth faults, salt diapirs and crestal grabens are common (Dupré et al., 2007; Garziglia et al., 2008; Loncke et al., 2009). Gravity spreading of the salt/overlying sediments "system" has induced proximal thin-skinned extension along the shelf and upper slope, and distal contraction along, and at the base, of the continental slope (Morley and Guerin, 1996). As a consequence, most of the NDSF Plio-Quaternary sedimentary cover is strongly tectonized and is thus particularly susceptible to fluid migration to the seafloor (Dimitrov, 2002). In contrast, the Messinian evaporites are almost absent in the upper slope where post-salt sediments can be up to 2-3 km thick (Loncke et al., 2002; Loncke and Mascle, 2004; Dupré et al., 2007). Pliocene to present day post-salt sedimentary deposition on the deep-sea fan is concentrated on the continental slope

rather than shelf edge due to the extended location of the Nile mouth during this period (Loncke et al., 2002).

The River Nile bifurcates into two main tributaries, the Rosetta and Damietta Rivers (Western and Eastern tributaries respectively), as it transects its arcuate delta (Fig 3.2). The offshore extension of the Rosetta River, the Rosetta Canyon and the Rosetta Channel, lies in a region of interrelated channel and slope processes. The study area for this research is located in and around the Rosetta Canyon/Channel, a prominent sediment delivery pathway to the lower fan (Loncke et al., 2002; Loncke and Mascle, 2004; Loncke et al., 2009). This feature consists of a deep canyon in the upper slope and a prominent modern channel-levee system in the lower slope. The channel-levee system has migrated, avulsed and been abandoned throughout its history. Multiple stacked abandoned buried channel and channel levee complexes can be identified from regional seismic data (Samuel et al., 2003) (Fig. 3.2). Palaeochannels and levees can provide either a fluid source or fluid focusing route for biogenic gas (Gay et al., 2003) or provide sedimentary traps or secondary migration routes for migrating hydrocarbons (Samuel et al., 2003).

Multiple tiers of buried mass transport deposits (MTDs) occur at various stratigraphic levels and at various depths within the Holocene-Pleistocene within the Rosetta region (Garziglia et al., 2008) (Fig. 3.2). Referring to the immediate area (~100 km^2) surrounding the Rosetta Channel, the Rosetta Slide Complex (Loncke et al., 2009) is composed of 10 episodes of sliding. The first period of instability (incorporating at least 4 sliding events) is probably partly responsible for a >30 km long, ~500 m high head scarp and sidewall, delimiting the Rosetta Slide Complex (Loncke et al., 2009) (Fig. 2.5). The mass wasting events produced a residual asymmetrical topography which is deeper towards the east of the complex. This topography controlled the location of turbidite depocentres and superimposed channel-levee systems (Loncke et al., 2009).

Widespread slope instability in this region may be related to changes in sediment supply, sea level change, earthquakes or the circulation of gas rich fluids within subsurface sediments (Loncke and Mascle, 2004; Garziglia et al., 2008; Loncke et al., 2009). Mass transport deposits (MTDs) have the potential to retard or promote

fluid flow (Bünz et al., 2005; Paull et al., 2008). It is possible that MTDs in this region may act as barriers to vertical fluid flow, may promote localised lateral up dip fluid migration or promote fluid expulsion due to the generation of overpressures through rapid loading or unloading (Garziglia et al., 2008; Loncke et al., 2009).

Information on the stratigraphic framework of the NDSF is restricted to descriptions of a limited number of sparsely distributed piston cores. These cores are not close, >20 km (Garziglia et al., 2008), to the area under investigation in Chapters 6 and 7. Sediment supply during the Holocene mainly consists of two fractions, a coarser fraction of turbiditic sands on the lower slope, and a finer fraction composed of hemipelagic clays on the upper slope (Maldonado and Stanley, 1976, 1979). Sedimentation rates in the Late Pleistocene to Holocene are high on the western NDSF with average rates of 32 cm/1000 yr for the last 58,000 years and 280 cm/1000 yr in distal lobes of the Rosetta sub-aerial fan during the Pleistocene (Maldonado and Stanley, 1979; Ducassou et al., 2007; Loncke et al., 2009) where the highest proportions of turbidites occur. The Central NDSF is not influenced by highly effective sediment by-pass systems (channels) and average sedimentation rates are in the order of 2–4 cm/1000 yr for Late Pleistocene to Holocene times (Loncke et al., 2009). This may more closely resemble the hemiplegic sedimentation in the Rosetta Region. Sapropels and carbonate sediments are also common (Maldonado and Stanley, 1979; Ducassou et al., 2007; Loncke et al., 2009).

The NDSF is widely known as an important petroleum province. Thermogenic hydrocarbon accumulations have generally been discovered in 1) Pliocene-Pleistocene deepwater channel and basin-floor turbidite sands; 2) Upper Miocene fluvial and/or turbidite sands; and 3) pre-salt distal turbidities (Abdel Aal et al., 2001; Samuel et al., 2003).

Chapter 4

This chapter has been published as Moss, J.L., and Cartwright, J., 2010, 3D seismic expression of km-scale fluid escape pipes from offshore Namibia: Basin Research, v. 22, p. 481-501.

The work presented in this chapter is that of the lead author (JLM), editorial support was provided by the project supervisor (JAC) in accordance with a normal thesis chapter.

4 3D SEISMIC EXPRESSION OF KM-SCALE FLUID ESCAPE PIPES FROM OFFSHORE NAMIBIA

4.1 Abstract

This chapter documents a large number of large km-scale fluid escape pipes with complex seismic expression and a diatreme-like geometry from the mapping of a 3D survey, offshore Namibia. These pipes are crudely cylindrical, but occasionally have steep conical geometry either narrowing upwards or downwards. They are generally ovoid in planform and their ellipticity varies with pipe height. Vertical dimensions range from c.100 to > 1000 m and diameters range between 50 m and 600 m. The lower part of the typical pipe is characterised by a sag-like or collapse type of structure, but this is only imaged well in the wider pipes. The upper part of the typical pipe is characterised by gently concave upwards reflections, with a negative relief of tens of metres. There is some evidence that these concave upwards reflections are vertically stacked palaeo-pockmarks. A conceptual model for pipe formation is proposed that involves hydraulic fracturing and localisation of focused vertical fluid escape with volume loss at the base of the pipe inducing collapse within the pipe. Continuing episodic fluid migration through the pipe produces further collapsing of the core of the pipe and pockmark structures at the top of the pipe. Longer term seepage through pipes is manifested in zones of amplification of reflections above the top of the pipe.

4.2 Introduction

One of the least understood aspects of fluid flow in sedimentary basins is the precise nature of the flow across thick sequences of low permeability claystones, and the degree to which this flow is pervasive through the pore network, or more focused through faults or other features of enhanced vertical to sub-vertical permeability. This question has important implications for petroleum exploration and more generally for basin analysis (Downey, 1984; Watts, 1987; Cartwright et al., 2007). In particular, the evaluation of secondary migration pathways is a critical element in hydrocarbon play analysis, and recognition of features that promote vertical hydrocarbon migration is an important component of this type of analysis. Equally, prediction of the integrity of petroleum seals should ideally incorporate an appraisal of seal bypass systems, a group of features that are embedded in the sealing sequence and offer preferential flow pathways for hydrocarbons through the seal (Cartwright et al., 2007).

One of the main families of seal bypass system as defined by Cartwright et al. (2007) is pipes. A number of recent studies have documented different types of pipe-like structure from a diverse range of geological settings. The first detailed description of fluid expulsion pipes was by Løseth et al. (2001) who termed them blowout pipes, based on their mapping of these columnar disturbance zones from depths of c. 1000 m to the seabed, where they terminated in pockmark craters (King and MacLean, 1970; Hovland and Judd, 1988; Judd and Hovland, 2007). This pioneering study was followed by investigations using high-resolution (single-channel and multichannel) 3D seismic data from offshore Norway (Mienert et al., 1998; Bouriak et al., 2000; Berndt et al., 2003; Hovland et al., 2005; Hustoft et al., 2007; Paull et al., 2008; Westbrook et al., 2008b), the North Sea Basin (Løseth et al., 2003; Ligtenberg, 2005), offshore Ireland (Van Rensbergen et al., 2007), offshore West Africa (Gay et al., 2007a; Gay et al., 2007b), offshore Korea and using 2D seismic data from the Mediterranean region (Loncke and Mascle, 2004; Trincardi et al., 2004). The pipes in these studies have been referred to as gas chimneys, seismic chimneys, acoustic pipe structures or blowout pipes, but all share a common basic

seismic expression albeit with considerable variation of specific acoustic characteristics.

In seismic profiles, pipes appear as vertical to subvertical zones of highly discontinuous or disturbed reflections, or even as zones of complete loss of coherence (Fig. 4.1). In planform, pipes range from circular to elliptical, with variable geometry upwards over the full vertical extent of the pipe (Løseth et al., 2001; Hustoft et al., 2007). The reflection amplitudes within the pipe are generally highly variable, with localised amplitude anomalies distributed within or immediately adjacent to the pipe, in some cases high amplitudes due to gas pockets or cemented zones are inferred (Gay et al., 2007a; Hustoft et al., 2007). Where reflections are more coherent surrounding the pipe, they are often seen to either bend sharply upwards around the pipe perimeter towards the centre of the pipe, or to bend downwards into the pipe (Berndt et al., 2003; Hustoft et al., 2007). All these acoustic characteristics are considerably influenced by the survey parameters and specifics of the processing sequence (Løseth et al., 2003). Seismic artefacts (velocity anomalies, attenuation, transmission, and scattering) and the complexity of imaging the margins of a near vertical geological feature whose width of often not much greater than the spatial resolution combine to make the interpretation of true structure extremely difficult.

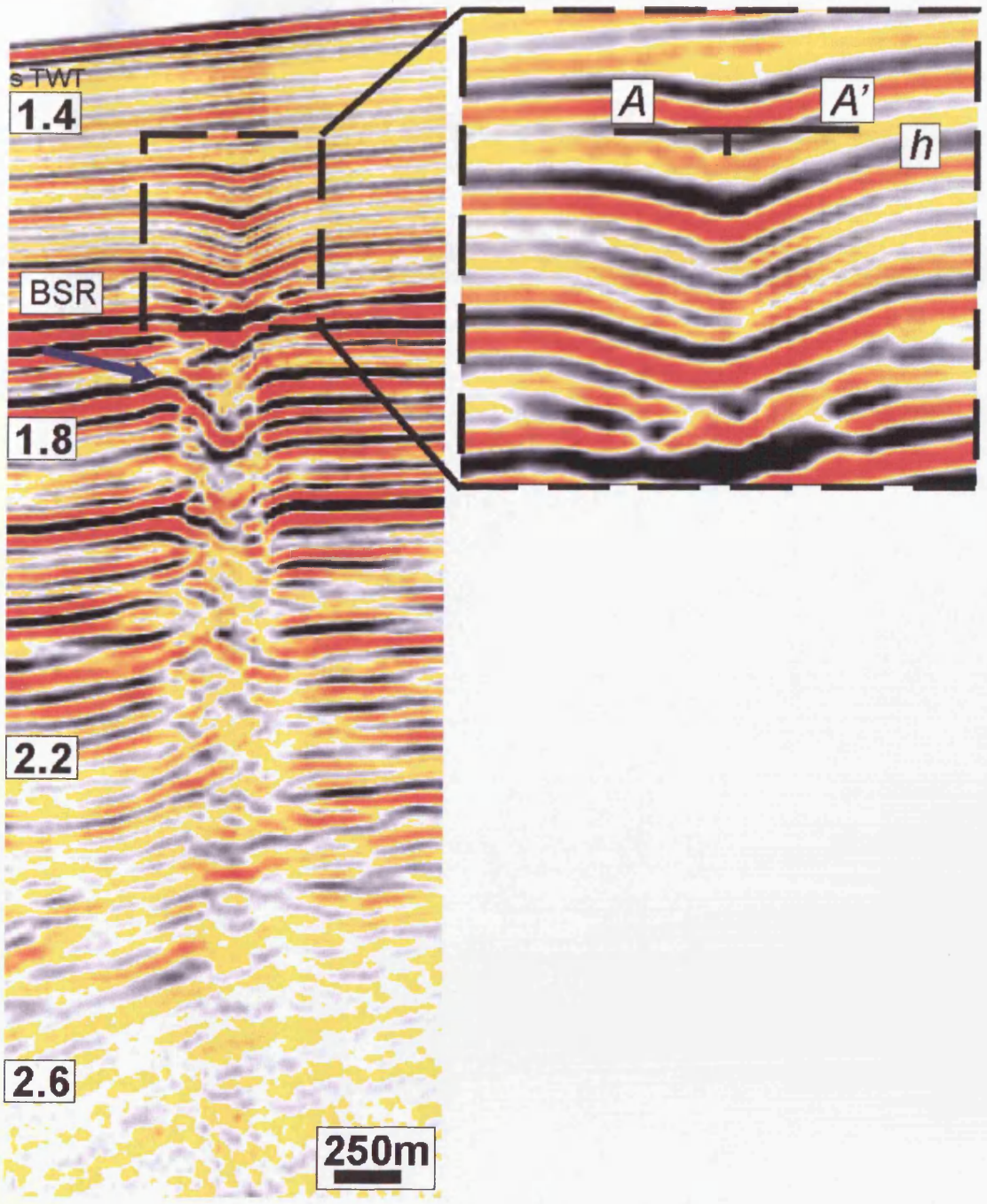

Figure 4.1 Seismic profile through pipe 24. Pipes appear as vertical to subvertical zones of highly discontinuous or disturbed reflections, or even as zones of complete loss of coherence. The observed stratal thickening (blue arrow) on the flanks of the pipe is believe to represent the levee-like deposition of fluidized material from the base of the pipe. Pipe measurements include height and diameter and reflections width (A-A') and relief (h). Pipe 24 passes through the Bottom Simulating Reflection (BSR). Seismic scale is in seconds TWT.

I present a study of pipes from the West African continental margin. The study area is located in the Namibe Basin of northern Namibia, and is based on a 3D seismic survey located in the basin axis, in a modern slope setting. There are two prime advantages to this study area: (1) the data is high quality with very good spatial resolution of < 25 m, and (2) there are a large number (366) of seismically resolved pipes within the region covered by 3D seismic data. The large number of pipes means that I can investigate the range in acoustic expression in a single geological province where the basic stratigraphy and hydrodynamic boundary conditions are unlikely to vary laterally to any significant degree.

This chapter has two aims: (1) to extend the descriptive base for pipe structures by capturing the variability in acoustic expression of the pipes in this area and so aid their future interpretation elsewhere, and (2) propose a model for their genesis. This study is largely based on qualitative or semi-quantitative description of pipe geometry with a main focus on interpreting the internal and external structure of the pipes. Chapter 5 will deal more specifically with the spatial and temporal analysis of the pipe distribution, and relate the statistics of their distribution to their genesis. Hence in this chapter, I do not address the question of the diachroneity of pipe formation, nor attempt to explain in any detail why pipes and pipe clusters are located in specific positions in the basin. However, I do make some simple observations on the specific context in which some pipes are formed and relate this to their genesis.

4.3 Seismic Data and Methods

The data volume used for this chapter consists of a ~900 km^2 grid of pre-stack time migrated 3D seismic data from North Namibia acquired on behalf of NAMCOR in 2002 (Fig. 2.4). Pipe analysis focused on the geometric attributes of the constituent reflections, their seismic character, shape, reflection thickness and amplitude using methods outlined in Chapter 2.

The quantitative analysis of the upper portions of the pipe structures undertaken in this chapter expands on measurements that have previously been employed with seismically resolvable sag structures (Bertoni and Cartwright, 2005; McDonnell et al., 2007) or for the measurement of growth fault slip histories (Thorsen, 1963).

4.4 Results

4.4.1 Regional distribution and geometry of the pipes in the Namibe Basin

Qualitative and semi-quantitative analysis was undertaken on a large population of pipes from the study area within the Namibe Basin. The 3D seismic cube covers an area of ~900 km^2, and contains over 366 buried pipes at an average density of 2 pipes per km^2. Densities range from 1 pipe per km^2 to a maximum density of 7 pipes per km^2 in the south. The largest pipes (height > 800 m and diameter > 200 m) are in the south of the study area with smaller pipes located towards the centre and north of the study area (Fig. 4.2).

The pipes are stratigraphically restricted to Post-Rift 2 and 3. The precise depth range for many of the pipes is one of the most challenging parts of their interpretation, and is discussed in more detail in later sections. However, many of the pipes in the southern part of the study area can be traced at least as deep as the channelized interval in Post Rift 2 (Fig 4.3). They terminate upwards at various levels within Post Rift 3. Again, this interpretation is problematic, because there is considerable variation in the geometry of the uppermost parts of pipes.

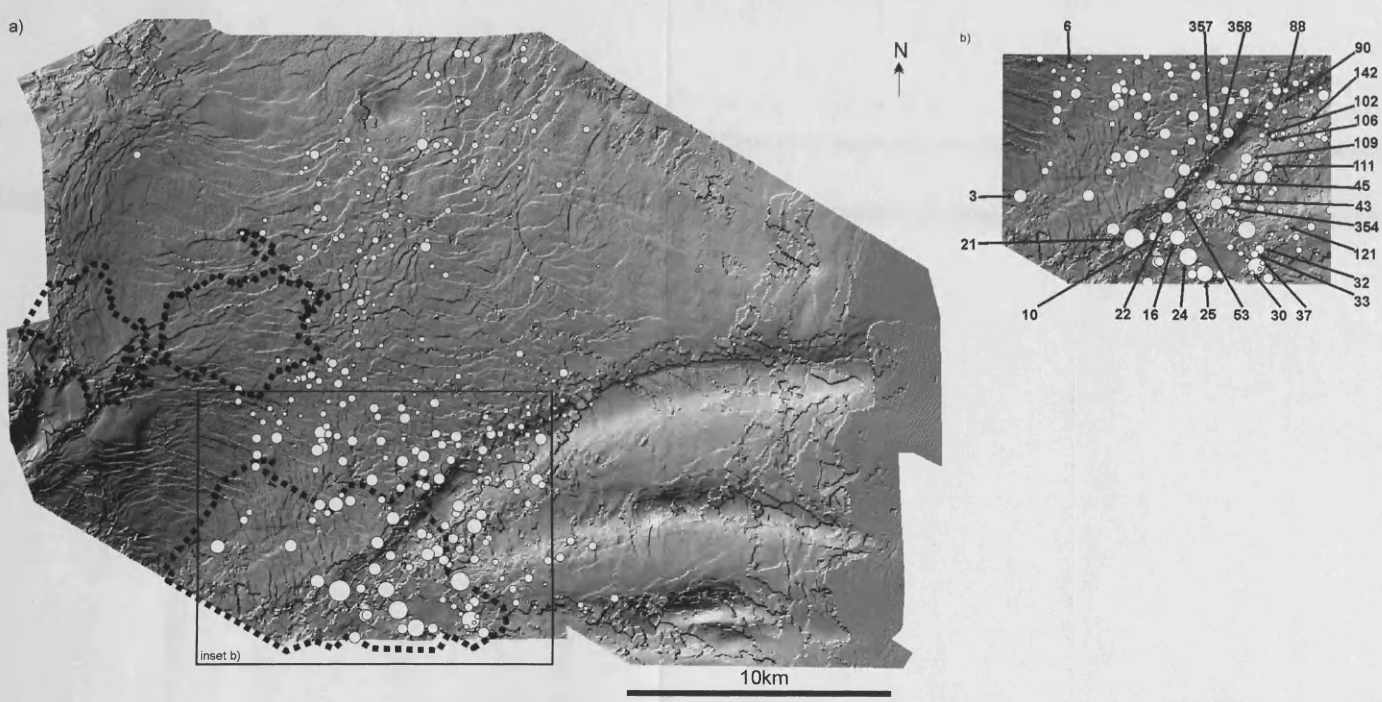

Figure 4.2 Pipe distribution. a) Dip map of the base of Post Rift 3 showing the location of the palaeo channels, polygonal faults, BSRs (black dashed outline) and pipes (white circles). The size of the pipe symbol is directly proportional to the maximum diameter of the pipe. The map is to scale. b) Inset map showing the location of the pipe examples referred to in the text (Chapter 4 only).

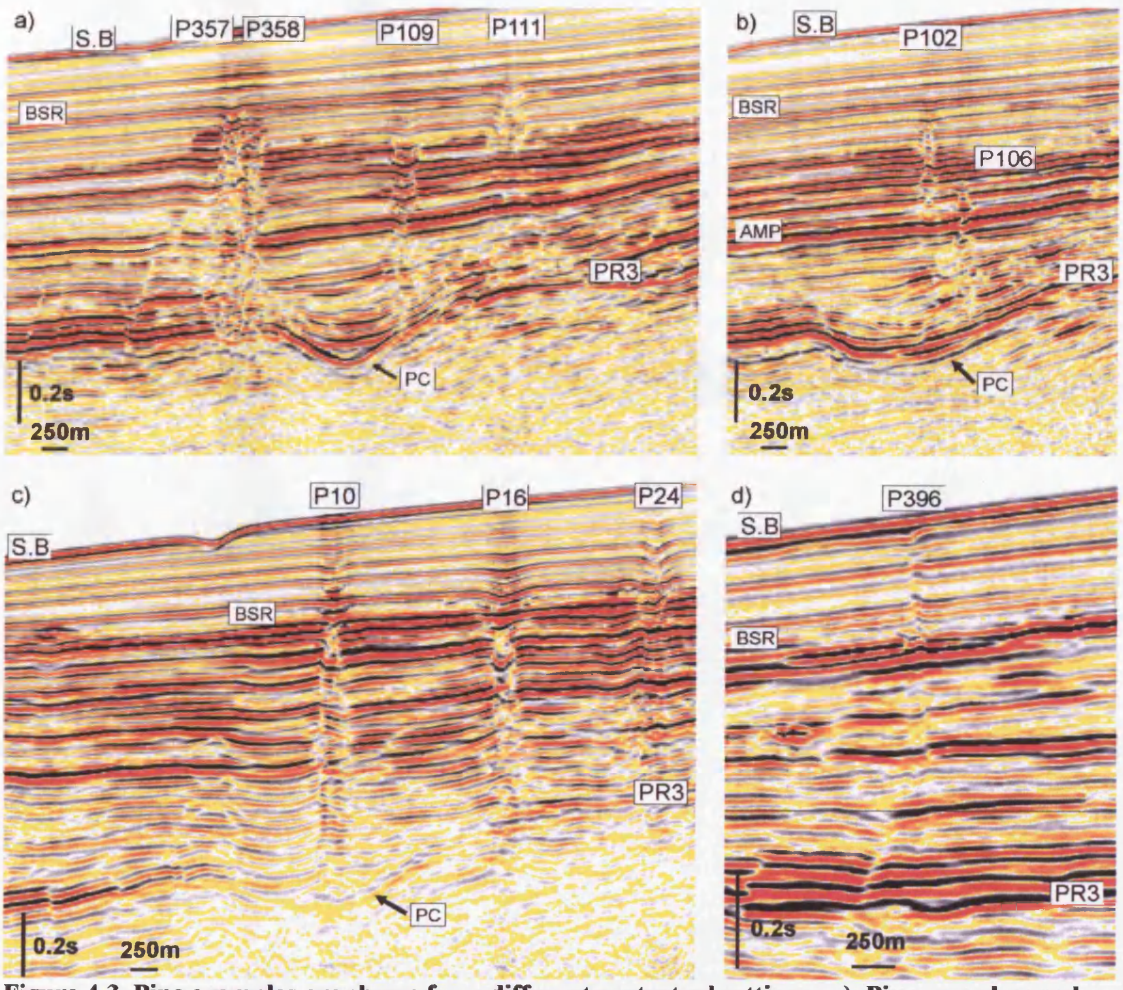

Figure 4.3 Pipe examples are shown from different contextual settings. a) Pipes are observed to emanate from palaeo channel levees at the base of Post Rift 3 (PR3), for example Pipe 109, Pipe 357 and Pipe 358. b) A narrow pipe (Pipe 106) is feeding a high amplitude body trapped beneath the modern BSR from a probable palaeo channel (PC) source. Narrow pipe (Pipe 102) is sourced from the base of the high amplitude body (AMP), terminating at the lateral edge of the seismically determinable modern BSR. c) Pipes have been observed to extend vertically through channel beds without interacting with the bed or rising up dip on levees, for example Pipe 10. This suggests that the pipes may be sourced deeper than Post Rift 3 (PR3). Pipe 10, pipe 16 and pipe 24 are examples of pipes which transect the BSR. d) Narrow pipe 396 is sourced from the modern BSR. Acoustic anomalies (push down) are observed beneath the pipe. The modern BSR is indicated (BSR). Seismic scale is in seconds TWT.

The 366 pipes are distributed in a clustered and uneven pattern in the basin. They occur in a broad north-south zone in the basin axis (Fig. 4.2). They are spatially coincident with buried channels in the south and a more axial region of polygonal faulting within Post Rift 3. On a gross scale, the pipes are distributed in a horseshoe pattern. This pattern correlates with the flanking depressions to the large lensoid mound body defining the Post Rift 1 sequence (Fig. 4.4). The structure map of the top of Post Rift 1 shows the pipe distribution to be anti-correlated with the central mound-like high of this lensoid body. The thickness map of Post Rift 2 and the structural and thickness maps of the Syn-Rift are the only maps that show any spatial correlation of mapped features (thickness or topography) to the distribution of pipes (Fig. 4.4).

There is no obvious relationship between the geometry of the present day seabed and the distribution of the pipes*. A prominent failure scar occurs in a mid slope position, but there is no obvious correlation between this feature and the underlying pipe distribution. Similarly, there are few seabed pockmarks, and these do not uniquely correlate with the position of underlying pipes. The pipes are distributed across a range of present day bathymetry from -600 m to -1800 m. Since there has been relatively limited subsidence in the Neogene along this part of the margin, this bathymetric range probably closely approximates the bathymetry at the time of their formation.

The stratigraphic distribution of the pipes is difficult to determine precisely, mainly because the base of many of the pipes occurs within the very low amplitude seismic facies of Post Rift 2, and the true base is often masked by seismic artefacts or background noise. Of the pipes with a confidently interpreted base (about 40% of the total population), the majority of these emanate from the lower part of Post Rift 3*. Pipe bases are observed to emanate from buried channel levees (Fig. 4.3) and amplitude anomalies beneath the modern BSR in the south of the study area. In these instances it is feasible that the channel levees and gas trapped beneath the BSR supplied the pipes with fluid and/or free phase gas (Bünz et al., 2003; Gay et al., 2003; Hovland et al., 2005; Gay et al., 2006a; Gay et al., 2006b).

* Map presented in Appendix A2

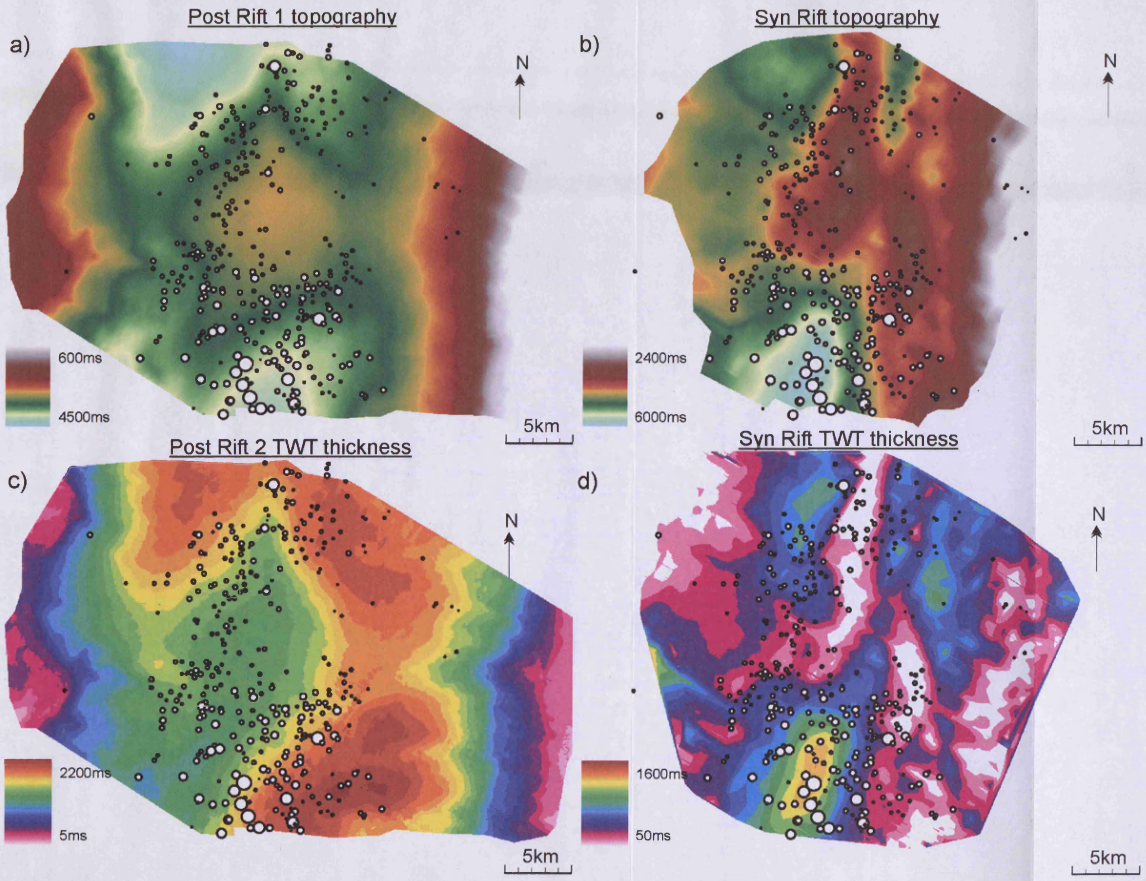

Figure 4.4 Mega unit topography (unit top) and thickness maps. a) Post Rift 1 topography. b) Syn-Rift topography. c) Post Rift 2 (TWT) thickness map. d) Syn-Rift (TWT) thickness map. Pipe distribution is indicated by the white dots. White dots are proportional to maximum pipe diameter (m).

Direct observations of pipes associated with channel levees and sub-BSR amplitude anomalies account for c. 20 % of the total population. For the majority of pipes the deepest recognisable seismically disturbed reflection is either coincident with the Post-Rift 2 / Post-Rift 3 unit boundary or in the upper part of Post-Rift 2. Seismic amplitude and continuity is poor in Post-Rift 2 and tracing pipe structures through this sequence is difficult, limiting interpretation of pipe structure to the uppermost 400 m of this sequence. Observations of pipes that vertically transect channel fill units without any obvious change in their geometry or position may suggest that the pipes are sourced deeper than Post-Rift 3 (Fig. 4.3).

The pipes exhibit a complex relationship with a prominent BSR in the south of the study area. The spatial location of the BSR is coincident with some 59 pipes, among which include some of the largest in the population. Pipes are observed to (1) terminate upwards at the BSR (Fig. 4.3b), (2) originate at their base from the BSR (Fig. 4.3d) and (3) originate beneath and then pass straight upwards through the BSR (Fig. 4.3c). Only the smallest pipes originate at the BSR and only the largest pipes pass straight through the BSR. The smaller isolated 'patches' of a less prominent BSR in the central-west of the study area are devoid of pipes.

4.4.2 Seismic expression

The 366 pipes in the study area represent a broad spectrum of geometrical forms and dimensions, and also occur in a range of stratigraphic intervals. Hence much of the acoustic variation can be related to the background reflectivity of the intervals that the pipes individually transect. All the pipes are recognisable as circular to elliptical columnar zones of disturbed or disrupted reflections (Fig. 4.1). They stand out from the background reflectivity in Post Rift 3, but are less easily observed in the lower amplitude background reflectivity of Post Rift 2. Hence the ease of interpretation depends to some extent on the amplitude characteristics of the host stratigraphy. In general, they are more easily observed and more accurately defined within intervals with higher dominant frequency.

The defining characteristic of all the pipes is the disrupted nature of the seismic reflections. This immediately flags an important if somewhat obvious point: formation of the pipe involves disrupting the sedimentary layering to the extent that the reflections are disrupted. This implies a scale of disruption that is imaged by the seismic wavefront. Disturbed seismic data quality is associated with reduced acoustic velocities and the specific distribution of gas within the sediments (Dangerfield, 1992; Granli et al., 1999; Arntsen et al., 2007). Gas charged zones can cause significant velocity anomalies which can produce distortion in the seismic data that can propagate downward below the pipe. The degree of disruption is important to quantify, but this is very difficult in practice because the disruption varies vertically and laterally, but is often masked or influenced by the presence of artefacts and coherent noise. The quality of the imaging of the pipes generally degrades with increasing depth.

The pipes in the study area vary considerably in gross dimensions and seismic expression. The narrowest pipes are at the limit of seismic resolution (one to two traces wide; 25-50 m) and therefore any internal structure is not clearly resolvable. The wider pipes can have diameters of c. 300-500 m, hence their internal structure is imaged, albeit subject to the distortions associated with lateral and vertical velocity anomalies, more clearly. In general, the larger the pipe is, the better the internal structure is resolved and imaged, and the more clearly it is possible to recognise probable artefacts.

In general, the pipe diameter is not constant with depth, irrespective of the size of the pipe. Pipe height and diameter are positively correlated implying there is a scaling relationship between pipe geometries (Fig. 4.5). Comparisons between pipes indicate that individual pipes have a different planform shape at consistent unit boundaries, and pipe size, shape and spatial location change with depth (Fig. 4.6b). The planform geometries of coalescing pipes (Fig. 4.6b(b)) typically show that pipes are separate at depth becoming more conjoined towards the seabed. Ellipticity measurements show that pipes are more elliptical at their base and more circular towards the top (Fig. 4.6c). This alteration in ellipticity with depth is reflected in the orientation measurements which show pipe orientations are unidirectional at depth (NW-SE) and bidirectional in the top zone (NW-SE and NE-SW) (Fig. 4.6c).

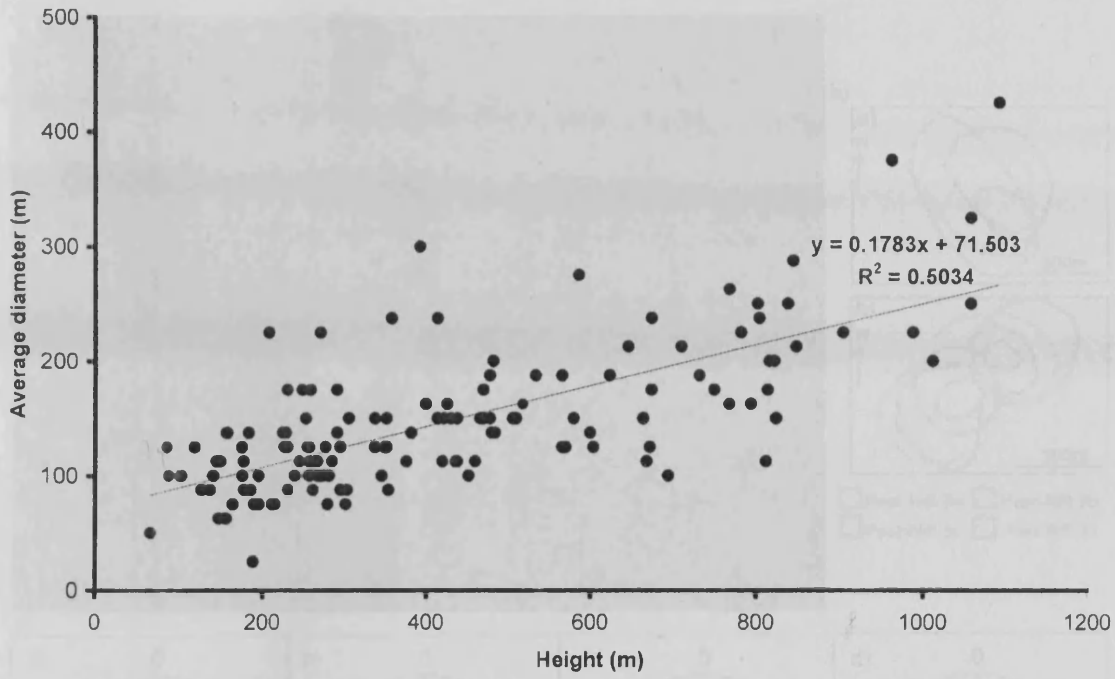

Figure 4.5 Pipe dimensions. The positive correlation between pipe height and diameter implies a scaling relationship exists between pipe geometries.

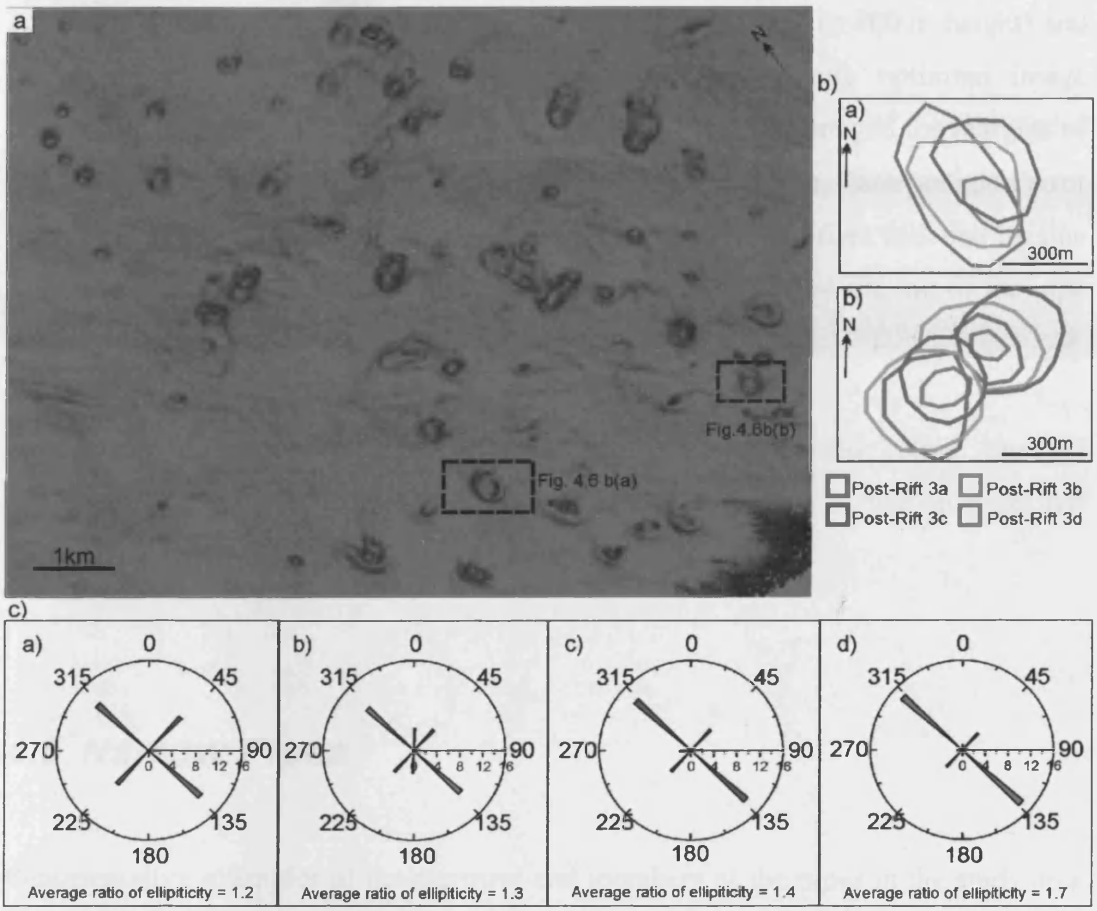

Figure 4.6 Pipe planform geometries. a) coherence slice through Post Rift 3 showing circular to elliptical pipes and coalescing pipes. Coherence cube sliced at Post Rift 3c c.2200ms TWT. b) digitised pipe perimeters from various depths in Post Rift 3 showing that pipe planform shape and spatial location change with depth for (a) single pipes e.g. pipe 53 and (b) coalescing pipes e.g. pipes 32 and 33. Note that pipes are single at depth but coalesce towards the seabed. From the digitised perimeters pipe a and b axis were measured. The data is displayed in figure c. c) Pipe orientation and ellipticity. Pipes become more elliptical and unidirectional with depth. (a) Post Rift 3a; (b) Post Rift 3b; (c) Post Rift 3c; (d) Post Rift 3d.

Analysis of planform geometries was restricted to large pipes (> 800 m height) and measurements were only taken within Post-Rift 3 to ensure optimum image resolution and clarity. Potential errors are based on how well imaged the margins of the pipes are, consequently estimated errors increase with depth. Interpretation error is based on objective picking of pipe margins on adjacent profiles and line by line comparison of positional errors. Estimated errors are < 25 m at the top of the pipe (seismic spatial resolution), increasing to < 100 m at the base.

More detailed descriptions of seismic expression are presented below, grouped arbitrarily into narrow and wide pipes, based on the quality of the imaging that results from their size.

4.5 Narrow Pipes

Representative examples of the narrower end members of the pipes in the study area are presented in Fig. 4.7 (Pipes 30, 37, 121, 142). These examples all have minimum diameters of less than 100 m (Fig 8 a', b', c', d'). In Fig. 4.7(a), the pipe (P30) is visible as subtle breaks in the reflection continuity that are 1-2 traces wide that stack vertically in a systematic fashion over a distance of about 200 m above a prominent unbroken reflection (R1). Above this, the reflections are more disrupted for c. 100 m, and then towards the top of the pipe, a prominent negative polarity reflection (R2) is deformed into a bowl shaped feature c. 100 m across, with a negative relief of c. 20 m. Above this reflection, there is minor disruption and concave deflection of reflections for 50 m up the pipe, and then at shallower levels there is no more disruption visible, but there is a subtle amplification of the background reflectivity in a column of almost constant width (c. 100 m across) up to the seabed.

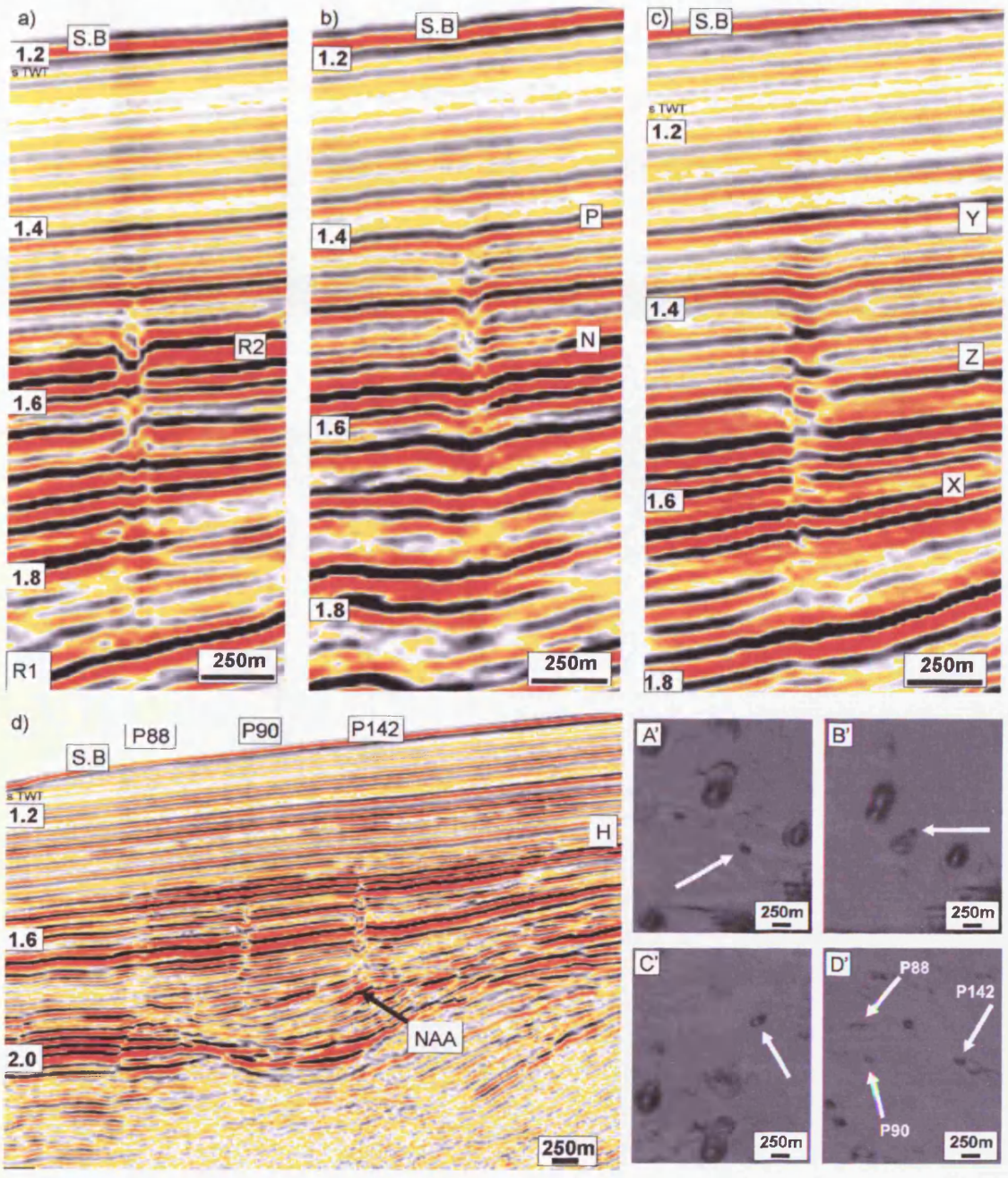

Figure 4.7 Examples of narrow pipes. Pipes are imaged as zones of disturbed reflections. a) Pipe 30 extends from reflection R1 to c.1500ms TWT. (A') Coherency slice through P30 (white arrow) at c.1550ms TWT. b) Pipe 37 from reflection N to P. (B') Coherency slice through P37 (white arrow) at c.1500ms TWT. c) Pipe 121 from reflection X to Y. (C') Coherency slice through P121 (white arrow) at c.1500ms TWT and d) Pipe 142 extends from reflection NAA to H. Only the flanks of pipes 88 and 90 are imaged in this cross section. (D') Coherency slice through P142, P88 and P90 (white arrows) at c.1650ms TWT. Seismic cross section taken NW-SE (top left to bottom right) through the coherency slice. Seismic cross section scale is in seconds TWT.

In Fig. 4.7(b), the pipe (P37) is interpreted based on the extent of disrupted reflections from 1550 ms TWT to 1400 ms TWT, from a prominent negative polarity reflection (N) at the base, to a positive polarity reflection (P) at the top. The disruption deep in the pipe is 1-2 traces across (c. 50 m), with strong de-amplification of the background reflectivity in the pipe above a small depression visible on the basal reflection (N) amounting to c. 10 ms TWT of negative relief. Again, there is a sharp downward disruption of a reflection towards the upper part of the pipe by c. 15 m. There is no visible amplification above reflection P. Beneath basal reflection N a series of vertically stacked push downs are observed from 1550 ms TWT to 1800 ms TWT.

In Fig. 4.7(c), a narrow pipe (P121) can be interpreted with a base that lies just above a high amplitude negative reflection (X), and is delimited upwards by a negative reflection (Y), some 200 m shallower in the section. The pipe is expressed in the lower portion as minor breaks in the reflections combined with dimming of amplitude across a zone 3-4 traces wide. Above 1500 ms TWT, several prominent reflections (e.g. Z) are offset downwards by 20-30 ms TWT, and a series of reflection doublets have significantly higher amplitudes than their lateral equivalents outside the pipe. In the uppermost 100 m of the pipe, the reflections are continuous across the structure, but are systematically depressed downwards over a zone that widens upwards from 100 to 250 m. There is no clear amplification of reflections above reflection Y.

The example in Fig. 4.7(d) (P142) differs from the previous three examples in its context. The examples in Figs. 4.7(a) to (c) all have bases that are defined by unbroken reflections on a gently dipping flank. In Fig. 4.7(d), the right pipe (P142) emanates from a seismic unit that can be clearly seen to be a channel fill deposit. Nearby, other narrow pipes (P88 and P90) are also seen to 'root' into this channel (this is not shown in Fig. 4.7(b)). The pipe (P142) can be traced from a strong negative amplitude anomaly typical of a free gas accumulation (labelled NAA), and extends upwards some 350 m to terminate at a negative reflection (H). There are no amplitude anomalies above reflection H that can be clearly linked to P142. The reflections within P142 are disrupted mainly by downwards deflection or offset,

typically by 10-15 m. There are no strong enhanced amplitude anomalies within the pipe, but a reflection at 1550 ms TWT is dimmed within the pipe.

4.5.1.1 Summary and Interpretation

The examples in Fig. 4.7 illustrate the variety in seismic expression amongst the narrowest pipes in the study area. They show that pipes can be reliably detected from recognition of systematic disruption and/or offset of the reflections within the pipe, augmented by observations of amplitude enhancement or dimming. The lateral margins of these types of pipe are thus defined as the edge of the stratal reflection disruption or offset. Edges of amplitude anomalies are treated with caution in this regard, as they may not be confined to the pipe itself, but may extend across the pipe margin and into the surrounding sediments.

Although at diameters of < 100 m, imaging of internal structure must be regarded with caution, all of these examples exhibited greater or lesser degrees of downward bending or depression of stratal reflections within the pipe relative to their position outwith the pipe. The recognition of the bases of pipes is a critical observation that can help constrain the location of the source of the fluids. All four examples have bases defined by a basal reflection that exhibits no disruption beneath the pipe. The recognition that the base can be defined as the first continuous reflection to cross beneath the pipe is thus important as a guide to the source layer for the fluid. In Fig. 4.7(d), for example, Pipe P142 emanates from the channel fill unit. The base of the pipe is a strong negative polarity amplitude anomaly that has the acoustic character expected for a small gas pocket which is probably trapped in coarser facies within the channel fill (Gay et al., 2006b; Gay et al., 2007a). By defining the base in this way, it is also possible to examine the seismic character in the region beneath the pipe to see if there are velocity anomalies (push down, pull up) or any evidence of scattering or distortion due to the complex ray paths through the pipe (Fig 4.7b). For 3D seismic data acquired with cable lengths greater than a few kilometres, the wider offset data will undershoot the base of the pipe, and hence deeper reflections should not lose continuity because of ray path complexity within the pipe, as is often the case with, for example, shallow channels or shallow reefs (Brown, 2004).

Definition of the upper termination of pipes in the study area is more problematic than defining the base. The only systematic way to define the upper terminus is by taking the first reflection to cross above the pipe with no loss of continuity or downward deflection. This works well for pipe examples in Figs. 4.7a, b and d. However, when this criterion is applied to Fig. 4.7c, the terminus is located in a zone of the feature where there is still a considerable downward deflection of several otherwise continuous reflections. Local amplification of reflections in a narrow linear zone above the pipes is also observed. These question are addressed again in the following section, in more detail, because the observation of systematically downwards deflected reflections in the upper sector of the pipe and local reflection amplification is recognised for the majority of the wider pipes in the study area, and where these wider examples offer better imaging and grounds for discussion.

4.5.2 Wide Pipes

Some representative examples of wider pipes are presented in Fig. 4.8. These pipe examples are located in the south of the study area (Fig. 4.2).

The base of the first example (Pipe 3) (Fig. 4.8a) is defined similarly as for narrow pipes i.e. by identifying the shallowest continuous reflections to cross beneath the pipe without disruption and/or offset. In this example, the base is located within the low amplitude reflections that are characteristic of Post Rift 2. Because the signal to noise ratio is generally lower in this type of seismic facies, it is harder to be confident of true continuity, since coherent noise emanating from the pipe above can interfere with the low amplitude reflections, as seen to some extent in this example. For the same reason, it is harder to interpret true breaks in the data, and thus difficult to define a perimeter to the pipe. Both these tasks are easier to achieve accurately in the high amplitude seismic facies of the basal part of Post Rift 3, above reflection P, in Fig. 4.8a. Here the pipe has a diameter of c. 300 m, and the reflections are both disrupted and deflected downwards by c. 10-20 m. Localised dimming and brightening is seen within the surrounding sediment adjacent to the pipe in this interval. Above 2300 ms TWT, the downward 'sag' of the reflections increases

upwards to a maximum relief of 40 ms at 2100 ms TWT. No clear indications of erosional truncation can be seen towards any of the concave reflections, but there are numerous amplitude anomalies distributed up this part of the pipe, confined to the pipe interior. The pipe is interpreted to terminate at 2050 ms, into a lower relief depression, in which there appears to be an infill (X), which has a circular planform and is therefore interpreted as a buried and infilled pockmark crater. Coherence slices throughout this interval from 2050 to 2500 ms indicate that the gross geometry of this pipe is an almost constant diameter cylinder with a circular planform geometry (Fig 4.8a').

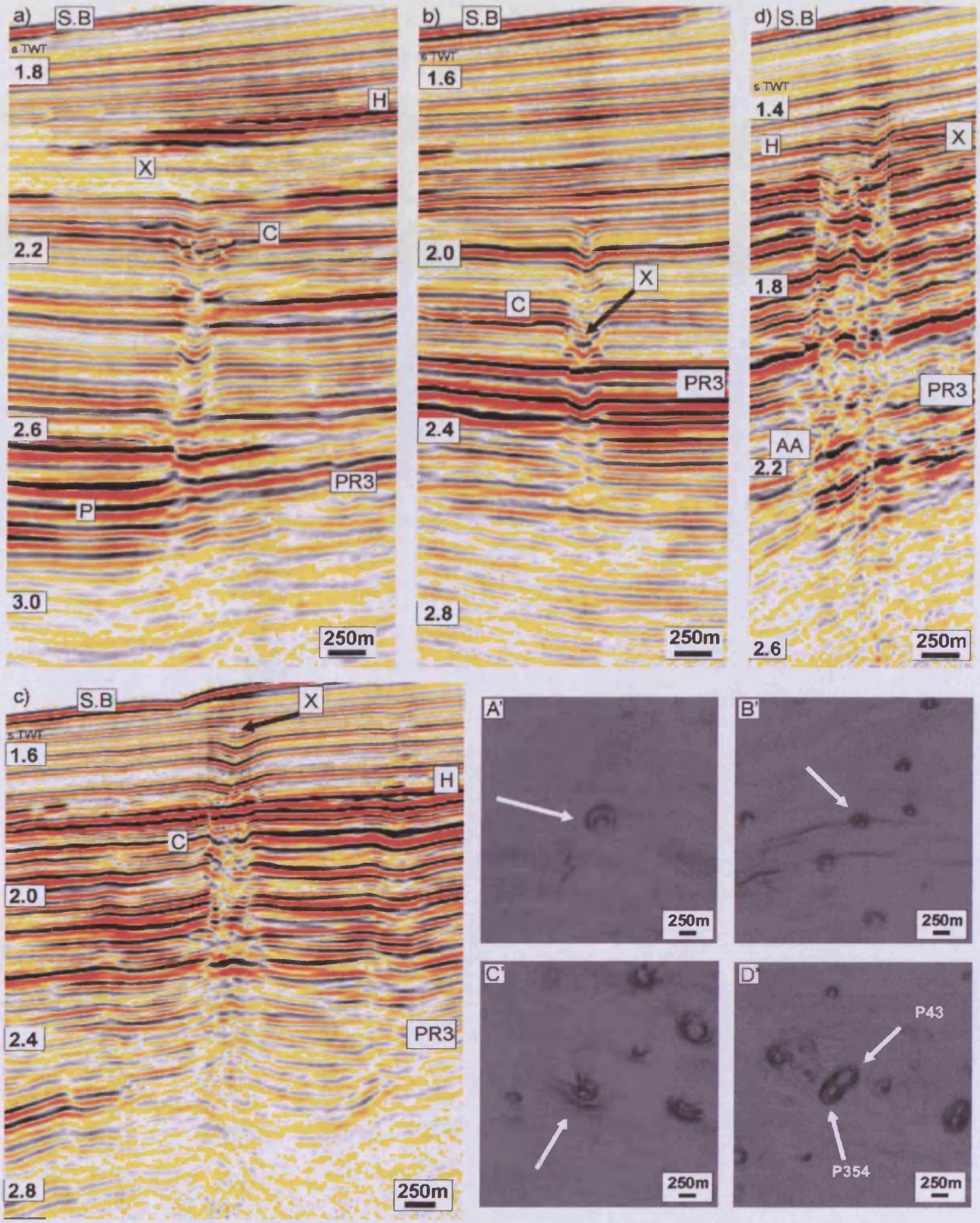

Figure 4.8 Examples of wide pipes. Pipe 3 a) and Pipe 6 b) transect the Post Rift 3 unit boundary (PR3) and are rooted in Post Rift 2. A BSR is interpreted at position H (a). (A') Coherency slice through P3 (white arrow) at c.2200ms TWT showing a well developed crater (C). (B') Coherency slice through P6 (white arrow) at c.2100ms TWT. Pipe 21 c) transects the Post Rift 3 unit boundary (PR3) at the location of a palaeochannel levee and passes through the theoretical base of the gas hydrate stability zone (H). (C') Coherency slice through P21 (white arrow) at c.1900ms TWT d). Pipes 43 and 354 are coalesced or composite pipes rooted in the strong amplitude anomaly (AA). (D') Coherency slice through P43 and P354 (white arrows) at c.1600ms TWT. Seismic cross section taken NW-SE (top left to bottom right through the coherency slice, with the exception of (D') which is taken SW-NE. Seismic cross section scale is in seconds TWT.

The second example (Pipe 6) (Fig. 4.8b) is similar in its seismic expression in many respects to Fig. 4.8a in that (1) the base occurs within Post Rift 2, in the low amplitude seismic facies, (2) the pipe is sharply defined laterally by a pronounced downward 'sag' of the background reflections, and (3) there are amplitude anomalies distributed vertically within the pipe. In addition, there are several features worth noting. Firstly, the relief of the 'sag' increases from c. 15 m at the base to a maximum of 60 m at 2150 ms TWT, and thereafter decreases steadily upwards to the upper pipe termination at 1900 ms TWT. The maximum relief position is marked by several reflections that are erosionally truncated against reflection C. Above this erosional surface, the suprajacent reflections appear to define an infill geometry over a vertical extent of 100-150 m, with alternating reflections exhibiting greater and lesser negative relief. A good example of an infilling reflection is shown at point X. Secondly, the diameter of the pipe systematically decreases upwards from the point of maximum relief (300 m) to the upper terminus (100 m), and the geometry is that of a steep sided cone (carrot shaped). There are no obvious amplitude anomalies above the upper terminus. A polygonal fault transects the pipe at 2100 ms TWT (Fig 4.8b') at an acute angle. The pipe is not deflected by the fault.

The third example (Pipe 21) (Fig. 4.8c) represents a group of wider pipes whose depth of origin is problematic. The 'roots' of this pipe lie within Post Rift 2, but the quality of the imaging at depth is too poor to lead to confident interpretation of true continuity as opposed to reflections that appear broken because of migration artefacts or other interference with coherent noise. Nevertheless, the imaging within Post Rift 3 is excellent and allows clear comparisons to be made with other wide pipes. In this interval, the pipe has an almost constant diameter of 450 m and an almost circular planform (Fig 4.8c'). The seismic expression of the pipe changes markedly, however, at a prominent negative reflection (H) at 1720 ms TWT. Below this, reflections within the pipe are dimmed, disrupted and exhibit the sag morphology, with a negative relief of c. 20 m. Above reflection H, the reflections exhibit a morphology that is a more gentle, bowl shaped depression, with a negative relief of 15-25 m, and with local amplification. Reflection H crosses the pipe with a much smaller downward deflection of c. 3-5 m, compared to the 20 m relief above and below. Reflection H is interpreted as corresponding to the theoretical base of the gas hydrate stability zone from its polarity and by regional correlation to a suite of amplitude

anomalies terminating at a fixed depth below the present day sea bed. The pipe terminates upwards about 100 m below the seabed, with a clear infill of the shallowest concave reflection (X), similar to the pockmark geometry interpreted at the upper terminus in Fig. 4.8a. There is a localised zone of amplification above the upper terminus extending up to the seabed.

The fourth wide pipe (Pipe 43 and Pipe 354) (Fig. 4.8d) has a base at a strong amplitude anomaly (AA) within the upper part of Post Rift 2. This pipe consists of two closely spaced or conjoined pipes, and it thus represents an important variation of the total population, of which some 5 % are conjoined or composite structures. This composite pipe structure is very clearly revealed by coherence attribute slices (Fig 4.8d'). Both component pipes share a common root zone with a base in the strong amplitude anomaly (AA). The combined diameter is c. 500 m, but with an elliptical planform for the combined structure. Both pipes are characterised by similar reflection geometry as seen in singular pipe structures i.e. dominant downward deflections with sporadic amplitude anomalies. As with Fig. 4.8c, the reflection geometry of the pipes changes upwards (X) across the level interpreted to be the base of the gas hydrate stability zone (H). The locus of downward deflection of reflections shifts to the more upslope of the two pipes above this level, and terminates at 1300 ms TWT, with only diffuse amplification of the overlying stratal reflections.

4.5.2.1 Summary and Interpretation

The wider pipes presented here represent the variation seen in the total population of pipes. Geometrically, they vary from cylindrical, to conical, to conjoined. They predominately root in Post Rift 2 or at the Post-Rift 2 : Post-Rift 3 unit boundary. They are characterised by an internal structure in which the majority of reflections are deflected or offset downwards relative to the host stratigraphy by amounts that vary upwards within the pipes. The negative relief ranges from c. 10 to c. 60 m. In some cases, the negative relief changes upwards gradually, but in other cases there is evidence of abrupt alternations of greater or lesser relief, and evidence of erosional sculpting of this relief, and subsequent and episodic infill. This latter observation is

critical, since it strongly suggests that the negative relief is real and not artefactual (i.e. a velocity push down in pre-stack time migrated data), and hence implies a genetic process that is capable of removing material at the seabed and forming a crater shaped depression, that is then later infilled. This process seems to have been episodic in some cases (e.g. Fig. 4.8b). The upper terminations of these pipes are commonly, but not ubiquitously, features that can be interpreted as pockmark craters, also strengthening the notion of a dynamic process capable of erosion of sediment in the near surface.

An important common observation is the contrast in the internal geometry of the deeper and shallower parts of the pipes. In the deeper part of the pipes, the 'sag' is abrupt and sharply delimits the lateral margins, whereas the depressions in the shallower portions of the pipe are more gently curving, and the pipe margins are less abruptly defined. This systematic change in geometry is discussed further in a later section.

The wider pipes that root in Post Rift 2 are invariably seen to transect a large part of Post Rift 3, terminating within a few hundred metres of the present day seabed. The wide pipes demonstrably cross the base of the gas hydrate stability zone, and the observation that the reflection most closely corresponding to this is almost unaffected by the downward deflection can be interpreted as evidence that the hydrate has re-equilibrated across the pipe i.e. the pipe predates the current stabilisation of the hydrate in this area.

4.6 Discussion

4.6.1 Internal Sag Geometry: Real or Artefact?

As documented above, one of the most systematic observations of the widely varying pipe forms in the study area is the downward deflection of reflections relative to the host stratigraphy. This observation is potentially critical for any understanding of

pipe genesis, since if genuine it implies that the process of pipe formation involves some collapse of the column by loss of material (solid or fluid) from the column. A key question therefore is whether the interpreted downward deflection is due to a velocity effect (push down) or some other imaging artefact or whether it faithfully records true deformation of the strata?

To answer this question, I plotted the negative relief exhibited by successive stratal depressions in the shallower portions of the pipe by extrapolating a local datum across the pipe from the undisturbed correlative reflections around the pipe, and measuring the downward shift relative to that datum (Fig. 4.1). Measurements are reported here in two way travel time, because I was aiming to evaluate systematic shifts in travel time that might be indicative of velocity artefacts.

Plots of negative relief for 2 representative pipes are presented in Fig. 4.9*. In general, I observe a systematic reduction in negative relief from the base to top of the pipes. The relief at the base ranges from 10-55 ms in the population as a whole. I am typically able to measure 1-22 values of relief upwards from the base to tops of individual pipes, and the plots exhibit a typically staircase shape, with intervals of upward reduction in relief alternating with intervals of almost constant relief (Figs. 4.9a and 4.9b). Less commonly the relief increases locally, before decreasing again (Figs. 4.9c and 4.9d). This was also noted in the description of pipe geometry and internal structure, and a good example of this was explained in Fig. 4.8b, where a pockmark crater was interpreted as the origin of the anomalous increase in relief. Many of the plots exhibit gradational upward decreases constrained by measurements every 30-40 m or so. These are particularly associated with the change in reflection geometry from a sharp downward deflection, to a more gently bowl shaped reflection geometry that is often noted to occur in the top 100-300 m of most of the wider pipes (Fig. 4.8a, b, c), and some of the narrower pipes too (Fig. 4.7).

* Additional plots are in Appendix A2

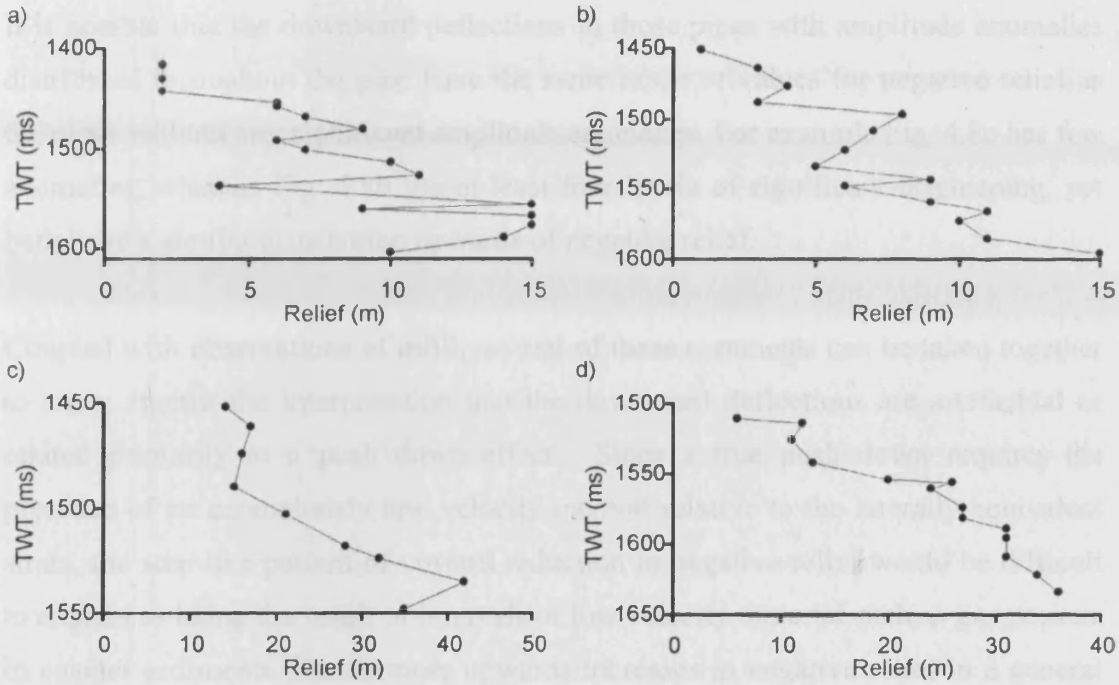

Figure 4.9 Pipe relief. Pipe reflection relief is plotted against TWT. Plots typically exhibit a staircase shape, with intervals of upward reduction in relief alternating with intervals of almost constant relief, for example pipe 22 (a) and pipe 25 (b). Less commonly the relief decreases gradually, for example pipe 45 (c) and pipe 16 (d)

It is notable that the downward deflections in those pipes with amplitude anomalies distributed throughout the pipe have the same range of values for negative relief as the pipes without any significant amplitude anomalies. For example Fig. 4.8c has few anomalies, whereas Fig. 4.8b has at least four levels of significant brightening, yet both have a similar distribution upwards of negative relief.

Coupled with observations of infill, several of these comments can be taken together to argue against the interpretation that the downward deflections are artefactual or related primarily to a push down effect. Since a true push down requires the presence of an anomalously low velocity interval relative to the laterally equivalent strata, the step-like pattern of upward reduction in negative relief would be difficult to explain as being the result of intervals of low velocity material such as gas pockets in coarser sediments. Furthermore upwards increases in negative relief in a general trend of upward reduction cannot be due to a low velocity interval, since this interval would necessarily affect the interval below and not just that with the anomalous negative relief. Lastly, the systematic changes in geometry of the deflected reflections apply to nearly all of the wider pipes, irrespective of the presence of any amplitude anomalies, suggesting they are geological, rather than artefactual.

It is undeniable that there must be some element of push down present, and possibly pull up, and this might vary vertically through the pipes according to the distribution of gas pockets or cemented zones (Hustoft et al., 2007), but the measured values of the negative relief argue forcefully that this is likely a much lower value than the gross values of total negative relief, and probably accounts for some of the fluctuations in values seen on the plots in Fig. 4.9. Changes in the velocity model across space and time may account for some of the variations observed but I am unable to establish any accountability for this variation at such a local scale. In summary, these data strongly suggest that the downward deflection is a fundamental geometrical feature of the pipes.

Finally, linear zones of local amplification are observed to stretch from the pipe top towards the seabed from both narrow and wide pipes (Figs. 4.1, 4.3, 4.7 and 4.8)*.

* Raw RMS amplitude data (table) measured for selected pipes is available in Appendix A2

Not all pipes exhibit this local amplification. This amplification is more apparent from wider pipes and larger narrow pipes which display a degree of downward deflection above narrow sag-like, loss of reflection continuity, v-shaped notches (see narrow pipe interpretation above). The linear zones share a similar planform geometry and diameter to the underlying pipes (Fig 4.10), although seabed pockmarks are not observed (at the resolution of this dataset). The seabed reflection does exhibit localised higher amplitudes above these columnar amplifications. Local amplitude amplification may result from some form of trace normalisation or amplitude anomaly. Due to the spatial distribution of these amplifications, and the specific association with pipes, amplitude anomalies resulting from processing problems, geometric or velocity focusing are unlikely but not improbable. Localised changes in lithology brought about by chemical alteration, cementation or carbonate deposition may be feasible if a fluid migration route can be established and maintained. Following the cessation of morphology forming fluid migration, low saturation gas migration through the pipe to the seabed would need to be maintained. Gas concentrations would need to be high enough to be seismically detectable and encourage lithological transformations yet low enough not to cause reflection downward deflection. Without sediment sampling this supposition must remain highly speculative.

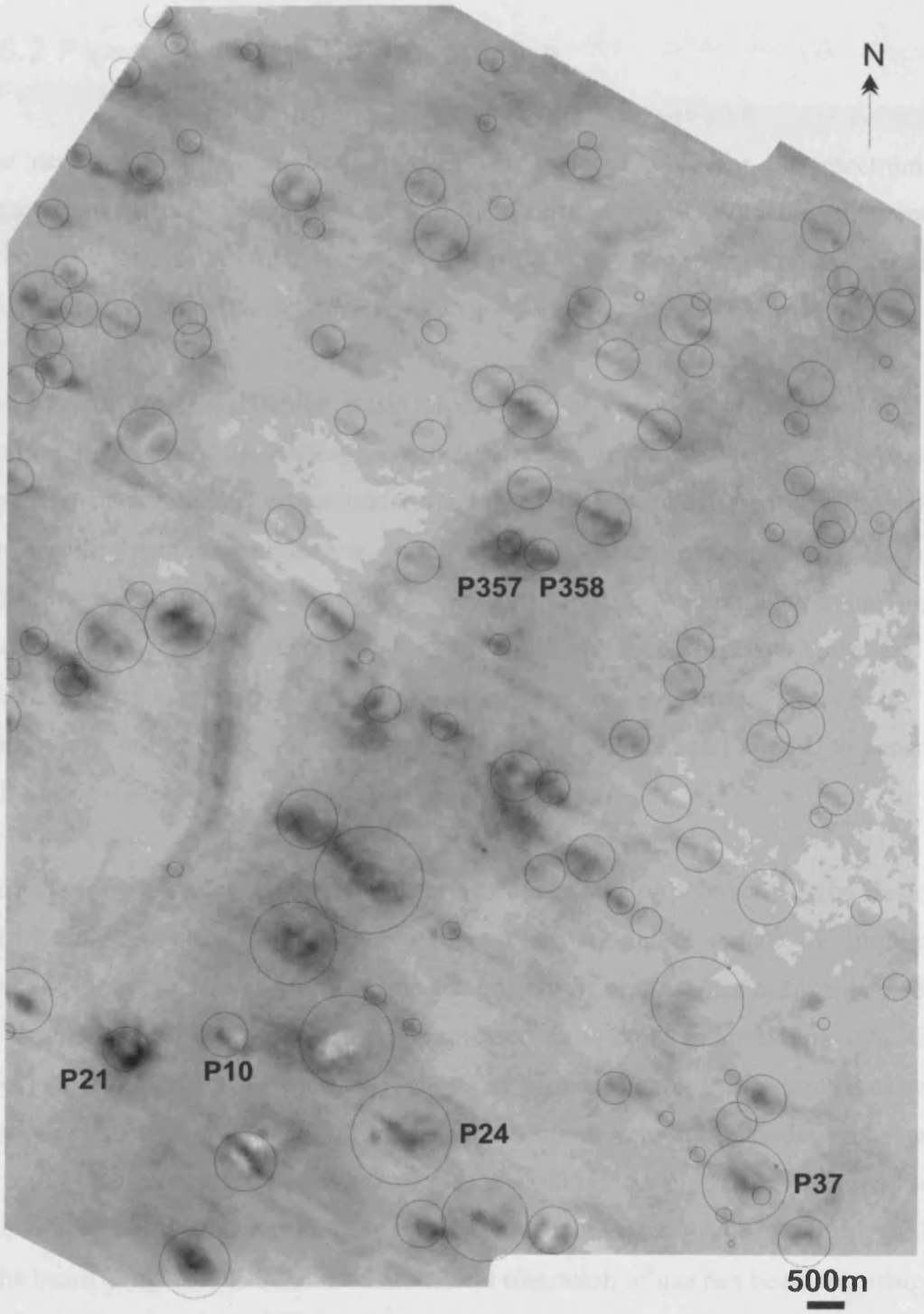

Figure 4.10 RMS amplitude extraction window 150-200ms below the seabed. Near vertical columnar zones of localised amplification are imaged above the pipes. The amplitude extraction window was taken at an arbitrary distance above the pipes (150-200ms below seabed). Local amplification of amplitude is imaged as circular to elliptical high amplitude regions (dark grey) against a lower background amplitude (light grey). Average pipe diameters are shown. Pipe diameters vary with pipe height, therefore average pipe diameters are taken at different stratigraphic depths. In the majority of examples, the spatial overlap of average pipe diameters is simply a function of the depth at which the measurement was taken and not a representation of conjoined pipes. Pipe examples previously mentioned in the text are labelled. Not all pipes exhibit this local overburden amplitude increase.

4.6.2 Pipes: A link to fluid expulsion

The network of pipes in the Namibe Basin is remarkable for the spectrum of geometrical forms, for their density and their vertical extent. Whatever the genetic mechanism involved in their formation, it is evident that this suite of pipes represents a significant vertical anisotropy in an otherwise highly stratified sequence.

The similarity of the Namibe Basin pipes to most previous descriptions of fluid escape pipe makes a compelling case that the pipes in the study area also represent expulsion of pore fluids or gas under a significant pressure differential. Alternative pipe forming mechanisms such as collapse of carbonate or evaporite karst (Bertoni and Cartwright, 2005; McDonnell et al., 2007), or hydrothermal venting pipes (Hansen, 2006) can be considered highly unlikely here, because there are no indications of dissolution of either carbonates or evaporites deeper in the stratigraphy, nor any seismic indications of intrusions of the scale needed to generate hydrothermal pipes.

The case for a genetic link to some form of fluid expulsion for the Namibe Basin is considerably strengthened by the large number and areal extent of amplitude anomalies that can be attributed to free gas trapped in near surface sediments, and to the development of a hydrate layer, expressed in a bottom simulating reflection (BSR) (Swart, 2009). Most tellingly, there are numerous amplitude anomalies with negative polarity within many of the pipes, and minor velocity push-downs beneath the pipes also point to the presence of free gas within the pipes at the present day. These observations together indicate that a petroleum system has been recently active in the basin (England, 1987), and that vertical migration of gas has been occurring in the relatively recent past (Cunningham and Shannon, 1997). Analysis on the timing of pipe formation is further developed in Chapter 5.

Previous studies have generally invoked some form of natural hydraulic fracturing mechanism to explain the vertical focusing of fluids and their ascent through otherwise low permeability sediments (Hovland and Judd, 1988; Mienert et al., 1998; Van Rensbergen et al., 1999; Berndt et al., 2003; Hustoft et al., 2007; Judd and

Hovland, 2007). In recent studies of focused flow of free gas through shallow buried sediments within the hydrate stability zone, the buoyancy pressure of free gas columns trapped beneath the hydrate layer has been implicated as the driver for hydraulic fracturing and the propagation of pipe like vents for methane migration through to the seabed (Gorman et al., 2002; Flemings et al., 2003; Tréhu et al., 2004). Flemings et al. (2003) computed that quite modest free gas column heights of 150-250 m might be sufficient to induce failure through hydraulic fracturing for a gas at shallow depths of a few hundred metres. This is comparable to the column heights I have observed for many of the stratiform amplitude anomalies in the study area below the base of the hydrate stability zone, so it is therefore conceivable that one of the main drivers for focused fluid flow in the area may be gas overpressure resulting from trapped free gas columns.

4.6.3 Source of fluids implicated in pipe formation

We have no geochemical data to constrain the presence of gas, or to identify the composition and origin (biogenic versus thermogenic). Thermogenic gas has been encountered in a number of exploration boreholes further south in Namibia (Cartwright et al., 2008), and basin modelling studies indicate that Cretaceous source rocks in the Namibe Basin could certainly be in the gas generative window (Holtar and Forsberg, 2000). Biogenic gas generation is common in the slope sediments along the west African margin (Cunningham and Lindholm, 2000), and the organic content of the slope sediments of the Namibe Basin is likely to be reasonably high due to the sourcing of this sediment wedge from the Kunene Delta. Potentially enriched source regions for biogenic gas generation include the slope channel fills in Post-Rift 2

The upper temperature limit for biogenic gas generation is debated (Whiticar, 1999; Holm and Charlou, 2001; Sleep et al., 2004; Kieft et al., 2005; Lollar et al., 2006; Roussel et al., 2008), but is commonly taken as c. 70 degrees C. Using present day temperature gradient data from the Walvis Basin, this would equate to a sub seabed depth of c. 2000 m, which would mean that biogenic sources of fluid would be

restricted to Post-Rift 3 and the upper portion of Post Rift 2. It should be noted that the deepest level a single pipe can be traced with confidence is to the middle of Post Rift 2, which is just at the notional deepest limit of biogenic gas generation.

Although it lies beneath the deepest level of confidently interpreted pipe bases, the likely source interval for thermogenically generated hydrocarbons (Syn Rift Sequence) could nonetheless be supplying hydrocarbons to the overburden sediments in the region of most widespread pipe development. Direct (thermogenic) hydrocarbon indicators are indeed observed in the Transitional / Post-Rift 1 interval (Fig. 3.1) and it is conceivable that a deep thermogenic source was implicated in pipe formation. It would be necessary to invoke a vertical migration pathway across the lower part of Post Rift 2, and no obvious routes can be seen because the seismic data in this interval is so low in signal/noise ratio, therefore this suggestion must remain highly speculative.

4.6.4 Significance of the Internal Structure

It has been documented that the internal structure of the typical Namibian pipe consists of two or three contrasting reflection geometries. Loss of coherent acoustic character in the basal area of the pipe, the downward or sag like deflection of reflections and the more gently and subtly diminishing concave dish-like geometry in the upper portions of the pipe.

Perhaps the most significant observation presented in this study is the ubiquitous downward deflection of reflections into pipes, across the full dimensional and contextual spectrum. I have argued that this negative relief is too large to be due entirely to velocity effects (push down), although minor push down is commonly observed at pipe bases. I have also shown that in some examples the negative relief is largely erosional, in the form of pockmark craters, embedded into the structure of the pipe as is also found at Nyegga, offshore Norway (Hovland et al., 2005; Westbrook et al., 2008a). This latter observation implies that fluid flux upwards through the pipe was sufficiently vigorous to excavate seabed sediments for depths of c. 30-50 m from

the palaeo-seabed, and the pipe continued to grow upwards thereafter, as more sediments were deposited on top of the buried pockmark. However, it is clear that the downward deflection in the deeper parts of the pipes cannot be linked directly to seafloor erosion, and hence some other explanation is required.

Instead I suggest that this 'sag-like' geometry results from collapse by removal of material from near the base of the pipe. It is notable that the negative relief in the basal third to half of many pipes is almost a constant value, an observation that is consistent with a collapse origin. Although these pipes cannot be linked to any carbonate or evaporite karst collapse, the concave upwards geometry is very similar to that described for cylindrical collapse structures above karst in the Ordovician of West Texas (McDonnell et al., 2007). I speculate therefore, that pipe formation begins with focused fluid flow that either induces removal of material from a zone near the base of the pipe (e.g. by fluidization) or some other process induces liquefaction, and the flow of fluid upwards from the liquefied interval provides the volume loss necessary to induce collapse of the overburden. Evidence for fluidisation is proposed in the form of the levee-like deposition of material observed in the stratal thickening of some pipes (Fig. 4.1). Where the upward escape of fluid and/or entrained solids was sufficiently vigorous, a surface crater was formed as the multiphase flow egresses at the seabed (Hovland et al., 2005; Hovland and Svensen, 2006). Where fluid escape is less vigorous the seabed may simply have had a modest depression as the surface expression of the underlying zone of collapsed pipe interior. It is also conceivable that in some cases pipes may have terminated into shallow aquifers, where the high porosity of the sediments may have allowed the upwards flowing fluids to disperse laterally, reducing their overpressure, and thus preventing their upward escape to seabed.

Gas hydrates are a very important component of the fluid flow system. The base of the gas hydrate stability field may represent a strong permeability boundary affecting the flow of fluids through the sediments, therefore the relationship between the BSR and pipe formation must be considered. It is plausible that the gas hydrate zone (GHZ) forms a low permeability seal, because present-day free gas accumulations are evidently trapped beneath the base of the GHZ. Underconsolidated sediments within and beneath the GHZ are likely to be overpressured, permitting lateral

migration of fluids. Free gas is trapped beneath the BSR and migrates laterally to an up-dip location. At the up-dip location, if the buoyancy pressure of the free gas column is sufficiently high, it is likely that failure will occur, and a pipe could form as a result (Flemings et al., 2003; Tréhu et al., 2004). The vertical depth limit of the stability field of the hydrate restricts the height of pipe formation. The modern GHZ is 250-350 ms from the seabed, thereby restricting BSR sourced pipes to heights of < 350 m. Fifty six percent of pipes are less than 350 m tall but only < 5 pipes emanate from the modern BSR. The remainder are sourced from Post-Rift 2 or the base of Post-Rift 3.

The flow of fluids through a migration conduit is often associated with the loss of coherent acoustic character (Berndt et al., 2003). Hence, focused fluid flow towards the palaeo seabed may seem to be in contradiction with the well imaged sag-like geometry of reflections. It is suggested that the concentration of gas and spacing of any fractures are insufficient to scatter seismic energy and prevent good imaging. It is acknowledge that imaging artefacts associated with the seismic wavefront and velocity anomalies are still present towards the base of the pipe.

This sequence of events does not capture the full set of observations however, because it fails to explain the systematic change of geometry observed in the internal reflections of most of the pipes, from the more abrupt sag at depth to more gently and subtly diminishing concave dish-like geometry in the upper portions. This change often coincides with an upwards widening of the pipe (e.g. Fig. 4.8). The upwards reduction in negative relief could be interpreted as a result of a collapse mechanism (Branney, 1995), but the combination of upwards widening, gentle curvature and upwards reduction in negative relief are difficult to reconcile with a purely collapse origin. Where clear evidence of pockmark craters can be seen within the pipe (e.g. Fig. 4.8b), these occur beneath this upper zone of gentle curving depressions, and this implies that the mechanism responsible for this upper region of pipe development occurred after the initial phase of pipe growth. This excludes the possibility of a simple single phase collapse mechanism for the entire pipe, since the collapse invoked to form the pipe initially can only have propagated up to the seabed at the position of the palaeo-pockmark crater.

Following the initial phase of pipe growth, the deposition of sediments and the burial of palaeo-pockmark craters beneath successive layers of sediment may be influenced by differential compaction. Sediment accumulation above the pipe may develop different degrees of porosity or settle unevenly during pipe burial, a common process in differential compaction. Therefore differential compaction of sediments above the pipe as the pipe was buried could explain the sag like geometry in the upper zone of the pipe. Reflection thickness differences are observed between measurements taken within and outwith the pipes suggesting differential compaction as a viable mechanism to explain sag like geometry for individual reflections. The apparent sag in reflection is stacked between 1 and 22 reflections, with each reflection exhibiting a unique pipe width, sag relief and difference in reflection thickness between pipe shoulder and pipe centre. It is anticipated that differential compaction would produce a more uniform geometry that flattens out as the differences in sediment compaction between the pipe and background strata equilibrates through time. This is not uniquely observed. The importance of differential compaction should not be dismissed and is considered to be an ancillary mechanism in pipe propagation.

Instead of a collapse mechanism to explain the upper zones of the pipes, I prefer an episodic or continuous seepage mechanism that operates after the phase of initial formation, and exploits any permeability enhancement in the pipe from its initial phase of growth (Fig. 4.11). As sedimentation occurs, fluid flow upwards through the pipe could reduce net sediment accumulation in the region above the pipe, or could locally redistribute the deposited sediment into the water column, similar to the process often invoked for pockmark development and columnar fluidization structures (Fig. 4.11) (King and MacLean, 1970; Hovland and Judd, 1988; Davies, 2003; Judd and Hovland, 2007).

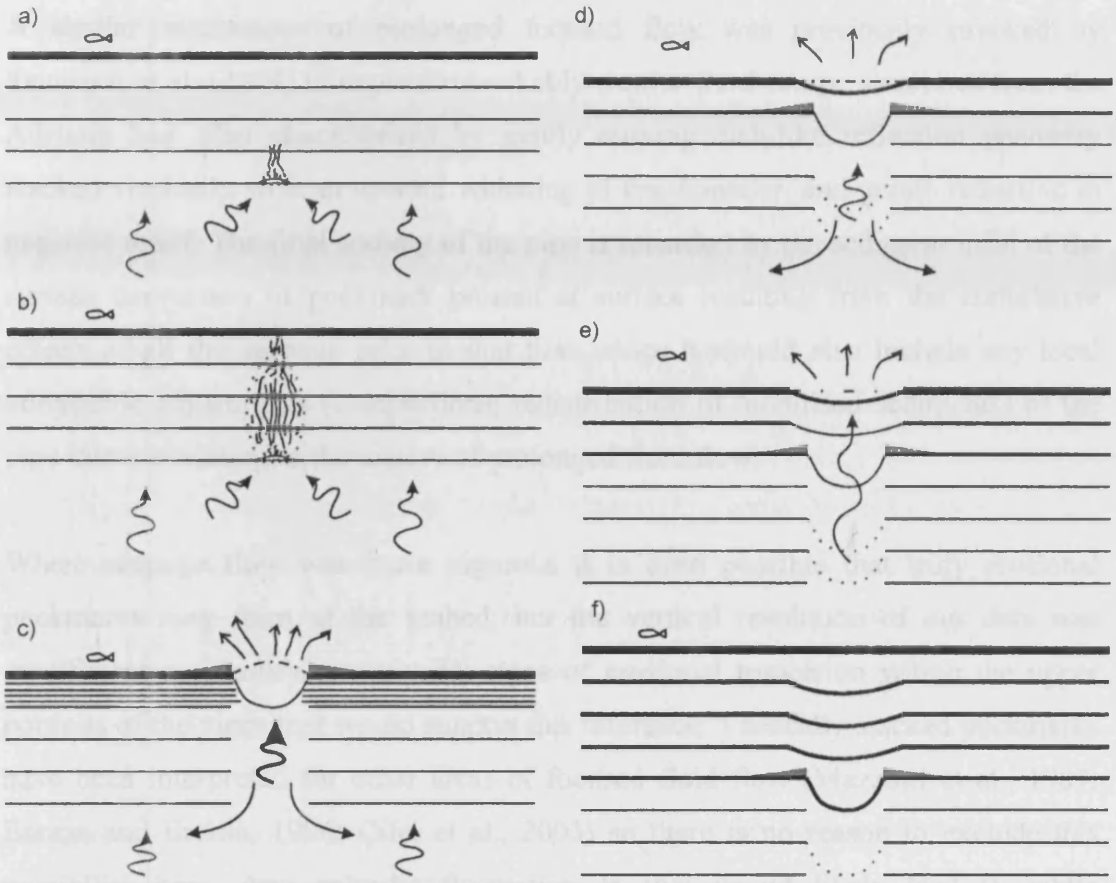

Figure 4.11 Conceptual model for pipe formation. a) Increase in pressure induces reservoir cap rock failure by hydraulic fracturing; b) Upward propagation of fluids and fractures dilate, flow self-organises and the hydrofractured region propagates towards the seabed; c) Fluid pressure builds in the shallow subsurface, and deformation (doming) of the seabed occurs. A hydraulic connection is established, reducing pressure and resulting in a violent burst of escaping fluids. Fluids/sediment is expelled into the water column and laterally onto the seabed. Deposited sediments form a levee-like structure on the seabed. Collapse of the overburden is induced by fluidization and liquefaction that initiates sediment removal at the base of the pipe, providing the volume loss necessary for collapse; d) Following the phase of initial formation, less vigorous, episodic or continuous seepage through the pipe continues; e) as sedimentation occurs, fluid flow through the pipe reduces net sediment accumulation in the region above the pipe and/or locally redistributes the deposited sediment into the water column producing bowl-shaped depressions above the pipe; f) Fluid flow ceases and the pipe/pockmark is infilled with sediment. A similar model has previously been suggested by Davies (2003) for columnar fluidization structures from the Niger Delta.

A similar mechanism of prolonged focused flow was previously invoked by Trincardi et al. (2004) to explain remarkably similar fluid escape structures from the Adriatic Sea, also characterised by gently curving dish-like reflection geometry stacked vertically with an upward widening of the diameter, and gentle reduction in negative relief. The final activity of the pipe is recorded by the sediment infill of the surface depression or pockmark present at surface resulting from the cumulative effects of all the seepage prior to that time, since it should also include any local volumetric adjustments (compactions, redistribution of mobilised sediments) of the pipe interior relating to the history of prolonged fluid flow.

Where seepage flow was more vigorous it is even possible that truly erosional pockmarks may form at the seabed, but the vertical resolution of our data was insufficient to identify unequivocal signs of erosional truncation within the upper portions of the pipes that would support this inference. Vertically stacked pockmarks have been interpreted for other areas of focused fluid flow (Mazzotti et al., 1987; Baraza and Ercilla, 1996; Çifçi et al., 2003) so there is no reason to exclude this possibility here. Any episodic fluctuation in flux would likely lead to subtle expressions of differential negative relief, and these may perhaps be observed in the profiles presented in Fig. 4.9, although I caution that these minor fluctuations are close to the vertical resolution limit.

If this mechanistic interpretation of instantaneous pipe formation follow by long term seepage is correct, it means that I should be able to date the initial phase of pipe formation from observations of the geometry and vertical reduction in negative relief of the internal reflections and also bracket the time interval for subsequent leakage through the pipe conduit. It also implies that once formed, the pipes in the Namibe Basin have a tendency to act as long term conduits, as was also suspected for some pipes on the Norwegian margin (Hustoft et al., 2007). This mechanism also explains the zones of modest amplification of overburden reflections above the upper terminus of the pipe observed for many of the pipes (e.g. Figs. 4.8a,c), as an expression of probably low flux seepage of gas towards the seabed.

The specific processes occurring within the pipe during this second phase of growth will ultimately depend on the flux, the nature of the flow (single, multiphase), the

pressure regime, and the physical properties of the deformed sediments comprising the pipe. It seems likely that gross lithology exerts a first order control on pipe geometry. The pipes described by Van Rensbergen et al (2007), for example, from the sand rich sequence of the Porcupine Basin look markedly different than those described here, with a generally convex upwards internal structure, as opposed to the concave downwards structure described here for probable clay-rich host strata, and this presumably relates to the different mobilisation mechanisms likely for sand rich versus clay rich sediments. Van Rensbergen et al. (2007) make a very convincing case for sand fluidization as a dominant process. In clay-rich pipes, the likeliest mechanism for continued focused flow is through dilational exploitation of pre-existing fractures (from the initial phase of pipe formation) under renewed conditions of overpressure in the underlying fluid reservoir (Sibson, 1995). Longevity of activity therefore places constraints on the gross basin plumbing and hydrodynamic regime, since it implies a renewal of the driving overpressure conditions.

Comparisons can be drawn between the pipes described here and sedimentary diatremes. Sedimentary diatremes are narrow vertical structures formed by the fluidization and entrainment of nitrified sediment by flowing liquids or gases producing an explosive eruption at seabed and resultant blowout crater (Brown, 1990; Løseth et al., 2001). The formation mechanism invoked for sedimentary diatremes is highly similar to the conceptual model described above although a considerable size difference exists between the width of the Namibian pipes and examples of sedimentary diatremes from offshore Nigeria (Løseth et al., 2001). The blowout pockmarks are of a comparable size. Hanken et al 1999 ((Hanken et al., 1999) cited by Judd and Hovland 2007) proposed a formation mechanism for onshore sedimentary diatremes involving hydraulic fracture and vertical blowout. The authors propose that after each gas escape, the diatreme becomes blocked as clasts of the overlying rock fall into the newly created void and become embedded in the clay matrix. Subsequent gas pressure release requires the formation of a new diatreme and blowout crater. The pipes described here conform to diatremes-like collapse of the overburden, but I have shown that this collapse zone is possibly quite permeable, permitting a degree of fluid seepage. Chapter 5 will further examine the spatial distribution of overpressure build up and demonstrate how the blowout of a single pipe affects the formation of subsequent pipes.

A final consideration is the question of a possible scaling relationship between height and width of the pipes (Fig. 4.5), and how this might be linked to the two stage genetic model being proposed here (Fig. 4.11). Is it possible, for example, that the height and width are partly controlled by the initial conditions of formation (e.g. flux, magnitude of overpressure, host stratigraphy), but then modified by gradual enlargement during the second phase of growth? It seems reasonable to infer that long-term and possibly episodic flux of pore fluids, gas and possibly entrained solids through the initial pipe structure, would lead to some degree of widening. This might not necessarily require high velocity flow and abrasion of the pipe walls, but could be a combination of stopping and collapse of the walls, abrasion, liquefaction and brecciation by additional fracture propagation, similar to that described for many breccia pipes and sedimentary diatremes (McCallum, 1985). Alternatively, in much lower flux systems, with low seepage velocities, the widening of a pipe with time might be the result of percolation invasion of the previously intact host stratigraphy, and of opening up of new higher permeability routes around blockages resulting from cementation or collapse. The numerous examples of positive polarity amplitude anomalies observed in the pipes in this study area lend support to this notion, since they are most likely due to methanogenic carbonate precipitation in and around the pipe core (O'Brien, 2004). In summary, although speculative at this stage, in the absence of examples calibrated by targeted scientific drilling, some form of widening of pipes could reasonably be expected to occur with longevity of activity as a conduit, and this would go some way to explaining the observed scaling relationship.

4.7 Summary

This study has focused primarily on describing the internal structure of pipes from a single, well defined area of focused fluid flow. Examples of narrow (< 100 m diameter) and wide pipes (> 100 m diameter) have been used to display the diversity and similarity between pipe seismic characteristics. Pipes can be reliably detected from recognition of systematic disruption and/or offset of the reflections within the pipe, augmented by observations of amplitude enhancement or dimming. Pipe bases

are defined by a basal reflection that exhibits no disruption beneath the pipe, although occasionally velocity push-down or sag can be seen, and the upper terminus is defined by taking the first continuous reflection to cross above the pipe. Often this reflection exhibits a fill morphology.

A conceptual model for pipe formation is proposed. An increase in pressure induces reservoir cap rock failure by hydraulic fracturing. As fluids propagate upwards, fractures dilate and the flow self organises building pressure in the shallow subsurface. A hydraulic connection is established at the seabed reducing pressure and producing a violent burst of escaping fluid/sediment. Subsequent collapse of the overburden is induced by volume loss due to fluidization at the base of the pipe. After the phase of initial formation, less vigorous episodic or continuous seepage through the pipe continues reducing net sediment accumulation in the region above the pipe and/or locally redistributes the deposited sediment into the water column producing a bowl-shaped depression above the pipe. Upon cessation of fluid migration the pipe/pockmark is infilled with sediment.

The examples shown exhibit different degrees of clustering, and different ages of activity, which can potentially be dated using the interpretational framework established in this chapter. In the next chapter I concentrate more on explaining the distribution of the pipes in space and time.

Chapter 5

This chapter has been published as Moss, J.L., and Cartwright, J., 2010, The spatial and temporal distribution of pipe formation, offshore Namibia: Marine and Petroleum Geology, v. 27, p. 1216-1234.

The work presented in this chapter is that of the lead author (JLM), editorial support was provided by the project supervisor (JAC) in accordance with a normal thesis chapter.

5 THE SPATIAL AND TEMPORAL DISTRIBUTION OF PIPE FORMATION, OFFSHORE NAMIBIA

5.1 Abstract

A group of nearly 400 pipe structures from the continental slope of northern Namibia are analysed for their spatial and temporal distribution. The pipes most likely formed as a result of highly focused fluid venting, and understanding the factors controlling their distribution in space and time is key to their genesis. I analysed their spatio-temporal distribution using an arbitrary chronostratigraphic timescale, from which it is concluded that the pipes did not form at the same time. Pipe formation is shown to be intermittent and persistent, with 2-29 pipes forming in each of the > 20 arbitrary time intervals that are considered to span the Neogene period. The spatial distribution of these pipes is clustered to dispersed. Spatial statistics conducted on the distribution of pipe formation timings have shown that two statically significant groups of pipes exist within the population, (1) in the North and West and (2) in the South, with the former occurring prior to the latter. Locally, pipe formation is sporadic with clusters and outliers occurring during the same time period. A conceptual model is proposed whereby pipe formation in specific locations is the result of localised breaching of the seals for isolated pressure cells which are locally independent yet broadly controlled. An inferred basinal fluid source is thought to determine the broader patterns of pipe formation, and the focus of this fluid source shifts from North to South with time. At a local scale, multiple local factors interact producing a sporadic pipe formation distribution through a prolonged period of highly focused fluid migration. Once formed, the pipes continued to focus fluids intermittently, leading in some cases to later pockmark formation.

5.2 Introduction

Focused fluid migration is an important process in sedimentary basins, and is manifested in a range of structures such as sand intrusions, mud volcanoes and fluid expulsion pipes (Berndt, 2005; Cartwright et al., 2007). Pipes are vertical columnar zones of seismic disturbance, which are interpreted to be the expression of highly focused migration of fluids through low permeability sequences (Fig. 5.1) (Løseth et al., 2001). Fluid migration is focused into narrow, near-vertical zones where presumed increased permeability permits fluids to bypass the pore network. Pipes propagate from shallow fluid sources (< 1 km below the seabed) and terminate at seabed pockmarks, craters or vents. Pipes are considered to form by the catastrophic breaching of top seals to shallow gas reservoirs in a highly dynamic process involving hydraulic fracture under elevated pore fluid pressures, and fluid driven erosion and collapse (Løseth et al., 2001; Berndt et al., 2003; Ligtenberg, 2005; Cartwright et al., 2007; Hustoft et al., 2007; Judd and Hovland, 2007). Pipes have recently become a major research focus because they have implications for basin analysis, modelling overpressure development, seal failure and gas hydrate development.

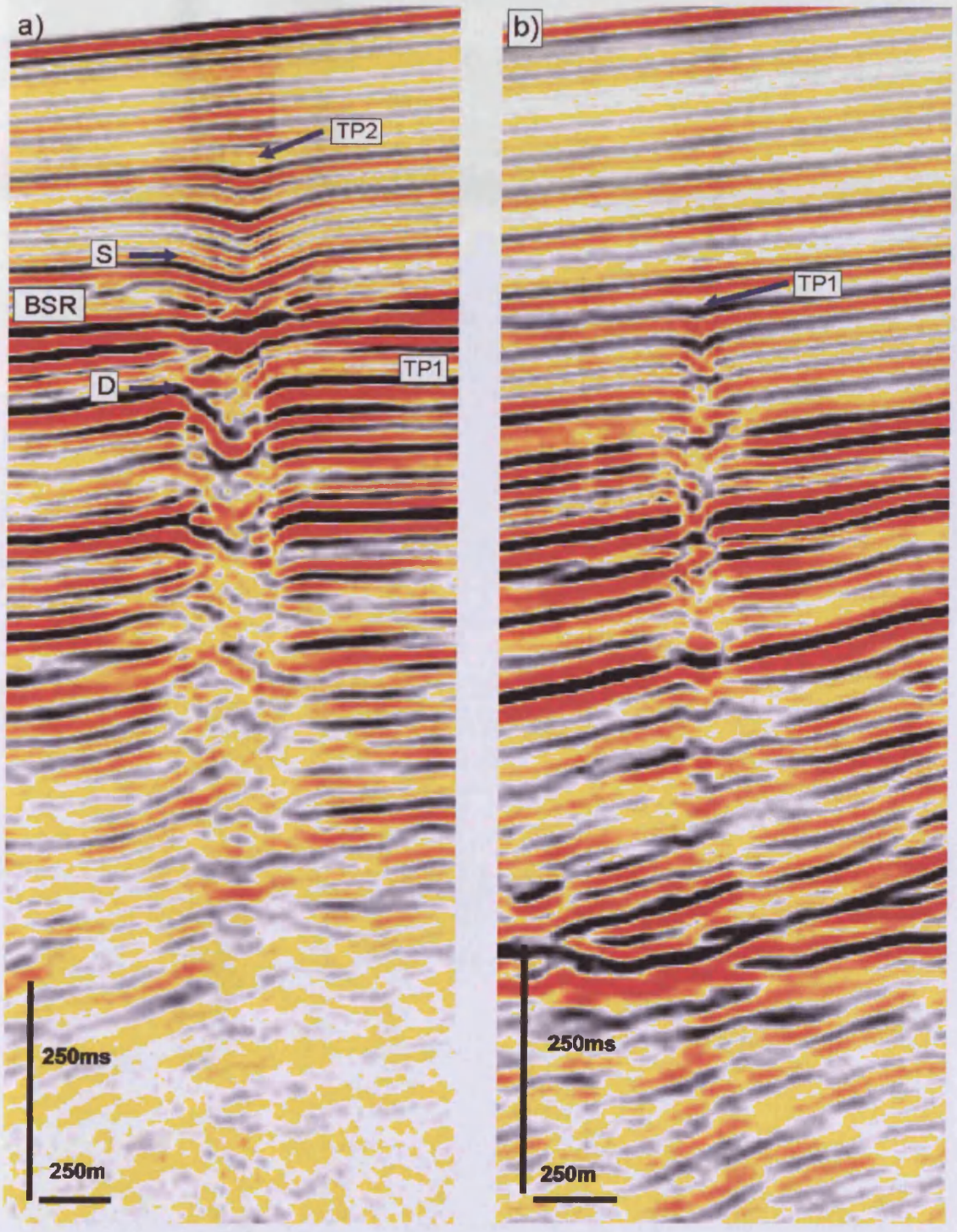

Figure 5.1 Pipe examples. These vertical columnar zones of seismic disturbance are interpreted to be the expression of highly focused fluid migration. a) Wide pipe (Pipe P24). Time Point 1 (TP1) is towards the base of the pipe and marked by steeply dipping, truncated reflections (D). The blue arrow also indicates stratal thickening interpreted as levee-like deposition of fluidized material from the base of the pipe. Shallow reflections towards the top of the pipe are more gently curving (S). Time Point 2 (TP2) is at the top of the pipe and marked by fill geometry. This example of a wide pipe is transected by the hydrate layer (BSR). b) Narrow pipe (Pipe P116). Time Point 1 and Time Point 2 are marked by the same reflection. This reflection is at the top of the pipe and marked by fill geometry.

A large population of nearly 400 pipes from offshore northern Namibia was described in Chapter 4 (Fig. 4.2a), which extended the descriptive base for pipe structures. Based on a geometrical-acoustic description, I proposed a genetic model that built on previous studies in favouring a mechanism involving hydraulic fracturing and pressure release from a locally overpressured 'cell.' Other pipe genetic models were considered including dissolution of carbonate or evaporite units (Bertoni and Cartwright, 2005), fluid escape by slow seepage (Cartwright et al., 2007) and rapid hydrothermal venting (Davies et al., 2002), but I was able to discount these possible alternatives based on the regional geological setting and knowledge of the likely stratigraphy. No evaporites are known in northern Namibia, the seismic stratigraphy does not indicate the presence of thick carbonates and no igneous intrusions have been interpreted within the post-Karoo sedimentary sequence in this part of the Namibian margin (Clemson et al., 1997; Corner et al., 2002), making dissolution and hydrothermal venting unlikely. I considered pipe formation utilising a purely seepage based genetic model unlikely for the majority of Namibe Basin pipes due to the observations of erosional truncation (e.g. defining the craters) but acknowledged that seepage may be involved.

The timing of pipe formation is generally quite poorly constrained in all previous descriptions of pipes. One approach has been to constrain the maximum period of pipe formation from the accurate identification of pipe fluid sources. This methodology is only feasible where it is possible to determine when overpressure started to develop, and where precise delineation of the pipe base and its interaction with a fluid source can be established (Heggland, 1998; Gay et al., 2003; Duck and Herbert, 2006; Gay and Berndt, 2007; Van Rensbergen et al., 2007; Pinet et al., 2008). This method is limited by commonly occurring seismic artefacts obfuscating the diagnostic identification of the bases of pipes, but even when this interpretation can be made, this approach provides no constraints on the timing of subsequent pipe evolution.

The main aim of this chapter is to tackle the outstanding question of the dating of pipe formation and subsequent behaviour as fluid flow conduits. Firstly this chapter extends the initial description of Chapter 4 by placing pipe genesis within a more quantitative spatial and temporal framework, permitting the examination of how the

distribution of pipes evolved through the basin's history. Secondly, it introduces a more rigorous quantitative approach to the analysis of fluid escape pipes. It is acknowledged that the analysis of timing of pipe formation cannot be separated from the conceptual model for pipe formation. I note the uncertainties in this approach and attempt to overcome these by including alternative approaches to dating pipe activity. Irrespective of which specific approach is taken to dating pipes, the conclusion reached here is that pipe formation is intermittent yet persistent through time and space, and this should prompt further evaluation of the current group of genetic models.

5.3 Seismic data, interpretation and methodology

The data volume used for this study consists of a ~900 km^2 grid of time migrated 3D seismic data from North Namibia acquired on behalf of NAMCOR in 2002 (Figs. 2.4 and 3.1).

5.3.1 Dating formation from the interpretation of pipe morphology

Chapter 4 subdivided the population of pipes into narrow and wide pipes based on the quality of the imaging which results from their size, and this distinction is maintained here. Narrow pipes are imaged as systematic disruptions and/or offset of the reflections within the pipe, augmented by observations of amplitude enhancement or dimming (Fig. 5.1b). The pipes exhibit a greater or lesser degree of downward bending or deflection of stratal reflections within the pipe relative to their position outwith the pipe. A sharp downward disruption of a reflection towards the upper part of the pipe is interpreted as the top of the pipe (Fig 5.1b). It is inferred that the top of a narrow pipe marks the stratigraphic datum at which focused fluid flow was initially expelled at the palaeo seabed. The reflection at which this morphology is observed is

taken here to indicate the stratigraphic position of pipe formation or Time Point 1 (TP1).

Wide pipes represent c. 45 % of the total population. Seismic imaging of wide pipes is enhanced by the larger size (100-500m diameter) of the feature permitting an assessment of their internal structure (Fig. 5.1a). Wide pipe internal structure is characterised by reflections that are bent or offset downwards relative to the host stratigraphy by c. 10 to c. 60 m, and the magnitude of this relief varies upwards within the pipes. A contrast in internal geometry is observed between the deeper and shallower parts of the pipes. In the deeper part of the pipes, the 'sag' is abrupt (max 60 m relief) and sharply delimits the lateral margins. This maximum relief position is commonly marked by localised erosional truncation, suggestive of pockmark development. The depressions in the shallower portions of the pipe are more gently curving (c. 15 m relief) and the pipe margins are less abruptly defined (Fig. 5.1a). The reflections exhibit variation in pipe negative relief, ranging between a gradual upwards trend of diminishing relief and abrupt alternations of greater or lesser relief over a vertical extent of 10-150 m. Amplitude anomalies of 'soft' and 'hard' impedance contrasts are distributed vertically within, above and below the pipes.

The position of maximum relief is interpreted as an expression of surface venting and pockmark formation, and is consequently categorised as the temporal point of initial pipe formation (Time Point 1 , TP1) (Fig. 5.1a). The upper limit of the pipe is taken at the first reflection that crosses the pipe with no measurable offset or deflection, although there can often be amplification of the background reflectivity above this position. The gentle sag-shaped reflections between TP1 and the top of the pipe are interpreted as having formed during a period after the initial pipe formation when continuous or episodic seepage resulted in reduced sediment accumulation above the pipe axis, and occasional pockmark formation at the seabed (see Chapter 4 Discussion). The top of the wider pipes is interpreted as the datum when this seepage ceased to shape the seabed. This datum is used in the analysis of pipe distribution as Time Point 2 (TP2) (Fig. 5.1a).

5.3.2 Seismic stratigraphic dating

In the absence of direct chronostratigraphic calibration from boreholes, I established a relative chronostratigraphy by correlating 80 seismic reflections through an interval (TWT) that would include the positions of TP1 and TP2 for all 366 pipes in the study area. At least 27 reflections were correlated in their entirety throughout the survey area. I numbered these reflections consecutively from the seabed to the base of Post Rift 3 and for each pipe interpreted the reflection which correlated closest to the position of TP1 and TP2. For the narrow pipes, only a single datum (TP1) could be correlated. Where individual reflections provided only a local constraint on relative timing, groups of reflections were chosen to provide full areal coverage, albeit at a lower temporal resolution (Fig. 5.2).

5.3.3 Errors and Limitations

No absolute dates are given for pipe formation because I lack direct biostratigraphic calibration. Errors in the relative dating are related to the correlation of the individual seismic reflections to the interpretation of TP1 and TP2 for each pipe. Individual dating of each pipe is therefore limited by the subjectivity of interpretation of each Time Point, combined with any correlation error attached to any given seismic reflection. Because the data used is a 3D seismic survey, and there are no major obstacles to lateral correlation such as major faults, I can estimate the correlation error as 10milliseconds (c. 10 m) over the area of the survey. It is important to note that the relative time scale is in reflection number, and is not likely to correlate linearly with geological time. Based on average sedimentation rates from nearby ODP boreholes during the Pleistocene, the periods defined by successive reflections represent c. 200,000 yrs.

Spatial statistics are highly susceptible to the precision of the coordinates in the point dataset and the mathematical boundary area imposed on the spatial analysis. The calculation of nearest neighbour statistic utilises coordinates which do not take into

account pipe diameter, therefore pipes which have a minimum distance < 150 m from their nearest neighbour are in actual fact conjoined pipes. This applies to < 5 pipes. In order to compare Moran's I statistics between time intervals the mathematical boundary conditions on the search area had to remain fixed, and was therefore extended beyond the immediate area of the pipes in the calculation to cover the entire pipe coverage. Extending the boundary conditions will produce a tendency towards clustering as the proportion of pipes to free space is extended.

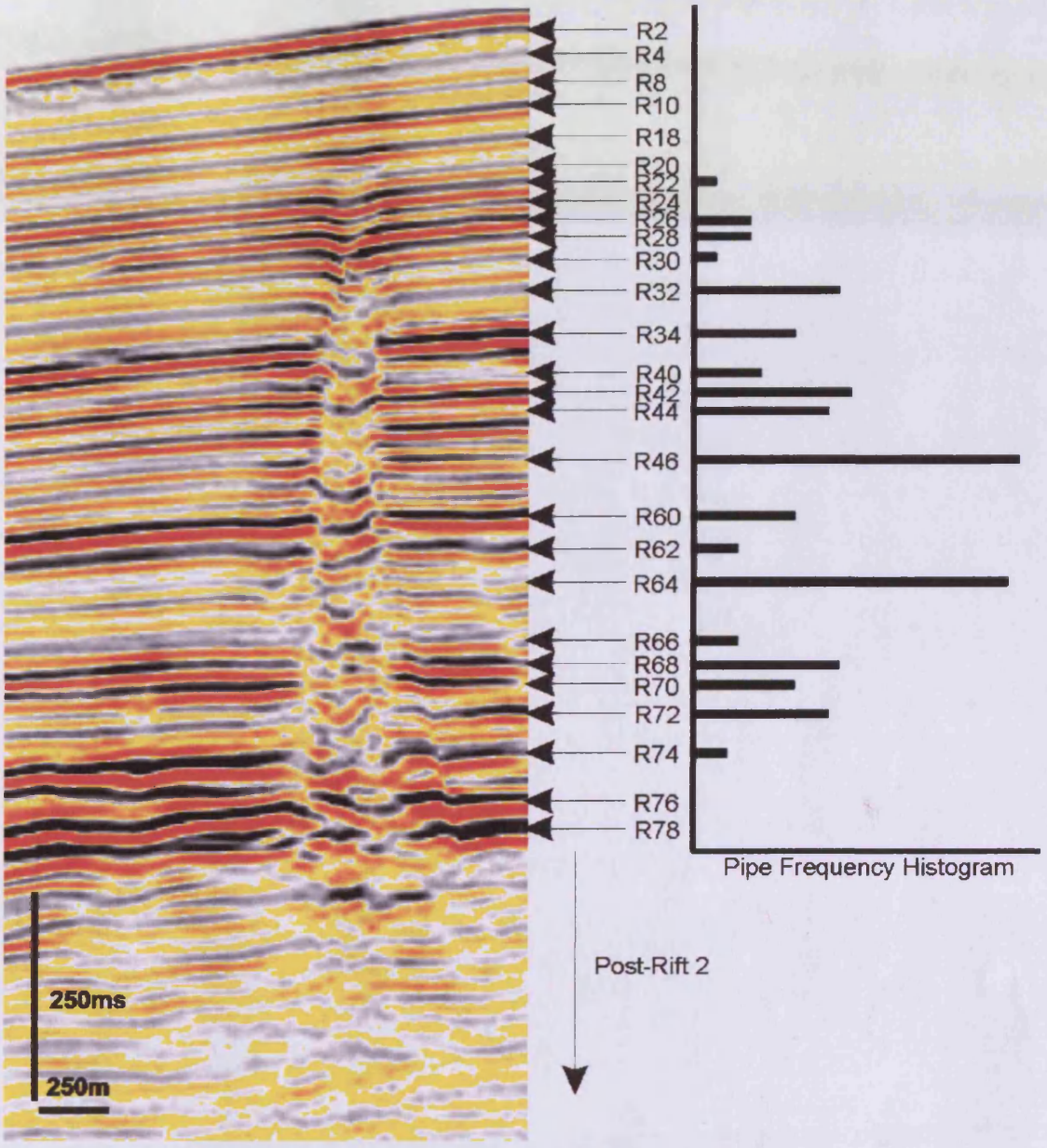

Figure 5.2 Arbitrary chronostratigraphic dating methodology. Each reflection and reflection package was consecutively numbered from seabed to the base of Post Rift 3. Example histogram does not display collected data. Only negative polarity reflections are labelled on the histogram. Reflection packages are not labelled. Pipe example is wide pipe P74.

5.4 Results

5.4.1 Gross Distribution of the Pipe Population

The population of 366 pipes are irregularly distributed in the basin across a range of present day bathymetry from -600 m to -1800 m (Fig. 4.2a). The pipes have an average density of 2 pipes per km^2 and occur in a broad north-south zone in the basin axis (Figs. 4.2a and 5.3). The largest pipes (height > 800 m and diameter > 200 m) are in the south with smaller pipes located towards the centre and north of the study area (Figs. 4.2a and 5.3). The large pipes in the south are spatially coincident with buried channels developed in the basal Post Rift 3 : upper Post Rift 2 sequence. This may imply that fluids were focused via more permeable units within the channel-levee complex (Bünz et al., 2003; Gay et al., 2003; Gay et al., 2006a; Gay et al., 2006b; Hovland and Svensen, 2006). A zone of polygonal faulting covers the basal third (300-400 m) of Post Rift 3 and top section of Post Rift 2 (c. 100 m - 400 m). In contrast with relationships identified elsewhere (Berndt et al., 2003; Gay et al., 2006b) there is no causal link between polygonal faulting and pipe formation or location.

On a gross scale, the total pipe population is distributed in a horseshoe pattern. The geographical distribution of the pipes does not show any quantifiable correlation with the structural or thickness maps of the main stratigraphic intervals, for example i.e. pipe diameter vs unit thickness* (Fig. 5.3). The crude horseshoe pattern loosely correlates with the thickest development of the Post Rift 2 succession (Fig. 5.3b) where it infills the flanking depressions to the large lensoid constructional mound within the Post Rift 1 sequence (Fig. 5.3a). The majority of the pipes are arrayed around the margins of this mound suggesting that the source of the fluid was neither within the mound or focused upwards by it, since there are no pipes above the topographic culmination of this body.

* Graphs shown in Appendix A3

There is a crude correlation between the pipe distribution and the thickest development of the Syn Rift and Transitional sequences above the basement half graben (Fig. 5.3c,d). The largest pipes are observed above the thickest development of the Syn Rift, and this spatial pattern is also consistent with the location of the BSR in Post Rift 3 (Fig. 4.2). If the pipes are sourced from this depth, then it is conceivable that the pipes are sourced direct from a probable hydrocarbon kitchen (given the analogous depths to known kitchens in the Orange Basin, South Namibia) and that these pipes are spanning over 4 km of sealing sequence. If shown to be correct, these pipes are the first reported pipes sourced from a kitchen and to have column heights in excess of 1 km and are therefore unique within the published literature.

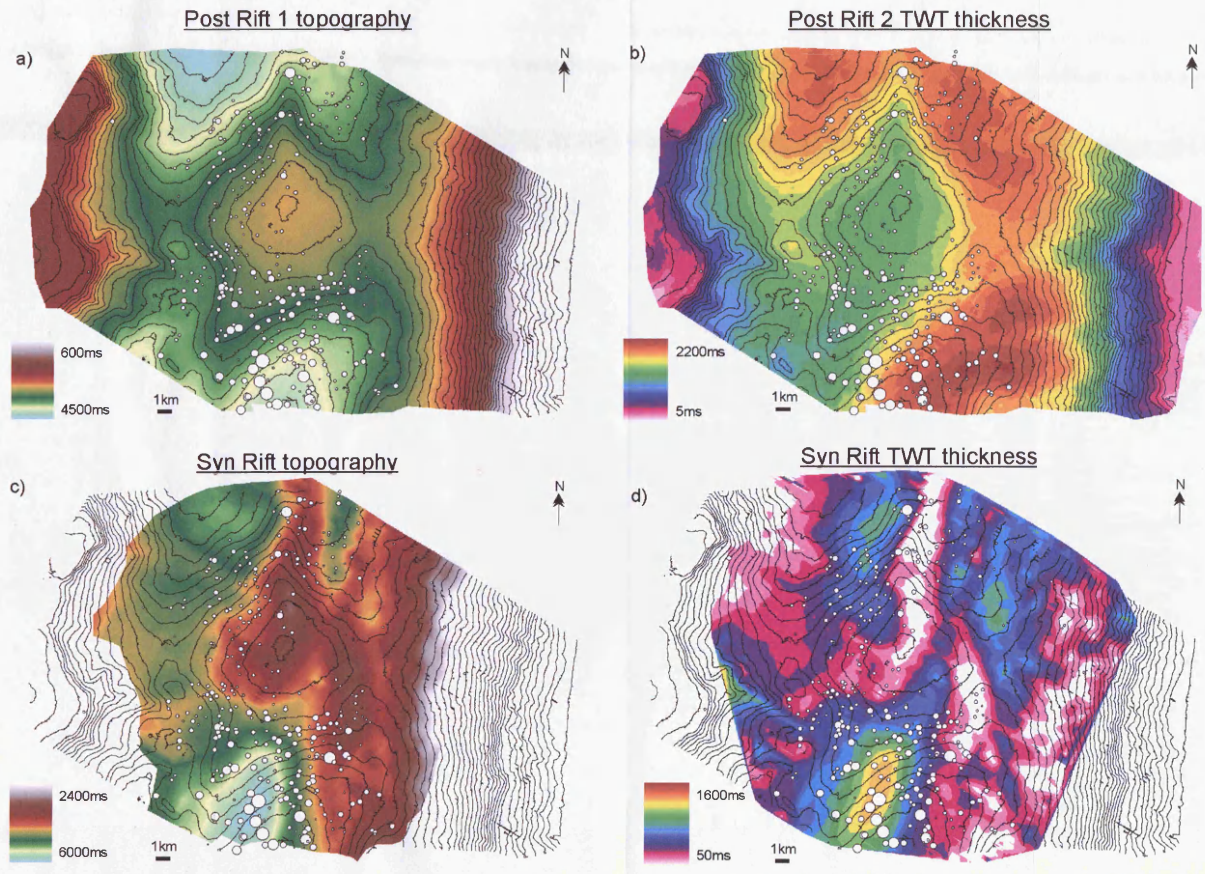

Figure 5.3 Spatial distribution of pipes in relation to underlying geology. a) Topographic surface of Post Rift 1. b) Thickness (TWT) map of Post Rift 2. c) Topographic surface of the Syn-Rift. d) Thickness (TWT) map of the Syn-Rift. All contours refer to the Post Rift 1 topographic surface and are spaced at 100m intervals. Pipe locations are represented by the white points. Point size is directly proportional to maximum pipe diameter.

Similarly, there are no obvious correlations between the pipe distribution and the following features/structures; a) a prominent seabed failure scar*. b) 6 small circular seabed depressions. c) there is no direct relationship between the occurrence of BSR (Bottom Simulating Reflection) and the large number of pipes (< 20 %) which occupy the same spatial area (Fig. 4.2a). A minority of pipes (< 5) have been observed to emanate from the BSR (Fig. 5.4). d) with the exception of localised brightening of reflections and the high amplitude reflections trapped beneath the BSR (Fig. 5.4a), pipes are rarely observed to emanate from amplitude anomalies in Post Rift 3 (< 5 % of pipes). The paucity of amplitude anomalies associated with the presence of gas in Post Rift 3 is suggestive of a fairly efficient sealing unit overlying a fluid source which is deeper than Post Rift 3.

* Map shown in Appendix A2

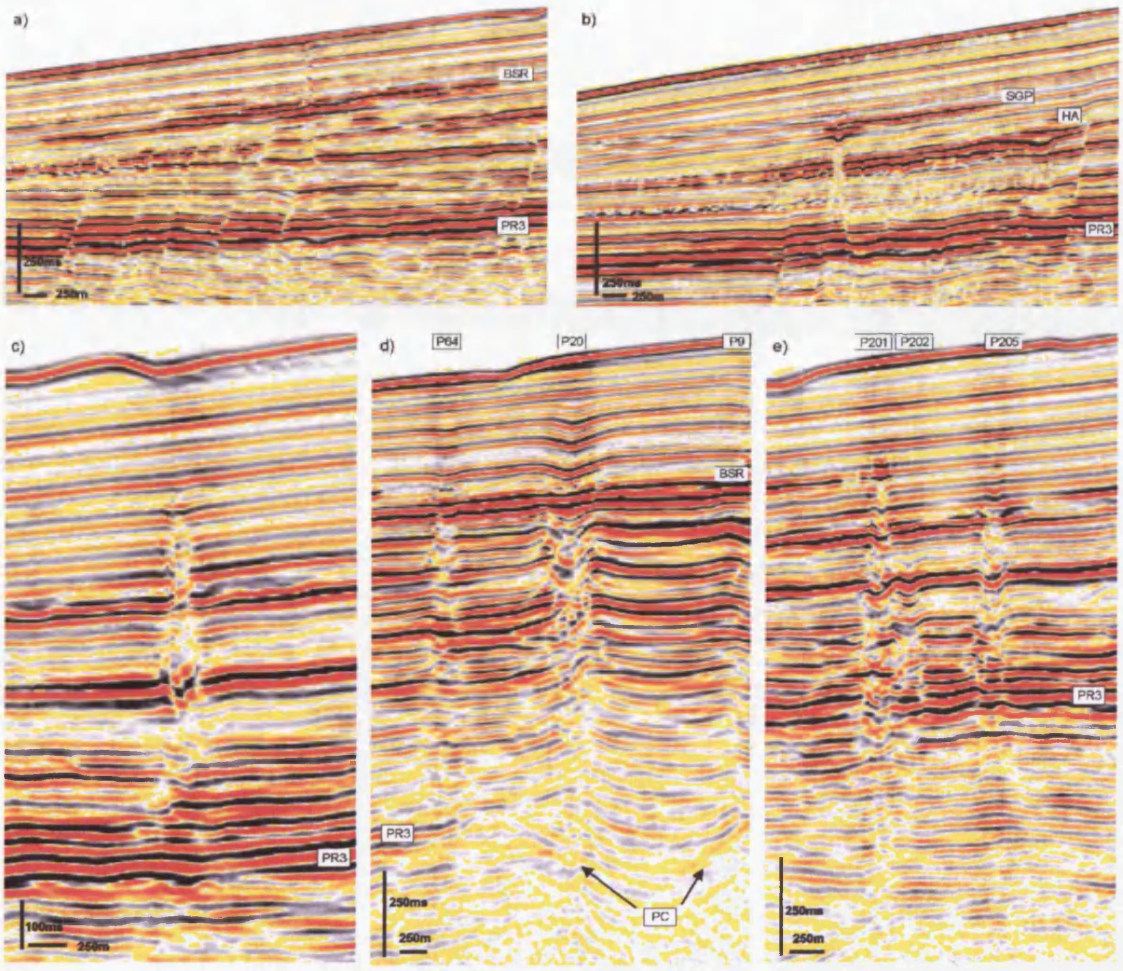

Figure 5.4 Variation in pipe base setting. a) Narrow pipe P396 bleeding from a BSR (Bottom Simulating Reflector). b) Narrow pipe P231 bleeding from the high amplitude and polygonally faulted basal section of Post Rift 3, passing through a high amplitude body (HA) trapped by a polygonal fault and terminating in a shallow gas pocket (SGP) at the level of the current BSR. The shallow gas pocket appears to be sourced from the pipe. c) Narrow pipe P209 bleeding from an un-known position mid Post Rift 3. d) Wide pipe P20 bleeding from a palaeochannel levee (PC). The edges of neighbouring pipes are imaged on the far left (P64) and right (P9) of this figure. e) Conjoined pipes P201 and P202, and pipe P205. P201 has its base in Post Rift 2 compared with P202 which has its base in Post Rift 3. Both pipes terminate at different stratigraphic depths in Post Rift 3. P205 has its base in Post Rift 3. PR3, mega unit boundary between Post Rift 2 and Post Rift 3.

The Namibe Basin pipes are stratigraphically restricted to the Post Rift 2 and 3 sequences (Fig. 3.1). No pipes have been observed in Post Rift 1 or older units. The identification of the upper limits to the pipes can be made with a high degree of precision. The vast majority (> 95 %) of the pipes terminate upwards at various levels within the Post Rift 3 sequence. The specific distribution of the upper zones of the pipes is considered more fully in the section below on timing of pipe formation.

The stratigraphic distribution of pipe bases is difficult to determine precisely. A large proportion of the population emanate from the very low amplitude seismic facies of Post Rift 2. Seismic interpretation within this unit is limited to the uppermost 100-400 m. Below this level seismic artefacts, background noise, amplitude anomalies and poor seismic continuity mask the true basal position of pipes. Continuity of stratal reflections is sufficiently high in the southern part of the study area to trace the majority of pipes 400 m into this unit. Coupled with observations of a small number of pipes that vertically transect channel fill units without any obvious change in their geometry or position, it is feasible that the majority of pipes in the north and west which become untraceable at the Post Rift 3 : Post Rift 2 unit boundary are indeed sourced from below this level.

In summary, it remains possible that the pipes cut deeper than I generally recognise, but no firm evidence can be found to support this at present. Overall, 40 % of pipes can be traced confidently into Post Rift 2, a further 40 % of pipes have their base within the high amplitude, highly faulted lower interval (c. 300-500 m thick) of Post Rift 3 and 20 % of pipes can be traced to channel levees or gas accumulations that are trapped at the base of the gas hydrate stability zone (Fig. 5.4).

5.4.2 Timing of pipe formation

The timing of pipe formation within the Namibe Basin is established using an arbitrary chronostratigraphic dating technique. As noted in the methodology (Chapter 5), different methods are required for wide and narrow pipes respectively, due to differences in the imaging of pipe interiors. Consequently, three age distribution

frequency histograms are presented: (1) time of formation taken as TP1 for all pipes; (2) time of cessation of pipe activity taken at TP2 for all pipes (and for narrow pipes this is assumed to coincide with TP1); (3) time of formation taken as TP1 for wide pipes (narrow pipes are excluded). The time scale used is relative and applies only to the study area.

Pipe formation frequency during the Neogene is presented in Figure 5.5 and 5.6. Figure 5.5 has been re-graphed in Fig 5.6 to express the difference in the number of reflections between TP1 and TP2 as box plots. This will be discussed in more detail below and mapped in Figure 5.7. All three histograms (Fig. 5.5) exhibit a longevity of pipe formation which stretches throughout the temporal period captured by Post Rift 3 (Fig. 5.5). In scenario 1 (TP1 for wide and narrow pipes), pipe formation spans the period from R71 to R10 (Fig. 5.5a). There are only two intervals (R9- R0 and R18-19) with no pipe formation. This younger interval of inactivity probably represents the larger part of the Pleistocene, and possibly some of the Pliocene, based on extrapolations from nearby ODP drill sites. There are a number of distinct peaks in the histogram however some may be artificial because they represent groups of reflections rather than individual reflections (e.g. R46-60). Although there are some intervals with generally lower numbers of pipes forming than in others (e.g. R69-R71 and R22-R23), the distribution can not be described as episodic. Instead, I propose pipe formation persisted through the gross time interval, with some periods of increased occurrence above the background level of c. 5 or 6 pipes per reflection increment.

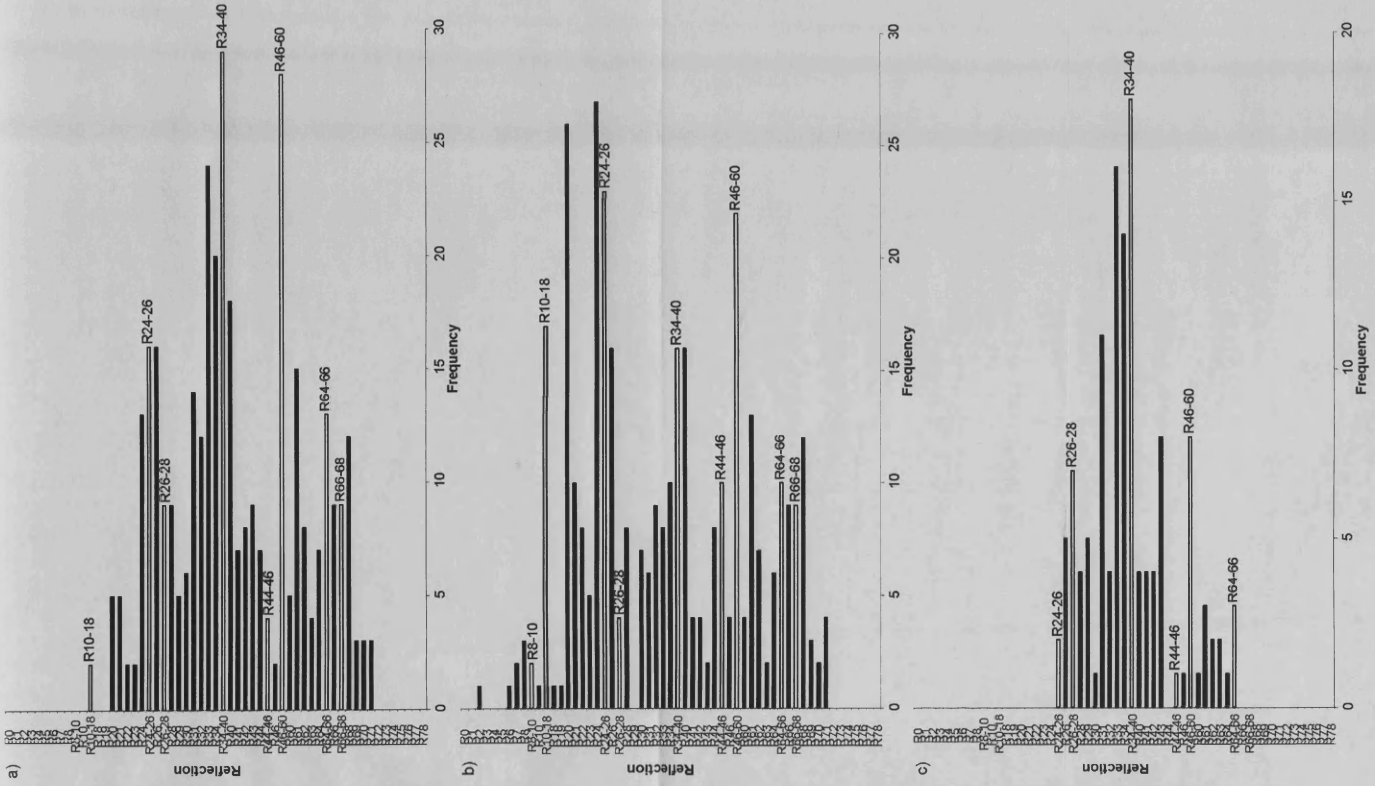

Figure 5.5 The timing of pipe formation. a) Time Point 1 frequency histogram. b) Time Point 2 frequency histogram. c) Time Point 1, wide pipes only, frequency histogram. Reflection packages are labelled.

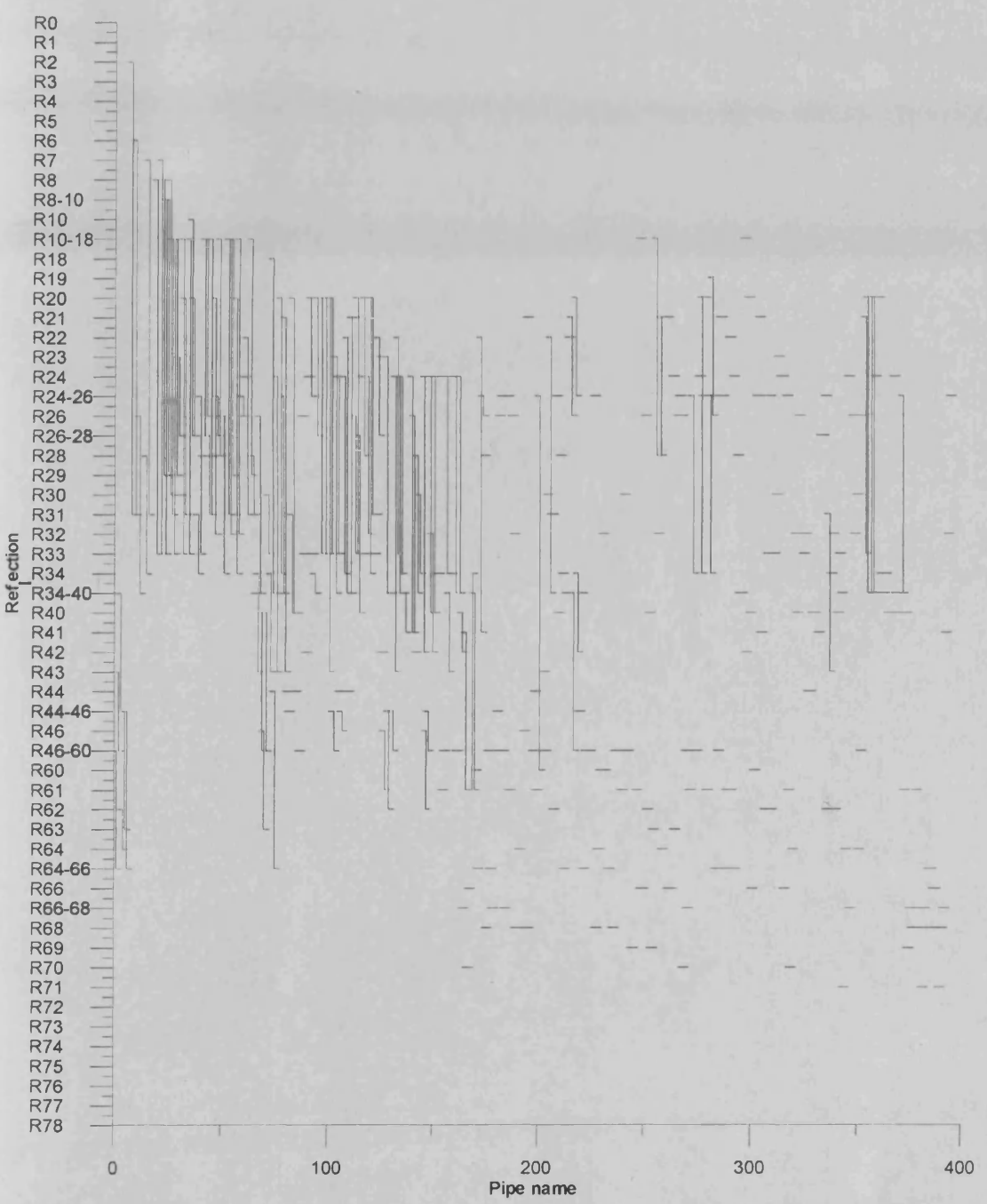

Figure 5.6 Difference in reflection between TP1 and TP2. Box plots span the time period represented by the difference in reflection number between the time of pipe formation (TP1) and the time when seepage ceased (TP2). Horizontal lines represent those narrow pipes where only TP1 values could be measured. Pipes were number from South to North in the dataset; therefore the increase in pipe name broadly corresponds to a south to north shift in pipe location.

Scenario 2 (TP2 for wide and narrow pipe) spans a greater range of reflections from R71 to R2, with two intervals where no pipes are recorded as being active (R3 to R5 and R29) (Fig. 5.5b). This histogram shows a similar gross temporal distribution to that presented for TP1 (scenario 1)*. There is evidence for persistent activity throughout the Neogene and considerable fluctuation in the numbers of pipes forming per reflection increment.

Scenario 3 (TP1 for wide pipes) spans the smallest range of reflections from R24 to R66 (Fig. 5.5c)*. By excluding the smallest pipes whose time of formation is almost impossible to determine with confidence, and concentrating on the largest, most reliably imaged pipes, this histogram perhaps provides the most realistic representation of the true duration of pipe formation in the basin. Using the extrapolated average sedimentation rates from nearby ODP sites, this span of reflections may represent 7-8 Ma. Even if this was in error by a factor of two, this still suggests that pipes formed on a multi-million year time scale, with no strong evidence of episodicity, and no prolonged periods where there was a total absence of pipe formation.

The striking conclusion derived from these three contrasting approaches to 'dating' pipe formation or activity, is that the phenomenon of pipe growth was persistent through a long period of time, and was not episodic at the time scale captured by the seismic resolution of stratal reflections. Although the reflection-based chronology is unlikely to approximate a linear time scale, the fact that the three contrasting methodologies all convey a similar behaviour strengthens the basic conclusion of persistent activity of pipe growth.

* Spatial distribution maps shown in Appendix A3

5.4.3 Temporal distribution

5.4.3.1 Correlation with measurable geological parameters

Taking TP1 (scenario 1, Fig 5.5a) as a holistic representation of pipe formation within the Namibe Basin, pipe formation was quantitatively assessed against various geological parameters. I could find no systematic correlation between the timing of pipe formation and the depth (m), slope (°), aspect (°) and thickness (m) of the Post Rift 2 and the Syn-Rift sequences*. This supports the earlier qualitative conclusion that there is no obvious visual correlation between any of the mapped geological features and the pipe distribution.

Pipe bases are observed at a range of depths and stratigraphic intervals*. There is no systematic relationship between the timing of pipe formation (TP1) and a) the depth of the pipe base or b) the reflection value assigned to the pipe base. This suggests that pipe base depth can not be used as a proxy for determining when pipe formation occurred, and implies that pipes with common basal horizons do not necessarily form at the same time.

5.4.3.2 Incremental evolution of the population

Spatial statistics conducted on the total population of 366 pipes have shown that the pipes are statistically significantly clustered within the study area at the 95 % significance level (*Rn* 0.77 and a *z* score of -8.38, equations 1, 2, 3). This result is too coarse to provide insight into what factors might have influenced the clustering of pipes. Higher resolution analysis requires a subdivision of the total pipe population into subpopulations. This subdivision is based on distinctive frequency peaks within the pipe formation timing histogram (Fig 5.5a). These sub-populations can be regarded as early (R71 to R46), middle (R44-46 to R30), and late (R29 to R10) 'phases' of formation. Mapped distributions of the three 'phases' indicate a spatial trend of older pipes in the north and west, and younger pipes in the south of

* Graphs shown in Appendix A3

the study area. The youngest forming pipes (R29 to R10) are distributed in a horseshoe pattern throughout the study area, similar to the general spatial pattern for the total pipe population (Fig. 5.6a).

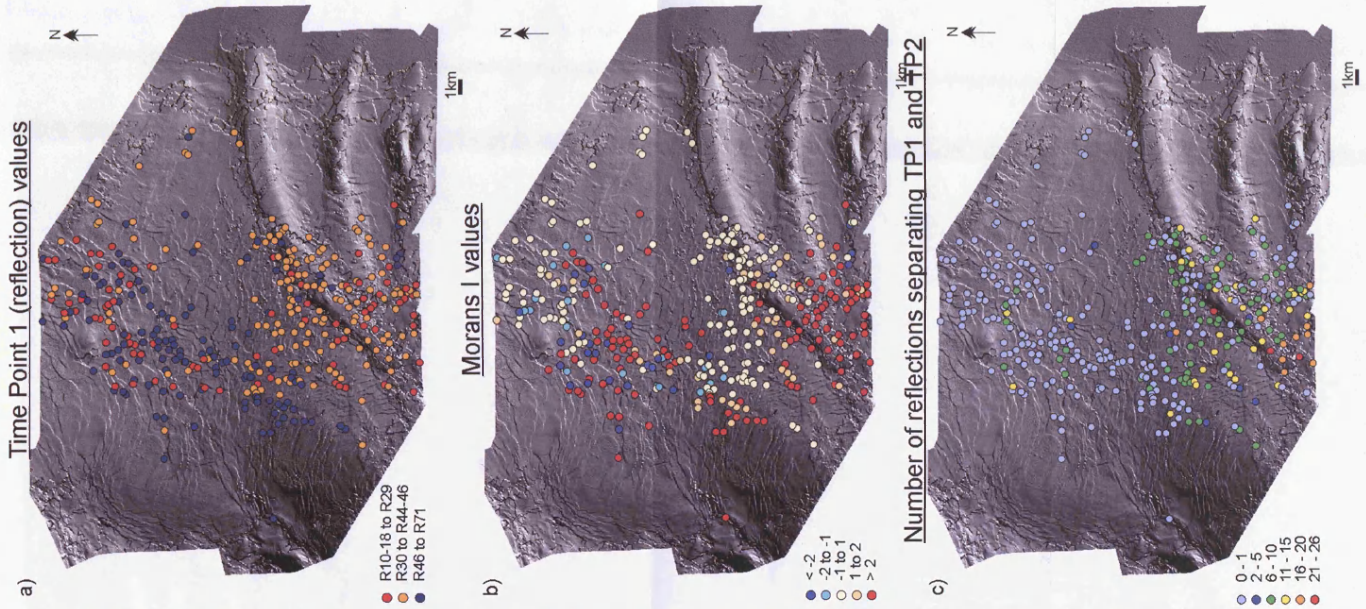

Figure 5.7 Spatial distribution of Time Point 1 values and statistical significance. a) Spatial distribution of Time Point 1 (TP1) values. Distribution shows a general trend of older forming pipes (R46 to R71) in the North and West, and younger forming pipes in the south (R30 to R44-46). b) Moran's I (Ii) cluster and outlier analysis. Spatial statistics z values are shown. A positive value for z indicates that the pipe is surrounded by pipes with similar TP1 values. Such a pipe is part of a cluster. A negative value for z indicates that the pipe is surrounded by pipes with dissimilar TP1 values. Such a pipe is an outlier. The null hypothesis that there is no pattern to pipe formation timing (TP1) is rejected at the 95% level for all pipes with a z score <-2 or >2 i.e. dark blue or red. c) Number of reflections separating TP1 and TP2.

The statistical significance of pipe formation spatial distribution was assessed using Moran's I cluster and outlier analysis (equations 2, 3, 4 Chapter 2) (Fig. 5.7b). Moran's I determines whether pipes of a given TP1 value are preferentially surrounded by pipes of either similar or dissimilar values. Pipes in the south of the study area have statistically similar TP1 values to those pipes around them (Ii z score > 2). The pipes in the north and west are a combination of statistically significant clusters and outliers (Ii z score > 2 and < 2). Outliers in this context are pipes that have a statistically significant different TP1 value to their neighbours. The pipes in the southern-central band are not statistically significant (Ii z score 1 to -1). The Moran's I spatial statistic therefore supports the notion of two broad zones of successive pipe formation, initially in the north and west, then later in the south. The spatial distribution of TP1 values is statistically significant, and the null hypothesis that there is absolutely no pattern to the spatial distribution of TP1 values is rejected at the 95 % level (Fig. 5.7b).

The difference in the number of reflections between TP1 and TP2 is recorded in Figure 5.7c and 5.6. Pipes with a single reflection difference i.e. narrow pipes where it was not possible to distinguish between TP1 and TP2 reflection morphologies are scattered throughout the study area but compose the majority of the pipes in the north and west. Pipes with 2-26 reflections are mainly found in the south. The interpretation of this "lag period" is open to debate however the spatial pattern of variation is consistent with the patterns described above (Fig. 5.7).

5.4.3.3 Individual time increment analysis

Incremental evolution has revealed a general pattern of younging of pipe formation towards the south of the study area. However, the time span represented in the tripartite grouping (Fig 5.7a) is still too crude to provide insight into what factors might have influenced the spatio-temporal distribution of pipe formation. The spatial distribution of pipes forming at individual reflections can also be displayed (Fig 5.5a), and allows a narrower time range for pipe formation to be analysed (Figs. 5.8 and 5.9). Furthermore, it permits the rapid comparison of pipe distributions in preceding and succeeding intervals (Figs. 5.9 and 5.11).

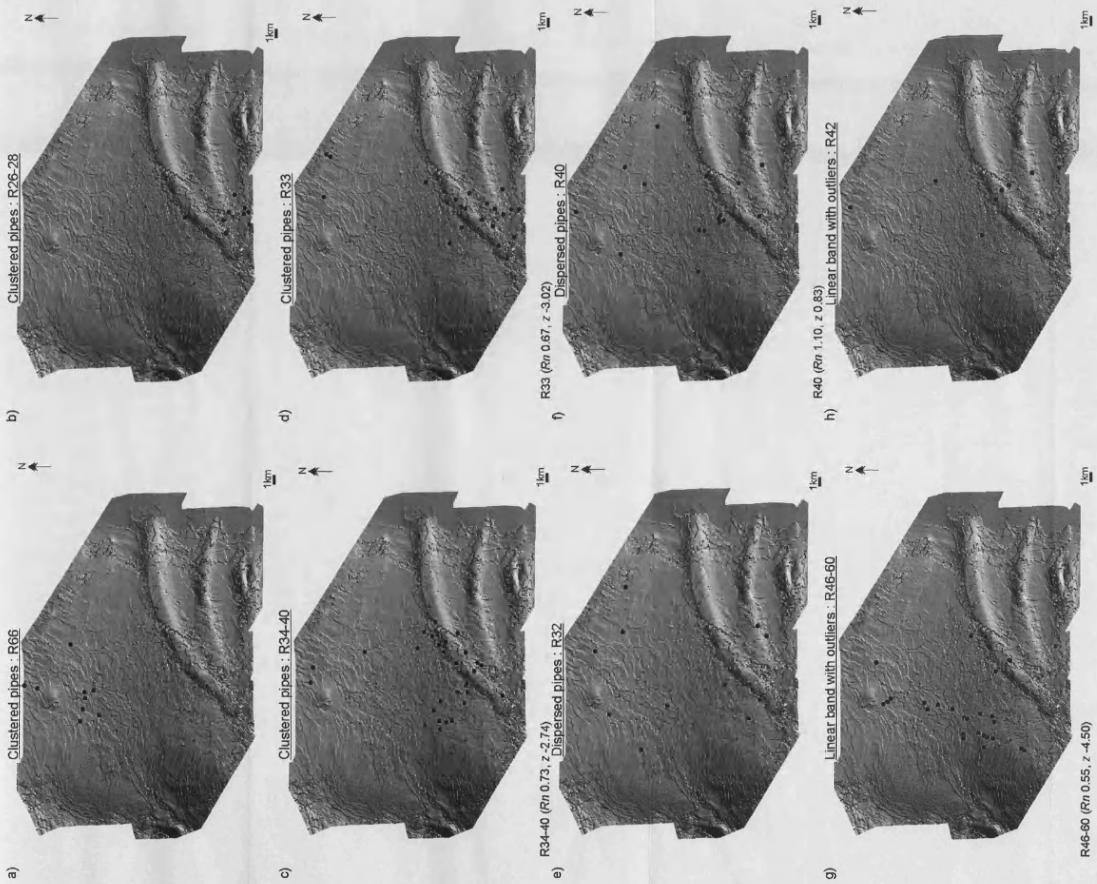

Figure 5.8 Spatial distribution of individual time periods. a) Clustered pipes forming during time period R66. b) Clustered pipes forming during time period R26-28. c) Clustered pipes with outliers forming during time period R34-40 (timing histogram peak). d) Clustered pipes with outliers forming during time period R33 (timing histogram peak). e) Dispersed pipes forming during time period R32. f) Dispersed pipes forming during time period R40. g) Linear band of pipes with outliers forming during time period R46-60 (timing histogram peak). h) Linear band of pipes with outliers forming during time period R42.

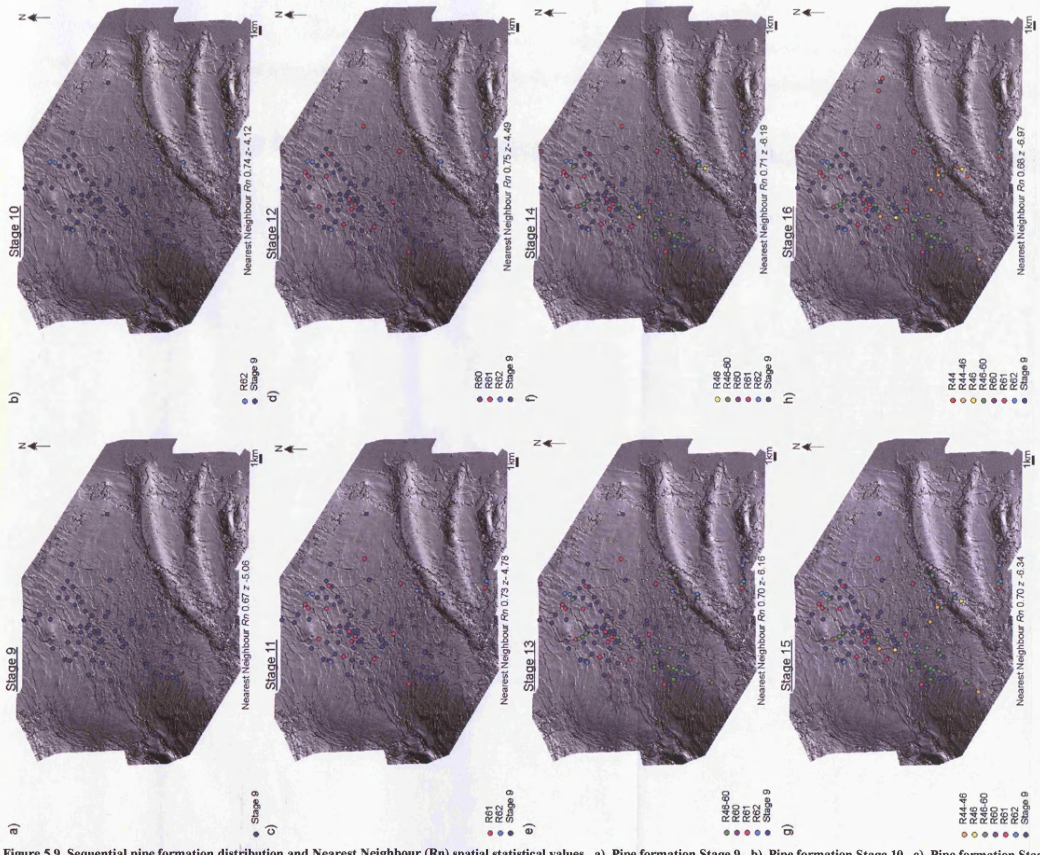

Figure 5.9 Sequential pipe formation distribution and Nearest Neighbour (Rn) spatial statistical values. a) Pipe formation Stage 9. b) Pipe formation Stage 10. c) Pipe formation Stage 11. d) Pipe formation Stage 12. e) Pipe formation Stage 13. f) Pipe formation Stage 14. g) Pipe formation Stage 15. h) Pipe formation Stage 16. Sequential pipe distributions show new forming pipes occupy space between existing pipes in addition to expanding the total pipe coverage by colonising outlying areas.

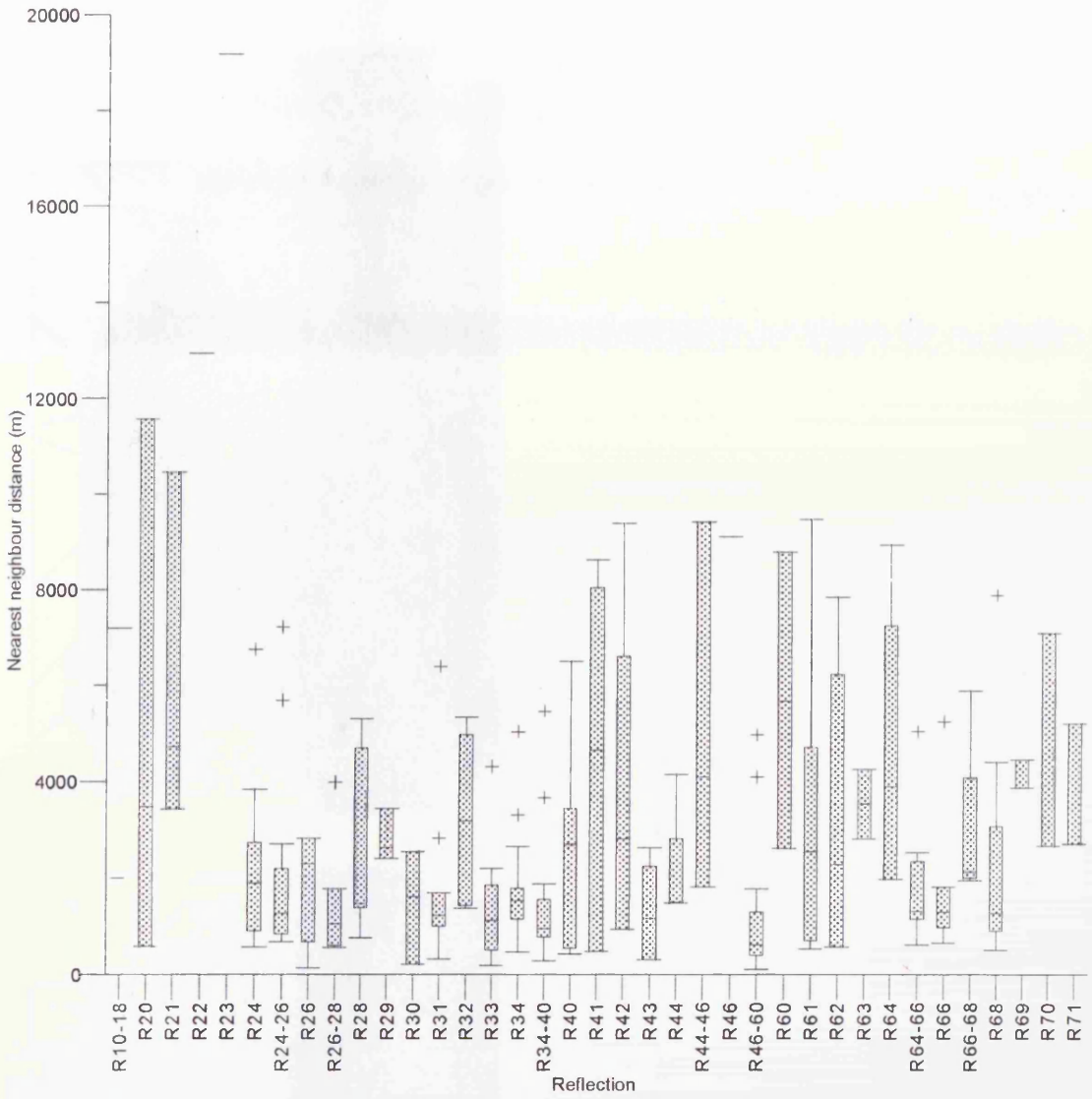

Figure 5.10 Nearest neighbour distance box plots. Box plots display the range of distances between an individual pipe and its nearest neighbour forming during a single time period. The lower and upper lines of the "box" are the 25th and 75th percentiles. The distance between the top and bottom of the box is the inter-quartile range (IQR). The line in the middle of the box is the sample median. The majority of reflections display a skewness in the range of nearest neighbour distances i.e. the median is not centred in the box. The whiskers show the extent of the nearest neighbour distances (unless there are outliers). An outlier (cross) is a value that is more than 1.5 times the IQR away from the top or bottom of the box. Reflections containing only 2 pipes are represented by a line.

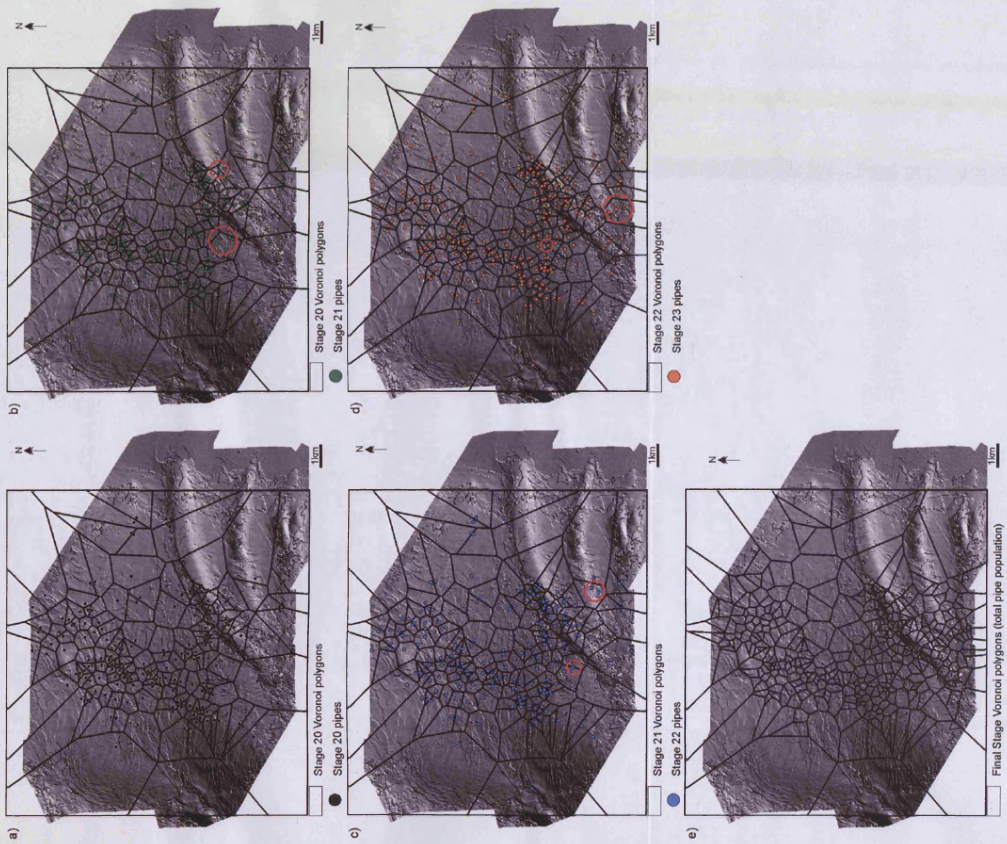

Figure 5.11 Voronoi polygons. Voronoi polygons were constructed for each pipe formation stage. a) In each individual stage, a Voronoi polygon contains a single pipe. b) Consecutively overlaying pipes formed in the latest stage (e.g. Stage 21) with Voronoi polygons from the preceding stage (e.g. Stage 20) displays a spatial pattern of available space for pipe formation with consideration of existing pipes. b), c), d) display a pattern of pipe formation within existing Voronoi polygons (solid circle) and at maximum distance from existing surrounding pipes (dashed circle). e) Stage 37, Voronoi polygons for the current total population of pipes. Boundary conditions have produced anomalously large edge polygons.

The individual increment plots (Fig. 5.8) show that a maximum of 29 pipes (R34-40) and a minimum of 2 (R10-18, R22, R23 and R46) formed during a single measurable time interval. For each time interval, the spatial distribution of pipes can be roughly categorised into clustered, clustered with outliers, dispersed, linear and linear band with outliers (Fig. 5.8). The low frequencies of pipe formation per time interval prevent robust statistical sampling, however *Rn* values have been calculated for those intervals with the largest frequency values (see Fig. 5.8). Some of these demonstrate clustering behaviour and are statistically significant at the 99 % level (intervals R34-40 (*Rn* 0.73, *z* -2.74), R33 (*Rn* 0.67, *z* -3.02) and R46-60 (*Rn* 0.55, *z* -4.50)) whilst others (e.g. R40 (*Rn* 1.10, *z* 0.83)) show no statistical clustering and are randomly distributed. The most frequently observed spatial distribution of pipes per increment is either dispersed or clustered with outliers. Figure 5.8 supports the qualitative assessment that pipes forming during the same time interval do not share a common pipe base datum.

The nearest neighbour distances of newly forming pipes are assessed for each individual time interval (Fig. 5.10). Minimum stand-off distances or nearest neighbour values range between 150-300 m. Of the 4 examples within the population, only a single conjoined pipe i.e. 2 pipes sharing a common pipe wall, is observed to form during the same time interval. This conjoined pipe is excluded from the analysis. The average distance between newly forming pipes are often lower than the median value, but maximum values are far in excess of the 75th percentile for individual time increments (Fig. 5.10). In summary, for a given time increment, the majority of newly forming pipes do not form in close proximity with one another.

The spatial positioning of newly forming pipes relative to existing pipes is expressed in Figure 5.9. The cumulative plots comprise a series of 37 incremental growth stages (younging from stage 1 to stage 37), of which, only a selection of these are shown to demonstrate some of the key observations. At stage 9, previously formed pipes (R63, R64, R64-66, R66, R66-68, R68, R69, R70 and R71) were scattered throughout the north and west of the study area (Fig. 5.9a). Newly forming pipes in stage 10 have formed within this area, but also formed as outliers in the south of the study area (Fig. 5.9b). Stage 10 (new pipe formation population at R62) is the first

stage to display pipe formation associated with the palaeochannels. Stages 11 and 12 continue the pattern of infill and spatial expansion, mainly in the northwest of the study area. With the exception of stage 15, pipe formation stages 13, 14 and 16 are also associated with the palaeochannels. Stages 13 to 16 represent the start of a considerable extension of pipe formation into the southern part of the study area when compared with previous pipe formation patterns (Fig. 5.9). In general, the pipes display modes of infill and expansion of the population as it accumulates pipes through time. Newly formed pipes occupy areas in between existing pipes and also expand the areal extent of the total population by penetrating the succession in outlying areas. I also observe that newly forming pipes rarely form in close proximity to pipes which formed in the immediately preceding stage, but are nearest neighbours with pipes which formed several stages previously.

Nearest neighbour (*Rn*) values were calculated using equation (1) (see Chapter 2) for the spatial distribution of pipes from Stage 9 onwards (thereby ensuring a statistically significant population size). Calculated *Rn* values range between 0.67 and 0.75 (Fig. 5.9). Since *Rn* values closer to 0 are equated to true clustering, and those closer to 1 as a truly random distribution, this observed range can be interpreted as a relatively weak tendency towards clustering. This statistic was subjected to a large search area to encompass the dispersed pipe distributions (see limitations in methods Chapter 5), and it is likely that more narrowly defined search area would yield *Rn* values closer to 1. These spatial statistics support the notion that sequential pipe formation is spatially sporadic. Additional pipes are not producing clusters within the population or creating a more random distribution of pipes.

Finally, Voronoi polygons were constructed for each incremental stage. Voronoi polygons are areas around each pipe with the unique trait that the distance inside the polygon is closer to that pipe than the pipe in the neighbouring polygon (Fig. 5.11a) (Dirichlet, 1850; Voronoi, 1907; Okabe et al., 2000). Voronoi polygon analysis has the ability to establish whether pipes are preferentially forming at the maximum possible distances from any pre-existing pipes, with the implication that there is a spatial ordering to their distribution. If this was true, then newly formed pipes are expected to be positioned on the Voronoi polygon boundaries.

It is evident from the sequential distribution of Voronoi polygons that there is no spatial control on the location of newly forming pipes. New pipes can be seen to have formed equidistant from pre-existing pipes but also within Voronoi polygons (Fig. 5.11b, c, d). There is no statistically significant relationship between the size of the final stage Voronoi polygons (all 366 pipes, Fig. 13e) and TP1, pipe height or diameter. The artificial boundaries on the perimeter polygons produce anomalously large polygons but it is evident that each individual pipe has a unique Voronoi polygon size and the polygons are not arranged in a uniform pattern.

5.5 Discussion

5.5.1 Pipe Genetic Model

Our preferred spatio-temporal framework for Namibian pipe formation is that of intermittent and persistent formation through time with a pipe distribution that can be generalised on two scales. At the larger scale the distribution exhibits two broad zones of pipe formation (TP1), an older zone in the North and West and a younger southern zone (Fig. 5.7). On a more local scale pipe formation is sporadic, forming as both clusters and outliers at the same time.

These key observations and interpretations raise important questions regarding pipe genesis. For example, what types of geological conditions trigger pipe formation, such that it persists for perhaps 5-10 M yrs? Why is there no obvious episodicity over time periods longer than that resolved by the sequential seismic reflections? Why is there a general shift in pipe formation from north and west to the south? Finally, how do existing models for pipe formation best equate to these observations? This chapter goes some way towards tackling these sorts of questions however it is evident that further research in this area is required to fully understand the relationship between geological triggers, spatio-temporal distribution and pipe formation.

Previous models for pipe formation share a common theme: namely, that they result from a cycle of pressure build-up and release in a shallow source region. It is considered that a pressure anomaly in a source region will lead to overpressure development and subsequent hydraulic fracturing in the overburden once pore pressures exceed the failure condition (Cartwright et al., 2007). Fracture dilation and vertical propagation towards the seabed follows seal breach as flow self organises. A hydraulic connection is established at the seabed, reducing pressure and resulting in a violent burst of escaping fluids forming a pockmark or crater (Berndt et al., 2003; Løseth et al., 2003; Ligtenberg, 2005; Hustoft et al., 2007; Judd and Hovland, 2007). The following sections of this discussion are based on the adoption of this genetic mechanism. As mentioned in the Introduction (Chapter 5), other models of pipe formation have been proposed in areas of evaporite or carbonate dissolution, or in areas of hydrothermal activity, but neither of these is considered plausible in the Namibe Basin in the past 10 M yrs.

How then, do we specifically relate the geometrical observations of pipes in the study area to the question of timing and of genesis? The majority of previous models explaining pipes as due to pressure release and fluid escape invoke a single episode of highly focused fluid escape. Cartwright et al. (2007) referred to this type of pipe as a 'blow out' pipe to convey this model of an initial high flux release of fluid, driven by high overpressure. If vented to the seabed, such an episode of fluid expulsion can lead to pockmark formation with often significant erosional truncation of sediments close to the seafloor. This is the most likely scenario for TP1 in this genetic model. Time Point 2 (TP2) is defined as a position of infill of relief of the depressed reflections located at the top of the pipe. What then, is the relationship between TP1 and TP2? This interval is clearly subject to seismic interpretational uncertainty (Fig. 5.7c), but it is also open to at least two alternative genetic explanations. It clearly represents a period post-dating initial pockmark formation and pre-dating the final stage of fill, but how can the vertically stacked gently concave upwards reflection geometry be explained? Two end member interpretations are tentatively suggested:

1. The reflections between TP1 and TP2 represent evidence for vertical seepage following pipe formation, including the possibility of vertically stacked pockmarks.

2. The deposition of dominantly hemipelagic or pelagic units following initial pipe formation results in a persistent drape of the original pockmark morphology until the depression in the palaeo-seabed is topographically healed.

Chapter 4 presented evidence in the form of localised columnar amplitude anomalies and measured variations in the concave reflection geometry between TP1 and TP2 to suggest possible post-formation fluid seepage. However, this seepage would have to be surprisingly uniform and long lived to give rise to the observed reflection geometries. As an example, in Pipe 9, there are 22 concave upwards reflections (c. 250 m) between TP1 and TP2, and at an average sedimentation rate of 40 m/My, seepage would need to remain active (either episodically or persistently) for over 6 My. Even if the maintenance of this concave upward reflection geometry was through low frequency, low magnitude, seepage promoting the winnowing of fines from the palaeo-seabed depression, the scale of a system required to maintain this level of activity is unclear.

Conversely, persistent drape could produce the resultant geometry without requiring any perpetuation of the focusing of fluid escape up the pipe. However, this explanation fails to explain the distinct infilling at or close to TP2 for many pipes, and the presence of amplitude anomalies both within (between TP1 and TP2) and above the pipe. The significance of this upper section of the Namibian pipes thus remains unclear and these two explanations must therefore remain speculative. Chapter 6 further develops the arguments presented here, utilising a higher resolution dataset from the Nile Deep Sea Fan, to illuminate the zone above TP1.

5.5.2 Fluid Sources

The large number of pipes within a relatively small area offshore Namibia advocates that a large potential for fluid generation existed within this part of the basin. This is perhaps not surprising when it is considered that the Kunene River did not build a delta during the Neogene, but instead fed its sediment load directly onto the mid-lower slope of the Namibe Basin (Aizawa et al., 2000). The largely low amplitude,

but partially channelised acoustic character of (upper) Post Rift 2 is strongly suggestive of a mid-dominated depositional system, and its progradational-aggradational geometry accords well with this concept of a diverted sediment load from the Kunene (Goudie, 2005). The rapid deposition of organic rich fine grained sediments of the 'displaced' delta would have been ideal for generation of excess pore pressure.

The Namibian pipe population described here provide much indirect evidence that their formation is linked to gas migration. Amplitude anomalies indicative of shallow free gas are common throughout the area (Figs. 5.1 and 5.4), and amplitude and velocity anomalies are abundant within and adjacent to the majority of the pipes (Figs. 5.1 and 5.4). It is therefore possible that in addition to disequilibrium compaction arising from the Kunene depositional system, gas generation may also play a role in pressure development (Osborne and Swarbrick, 1997). It is also possible that pressures were only built up locally through accumulation of gas into columns of sufficient height to exert a significant buoyancy pressure (Tréhu et al., 2004).

I was unable to determine the source of the fluids involved in pipe formation in the study area. The majority of the pipes transect the Post Rift 3 : Post Rift 2 boundary suggesting that a substantial fluid source exists within Post Rift 2 or deeper. The deepest pipes can be traced < 1500 m below seabed but deeper detection is prevented by the low amplitude, discontinuous and chaotic nature of Post Rift 2. At these minimum depths, pressures and temperatures, any gas in the system could be either biogenic or thermogenic methane.

The upper temperature limit for biogenic gas generation is debated (Whiticar, 1999; Holm and Charlou, 2001; Sleep et al., 2004; Kieft et al., 2005; Lollar et al., 2006; Roussel et al., 2008), but is commonly taken as c. 70 °C. Using present day temperature gradient data from the Walvis Basin, this would equate to a sub seabed depth of c. 2000 m. This would restrict biogenic methane generation to Post Rift 3 and the upper portion of Post Rift 2. Biogenic gas generation is common in the slope sediments along the west African margin (Cunningham and Shannon, 1997), and the organic content of the slope sediments of the Namibe Basin is likely to be reasonably

high due to the sourcing of this sediment wedge from the Kunene River with its large equatorial catchment (Fig. 2.4). Potentially enriched source regions for biogenic gas generation include the slope channel fills at the top of Post Rift 2 and gas hydrates within Post Rift 3.

Thermogenic gas has been encountered in a number of exploration boreholes further south in Namibia (Cartwright et al., 2008), and basin modelling studies indicate that Cretaceous source rocks in the Namibe Basin could certainly be in the gas generative window (Holtar and Forsberg, 2000). Direct (thermogenic) hydrocarbon indicators are observed in the Transitional / Post Rift 1 interval and the likely source interval for thermogenically generated hydrocarbons (Syn Rift Sequence). The onset of overpressure generation is generally thought to start c. 3000-4000 m below seabed in most basins (Swarbrick and Osborne, 1996). This would place the overpressure generation window or "transition zone" (Swarbrick and Osborne, 1996) below the Post Rift 1 mound and firmly within the Syn-Rift and Transitional intervals. Both suggestions must remain highly speculative because of the poor seismic resolution in Post Rift 2.

5.5.3 Spatio-temporal pipe formation

The spatial distribution of pipe formation is highly variable. In contrast, the timing of pipe formation is persistent throughout a long period, possibly extending to 5-10 M yrs. It is not possible to demonstrate synchroneity in the timing of pipe formation, although up to 24 pipes have formed within a single reflection, suggesting that they may have formed within 100-200 ka. It is evident therefore that any mechanism for generating anomalous pressure must have occurred many times in the overall period of pipe development and suggests a repetitive overpressure and release system.

The spatial analysis of pipe formation has established that there are two statistically significant broad zones of pipe formation, an older zone in the North and West and a younger, southerly zone. The distinction of two broad timing zones of older and

younger pipes is suggestive of a pressure generative process that migrated with time, either in the same general stratigraphic interval (Hunt, 1990), or in intervals of markedly contrasting source depth (England, 1987). It is also conceivable that each pipe has its own fluid generation (and subsequent overpressure) cell, but this is considered less likely because there are clear clustering phenomena at work at least in some of the pipe forming increments (Fig. 5.7). In the absence of much clearer data for the depth of origin of the pipes, this uncertainty in the likely organisation of putative pressure cells is inevitable, but the data do at least indicate that pipe formation migrates on a semi-regional basis, and this alone gives some clues for further research into pipe genesis.

The long term temporal migration of pipe formation on a semi regional basis implies a large-scale spatial control on the location (and possibly timing) of overpressure generation and pipe formation. This control would need to have a minimal spatial coverage of ~900 km^2 and a possible maximum coverage at a basinal scale. Basin scale influences on pipe formation include, but are not restricted to, possible hydrocarbon generation, the location of primary source rocks, degree (and any lateral direction) of primary migration, location of over pressure generation leading to primary or secondary migration, location of biogenic gas generation, subsidence patterns or sedimentary loading patterns. Our preferred model for the long term basinal controls on pipe formation in the Namibe Basin include those factors directly and indirectly relating to deep fluid sources.

Although the evidence suggests a broad scale basinal control on pipe formation over a longer time scale and an implied repetitive overpressure and release system, the evidence from a local scale suggests that pipe formation in the short term is more erratic, and not subject to any obvious, seismically resolvable structural controls. The incremental analysis of pipe formation indicates that over short time periods (c. 100-200 ka), 1) pipes form in both clusters and outliers often at great distances from one another, and 2) pipe formation takes advantage of the available space between existing pipes and colonises frontier locations. I interpret this as evidence of primary localisation phenomenon that is partially independent of the gross regional controls. Pipe formation in the available space amongst existing pipes suggests a spatial control which is common to all pipes forming in a specific area

regardless of formation time. In contrast, the colonisation of frontier locations is suggestive of an independent formation process which is spatially distinct from the other pipes. Based on the spatio-temporal analysis I conclude that pipe formation in the study area is the result of both basinal and local controls.

At any specific location within the study area I infer the spatio-temporal pattern of pipe formation to result from a combination of processes operating at both the basinal and local scales. The interaction of these two superimposed, synchronous and symbiotic spatial systems is responsible for the spatio-temporal evolution of pipe formation within the Namib Basin. At the broadest scale, fluid is generated and primarily migrated within the basin. The location of this broad scale control appears to move (North to South) over time. It is inferred that either a) the fluid migrates from a deep fluid source (primary migration has been discovered to occur over large km-scale distances), b) the location of widespread overpressure generation in a deep fluid source changes through time, or c) fluid is generated (and "overpressured") in (c. 2?) different locations at different times. At the more local scale, a multitude of factors interact to determine more specifically where and when pipe formation occurs. Factors which include sediment permeability and porosity, seal strength and heterogeneities in the seal permeability, overpressure build-up, fluid flux into the reservoir or fluid generation rate, high permeability migration routes or sealing features i.e. faults. These factors vary on a local scale and combine to produce locally independent pressure cells.

5.5.4 Conceptual model

Overpressure variations within individual pressure cells may be caused by complex geological structures, sub seismic faults providing barriers to lateral flow or low permeability units inside the cells acting as barriers to the migration of fluids. Pressure generation, lateral dissipation and vertical sealing will influence the distribution of the individual pressure cells. It is anticipated that lateral flow patterns will, to a large extent, govern the magnitude of the overpressure and if a considerable rapid change in overpressure occurs in one pressure cell e.g. as a result of fluid

generation or migration, the dissipation rates across cell boundaries will increase (Borge, 2002). This has implications for the spatial positioning of pipes. The pressure dissipation in one cell following the formation of a pipe may be transmitted to surrounding areas or cells reducing overpressure generation capabilities thereby preventing pipe formation in close proximity to the newly formed pipe. This spatial and temporal pattern is observed within the spatio-temporal analysis. Sequential pipe formation has shown that a new generation of pipes will form at a distance from existing pipes, and will rarely become the nearest neighbours to the pipes in the preceding time interval. Borge's (2002) modelling, despite omitting fluid expansion as an overpressure generation mechanism, has shown that hydraulic leakage in one pressure cell tends to prevent similar leakage in the pressure compartments nearby due to fairly high lateral connectivity. This concept is further developed in Chapter 7.

Within this conceptual model a multi-tiered, hierarchical system is in place permitting pressure redistribution post-dating its generation. Deep sourced, basin wide, fluid generation and/or migration into shallower, locally independent, pressure cells are envisaged. Pipe formation is intermittent and persistent through time, and the focus of the fluid source can shift with time, redistributing overpressures and varying pipe formation locations. This concept is not novel. Geological sections with multiple transition zones have previously been envisaged by Swarbrick and Osborne (1996). This research validates assumptions that periods of high overpressure interspersed with normal or reduced amounts of overpressure are typical phenomena and that the width of the transition zone can change with time (Swarbrick and Osborne, 1996).

5.6 Conclusion

A total of 366 pipes are distributed in a horseshoe pattern in the centre of a 3D seismic dataset from North Namibia. A spatio-temporal framework utilising spatial statistics was constructed to analyse the spatial and temporal distribution of pipe

formation. The outcome from this spatio-temporal analysis can be summarised as follows;

- An arbitrary chronostratigraphic timescale has shown the timing of pipe formation to be both
    - Intermittent; between 2 and 26 pipes formed during a single or group of reflections (approximately 100-200 ka).
    - Persistent; pipes are observed to form throughout a 5-10 My interval (Neogene).
- The Namibian pipes did not form at the same time, nor was their formation restricted to specific time intervals.
- The pipes are not uniquely related to the up dip limit of structures or underlying stratigraphic units.
- The pipes are anti correlated with the mound apex in Post Rift 1, a classic structural trap in the form of a four way dip structure. Pipes have formed around the perimeter of the mound leaving the fold crest devoid of fluid flow features.
- Pipes with a common basal reflection or structure e.g. palaeochannel levee, do not form at the same time.
- Spatio-temporal pipe formation is neither clustered nor regular i.e. pipe formation is neither clustered or regularly (evenly) spaced in time and space.
- In an individual time period (c. 100-200 ka) pipe formation can be clustered, dispersed or linear.
- The large scale distribution of pipe formation displays two broad zones, an older North : West zone and a younger southern zone.
- At a local scale pipes can form as both clusters and outliers within the same time interval.
- Sequential pipe formation analysis has established that newly forming pipes take advantage of free available space between groups of existing pipes but also colonise new areas at a large distance from the main group.

- New generation pipes are not nearest neighbours with pipes in the immediately preceding time interval, but form in closer proximity with pipes several time intervals older
- The Namibian pipes display no uniform spatial ordering to their formation i.e. newly forming pipes do not form at a maximum equidistance from existing pipes.
- A conceptual model is proposed in which pipe formation results from isolated pressure cells that are locally independent yet broadly controlled.

Chapter 6

This chapter will be submitted for publication as Moss, J.L., and Cartwright, J., 2010, "Vertically stacked pockmark arrays: Evidence for highly focused, episodic fluid flow in sedimentary basins" to Marine and Petroleum Geology. Currently seeking permission to publish.

The work presented in this chapter is that of the lead author (JLM), editorial support was provided by the project supervisor (JAC) in accordance with a normal thesis chapter.

6 VERTICALLY STACKED POCKMARK ARRAYS: EVIDENCE FOR HIGHLY FOCUSED, EPISODIC FLUID FLOW IN SEDIMENTARY BASINS.

6.1 Abstract

A group of large (100-700 m diameter) buried pockmarks from the Rosetta Region of the Nile Deep Sea Fan have been analysed in terms of their time of formation and longevity of post formation fluid migration. This study has shown that pockmark-like morphology of concave upwards reflections above a buried pockmark can result purely from drape-type deposition failing to infill the initial seabed crater, leaving vestigial relief. Definitive evidence is presented showing that this conduit can remain viable after lengthy periods of dormancy, and can be reactivated if the hydrodynamic conditions require a renewed phase of focused fluid expulsion (and pressure bleed-off). These conduits are interpreted as "pockmark arrays" and not stacked pockmarks. Chronostratigraphic dating has confirmed buried pockmark formation in the study area between 100,000 yrs BP and 15,000 yrs BP. The majority of buried pockmarks are observed to form at a single horizon, which arbitrary chronostratigraphic dating estimates to be c. 50,000-80,000 yrs BP. The formation of these large pockmarks is believed to result from a single triggering mechanism, possibly associated with eustatic sea level fall, releasing fluids trapped beneath a shallow level Mass Transport Deposit (MTD). Numerous (> 150) clustered unit pockmarks (10-20 m diameter) within the seabed expression of the pockmark arrays (depressions) are testament to a high frequency, low magnitude post formation fluid migration through these conduits. The longevity of post formation fluid migration is measured by the presence or absence of unit pockmarks and the

height of the pockmark array. Longevity is estimated to be ~50,000-100,000 years in this part of the Rosetta complex.

6.2 Introduction

Pockmarks are circular to elliptically shaped, erosional depressions formed at the seabed by the localised expulsion of fluid from an overpressured source at depth via a low permeability pathway or pipe (Hovland and Judd, 1988). Pockmarks are therefore a valuable expression in the stratigraphic record of localised pore fluid overpressure generation and vertical fluid migration during a geologically rapid time interval, and their identification can shed light on basin hydrodynamics.

However, one of the least understood aspects of pockmark formation is the precise timing of formation and the longevity of the fluid migration associated with the feeder pipe and the pockmark. A number of open questions can be considered: for example, do pockmarks form instantaneously by a catastrophic flux of fluid or gas to the seabed, or do they form by slower, longer term seepage processes? Once formed, do the conduits that supplied fluid/gas to the seabed at the pockmark retain their potential for focusing fluid flow thereafter, and under what conditions does any later activity through the conduit occur? How do we recognise and correctly interpret evidence for rejuvenation of a pockmark conduit on seismic data?

A number of previous studies have implied that vertical stacking of pockmarks at a number of discrete stratigraphic intervals is evidence for repeated fluid expulsion using the same conduit (Çifçi et al., 2003; Curzi and Veggiani, 1985; Hovland and Judd, 1988; Mazzotti et al., 1987)*. This evidence commonly consists of an initial (basal) pockmark identified on seismic sections, with a series of similar shaped (concordant) concave reflections developed above this basal surface. This specific reflection geometry has been argued to suggest a longevity of the fluid expulsion process responsible for the initial pockmark formation.

* see Appendix A4 for examples of buried and stacked pockmarks

This chapter presents some examples of vertically stacked pockmarks from the Nile Deep Sea Fan (NDSF) imaged on ultra high resolution (UHR) 2D seismic profiles, and uses these to analyse the evolution of fluid flow to the seabed in this region (Fig. 6.1). I show that vertical stacking of concordant concave reflections above a basal pockmark surface is not, by itself, an indication that successive pockmarks formed above the same conduit. I also provide evidence from a combination of side-scan sonar and Chirp profiler data gathered with AUVs (Automated Underwater Vehicles) calibrated with the high resolution seismic profiles that the same conduit can be re-utilised for a considerable period of time after initial pockmark formation to produce a younger generation set of pockmarks nestled vertically above the basal pockmark.

This study has a number of wider implications for how stacked pockmarks are interpreted on seismic data, and also for the plumbing system at shallow levels within slope depositional settings. This study also helps explain recent features of stacked concave reflections observed at shallow levels above pipe-like fluid expulsion conduits identified using 3D seismic data (Chapter 4).

I follow previous studies in adopting a classical overpressure model for pockmark formation (Cathles et al., 2010; De Boever et al., 2009b; De Boever et al., 2006b; Heggland, 1998; Hovland, 2002; Hovland et al., 2010; Hovland et al., 1984; Judd and Hovland, 2007; Nyman et al., 2009). I use the standard definitions for "normal pockmarks" (> 50 m diameter) and extend the definition of "unit pockmarks" to refer to small pockmarks < 20 m diameter. Normal pockmarks are thought to result from periodic, rapid gas flow eruptions, which are subsequently sealed by Methane-Derived Authigenic Carbonate (MDAC) (Hovland, 2002). According to standard definitions, unit pockmarks are inferred to be the result of cyclic pore-water seepage as either "singular" features or "related" features forced to migrate away from the sealed centre of a normal pockmark to edge or rim localities (Hovland et al., 2010). Unit pockmarks are suggestive of episodic seepage of a high frequency, low magnitude fluid flux, compared to the low frequency, high magnitude flux associated with normal pockmarks. It is acknowledged that the influence of surface and near-surface sediment grade (permeability and erodibility) would contribute to the manifestation of seepage.

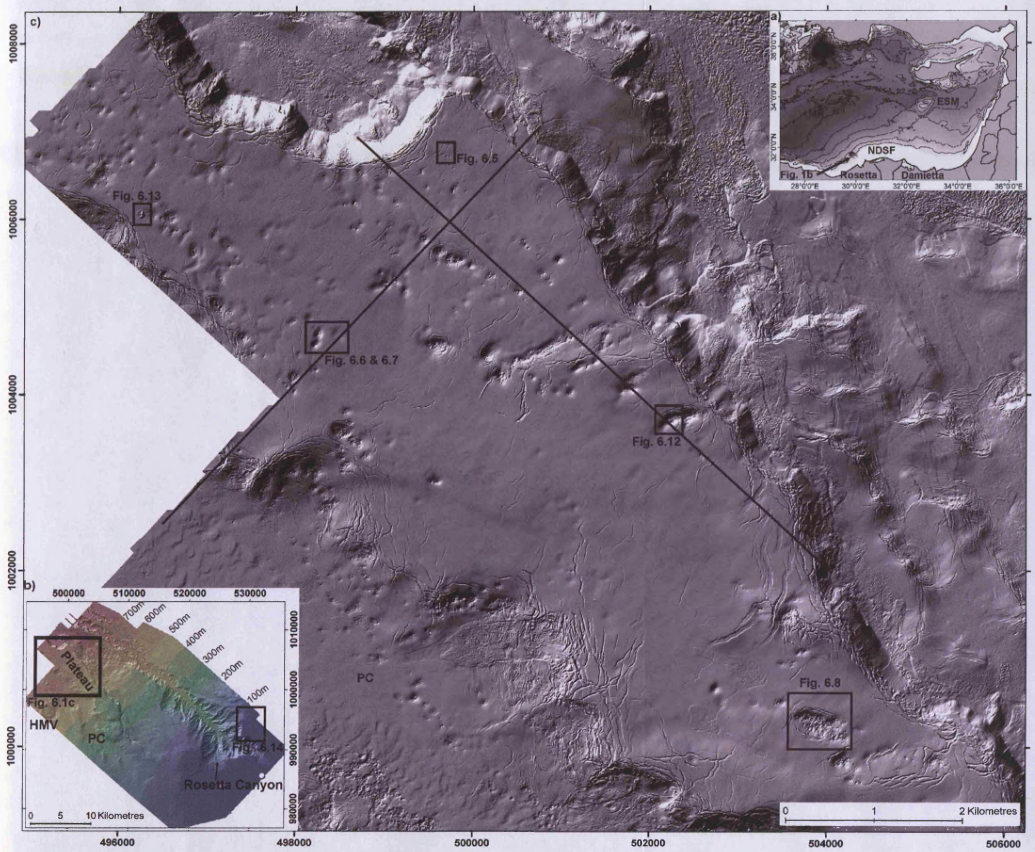

Figure 6.1 Location map. a) Location on Western NDSF, b) Rosetta bathymetry (metres), Horus Mud Volcano (HMV), Palaeochannel (PC), c) Plateau dip map showing location of figures and cross sections referred to in the text.

6.3 Geological setting

Regional geology and tectonic setting of the NDSF is given in Chapter 3

6.4 Seismic data and methodology

The data used for this study consist of ~1000 km^2 combined Autonomous Underwater Vehicle (AUV) sub bottom profiler (Chirp profiler) and side-scan sonar, and 2D Ultra High Resolution (UHR) seismic data collected by Fugro Survey, on behalf of BP, in 2004 and 2005 (see Chapter 2).

Seismic examples shown are restricted to those 2D seismic lines which pass straight through the centre of the unit pockmark / seabed depression.

6.4.1 Dating pockmark formation, chronostratigraphy and arbitrary chronostratigraphic dating

As previously defined in Chapter 4, buried pockmarks have been identified based on the erosional truncation of reflections onto a single concave upwards surface of stratal truncation. Seismic interpretation focused on the recognition and dating of the many small pockmarks in the Chirp profiler and side scan sonar data that were at or below the spatial resolution limit of the UHR profiles.

Dating pockmark formation relies upon correct identification of the erosional base of the pockmark. This is difficult to do with low frequency data, or when the pockmarks have diameters close to the spatial resolution limit. The age of the earliest onlap fill of the pockmark, or the earliest drape unit to be deposited on the pockmark erosional surface is taken as the approximate time for pockmark formation. It is common to see

localised high amplitude reflections associated with the pockmark surface, most likely due to authigenic carbonates (Judd and Hovland, 2007) and a considerable loss of signal directly beneath the pockmark surface due to scattering and localised velocity anomalies (Fig. 6.2).

Absolute dating of pockmark formation was not possible, but the seismic stratigraphy could be interpreted and referenced to three prominent horizons that have been dated chronostratigraphically using C^{14} methods (Fig. 6.2) from cores collected on behalf of BP in 2006 and extrapolated across the Plateau. Horizons are dated at 9,000 yrs BP (A200), 15,000 yrs BP (C0) and 100,000 yrs BP (D0). An arbitrary chronostratigraphic dating scheme was implemented following similar methodologies formally proposed in Chapter 5. Six well-defined horizons were identified and correlated throughout the study area to form an additional relative chronological framework between the chronostratigraphic dated horizons for the intervening time periods spanning c. 100,000 yrs (Fig. 6.2).

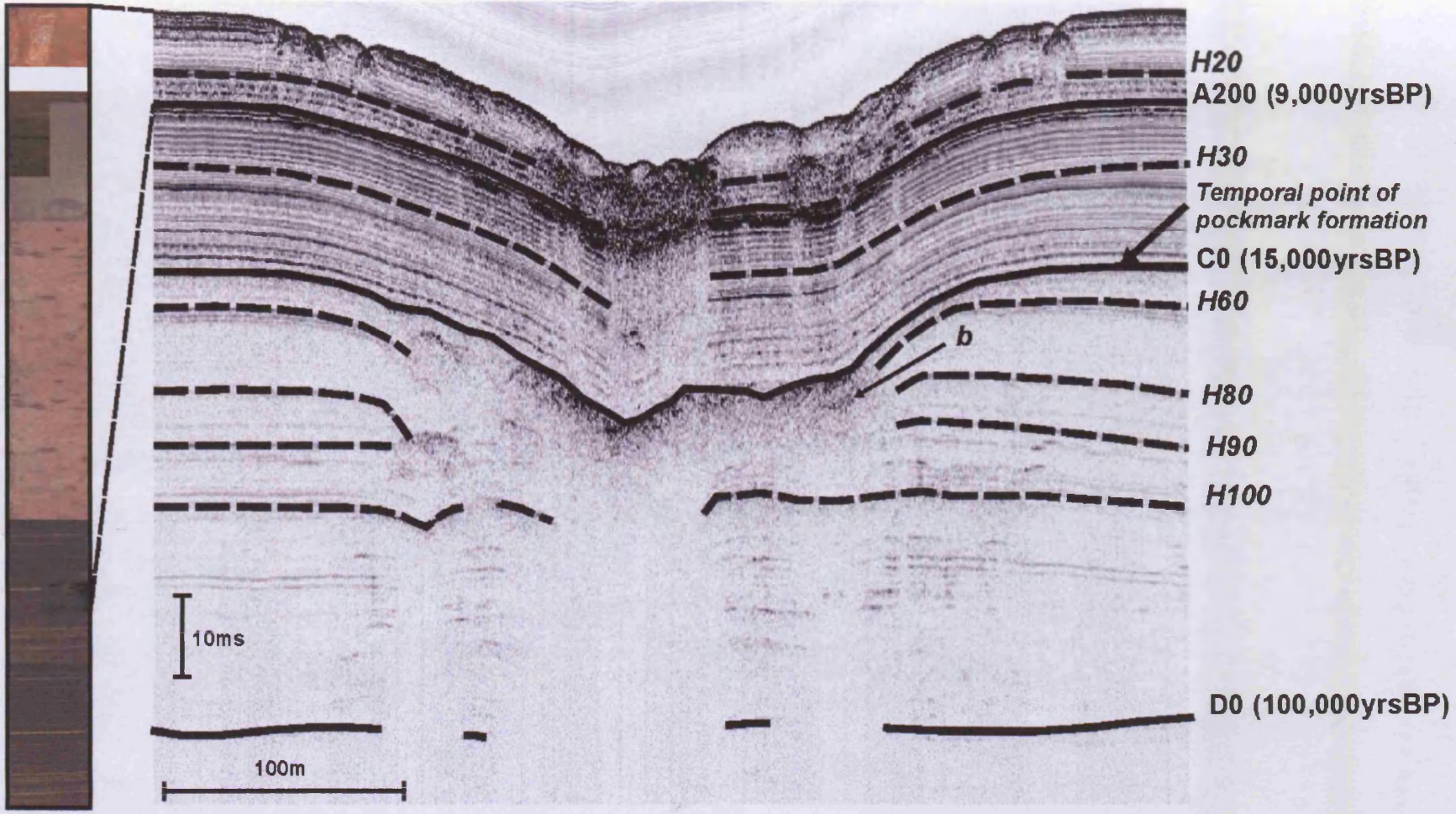

Figure 6.2 Chronostratigraphic dating. Chronostratigraphic age dates given in years BP (solid lines), arbitrary chronostratigraphic dated horizons (dotted lines). Example core taken from the top <20ms capturing horizon A200 (9,000yrsBP). Label b, anomalously high amplitude zone. The vertical resolution of the Chirp profiler data is captured from Seabed to D0 and is referred to in the text as Unit 4. Example shown is D117 (NE-SW transect).

6.4.2 Limitations

Buried pockmark formation timings are restricted to those pockmarks which are clearly imaged by an AUV line. Consequently only 20 % of identified pockmarks are arbitrarily dated. Buried pockmarks without a seabed expression are not included in the dataset as clear identification of the seismic expression as a pockmark (4-way dip structure) was not possible. Spatial statistics are highly susceptible to the precision of the coordinates in the point dataset and the mathematical boundary area imposed on the spatial analysis. The centre of the pockmark was used for the analysis, however this may produce anomalous results for elliptical shaped pockmarks. The mathematical boundary was a minimum enclosing rectangle thereby producing a tendency towards clustering.

6.5 Results

6.5.1 Regional setting

The Western Nile fan is a complex province of interacting channel, mass transport and fluid migration features (Loncke et al., 2009). The total area (~1000 km^2) of seismic coverage, hereafter referred to as the Rosetta Region, has been geomorphologically mapped to demonstrate the regional setting of the pockmarks (Fig. 6.3). A representative cross section is given in Figure 6.4. The Rosetta Region has been divided into zones based on the dominant geomorphological features in that area, and is briefly described below.

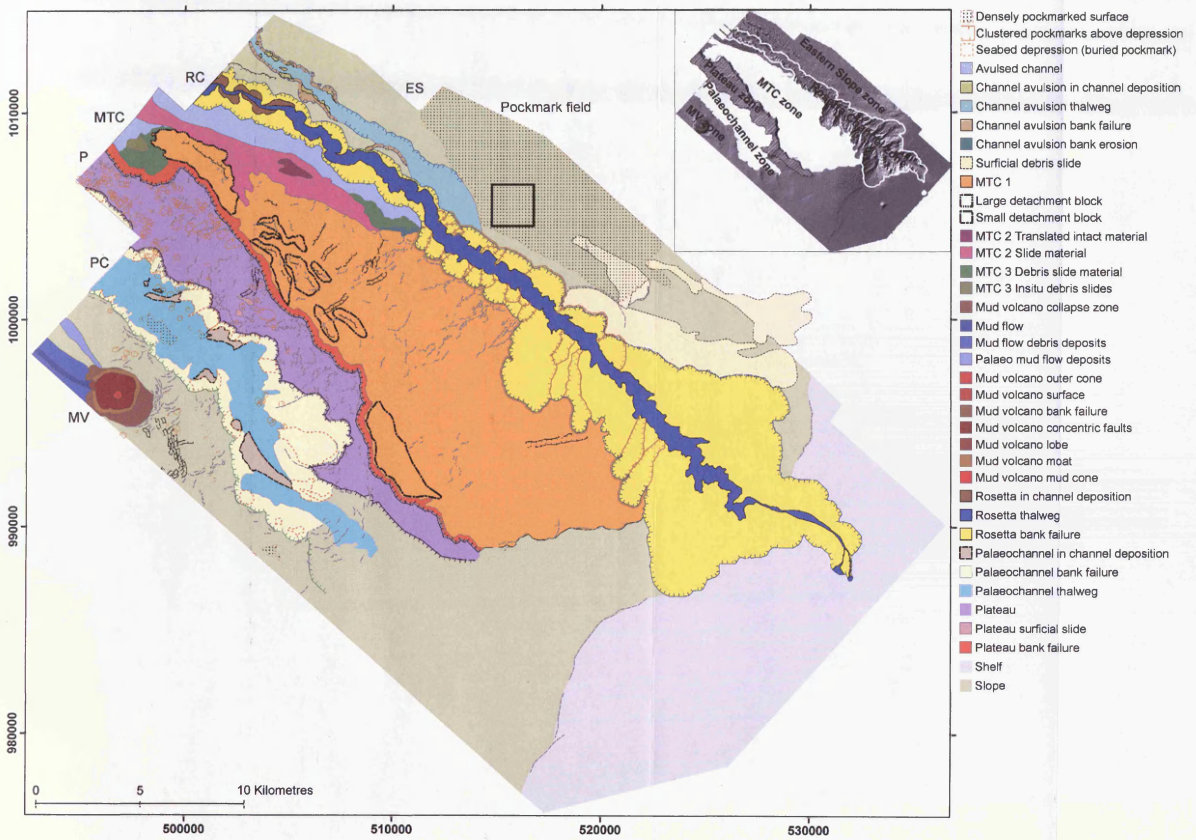

Figure 6.3 Geomorphological map. Broad geomorphological zones are shown. MV, mud volcano; PC, palaeochannel; P, Plateau; MTC, area of multiple MTC's; RC, Rosetta channel; ES, Eastern Slope including the pockmark field (Chapter 7) are shown in the inset map. Black box represents the spatial statistics study area utilised in Chapter 7. The entire Rosetta Region represents a relict topography. The majority of the features mapped are the surface expression of geomorphological features buried by drape.

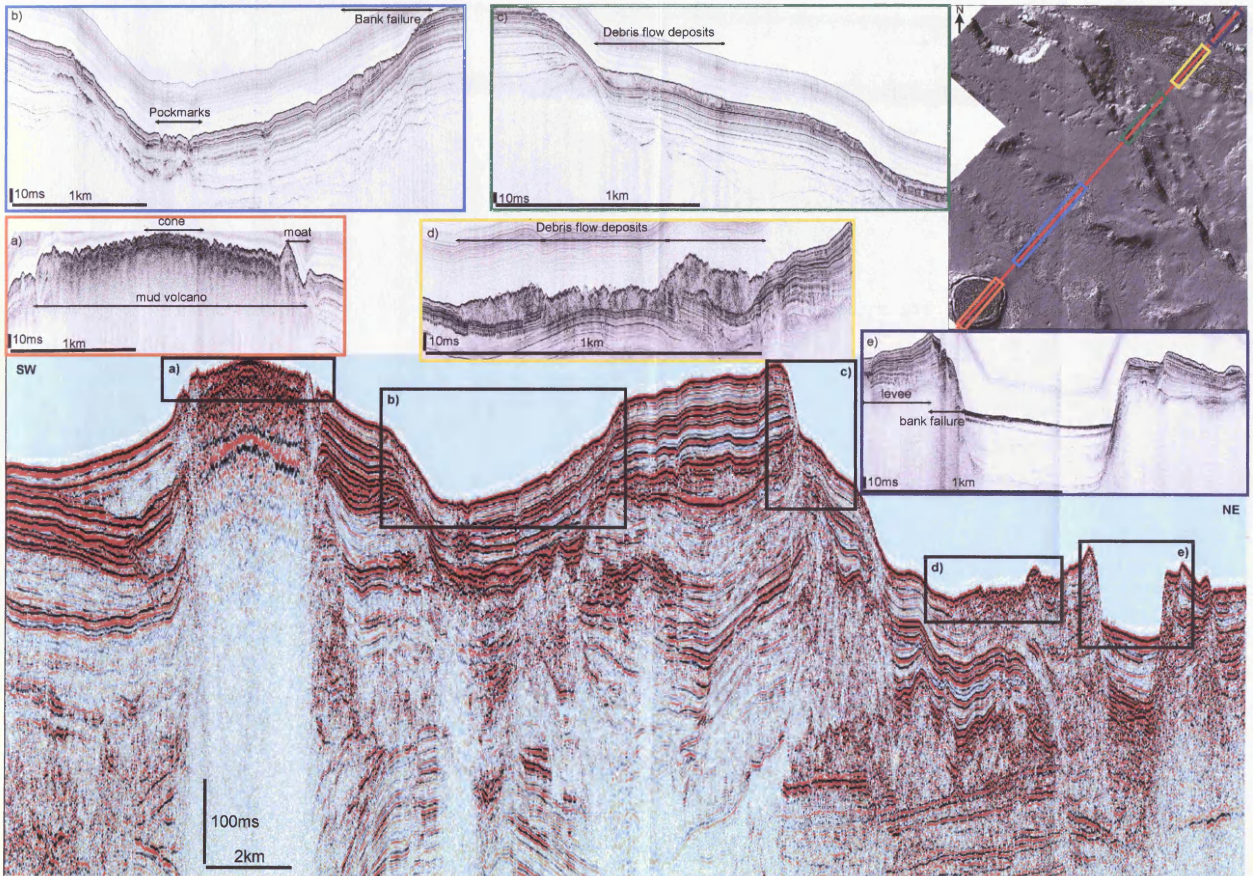

Figure 6.4 Cross section through the Rosetta Region showing a) mud volcano, b) palaeochannel, c) localised failures from the edge of the Plateau into the MTC zone, d) surfical debris flow material and e) Rosetta channel

6.5.1.1 Mud volcano zone (MV)

The western limit of the Rosetta Region is dominated by the Mud Volcano (Fig. 6.4). The mud volcano comprises a relatively flat, crenulated surface of radial concentric faults, surrounding a central cone. The mud volcano is surrounded by a moat which is breached at a single location by a mud flow. There is evidence to suggest that several generations of mud flow deposits are associated with the extrusive mud flow activity. The south-eastern margin of the mud volcano has collapsed and is marked by extensional faulting. Most of the faults have minor displacements of < 10 m.

The general slope area surrounding the Mud Volcano comprises localised normal faulting and isolated circular depressions and unit pockmarks. The circular depressions are interpreted as buried pockmarks (Chapter 6).

6.5.1.2 Palaeochannel zone (PC)

The palaeochannel represents a former position of the Rosetta Channel (Fig. 6.4). The palaeochannel is a relict feature delineated by marginal faulting and localised slope failures. The arcuate headscars of the rotational slope failures are lined with concentric tension cracks suggesting the failure maybe retrogressive. The palaeochannel bed contains surficial deposition from localised slope failures, buried pockmarks and surface pockmarks.

6.5.1.3 Plateau zone (P)

The Plateau zone is an undeformed section of slope which has remained vertically prominent by slope failures and erosion of the adjacent slope by the palaeochannel and Mass Transport Complexes (MTC) (Fig. 6.4). The Plateau is dominated by circular to elliptical depressions and unit pockmarks. The depressions represent buried pockmarks, and are often the loci for clustered unit pockmark formation (Chapter 6).

6.5.1.4 Mass Transport Complex zone (MTC)

This zone comprises multiple MTCs at varying depths and scales (Fig. 6.4). The zone is delimited by a large relict MTC which extends from the Plateau zone in the west to the Rosetta Channel in the east (MTC 1). MTC movement is likely to be in a downslope (north) and easterly trajectory towards the Rosetta Channel. The toe of the MTC appears to disintegrate into debris slides as it meets a former avlusion of the Rosetta Channel. There are fault scarps in a mid slide position, possibly indicating minor failures within the main slide body.

Large blocks of intact debris are observed on the Western side of the large slide (MTC 1). These blocks may represent successive back rotated slide blocks from incipient failures on the Plateau margin or detachment blocks of more solid material that have toppled/slid from the Plateau scarp post failure of MTC 1.

6.5.1.5 Rosetta Channel (RC)

The Rosetta Channel zone incorporates the main channel / canyon and surrounding bank failures. Sediment waves are observed in the axis of the channel indicating the likelihood of recurrent turbidity flows*. The arcuate bank failure scars are sharp and well defined suggesting that they were recently reactivated (Fig. 6.4). The absence of any in channel deposition implies that channel flows are removing any debris and may be actively eroding the channel banks, a precondition for further bank failure.

6.5.1.6 Eastern Slope (ES)

The Eastern Slope is an unbroken slope unit dominated by unit pockmark development (Figs. 6.3 and 6.4). A well developed pockmark field is located in a central slope position, however unit pockmarks are observed to cover the entire eastern slope.

* see Appendix A4 for a figure example of sediment waves in the Rosetta Channel

Subtle seabed debris slides and flows have been observed in an up-slope position, in a similar water depth as the Rosetta Canyon head. It is likely that these slides and flows transfer terrigeneous material from a shelfal to a slope setting. Minor faulting and debris material associated with these slides / flows can be found within and on the margins of the pockmark field.

6.5.2 Seismic sequence stratigraphy of the Plateau

The study area is located on the mid slope region of the western flank of the NDSF (Fig. 6.1). The northwestern limit of the study area is marked by a large failure scarp with a crescentic downslope-facing planform geometry (Fig 6.1). The Plateau seabed is generally smooth outside the immediate confines of the Rosetta Palaeochannel, MTD zone and the large scarp (Fig.6.3), but is punctuated by hundreds of small depressions that are clearly visible on the seafloor bathymetry map (Fig. 6.1). Many of these are aligned, but equal numbers are isolated or organised in small groups. Low relief palaeoscarps are visible and form loci for the clustering of many small extensional faults whose strikes generally follow the local topography.

The Late Pleistocene to Holocene seismic sequence stratigraphy of the slope sediments in the study area is divided here into a series of depositional units, based on their correlatability and on distinctive seismic facies characteristics. They are not subdivided based on sequence boundaries; hence they are referred to informally as seismic units rather than formal sequences. A representative seismic profile showing the typical acoustic features of each unit is presented as Figure 6.5. A summary of the characteristics of each unit is given in Table 6.1. The slope package consists of alternations of laterally continuous units interpreted here as consisting of mainly hemipelagic clays with interfingering of some discrete channel-levee complexes (Units 1-4 inclusive), with more chaotic units interpreted as mass transport deposits (MTDs 1-3). This interpretation accords with recent large-scale studies by Loncke and Mascle (2004), Garziglia et al. (2008) and Loncke et al. (2009).

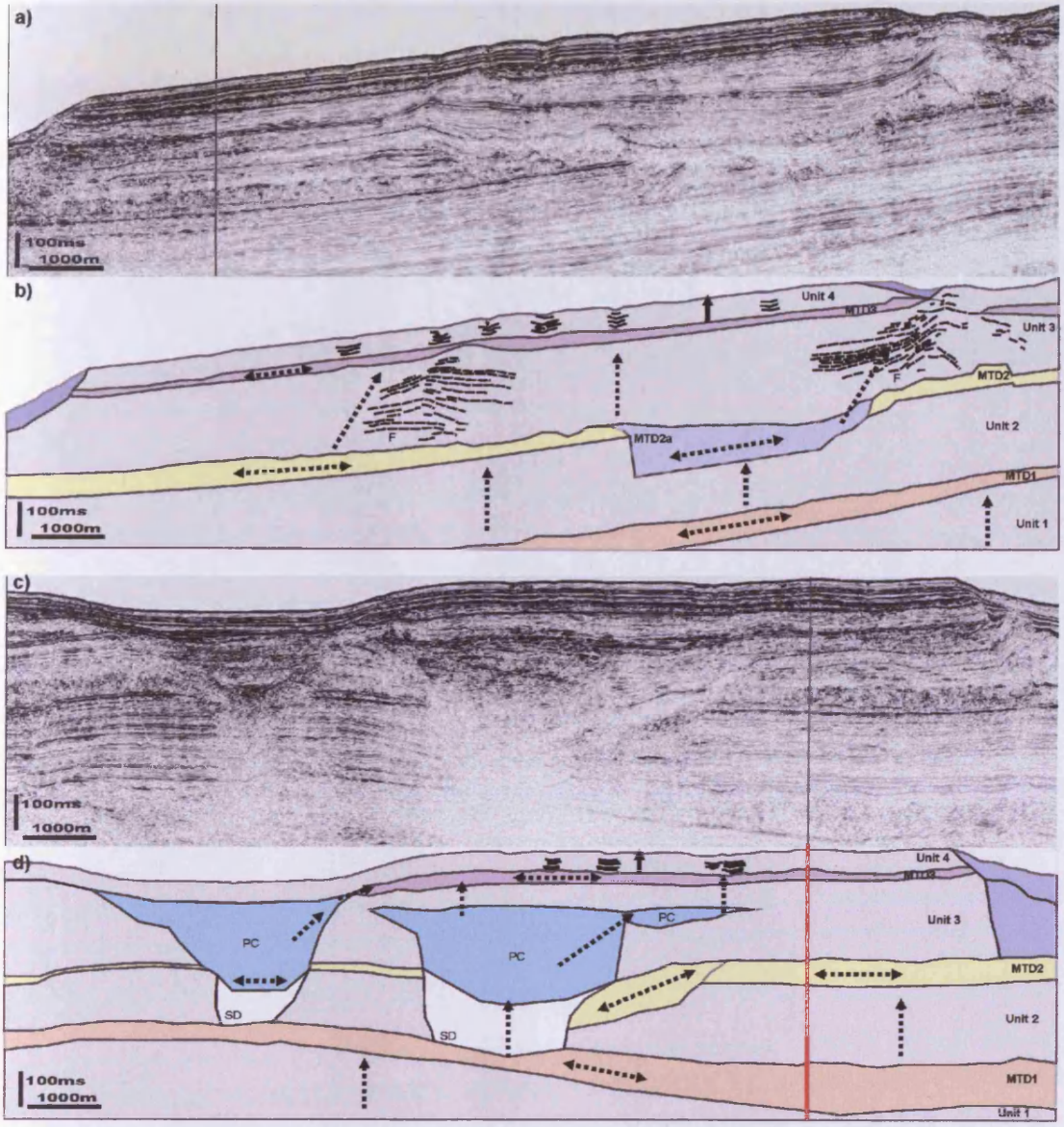

Figure 6.5 Stratigraphic cross section. a), b) NW-SE line. c), d) SW-NE line. Units 1, 2, 3 and 4, MTD 1, 2, 2a and 3, palaeochannel-levee complexes (PC) and folds (F) are shown. MTDs associated with sliding on the edge of the Plateau are shown (not labelled). Seismic distortion (SD). Arrows represent possible fluid migration pathways (only a minority of examples are shown). Horizontal arrows represent potential lateral migration and/or temporary storage of fluid. Vertical limit of Chirp profiler penetration is to the base of Unit 4.

Table 6.1 Seismic sequence stratigraphy

	Reflection characteristics					
Unit	Basal unit boundary	Upper unit boundary	Internal package	Unit geometry	Additional unit characteristics	Interpretation
Unit 4	Crenulated, near continuous	Continuous, seabed	Continuous, laminar, near horizontal reflections of varying amplitudes	Near uniform thickness c. 80-100ms	Near vertical, columnar zones of concave reflections transect Unit 4 for varying distances; The base of this unit is dated at c.100,000yrs (horizon D0), a mid-unit horizon at 15,000yrs (C0) and an upper horizon at 9,000yrs (horizon A200) (Fig. 6.2).	Fine grained, hemiplegic drape package
MTD 3	High amplitude, near continuous, sub horizontal, occasionally stepped	Crenulated, near continuous	Highly chaotic and disrupted reflections	Uniform thickness (c.50ms); thinning over the folds in Unit 3	Unlike MTD1 and 2, MTD3 is restricted to the lateral extent of the Plateau, due to subsequent slumping of sediments at the margins of the Plateau.	Mass Transport Deposit : composed of probable sandy layers above a distinct shear surface
Unit 3	Conforms with MTD2 and MTD 2a	High amplitude, near continuous, sub horizontal, occasionally stepped	Variable amplitude and reflection continuity	Near uniform thickness (c. 300ms)	Amplitude anomalies are numerous and range from brightening to acoustic wipeout; Three U-shaped, high amplitude channel-levee complexes; Contacts between the channel bodies and the host stratigraphy are erosional, some onlap can be observed on the margins of the eastern channel; Two folds within Unit 3.	Fine grained, hemiplegic package with coarser grained facies associated with the channelized intervals; folds
MTD 2	Above background amplification, continuous, near horizontal	High amplitude, near continuous, Highly crenulated, occasionally pitted,	Highly chaotic and disrupted	Uniform thickness (c.50-100ms); Pyramid-shaped reflections puncture the upper surface penetrating the unit above.	Unit contains seismic anomalies; MTD2a is observed to transect MTD2	Mass Transport Deposit : composed of probable sandy layers and large (<50ms) intact debris blocks

	Reflection characteristics					
Unit	Basal unit boundary	Upper unit boundary	Internal package	Unit geometry	Additional unit characteristics	Interpretation
MTD 2a	Above background amplification, continuous, near horizontal	Above background amplitude, crenulated, discontinuous	Amplitude and reflection continuity variation	Rectangular geometry c.100ms thick	MTD 2a erosionally truncates Unit 2; Possible indication of slumping or remobilisation of surrounding sediments caused by MTD 2a; MTD2a erosionally truncates Unit 2.	Mass Transport Deposit perpendicular in direction to cross section b (Fig. 6.4)
Unit 2	Crenulated, near continuous	Above background amplification, continuous, near horizontal	Sub horizontal, near continuous, laminar; amplitude and reflection continuity variation	Variable thickness (200-300ms)	Unit amplitude varies laterally from NE-SW, higher amplitudes observed in the SW; Faint trails of near vertical low amplitude columns transect this unit and may represent possible fluid migration routes.	Fine grained, hemiplegic drape package
MTD 1	High amplitude, near continuous, sub horizontal, occasionally stepped	Crenulated, near continuous	Highly chaotic and disrupted	Wedge-shaped package c.50-150ms thick; thickens towards the East and North.	Unit is broken by a distinct low amplitude seismic anomaly.	Mass Transport Deposit : composed of probable sandy layers and debris blocks, above a distinct shear surface
Unit 1		High amplitude, near continuous, sub horizontal, occasionally stepped	Low amplitude, continuous to discontinuous, sub horizontal	Unknown; Limit of UHR penetration.	Amplitude anomalies; Reflection signal of this unit is poor in places.	Fine grained, hemiplegic drape package

6.5.3 Distribution and geometry of pockmarks

The main focus of this study is the interpretation of pockmarks at the present day seabed and in the shallow subsurface. The AUV data is limited to shallow penetration of c. 80-100 ms, hence only Unit 4 is really encompassed by the highest vertical resolution profiles. Pockmarks are clustered at two main stratigraphic positions in Unit 4, the present day seabed, and at or just above a marker referred to informally as D0, the base of Unit 4. The distribution and acoustic expression of the pockmarks at these two levels are described separately below, and inter-relationships between them are considered later in this section. Reliable identification of pockmarks at deeper stratigraphic levels is prevented by poor imaging in the complex and chaotic seismic facies of the MTDs and within the deeper buried palaeochannel-levee complexes.

6.5.3.1 Recent Pockmarks

Over 25,300 small, circular depressions on the present day seabed that are here interpreted as pockmarks have been mapped within the ~1000km^2 Rosetta Region AUV coverage area. Seabed pockmarks are typically expressed as circular to sub-circular depressions, rimmed by multi azimuth slopes of 3 ° to > 6 °. Pockmark diameters vary from < 20 m to ~50 m and densities range between < 4 to > 400 pockmarks per 1 km^2. The density variation reflects disparities in pockmark spacing between isolated unit pockmarks on the upper shelf and a pockmark field immediately east of the Rosetta Canyon (Fig 6.3.). Recent pockmarks are described further (with figures) in Chapter 7.

6.5.3.2 Plateau unit pockmarks

A total of 1728 unit pockmarks have been mapped on the Plateau, 787 (or 46 %) of which are contained within large hollows or depressions on the seabed. The pockmark density varies dramatically between those relatively isolated unit

pockmarks located on the smooth 'Plateau' region and those distributed within the large seabed depressions. Isolated unit pockmark densities range between 1-2 pockmark per 1 km^2 whereas densities are > 90 pockmarks per 1 km^2 for unit pockmarks clustered in the largest depressions. Unit pockmarks range between 7 m and 45 m diameter (average diameter is 18 m) and 0.1 m to < 3.5 m deep (average depth is 0.5 m). Their geometry is near circular with an average ellipticity ratio of 1:1.5. The size and shape of the unit pockmarks within and outwith the depressions are comparable.

6.5.3.3 Depressions and buried pockmarks on the Plateau

The large depressions are an important feature of the Plateau region's physiography. They are recognisable on the seafloor bathymetry map (Fig 6.1). In profile, the depressions can be seen to occur directly above buried pockmarks. An excellent example of this relationship is shown in Figure 6.2, where a c. 350 m wide pockmark is interpreted to occur at the C0 horizon, based on an erosive margin and a zone of anomalously high amplitudes along the inferred pockmark base (labelled b). Above the buried pockmark, the highly laterally continuous reflections of the uppermost part of Unit 4 is interpreted to drape the underlying topography, since all the individual reflections up to the seabed are concordant with the pockmark base, and they therefore precisely mimic its geometry. The seabed depression can therefore be seen to be a vestigial feature that has formed solely due to drape of the topography of the underlying pockmark.

Also visible on the example shown in Figure 6.2, is the clustering of unit pockmarks at the seabed reflection in the area specifically encompassing the drape-induced depression. On this profile, for example, at least 6 unit pockmarks of variable size are transected, and high amplitude reflections are observed to be associated with several of these. Imaging quality is poor because of imaging artefacts (bow tie reflections and diffractions), and because they are narrow objects they are effectively below the lateral resolution of the method.

142 of these large bowl-shaped seabed depressions have been identified on the Plateau region west of the Rosetta Canyon. The depressions range in size from 100 m to > 700 m diameter and 0.5 m to > 20 m depth. On average, depression geometry is sub circular (average ellipticity ration 1:1.4) with a geometry ranging between circular (1:1 ellipticity ratio) to highly elliptical (1:3.7 ellipticity ratio).

The number of unit pockmarks clustered within depressions is highly variable. On average each depression contains 5 unit pockmarks, however 23 % of depressions do not contain unit pockmarks and 17 % contain only a single unit pockmark. The largest depression contains 152 unit pockmarks. The majority of the depressions appear to be geographically restricted to the northern end of the Plateau.

The depressions on the Plateau are unique within this ~1000 km^2 dataset. The depressions are geographically restricted to the Plateau, their seabed expression is larger and deeper than any other pockmark in the dataset, and they exhibit a greater variety in morphological expression than the smaller isolated unit pockmarks.

6.5.4 Seismic expression of pockmarks and depressions

The large population of unit pockmarks and depressions on the Plateau represent a broad spectrum of geometrical forms and dimensions. Seismic profiles through the seabed depressions and unit pockmarks indicate that despite a common concave geometry they occur at a range of stratigraphic levels in Unit 4. The identification and interpretation of these features is dependant, to a certain degree, on the amplitude characteristics and reflection geometry of the host stratigraphy. In general, they are more easily observed and more accurately defined within intervals with higher dominant frequency, acoustically finely layered and near-continuous reflections (Chapter 4). This limits clear identification of buried pockmarks to the top < 100 ms (limit of Chirp profiler resolution) of the sedimentary sequence.

The defining characteristic of all the unit pockmarks and depressions is the erosive nature of the seismic reflections in the host interval, suggesting formation of these

features involves removal or remobilisation of the sediments close to the seabed at the time of formation. It is not always possible to distinguish truly eroded forms from ones where the host reflections are merely disturbed in situ, particularly for smaller candidate pockmarks. Disturbed seismic data quality is associated with reduced acoustic velocities and the specific distribution of gas within the sediments (Dangerfield, 1992; Granli et al., 1999; Arntsen et al., 2007). Gas charged zones can cause significant velocity anomalies which produce distortion in the seismic data whose effects can 'propagate' downward below the pockmark. This disruption varies vertically and laterally, and is often masked or influenced by the presence of artefacts and coherent noise, for example in the form of bow-tie artefacts (Fig 6.6.). The quality of the imaging beneath the unit pockmarks and depressions is generally consistent with seismic interference due to the presence of gas and a possible pipe or fluid migration pathway (Chapter 4). The identification of seismic anomalies is dependent on the spatial and vertical resolution and on pockmark size.

Detailed descriptions of the seismic expression are presented below for some representative examples from the large data set that has been interpreted, grouped into unit pockmarks, large depressions and large depressions with clustered unit pockmarks.

6.5.4.1 Unit pockmarks

An example of a small unit pockmark is presented in Figure 6.6. Pockmark P448 is an isolated unit pockmark located at the northern end of the Plateau (Fig. 6.1), and is c. 16 m in diameter and is < 0.3 m deep at its deepest point so is at the limit of seismic resolution. It is identifiable on side scan sonar as an area of high reflectivity which is interpreted as resulting from the presence of carbonate cements or shallow gas (Fig. 6.6). It is expressed as a poorly resolved chaotic zone (between c. 1.119 s TWT and the seabed) with an acoustic impedance similar to the seabed and a bow-tie artefact at c. 1.119 s TWT (labelled *x*). Beneath the acoustic anomaly, concave deflection and subtle breaks in the reflection continuity are imaged that are several traces wide and stack vertically in a systematic fashion over a distance of c. 6-8 ms above a prominent disrupted reflection (A200) at c. 1.126 s TWT. Seismic distortion

and subtle amplification of the background reflectivity surrounding A200 is evident between c. 1.124 s TWT and c. 1.128 s TWT. Beneath this distortion a linear zone with the same diameter as the pockmark (1-2 traces) is imaged as a complete loss of signal.

It is important to note that all unit pockmarks on the Plateau (that are not contained within a depression) are observed to root at the level of the high amplitude horizon (*A200*) (±2ms) and the majority of unit pockmarks are observed to display a chaotic high amplitude zone (*x*) within several milliseconds of the seabed. Horizon A200 was deposited during an episode of Sapropel S1a formation in the wider Mediterranean (Ducassou et al., 2007), however definitive Sapropel formation in the Rosetta Region can not be confirmed here. Clays containing dark pyritic laminae, interpreted to have formed from individual dilute turbidity current/plume events, have been observed in some cores (Fig. 6.2). This suggests that bottom waters might have been anoxic during deposition and that it is likely that the dark laminae are associated with stratification of the water column during times of increased freshwater input.

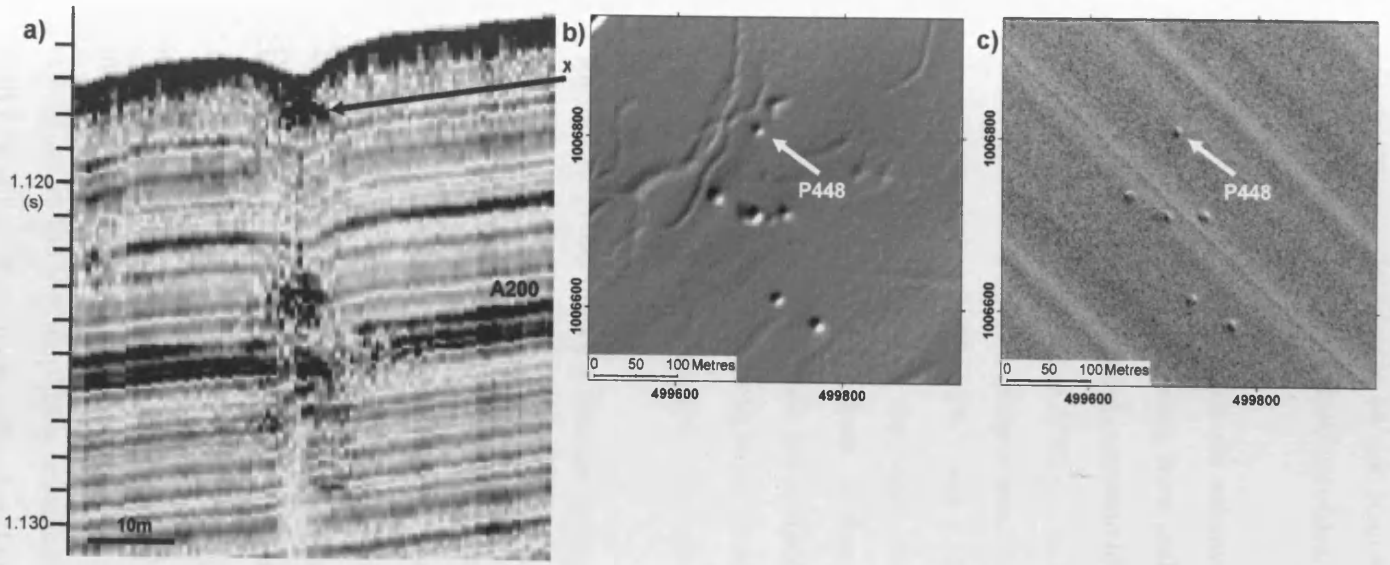

Figure 6.6 Unit pockmark P448. a) Chirp profiler data. A bow-tie artefact is imaged at position x. b) Seabed dip map c) Seabed side scan sonar. Cross section is taken NW-SE through the unit pockmark.

6.5.4.2 Large depressions

Two examples of large depressions are presented in Figure 6.7. Depression D85 and D140 are examples of subtle seafloor depressions in the northwestern sector of the Plateau. Depression D85 is c. 110 m in diameter and 1 m deep at its deepest point. Depression D140 is c. 70 m in diameter and c. 0.6 m deep. Depressions D85 and D140 are not identifiable on side scan sonar (Fig 6.7c). D140 is not crossed close to its centre by any of the seismic profiles.

Depression D85 is imaged on seismic as a vertically stacked series of concave upwards reflections extending from seabed to 1.146 s TWT where a reduction in the signal to noise ratio prevents accurate identification of the reflections (Fig 6.7a). The degree of concavity varies from c. 1 m at the seabed to c. 3 m near the base (H100). The relief of the concave shapes steadily decreases upwards with a prominent change in relief between 1.129 s TWT and 1.124 s TWT. It is observed that this change in relief is apparent within the same stratigraphic interval as a distinct change in reflection characteristics from diffuse to higher amplitude contrast reflections. Above interval *x* reflections are imaged as continuous, near parallel horizons with amplitudes above the background levels of the host unit. These reflections are neither disrupted nor distorted.

Reflection H100 marks a distinct change in reflection characteristics. H100 marks the deepest continuous traceable reflection and the maximum concave upwards relief. The reflections immediately below H100 are poorly imaged but show evidence of distortion, disruption and truncation. Several reflections are erosionally truncated against H100. Reflection H100 also represents a zone of reflection truncation for D140. Above this erosional surface, the suprajacent reflections appear to define an infill geometry over a vertical extent of c. 20 ms, with alternating reflections exhibiting greater and lesser negative relief. A good example of an infilling reflection is shown at point *y*. Above H100 reflections are observed to bend into the concave shape but show no evidence for truncation. Beneath H100 reflections in the low amplitude seismic facies are discontinuous due to loss of signal until a relatively prominent reflection (D0) at c. 1.164 s TWT.

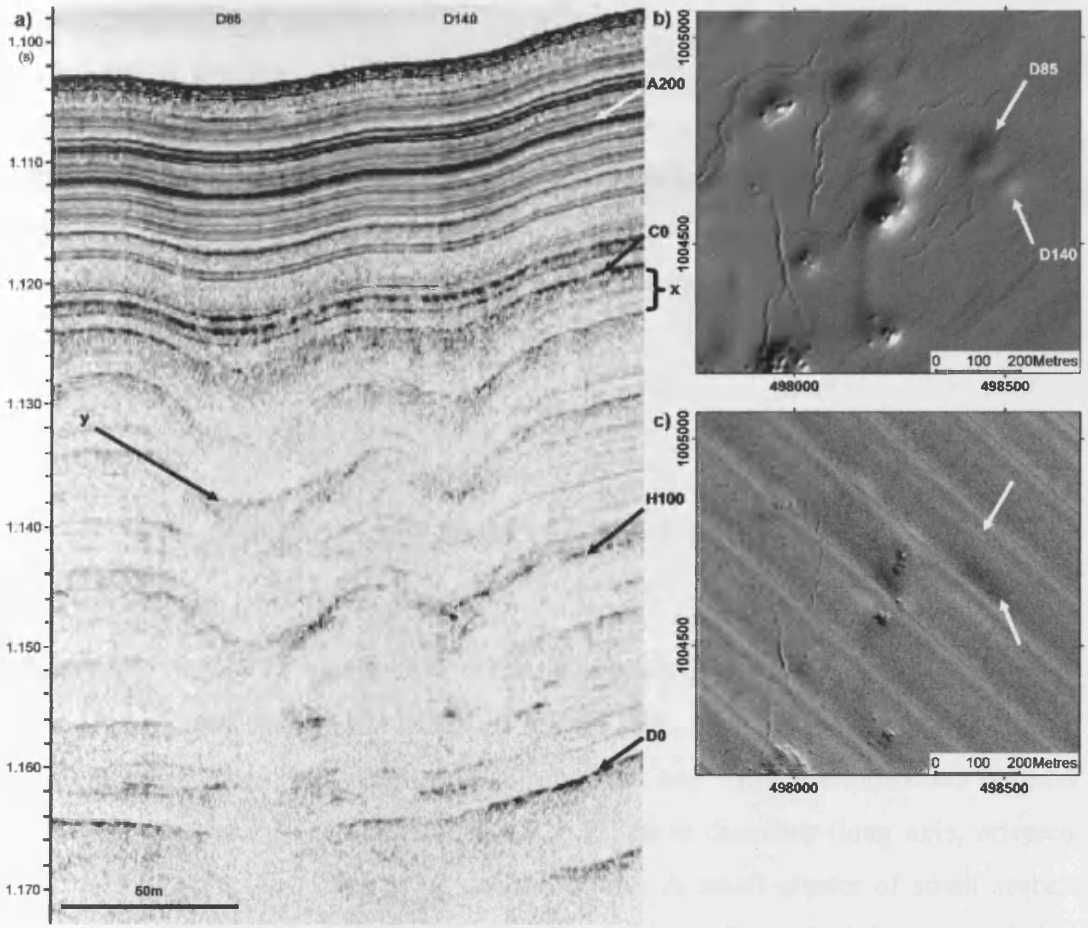

Figure 6.7 Depression D85. a) Chirp profiler data, b) Seabed dip map, c) Seabed side scan sonar (white arrows highlight location of depressions not detected by the sonar). Cross section is taken diagonally NW-SE through the depression

The interpretation of these reflection characteristics is that two buried pockmarks are interpreted at the level of H100, one each directly beneath the concave stack of reflections underlying the two depressions at the seabed. This therefore fits the characteristics noted earlier that depressions overlie buried pockmarks. The relief of these pockmarks was only partially infilled after initial burial, and vestigial relief was then draped by the more continuous seismic facies nearer the surface, leaving residual relief present at the seabed.

6.5.4.3 Large depressions with clustered pockmarks

6.5.4.3.1 D86

Depression D86 is an example of a prominent depression in the northwest of the Plateau containing 3 small pockmarks (Figs. 6.1 and 6.8). Depression D86 is located < 110 m away from D85 which does not contain any surface expressions of fluid flow. Depression D86 is elliptical and is > 125 m in diameter (long axis, oriented NNE-SSW) and c. 6 m deep at its deepest point. A small cluster of small seabed depressions interpreted as unit pockmarks are visible on the seabed dip map and side scan sonar imagery (Fig. 6.8), and are aligned along the long axis. The largest unit pockmark within the depression is < 30 m in diameter. The pockmarks within D86 are identifiable on side scan sonar as areas of high reflectivity associated with the presence of carbonate cements or shallow gas (Fig. 6.8).

The cross-sectional characteristics of D86 are illustrated using a Chirp profile (Fig. 6.8) that crosses through the largest pockmark at the westernmost end of the depression. Most strikingly, the subsurface beneath Depression D86 is imaged as a vertical stack of concave reflections that are generally concordant to the seabed down to interval z. The concave geometry of these reflections changes to a v-shaped geometry at the marker H100, although imaging plays a part in this geometry, with uncollapsed diffraction energy obscuring the true geometry. There is a slight increase in the diameter of the concave feature from c. 70 m at H100 to c. 100 m at the seabed.

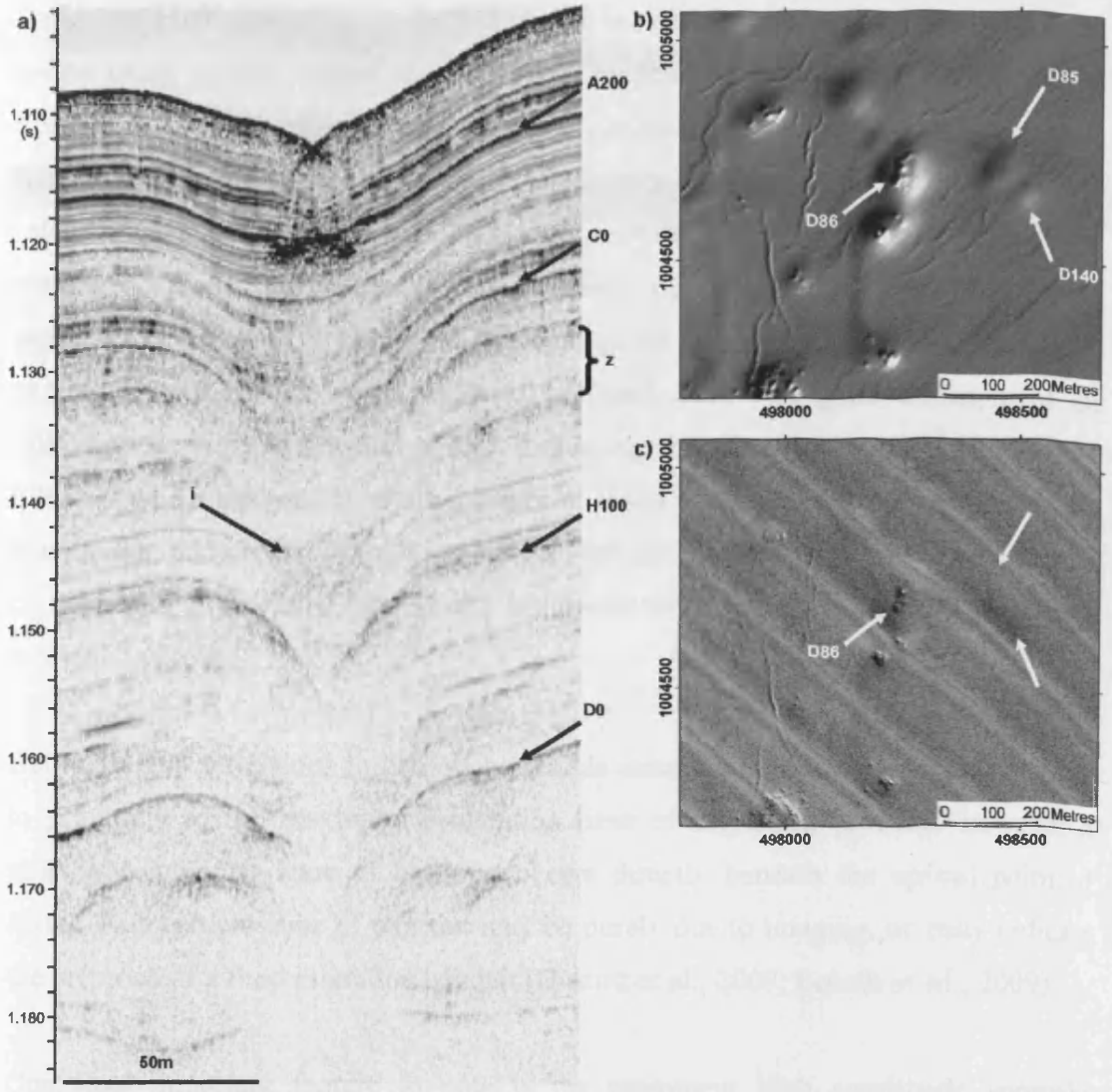

Figure 6.8 Depression D86. a) Chirp profiler data showing a unit pockmark within the depression, b) Seabed dip map. White arrow points to the precise location where the AUV line transects the pockmark, c) Seabed side scan sonar. Cross section is taken diagonally NW-SE through the depression.

Reflection H100 demarcates a distinct change in reflection characteristics, with those below being poorly imaged but with clear evidence of distortion, disruption and truncation. Several reflections are erosionally truncated against H100 on the steeper flanks of the concave feature. Above this locally eroded surface, the suprajacent reflections appear to follow the reflection geometry of H100 and bend into the structure. These suprajacent reflections show no evidence of truncation. Infill geometry is observed over a vertical extent of 40 ms, with alternating reflections exhibiting greater and lesser negative relief and infill. A good example of an infilling reflection is shown at point *i*. Taken together, the erosion at H100 and the infill above are diagnostic of a pockmark at H100, which as noted previously was then buried, and similarly to D85 and D140, left a vestigial feature at the seabed as a consequence of the inability of the sediments to completely infill the concave erosional hollow.

Beneath H100 reflections in the low amplitude seismic facies are discontinuous due to proximity to the maximum penetration limit of the Chirp profiler, however a strikingly columnar zone of blanking occurs directly beneath the apical point of H100. This vertical zone of wipeout may be purely due to imaging, or may indicate the presence of a fluid migration conduit (Hustoft et al., 2007; Løseth et al., 2009).

One final important feature to note is the prominent high amplitude anomaly observed at c. 1.117 s TWT at the level of reflection A200. The acoustic anomaly appears to disrupt and distort reflection A200 and several of the reflections immediately below, possibly by the scattering of incident energy. This anomaly is attributed to the presence of shallow gas or carbonate cements. A columnar seismic distortion of localised reflection discontinuities is observed from 1.117 s TWT to the seabed. Above the columnar zone a prominent v-shaped notch is apparent in the seabed that corresponds to the unit pockmark identified on the Chirp profiler and sonar data. It is evident therefore that Depression D86 initially formed at the time marked by H100, was buried, and then renewed fluid expulsion led to the formation of the seabed cluster of unit pockmarks.

6.5.4.3.2 D117

Depression D117 is the largest example of a depression with clustered pockmarks in the dataset, and is located in the centre of the Plateau at a distance (> 4 km) from the main population of depressions further North (Fig. 6.1). Depression D117 is elliptical, > 700 m in long axis diameter (oriented WNW-ESE), covers an area of 220 km^2 and is > 18 m deep at its deepest point (Fig. 6.9). 152 unit pockmarks with an average diameter of c. 10-20 m are clustered within the bounds of the depression (Figs 6.9b,c). The unit pockmarks are fairly regularly spaced within the depression, with an average density of ~10 pockmarks per 100 m^2 and an average nearest neighbour distance of c. 15-20 m. The pockmarks within D117 are identifiable on side scan sonar as areas of high reflectivity associated with the presence of carbonates or shallow gas (Fig. 6.9c).

In profile (Fig. 6.9a), Depression D117 is imaged as a set of vertically stacked concave reflections from a chaotic high amplitude zone (*b*) at the level of reflection C0 (c. 0.876 s TWT) to an undulating seabed. Above C0 the background reflections are generally continuous, parallel and of near uniform thickness. The concave relief remains near constant between C0 and the seabed as each subsequent reflection drapes underlying strata concordantly. A zone of high amplitude reflections is observed just above reflection A200.

Beneath C0 the signal to noise ratio is comparatively lower, with a columnar near complete loss of signal beneath the depression. Reflections at the level of the high amplitude interval *b* and those immediately below, show evidence of distortion, disruption and truncation. Several reflections are erosionally truncated against zone *b*. Strong de-amplification of the background reflectivity at depths greater than c. 0.875 s TWT prevents clear imaging of reflections however partial reflections can be tentatively traced across at deeper intervals e.g. c. 0.902 s TWT. Based on the evidence for erosional truncation and the gross geometry, a large buried pockmark is interpreted at the level of C0.

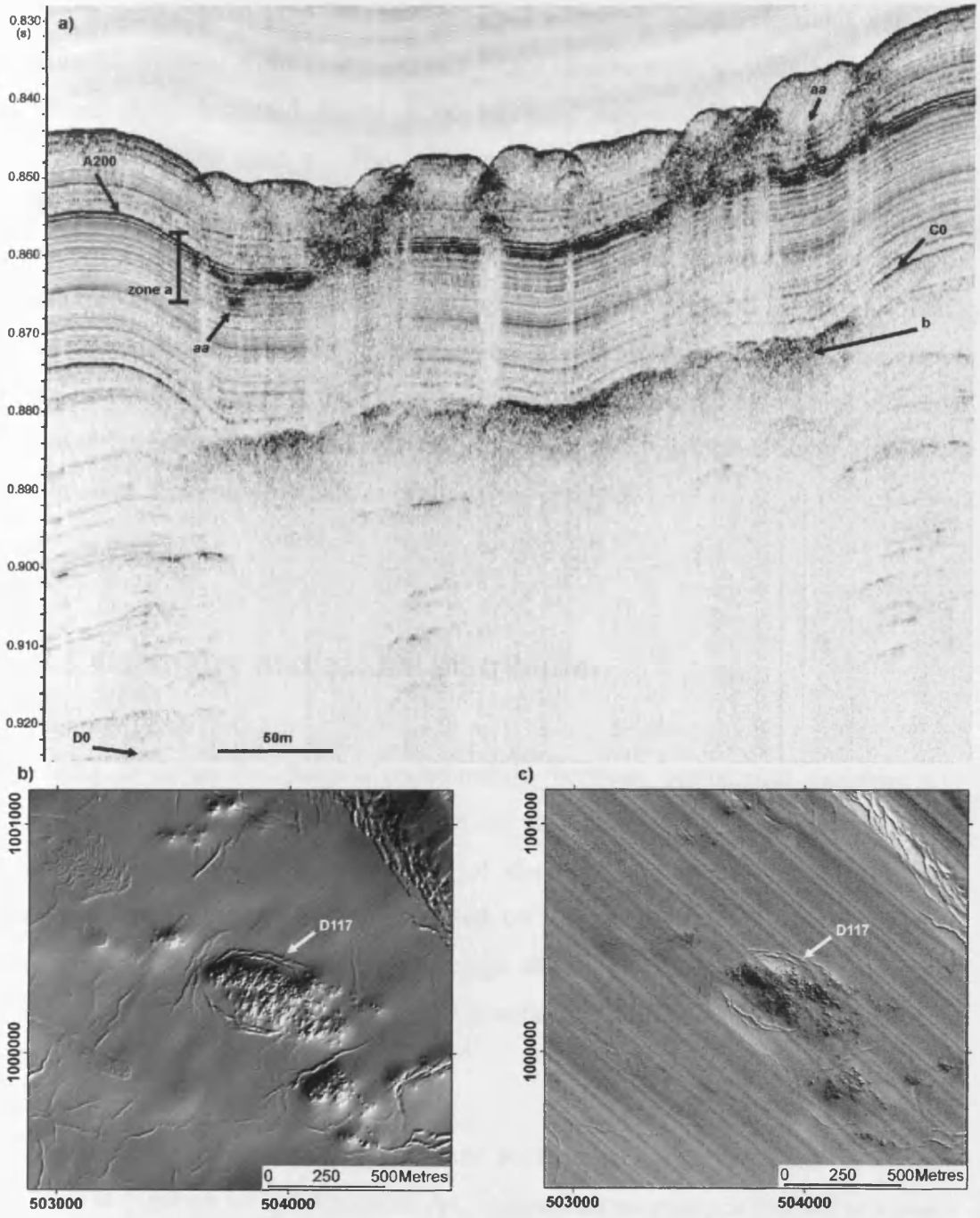

Figure 6.9 Depression D117. a) Chirp profiler data showing multiple unit pockmark within the depression, b) Seabed dip map, c) Seabed side scan sonar. Cross section is taken diagonally NW-SE through the centre of the depression

Zone *a* (at the level of A200) is a group of high amplitude reflections which are distinctly different from zone *b*. Zone *b* is a chaotic mass of distorted reflections whereas those localised above A200 represent sub-vertical swathes of distinct reflections within zone *a*. The host interval for these sub-vertical reflections is typified by near-continuous seismic facies, with localised amplification. Importantly, the sub-vertical high amplitude zones are not exclusively spatially consistent with v-shaped notches at the seabed that are interpreted as unit pockmarks (Fig. 6.9, labelled *aa*). Bow-tie artefacts are abundant beneath the unit pockmarks. Vertical blanking zones extend from the base of the high amplitude zones in zone *a* down to the level of the base of the large pockmark at C0, which as suggested above, could either be imaging problems or fluid flow conduits.

6.5.5 Geometry and spatial distribution

In order to determine potential relationships between geometrical variables e.g. diameter and depth, a sub population of unit pockmarks not associated with depressions, and the total population of depressions was analysed. The sub-population of unit pockmarks was based on a quadrate system of 1 km^2 grids. Representative samples (based on average diameter) were measured from each quadrate. In some quadrates the low number of unit pockmarks present made sampling inappropriate.

Basic geometrical measurements of unit pockmarks and depressions have been collated in Figure 6.10 and Appendix A4. Depression geometry is utilised as a proxy for buried pockmark geometry. Correlations between geometrical variables are not statistically significant but show a general positive trend between 1) unit pockmark diameter and depth, 2) depression diameter and depth, 3) unit pockmark area and depth, 4) depression area and depth, and 5) depression area, diameter and depth and number of unit pockmarks contained within the depression (Fig 6.10)*. Taken together, these correlations imply a scaling relationship to both unit pockmark and

* Not all graphs are shown – consult appendix A4

depression morphologies. Depressions which do not contain unit pockmarks show no correlation between geometries and therefore no scaling relationship (Fig. 6.10c).

Density plots of unit pockmark distribution show "hotspots" of unit pockmark occurrence (Fig. 6.11c,d). Density plots of total unit pockmark population (Fig. 6.11c) and unit pockmark populations not associated with depressions (Fig. 6.11d) are shown. A background density of 1-20 unit pockmarks/km^2 is evident, with a consistent zone of hotspots in the east of the Plateau. Above background densities (> 40 pockmarks / km^2) in the northwest and north east suggest depressions are a focus for the spatial formation of unit pockmarks.

The number of unit pockmarks contained within a single depression ranges from 0-152. There is no spatial pattern between the number of unit pockmarks contained by a depression and the spatial location of the depression (Fig. 6.11.b). At a local scale, unit pockmarks appear to be preferentially positioned on the lateral margins of the Plateau, leaving a pockmark-free central zone (Fig. 6.11a.). The only seabed features present within this zone are a minority of depressions which do not contain unit pockmarks. This small scale spatial absence of unit pockmarks (< 1 km width) is not detected by the density plots which average the number of unit pockmarks within a square kilometre.

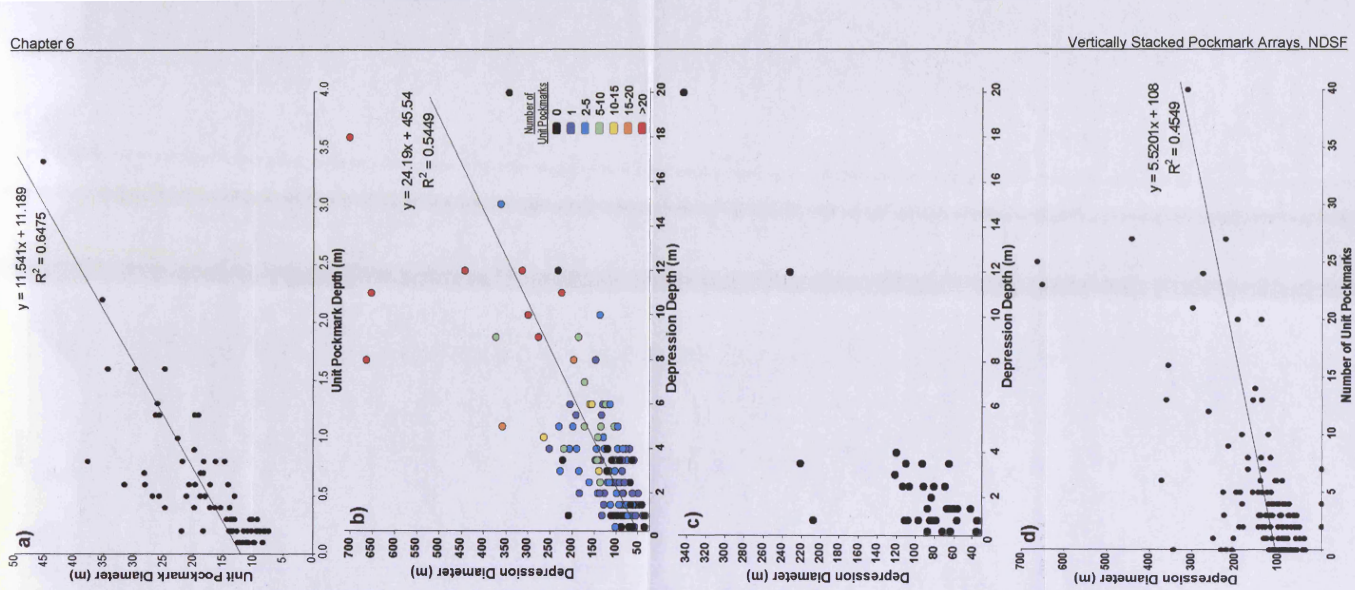

Figure 6.10 Geometrical relationships. a) Unit pockmark diameter and depth, b) Depression diameter and depth, coloured according to the number of unit pockmarks contained within the depression, c) Depression diameter and depth. Only those depressions without unit pockmarks are graphed, d) Depression diameter and number of unit pockmarks contained within the depression.

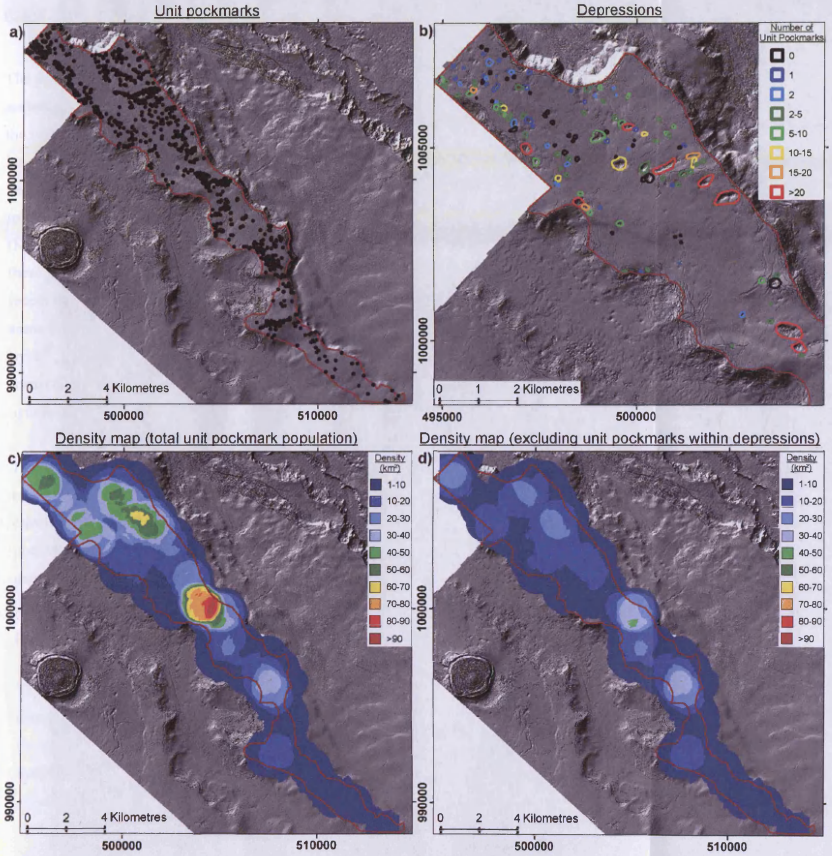

Figure 6.11 Spatial distribution. a) Spatial distribution of unit pockmarks on the Plateau (outline). Note the absence of pockmarks in the centre-North of the Plateau, b) Spatial distribution of depressions, coloured according to the number of unit pockmarks contained within the depression, c) Total unit pockmark population density plot, d) Unit pockmark density plot. Unit pockmarks contained within depressions are stripped out.

6.5.6 Timing of buried pockmark formation

The preceding descriptions show clear evidence that pockmarks have formed at the seabed, and also at shallow depths of < 100 ms beneath the seabed. Those forming at the seabed are generally < 30 m in diameter, whereas the buried pockmarks are much larger, typically > 100 m diameter (using diameters measured for associated seabed depressions as a proxy). The unit pockmarks occurring at the seabed are interpreted to have formed since 9,000 years BP. Recent sedimentation rates are high (Maldonado and Stanley, 1979; Ducassou et al., 2007; Loncke et al., 2009), and for these 1,728 unit pockmarks to have survived intact at the seabed suggests a very recent time of formation. It has been noted that the unit pockmarks all seem to link in some way through high amplitude trails to Horizon A200, and this surface is dated by C^{14} chronostraigraphy at c. 9,000 yrs BP. This sets an upper time limit for the formation of these unit pockmarks. It is not known whether they formed synchronously or diachronously within this time interval.

The timing of buried pockmark formation is based on the identification of erosional truncation of host strata at depth, and the assignment of a marker horizon at the envelope of the individual erosional truncation points. Confident assessment of pockmark timing is restricted specifically to those buried pockmarks that are clearly imaged by the seismic profiles (20 % of total population), therefore inferences made below are based solely on this sub-group and can not be extrapolated to the total population.

There is a distinct clustering of buried pockmark timing in the interval immediately above horizon D0 (Fig. 6.12). Buried pockmarks are only observed on half (4 out of 9) of the arbitrary chronostratigraphic and chronostratigraphic dated horizons mapped, namely C0, H80, H100 and D0. The results indicate that a significant proportion (75 %) of the buried pockmarks have formed at time period H100. A further 4 formed during C0, 2 at H80 and 1 in D0 (the horizon overlying MTD3). No large normal pockmarks have formed since C0. There is no correlation between the

relative age of the buried pockmark and depression depth, diameter or number of pockmarks*.

* Graphs presented in Appendix A4

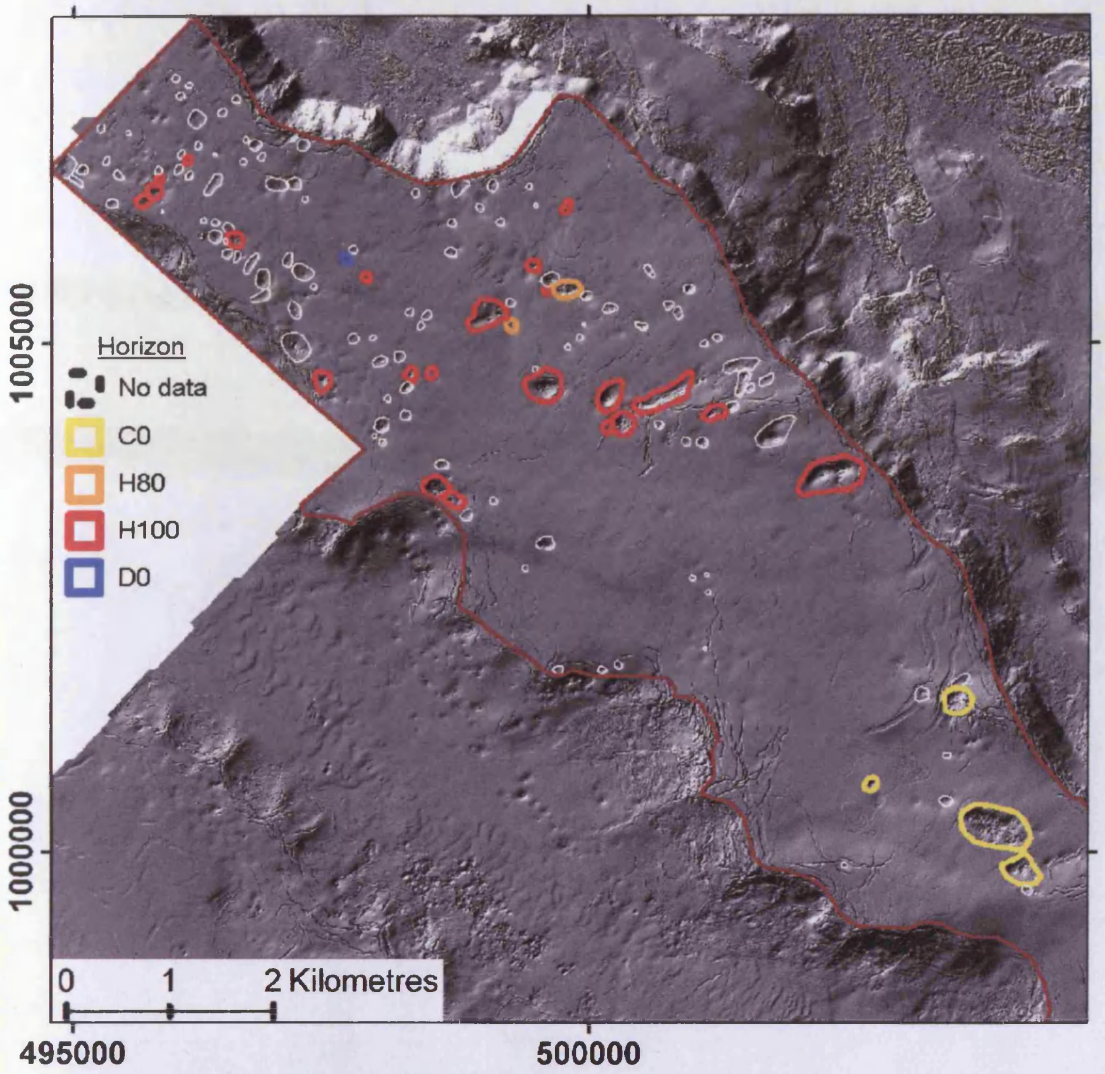

Figure 6.12 Spatio-temporal distribution of buried pockmark formation. Chronostratigraphic (C0 and D0) and arbitrary chronostratigraphic (H80 and H100) dating shows no spatial pattern to the temporal formation of buried pockmarks. White outlines indicate those depressions which could not be dated.

I infer from this that significant normal pockmark forming fluid migration on the Plateau has been intermittent yet persistent between the time of marker D0 and C0. The sampled data suggests that normal pockmark formation was restricted to specific events in time as indicated by their stratigraphic occurrence on only a few specific horizons between the period 100,000 yrs BP (D0) to 15,000 yrs BP (C0). The majority of buried pockmarks formed during a single fluid expulsion phase, over an interval (H100) midway between C0 and D0, tentatively estimated at c. 50,000-80,000 yrs BP.

6.5.7 Summary and interpretation

The large depressions observed at the seabed collectively represent a form of relict topography whereby pockmarks with diameters generally > 100 m formed in the Late Pleistocene, and were then buried by the mainly hemipelagic sediments (clay rich) of Unit 4. The deposition of hemiplegic drape across the Plateau was insufficient to completely infill the large pockmarks, topographically smoothing the seabed. The drape layer "moulded" to the original pockmark morphology creating a near uniform thickness of sediments over the crater, perpetuating the pockmarked morphology through time. Fill of the pockmark crater is observed, and this preferential fill may be a function of the crater morphology protecting deposited sediments from erosion by bottom currents. To date, the majority of the identified buried pockmarks have not been completely in-filled.

The large depressions are not always the locus for unit pockmark formation at or close to the modern seabed, but c. 77 % of the total of 142 large depressions have at least 5 unit pockmarks within their confines. These unit pockmarks are associated with high amplitude reflections at shallow depths, and by analogy with similar anomalies seen below other pockmarks these could either be due to carbonate cements or to the presence of shallow gas (Judd and Hovland, 2007; Hovland et al., 2010). In either case, there is evidently a renewed phase of fluid or gas expulsion in the very recent past. It seems most likely that whenever a conduit was formed during the initial stage of pockmark development, that this conduit was reactivated during

this latest stage of fluid expulsion. The main evidence for this is the confinement of the clusters of unit pockmarks to within the boundaries of the depressions themselves, suggesting a high degree of fluid focusing during this last stage of fluid expulsion, and with the same locus as for that responsible for initial, larger pockmark formation. It is also notable that depressions without unit pockmarks are more thoroughly infilled by the drape deposits of Unit 4 than those with unit pockmarks, suggesting that a) there may be a tendency for this latest fluid expulsion episode to have suppressed the effectiveness of any infill mechanism or b) repeated or renewed venting eroded any infilling sediment.

An interesting and important observation is made regarding high amplitude fluctuations in the largest depressions containing multiple unit pockmarks (Fig. 6.9, labelled *aa*). The sub-vertical high amplitude zones observed beneath the unit pockmarks are an enigmatic feature of this dataset. This phenomenon is also observed within other parts of the study area and is not uniquely related to the depressions (see Chapter 7). It is clearly not related to layer-bound acoustic impedance contrasts because the high amplitude reflections cross-cut stratal reflections. I therefore speculate that this phenomenon is the result of biological processes which produce either gaseous or cemented by-products, which are detectable using high resolution seismics. My preferred interpretation is carbonate precipitates as the product of palaeo(?) microbial activity e.g. sulphate reduction or the anaerobic oxidation of methane (AOM). Similar high amplitude waveforms have been reported from the Arafura Sea, Northern Australia (Rollet et al., 2009), but as yet, their origin remains a mystery.

6.6 Discussion

Having established that there are essentially two modes of pockmark occurrence in this part of the NDSF during the Late Pleistocene to Recent, the remaining focus of this chapter tackles the questions of what hydrodynamic system was responsible for

their formation, and what the wider implications of this work can be considered to be.

6.6.1 Fluid migration pathways and potential sources

A number of previous studies have shown that there is extensive evidence for widespread fluid migration within the NDSF (Loncke et al., 2002; Loncke and Mascle, 2004; Dupré et al., 2007; Garziglia et al., 2008; Bayon et al., 2009; Loncke et al., 2009). Highly focused fluid migration features such as mud volcanoes, mud pies, gas chimneys, pockmarks, carbonate crusts/pavements, chemosynthetic communities and mud mounds/diapirs are common (Bayon et al., 2009; Dupré et al., 2007; Loncke and Mascle, 2004). It is not known precisely when these features formed or whether they are currently active, however given the widespread distribution (approx. 600 km x 300 km area of the NDSF) and the considerable number of these features it is likely that a significant flux has occurred episodically throughout the Late Pleistocene to Recent during a time of rapid sedimentation on the fan (Loncke and Mascle, 2004).

Highly focused fluid flow via vertical conduits, be they pipes or mud volcanoes, is generally attributed to the generation of localised overpressured cells (Swarbrick and Osborne, 1996; Cartwright, 2007; Cartwright et al., 2007; Løseth et al., 2009). If we assume that the flux is crudely related to the magnitude and volume of the overpressure cell (Gallo and Woods, 2004; Cathles et al., 2010), then given the considerable size variation between features i.e. mud volcanoes (c. 1-5 km diameter) and pockmarks (< 20 m diameter) (Loncke and Mascle, 2004), it seems likely that overpressured cells must vary by orders of magnitude over the NDSF (assuming all other factors are equal).

Methane generation is one likely mechanism to generate these localised overpressured conditions (Swarbrick and Osborne, 1996), or at the very least prime the sealed cells for subsequent overpressure excursions during rapid loading or unloading (Ingram et al., 2004). Both thermogenic and biogenic methane sources

can be invoked in this area (Bayon et al., 2009), and results from exploration drilling confirm that both types of methane are present at relatively shallow depths in the sedimentary column (Vandré et al., 2007).

6.6.1.1 Buried pockmarks

Potential fluid migration pathways are presented in the plumbing diagram (Fig. 6.5). It is probable that both thermogenically and biogenically sourced methane migrates through the succession via a multitude of pathways to the level of MTD3. Vertical and lateral migration is considered to be facilitated by MTDs, faults, pipes, channel-levee complexes and folds in a range of seal bypass systems (Cartwright et al., 2007; Cobbold et al., 2009; Gay et al., 2003; Hustoft et al., 2010; Hustoft et al., 2009a; Hustoft et al., 2009b; Hustoft et al., 2007; Keller et al., 2007). For example, MTDs are commonly regarded as a potential seal unit, and migrating methane is often observed to be trapped at the basal shear surface of slides (Bünz et al., 2005; Frey-Martínez et al., 2006; Loncke et al., 2009). Localised amplitude brightening within MTD3 (Fig. 6.13) argues positively for methane migration through the slide complex, possibly via the complex juxtaposition of thin sandy layers contorted and connected via small faults and folds that are to be expected at the sub-seismic scale throughout such a deposit (Bull et al., 2009). These fluid migration indicators are frequently observed beneath buried pockmarks and may account for the spatial distribution of these larger pockmarks.

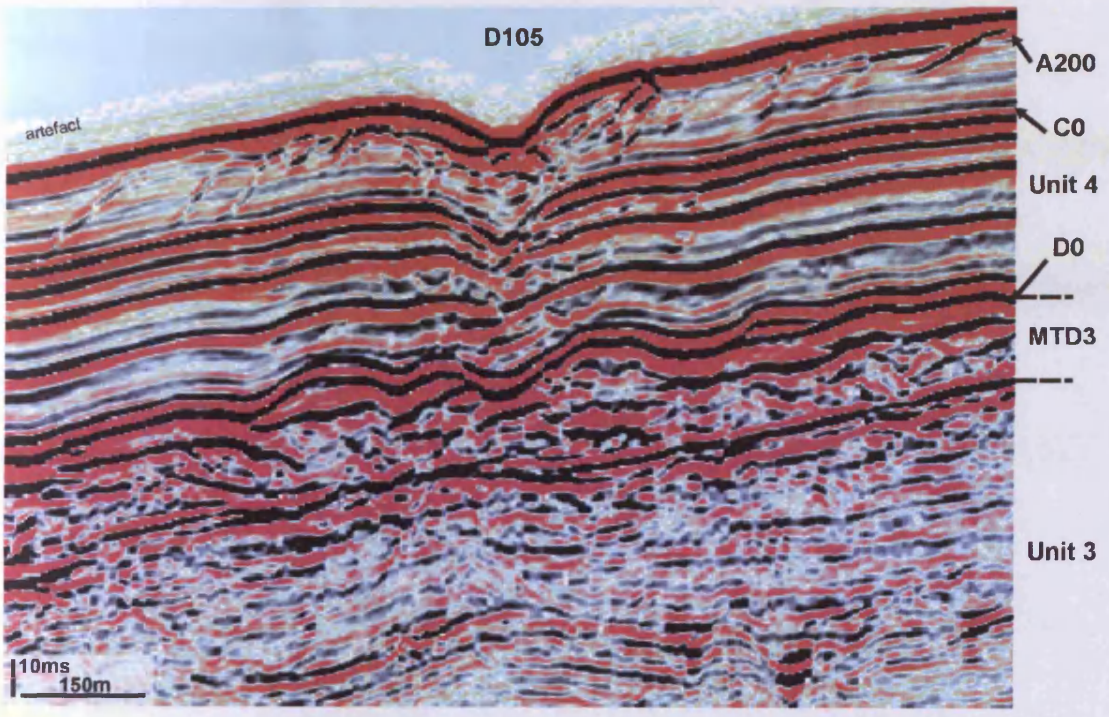

Figure 6.13 Depression D105. Depression D105 showing the relationship between the seabed depression, buried pockmark, the base of the pipe and MTD3 (2D UHR data). Cross section is taken diagonally NW-SE through the depression.

6.6.1.2 Unit pockmarks

In contrast to the buried pockmarks, unit pockmarks are thought to be sourced from cyclic pore water seepage (Hovland et al., 2010). This is a reasonable assumption given the random spatial distribution of background unit pockmarks, their small size, shallow routing depth and disregard for structures at depth. However, it has been interpreted here that all the unit pockmarks are observed to root at the level of *A200* (±2ms), a seismic horizon of Holocene age (9,000yrs BP). The inferred high organic Carbon content of this layer suggests that biogenic methane generation may play a role in their formation (Parkes et al., 2000; Gontharet et al., 2007; Pimenov et al., 2010). Chaotic acoustic disruption, high amplitude anomalies and acoustic wipe-out zones directly beneath unit pockmarks suggests that possible microbial activity associated with the *A200* horizon, in addition to possible pore water seepage, may have contributed to the generation and composition of the fluids responsible for pockmark formation (Fig. 6.6). This could certainly account for the large number of unit pockmarks that are found throughout the study area away from the large depressions at the seabed.

Clustered unit pockmarks in depressions may have a different genesis as suggested by their clear spatial association with buried pockmarks. Unit pockmarks within and outwith the depressions are of comparable size and geometry, are acoustically similar and rooted at the same horizon, however they are distinguishable based on several significant observations; 1) significant spatial clustering of the unit pockmarks is only observed within the depressions, indicating a point source within the depression may cause clustering, 2) there is no seismically observable difference between horizon *A200* on the Plateau and inside the depressions which could possibly account for this clustering effect, 3) horizon *A200* is observed within depressions which do not contain unit pockmarks suggesting it is not simply the presence of this horizon within a 4-way dip structure which influences unit pockmark location, 4) significant brightening and disturbance of horizon *A200* above background levels is only observed in depressions with unit pockmarks (Fig. 6.9.), 5) wipe-out zones which may be indicative of gas migration are observed to link buried pockmarks with unit pockmarks (Fig. 6.9). Based on these arguments I suggest that the unit pockmarks are sourced via the same conduits that fed the initial pockmark formation by a

combination of shallow-derived pore water and biogenic methane and deeper-sourced fluids (possibly pore fluid plus thermogenic or deeper biogenic methane). The plumbing system emplaced for the initial pockmark thereby provided a preferential focused fluid flow pathway for the migration of fluids to the seabed during this latest fluid expulsion episode.

6.6.2 Triggering mechanism

Multiple buried pockmarks on a single reflection implies widespread fluid migration and pockmark formation within a restricted time window. Based on a consideration of average sedimentation rates, available dating of specific shallow horizons and the c. 1-2 m vertical resolution of the AUV acquired high resolution seismic this is estimated to be < 1000 yrs. Potential deeper to shallow fluid migration routes on the plateau are likely to have been highly tortuous, involving vertical and lateral migration from depths in excess of 200 metres (Fig. 6.5). I suggest that fluid migrates across strata via bypass systems including faults and pipes, and then migrates up-dip along relatively permeable strata along local structures where it is temporarily trapped by low permeability seals such as the bases of MTDs or within levee complexes before migrating further upsection via crestal breakout features. At each trap locality on the vertical ascent route, fluid is trapped and accumulates to a threshold of local overpressure before seal breach is achieved and the fluid migrates out of this temporary storage. This model requires variable amounts of time for pressure build-up depending on the migration route, fluid flow pathway, number of temporary traps and the time taken to accumulate fluid in the trap and generate sufficient overpressures. Variability in the rate of ascent of fluid from a source at depth is inferred to produce pockmarks in a staggered time sequence as evidenced by buried pockmarks occurring at different reflections in the basal part of Unit 4.

Given that the majority of pockmarks formed at or very close to the same horizon, I suggest that the migration route for the initial phase of pockmark formation (leading to the set of large buried pockmarks) was probably of short distance and sourced from a single shallow storage layer. I suggest that MTD3 is the most likely source

for the buried pockmarks because it is the shallowest layer that has amplitude anomalies indicative of trapped gas that extends across the full area where buried pockmarks have been observed (Fig. 6.13). I envisage a hydrodynamic system where deeper sourced pore fluid plus methane migrated from depth to the level of MTD3 where it was trapped. Ingressing fluid accumulated through time building overpressure and priming the layer for fluid expulsion. I propose that an externally imposed triggering mechanism promoted multiple seal breaches and the formation of the suite of large pockmarks at the palaeoseabed, at some time post the 100,000 yr marker horizon (D0). It is probable that the significant difference between formation ages of those pockmarks in the North (H100) and South (C0) of the plateau are due to substantial differences between the geodynamic and fluid-dynamic locations of the pockmarks, requiring different overpressure cells possibly within the same source layer (MTD3), or conceivably with a different source layer.

A number of potential triggering mechanisms can be considered: (1) waves, tides and atmospheric pressure variations, (2) sediment loading and unloading e.g. MTDs, (3) earthquakes and (4) changes in eustatic sea level (Judd and Hovland, 2007). Waves, tides and atmospheric induced pressure variations has been proposed as a cyclic "pumping" mechanism for unit pockmarks (Hovland et al., 2010) but are considered insufficient to produce large-scale MTD seal failure. Sediment loading from MTDs is not observed in the sedimentary succession, however it is possible that undated slope failure at the NE edge of the plateau (Fig. 6.1), or reactivation of MTD3 may have induced laterally extensive pressure variations. Slope failure can potentially be triggered by earthquakes and/or sea level change (Leynaud et al., 2009; Piper et al., 1985; Reeder et al., 2002; Rothwell et al., 2000) therefore the triggering mechanisms may not be mutually exclusive.

Due to the position of the NDSF close to the zone of interaction between the Anatolian, African and Arabian plates (Fig. 3.2), the Egyptian passive continental margin has been affected by earthquakes, both in recent and historical time (El-Sayed et al., 2004). The Temsah and Rosetta fault trends are thought to have been mostly active in the early Cretaceous, however low magnitude earthquake epicentres (magnitudes not exceeding 6.7) have been reported offshore Egypt during the Quaternary and Holocene (McKenzie, 1970; El-Sayed et al., 1994; El-Sayed et al.,

2004). Mean return periods for earthquakes in the Gulf of Suez are predicted to be c. 10,000 yrs for magnitude 6 earthquakes (El-Sayed et al., 2004). Tentatively extrapolating the return period to the Late Pleistocene, it is possible that a magnitude > 6 earthquake could provide a triggering mechanism (Hasiotis et al., 1996), however the large distance from the epicentre may reduce the effects of pore pressure rise and sediment rearrangement due to shaking of the MTD seal.

Sea level has fluctuated in a generally falling trend during the late Pleistocene, reaching its lowest level c. 18,000 yrs BP (Fig. 3.2). Dates for significant normal pockmark formation at c. 50,000-80,000 yrs BP (approximated from sedimentation rates) and 15,000 yrs BP (chronostratigraphically dated) are of comparable age to two significant drops in sea level (Fig. 3.2). A dramatic fall in eustatic sea level is likely to reduce hydrostatic pressure and promote hydrofracturing and/or capillary migration in buoyant overpressured fluids (Judd and Hovland, 2007), such as those trapped beneath MTD3. Similar correlations between falling sea level and pockmark formation have been observed by Gay et al. (2007b).

6.6.3 Longevity of conduits

Although pockmarks have been recognised as resulting from highly focused fluid expulsion for nearly 40 years (King and MacLean, 1970), surprisingly little is understood of the conduits that presumably underlie the vast majority of these features. Pockmarks were first unambiguously linked to pipe-like conduits by Løseth et al (2001), since then a number of other studies have reported a close spatial association between pockmarks and a root conduit that is pipe-like (Gay et al., 2006b; Haacke et al., 2009; Hustoft et al., 2010; Hustoft et al., 2007; Ligtenberg and Connolly, 2003; Paull et al., 2008; Westbrook et al., 2008). This spatial association points to a relatively higher permeability for the pipe, but the manner in which the higher permeability is achieved, be it a static or dynamic property is poorly constrained (Cartwright et al., 2007). Nevertheless, it is often assumed that pipes contain a swathe of hydraulic fractures that propagated during the initial phase of

fluid expulsion that led to a pockmark forming at the top of the pipe (Chapter 4 and references therein). The lack of knowledge of the conduits stems from their poor representation in the rock record (Hanken et al., 1996; Roberts et al., 2010) and the inability of the seismic method to directly image their internal characteristics (Perez-Garcia et al., 2009).

The clear association described in this study between an underlying pockmark, and a later cluster of smaller pockmarks thus provides additional insights into conduit behaviour at a time scale that is high resolution by normal geological standards. The main conclusion reached in this study is that the conduits were reactivated after a lengthy period of inactivity, suggesting that whatever the mode of higher permeability was for the initial period of pockmark formation, that it could be resurrected for a later period, even after a maximum time gap of < 100,000 yrs (D0). This is perhaps not surprising, since if the conduit is indeed a zone of high fracture permeability, then a later pressure pulse could easily dynamically re-open pathways, or at least selected pathways from the available fracture network.

Several previous studies have shown examples of episodic use of a single conduit over longer time scales of millions of years (Cartwright et al., 2007; Hansen, 2006). Longevity has been implied, for example, in seep studies where persistent gas leakage through pockmarks is common, supporting vent communities and the generation of sonar-detectable carbonate hardgrounds (Gay et al., 2007a; Gay et al., 2006a; Gay et al., 2006b; Hovland, 2002; Hovland and Judd, 1988; Hovland and Svensen, 2006; Hovland et al., 2005; Paull et al., 2008; Paull et al., 1995). At the lower resolution of standard 2D or 3D seismic data longevity has been implied by the interpretation of vertically stacked concave reflection geometry as buried or stacked pockmarks (Çifçi et al., 2003; Curzi and Veggiani, 1985; Mazzotti et al., 1987) or by the localised high amplitude brightening above buried craters (Chapters 4 and 5). At outcrop, carbonate cemented pipes are testament to the endurance of fluid migration (Clari et al., 2004; De Boever et al., 2006b, a; De Boever et al., 2009b; Nyman et al., 2009).

Longevity of conduit activity must surely be related to the precise hydrodynamic context, and the degree of reactivation of conduits must then be related to fluid flux.

It seems reasonable that flux can be approximated from pockmark geometry (all other considerations being equal). In this study, the size of the buried pockmarks is several orders of magnitude larger than the unit pockmarks, and I suggest therefore, that an order of magnitude difference in flux was involved for the different sets of pockmarks. Given the size, number of features, planform geometry, spatial distribution, age and suggested mode of formation, buried pockmarks represent a low frequency, high magnitude flux. In contrast, unit pockmarks represent a higher frequency, lower magnitude process. Taking representative analogues it is possible this variation in observed flux is comparable with a violent eruptive phase followed by a quiet degassing phase as observed for some mud volcanoes (Clari et al., 2004; Clari et al., 2009).

Strong backscatter or hard sonar targets are indicative of MDAC or methane trapped within near-seabed sediments. The NDSF is an environment with high depositional and burial rates, therefore to see such a well-resolved, acoustically high amplitude expression of the seabed associated with unit pockmarks suggests a recent phase of activity. Those depressions without unit pockmarks are not visible in the backscatter sonar data, suggesting the Plateau hosts a combination of active, recently active, and totally dormant conduits.

Unit pockmarks have not been observed at depth within the drape package of Unit 4 suggesting that the unit pockmarks began to form within the depressions recently (since Horizon A200 or c. 9,000 yrs). Unit pockmark clustering in the depressions is related to a spatially specific fluid source suggested here to be the MTD3. I suggest that clustered unit pockmarks represent a bifurcation or local scattering of a single highly focused fluid supply. Observations presented here suggest bifurcation may be caused by two end-member mechanisms. Firstly, fluid expulsion through the centre of the buried pockmark to the seabed (Fig. 6.8). This is an analogous mechanism to that suggested for unit pockmark formation by Hovland et al (2010) but without the forced migration of fluids to the buried pockmark edge. Secondly, fluid pressure builds up beneath a diagenetic seal (carbonate?) formed by the buried pockmark leading to seal breach and continued vertical migration (Fig. 6.9) (Hovland et al., 2010). Fluid is focused by the pipe feeding the buried pockmark. By analogy with previous studies it is inferred that this pipe may represent an amalgamation of

hydrofracture networks or possibly small (below seismic resolution) "pipes" (Davies and Stewart, 2005).

Seepage through the system is perhaps implied but cannot be observed (Fig. 6.8). Seepage bifurcation suggests that fluid migration occurred under sufficiently low pressure gradients to permit migration along multiple branch-like hydrofracture networks (Fig. 6.14). Under low flux conditions, the fluid 'batch' selects random migration pathways based on paths of least resistance provided by heterogeneities in permeability. Each branch which reaches the seabed produces a single unit pockmark. It is assumed that each branch could potentially permit fluid migration on multiple occasions, however blockages due to sediment deposition and/or mineral precipitation would encourage the formation of additional unit pockmarks (Hovland, 2002).

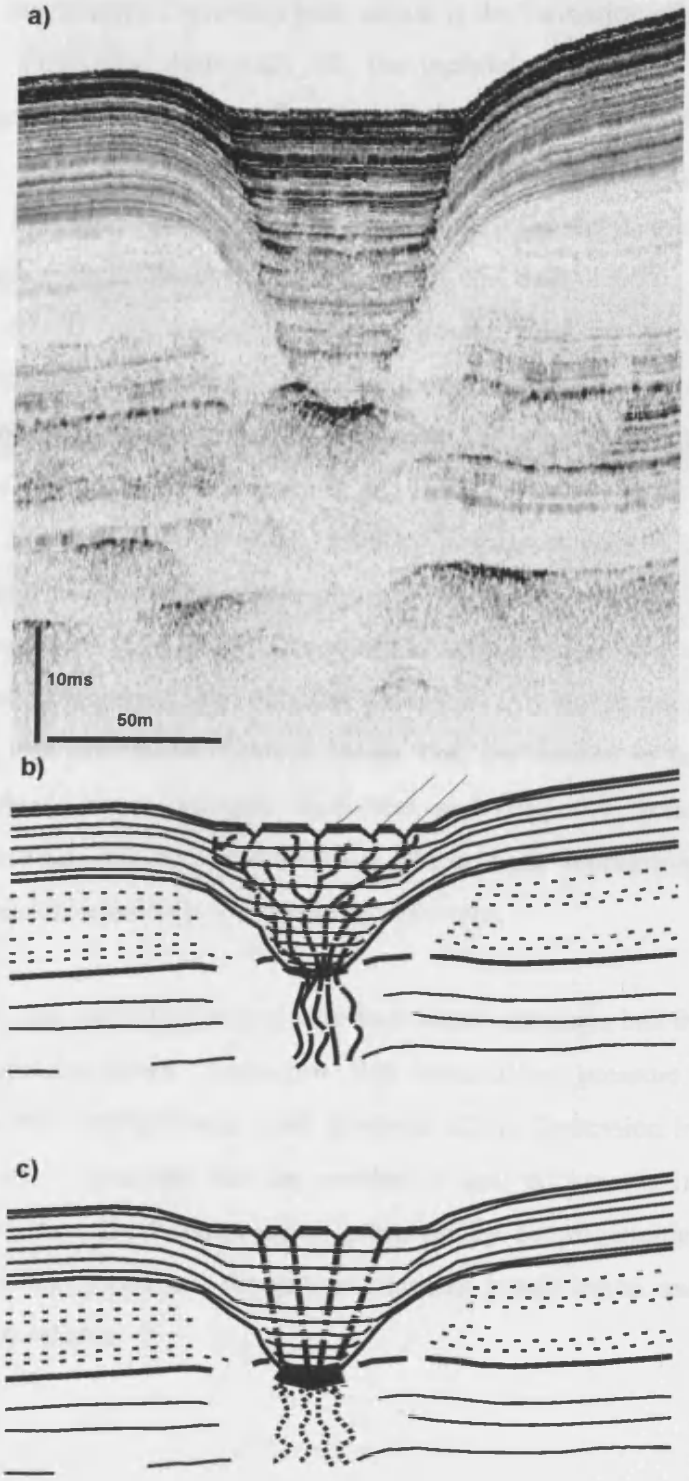

Figure 6.14 Conceptual model. A) Buried pockmark covered with drape. B) Post formation fluid migration via seepage. C). Post formation fluid migration following breach of a MDAC seal.

An alternative mechanism to produce bifurcation is the formation of a temporary seal (Fig. 6.14). Following formation of the normal pockmark, chemosynthetic communities grow, sustained by methane migration. Through time MDAC develop. Their growth seals the pockmark (Hovland, 2002), restricting fluid/methane migration and chemosynthetic community growth, and the normal pockmark is buried by drape. Overpressures build beneath the seal, leading to small-scale, localised seal breach. By analogy with seep studies, vertical "pipe" pathways are established to the seabed forming a unit pockmark. This pipe may represent either; a) an open conduit, possibly carbonate cemented, b) a brecciated conduit, or c) a hybrid of these two states (De Boever et al., 2009a; De Boever et al., 2009b; De Boever et al., 2006a, b; Nyman et al., 2009). Similar to normal pockmarks, unit pockmark formation could either be a one off (triggered) event or intermittent but persistent through time (Chapter 5). As with the seepage mechanism, pathways may be reused or sealed. Interestingly, only the youngest (C0) buried pockmarks with the most abundant unit pockmarks clusters above, that are located in the south plateau area show evidence for a potential carbonate seal (Fig. 6.9. zone b). Drawing comparisons between unit pockmarks within and outwith depressions, it is possible that unit pockmark formation is a single eruptive event.

A conceptual model consisting of multiple individual pathways has the advantage of diachronous formation times. Local low flux bleed-off of pressure is a small-step valving process that prevents large scale blowout of the depression in a single more catastrophic event. I propose that the number of unit pockmarks in a cluster is a function of fluid flux, fluid composition, permeability heterogeneities in the drape, MDAC development, sediment deposition, mineral precipitation and overpressure development and release.

6.6.4 Implications

The most significant implication of this study is the definitive evidence that conduits remain viable after lengthy periods of dormancy, and can be reactivated if the

hydrodynamic conditions require a renewed phase of focused fluid expulsion (and pressure bleed-off).

A secondary implication pertains to the interpretation of stacked pockmarks. This study has shown that some caution is required when interpreting concave upwards reflection configurations above buried pockmarks. This type of geometry has been referred to as "stacked pockmarks" in several previous studies (Baraza and Ercilla, 1996; Çifçi et al., 2003), and has been linked to the possibility of slow seepage after an initial phase of more catastrophic fluid expulsion especially when imaged in 3D data (Chapter 4). This study has shown, however, that pockmark-like morphology of concave upwards reflections can result purely from drape-type deposition failing to infill the initial seabed crater, leaving vestigial relief. I suggest that observations of erosional truncation of host strata should be used to distinguish drape perpetuation above buried pockmarks from true stacked pockmarks.

6.7 Concluding remarks

One hundred and forty two buried pockmarks from the Rosetta Region of the Western Nile Deep Sea Fan have been analysed in terms of their time of formation and longevity of post formation fluid migration. Stacked concave reflections above the buried pockmarks are interpreted as pockmark arrays. Pockmark arrays represent a perpetuation of pockmark-like morphology of concave upwards reflections resulting from a purely drape-type deposition failing to infill the initial seabed crater. The main findings can be summarised as follows;

- The Plateau area contains 142 buried pockmarks and 1728 unit pockmarks. 46 % of unit pockmarks are clustered within seabed depressions above the buried pockmarks. Depressions can hold between 1 and 152 unit pockmarks.
- Buried pockmarks formed between 100,000 yrs BP and 15,000 yrs BP. The majority forming at a single reflection estimated to be c. 50,000-80,000 yrs BP.

- The formation of the buried pockmarks is believed to result from a single triggering mechanism and is consistent with a steep drop in eustatic sea level c. 50,000-80,000 yrs BP.
- Pockmark arrays permit post-formation fluid migration through the buried pockmark to the seabed. These conduits remain viable after lengthy periods of dormancy, and can be reactivated if the hydrodynamic conditions require a renewed phase of focused fluid expulsion and pressure bleed-off.
- The longevity of post formation fluid migration is estimated to be ~50,000-100,000 years in this part of the Rosetta complex.

Chapter 7

This chapter will be submitted for publication as Moss, J.L., and Cartwright, J., 2010, Overpressure and release: The drainage cell characteristics of a pockmark field, Nile Deep Sea Fan to Marine and Petroleum Geology. Currently seeking permission to publish.

The work presented in this chapter is that of the lead author (JLM), editorial support was provided by the project supervisor (JAC) in accordance with a normal thesis chapter.

7 OVERPRESSURE AND RELEASE; THE DRAINAGE CELL CHARACTERISTICS OF A POCKMARK FIELD, NILE DEEP SEA FAN

7.1 Abstract

Over 25,000 seabed pockmarks were mapped from the Rosetta Channel region of the Western Nile Deep Sea Fan (NDSF) using concurrent Ultra High Resolution 2D, Chirp profiler and side scan sonar data which spans the Holocene-Pleistocene period. Within the region, a pockmark field containing > 13,800 pockmarks was analysed using spatial statistics to determine the distribution of pockmarks within the field. Pockmarks within the field are small (~16 m diameter), shallow (~0.5 m deep) circular depressions which formed within the last ~6,500 years. The fluid source for the field is identified as an accumulation/generation of gas beneath a hemipelagic seal c. 20-40 ms beneath the seabed. Statistical spatial analysis of the field confirms the distribution of pockmarks is not random. An exclusion zone surrounding each individual pockmark is identified. The exclusion zone is a unique minimum radius around each pockmark which is not penetrated by any other pockmark. The exclusion zone works in unison with Self-Organised Criticality (SOC) in determining the spatial distribution of pockmarks within the field. The exclusion zone is interpreted as a pockmark "drainage cell". A conceptual model for a pockmark drainage cell is proposed whereby pockmark formation dissipates a radius/area of fluid and overpressure, thereby preventing the formation of another pockmark within that cell. Consequently, pockmarks are observed to separate or produce anti-clustering tendencies within the field.

7.2 Introduction

One of the most significant processes involved in pockmark formation is overpressure and release. The presence of fluid escape features like seafloor pockmarks (Hovland and Judd, 1988) and seismic chimneys (Løseth et al., 2001) manifest localized zones of high fluid pressures in the subsurface (Judd and Hovland, 2007). Overpressure (i.e. pore pressure in excess of hydrostatic) may develop from rapid sediment loading (> 1 m/ka) (Gibson, 1958; Rubey and Hubbert, 1959), tectonic compression and the rapid generation or storage of methane (Judd and Hovland, 2007) in low-permeability environments. Overpressure and release contribute to fluid venting where pressure gradients drive lateral, downdip, localised updip and vertical flow (Hustoft et al., 2009a)

Pockmark/chimney structures are regarded as subsurface pressure valves (Judd and Hovland, 2007), where their spatial distribution roughly approximates the location of maximum overpressure in the subsurface. Pockmark fields by analogy are loci for widespread overpressure generation and fluid migration from the shallow subsurface (Scanlon and Knebel, 1989; Kelley et al., 1994; Christodoulou et al., 2003; García-García et al., 2004; Chand et al., 2009; Rollet et al., 2009; Webb et al., 2009). For example a) The Nyegga pockmark field, mid Norwegian margin contains ~400 pockmarks (density 4-10 pockmarks/km^2) is sourced from a contourite layer 300-400 ms TWT bsf (Hustoft et al., 2009b) , b) Fram Strait pockmark field, offshore NW Svalbard, contains > 100 pockmarks is believed to be sourced from the free gas zone beneath a BSR at ~200 mbsf (Hustoft et al., 2009b), c) it is proposed that the Patras Gulf, Greece pockmark field (density 80 pockmarks/km^2) is sourced from shallow gas trapped > 30 mbsf (Hasiotis et al., 1996), and d) Belfast Bay, Maine pockmark field contains 2,300 pockmarks (density 240-270 pockmarks/km^2) is understood to be sourced > 10-40 mbsf (Rogers et al., 2006).

Pockmark fields represent multiple points of overpressure generation and release from a spatially extensive shallow fluid source(s). The spatial location of the points of overpressure is of particular importance when interpreting the genesis of pockmarks within a field. Quantitative interpretation of the spatial distribution of

pockmarks is a relatively new technique within the fluid flow literature (Li et al., 2007; Olu-Le Roy et al., 2007; De Boever et al., 2009b; Galéron et al., 2009; Hammer, 2009; Webb et al., 2009; Jané et al., 2010). The strength of this technique lies in coupling pockmarks with variations in the distribution of overpressure, fluid source and shallow seals e.g. hydrates, and reconstructing fluid flow patterns and spatio-temporal fluid migration characteristics.

In order to enhance our understanding of the spatial distribution of overpressured fluids within pockmark fields I integrate ultra high resolution 2D, Chirp profiler and side scan sonar data from a pockmark field on the Western Nile Deep Sea Fan (NDSF) (Fig. 7.1) with statistical spatial analysis. I aim to quantitatively describe the spatial distribution of pockmark formation within a field in order to address questions like why are pockmarks not tightly packed in a wall-to-wall honey-comb structure given a spatially extensive fluid source?

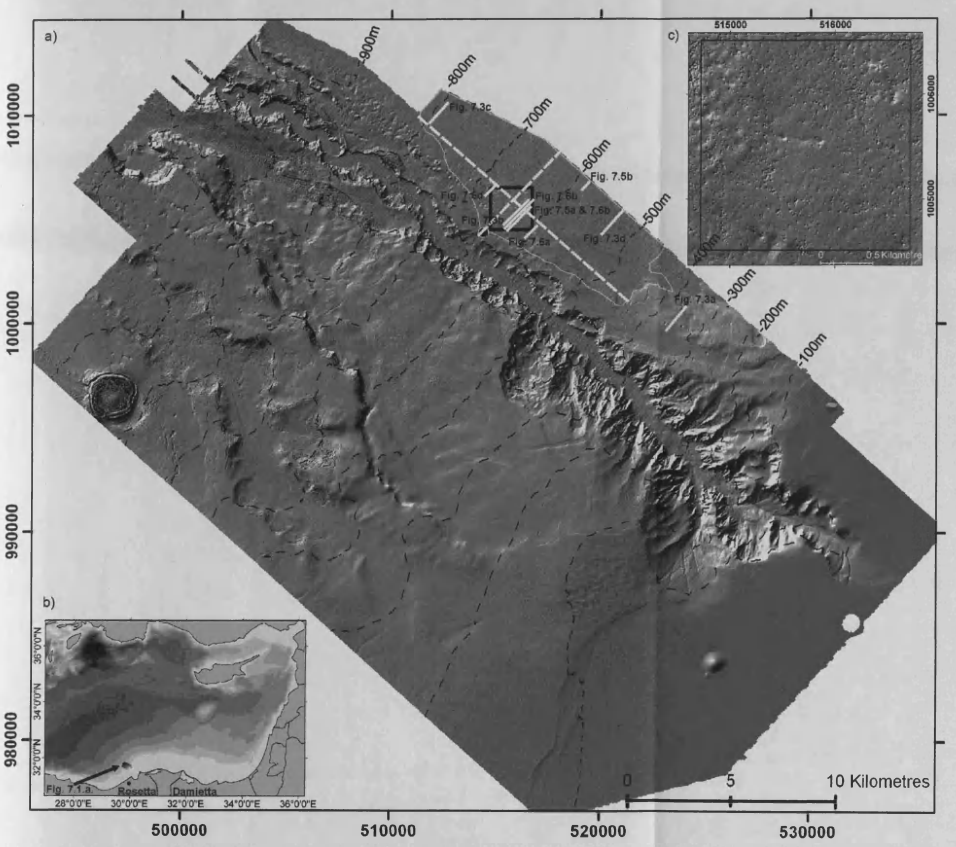

Figure 7.1 Location map. a) Dip map of the Rosetta Region. Area of Chirp profiler and side scan sonar coverage, showing location of STACOR (black dot), Rosetta pockmark field (grey outline) and study area (black box). AUV examples (solid white lines) and UHR examples (dashed white lines) are shown. b) Location of Rosetta Region in the Western Nile Deep Sea Fan. Tributaries of the Nile River, Rosetta River and Damietta River are shown. The location of Alexandria is shown (black dot). c) Dip map of the study area within the pockmark field.

7.3 Geological setting

Regional geology and tectonic setting of the NDSF is given in Chapter 3 (Fig. 3.2).

A 17.8 m STACOR core collected on behalf of BP in 2004 from the eastern bank of the Rosetta channel was geotechnically sampled (Fig. 2.5). The core indicated a Holocene-Pleistocene, predominantly clay (with some silt), package (Fig. 7.2). An important horizon, A030, was chronostratigraphically dated at 6,500 yrs BP.

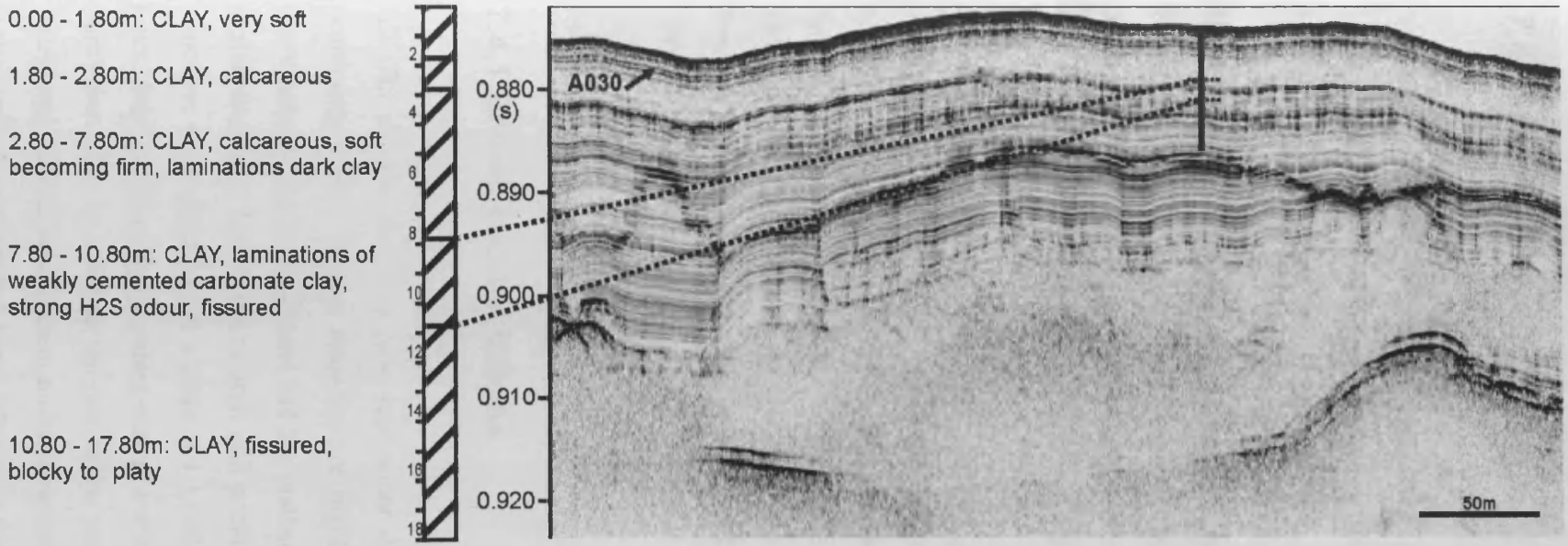

Figure 7.2 Basic STACOR information and core location. Horizon A030 is chronostratigraphically dated at 6,500yrs. STACOR (white triangle) location is given in Figure 2.5.

7.4 Data and methodology

The data used for this study comprised a combined survey of Autonomous Underwater Vehicle (AUV) and 2D Ultra High Resolution (UHR) seismic data were collected by Fugro Survey in 2004 and 2005.

Total AUV data coverage for this area (~1000 km^2) is referred to as the Rosetta Region in the text. Smaller areas on the eastern bank of the Rosetta Channel are defined as the Eastern Slope (~150 km^2), pockmark field (~75 km^2) and the study area (4 km^2) (Figs. 6.3 and 7.1)

For simplicity in handling a large pockmark population (> 13,800) a 2 km x 2 km study area was selected from within the pockmark field for the purpose of statistical analysis. Geometric information (diameter, depth, area, slope angle) was calculated for the 1,477 unit pockmarks within the study area based on the 3 m resolution bathymetry data. Density, nearest neighbour index, nearest neighbour distance, Ripley's K, Voronoi polygons and Minimal Spanning Tree (MST) spatial statistics were utilised in the analysis.

7.4.1 Errors and limitations

All GIS models based on side scan sonar data have a resolution of 3 m ±1.5 m positioning error. Spatial statistics are highly susceptible to the precision of the coordinates in the point dataset and the mathematical boundary area imposed on the spatial analysis. The centre of each unit pockmark (x,y,z), described by a 4-way dip structure, was determined at a scale of 1:1,000 using an aspect (°) model. A random point distribution of 1477 points within a 4 km^2 area was generated using the GIS (ArcView 9.2). A more robust test of the pockmark distribution against a random distribution would benefit from multiple random point generation models in addition to the single model applied here. Minimum Spanning Tree, hardcore distribution and Self-Organised Criticality simulations were compared to a random population

generated from 100 trials of statistically random data. Minimum bounding rectangle boundary conditions were applied to the spatial statistics. Boundary conditions were fixed by selecting a square quadrate and study area for the pockmark field. Ripley's K calculations were modelled using Ripley's Edge Correction Formula. The calculation of nearest neighbour and MST statistic utilises coordinates that do not take into account pockmark diameter thereby restricting minimum distances where pockmark perimeters touch i.e. wall to wall pockmarks. This applies to 2 % of the population.

7.5 Results

The pockmark field is located in a mid slope position on the Eastern Slope (~150 km^2) in 400-800 m water depth (Fig. 7.1). The pockmark field is identified as a large area of numerous, small, closely spaced pockmarks, distinct from the general background distribution of pockmark formation on the Eastern Slope. At the regional scale, the pockmark field is defined by pockmark densities in excess of > 100 unit pockmarks/km^2. This covers an area of ~75 km^2. The pockmark field is believed to extend east, beyond the limits of the data present here, possibly up to < 18 km, to the eastward limit of the large headscarp (Figs. 2.5 and 7.3).

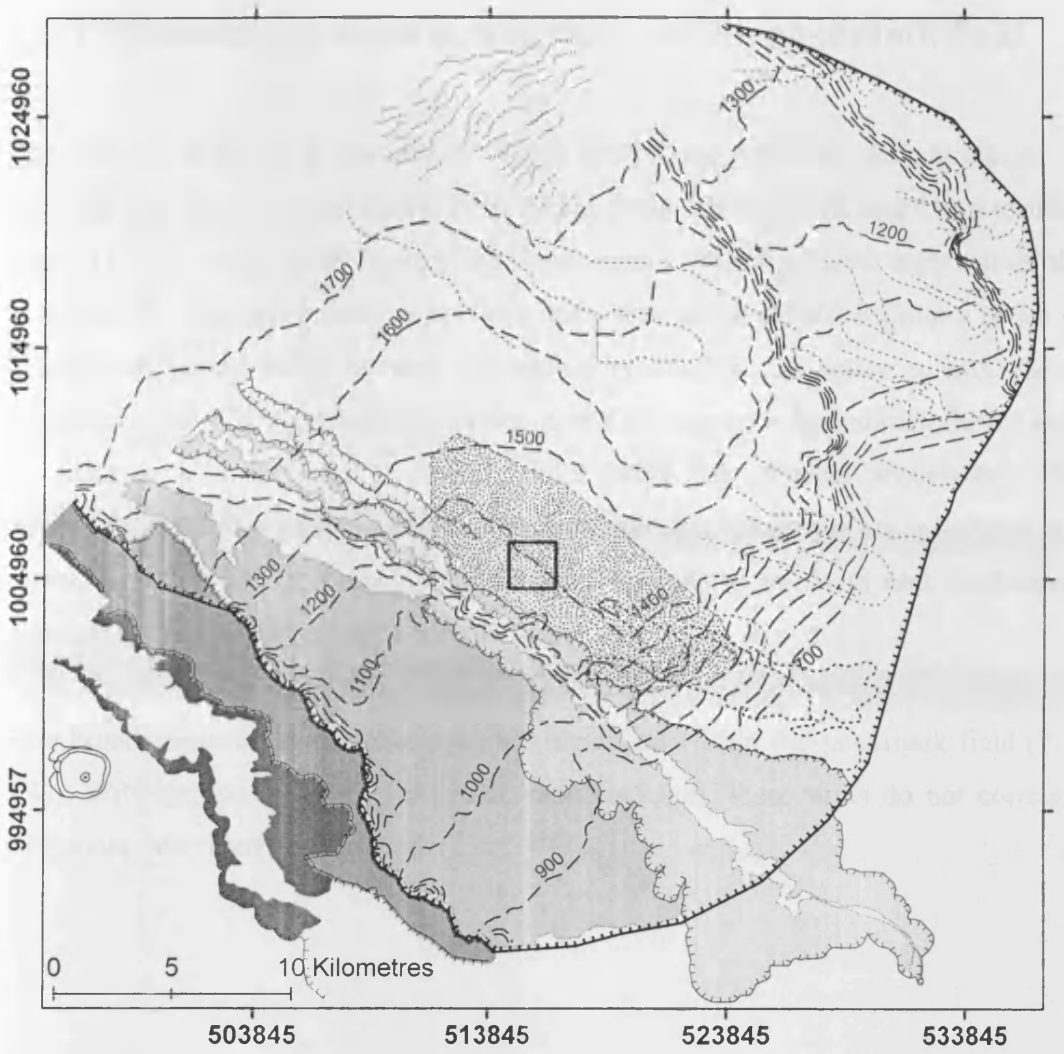

Figure 7.3 Structure map of the Rosetta Region. Structure map of the large Mass Transport Complex. Contours are depth to the MTC basal shear surface (ms) (based on 3D data). Area of greatest density pockmarks within the field (stippled area) and the study area is indicated (black box). The pockmark field is believed to extend beyond the boundaries mapped here. Slope failures associated with the headscarp (black line) are shown in grey dotted lines.

7.5.1 Seismic sequence stratigraphy of the pockmark field

The Eastern slope is a prograding wedge comprising complex seismic facies of interdigitated chaotic sequences at both the resolution of the UHR and Chirp profiler data. This led to difficulty in mapping continuous coherent seismic units within the stratigraphy. The slope sediments in the study area are divided here into a series of depositional units, based on their correlatability and on distinctive seismic facies characteristics. They are not sub-divided based on sequence boundaries; hence they are referred to informally as seismic units rather than formal sequences. The recorded sequence is of Holocene-Late Pleistocene age. The units are orientated in a downslope direction and display non-uniform unit thickness, with unit thicknesses diminishing and pinching out in a distal direction.

Five broad seismic stratigraphic units are identified within the pockmark field (Fig. 7.4). With the exception of Unit H5 (drape package), these units do not correlate with those described in Chapter 6.

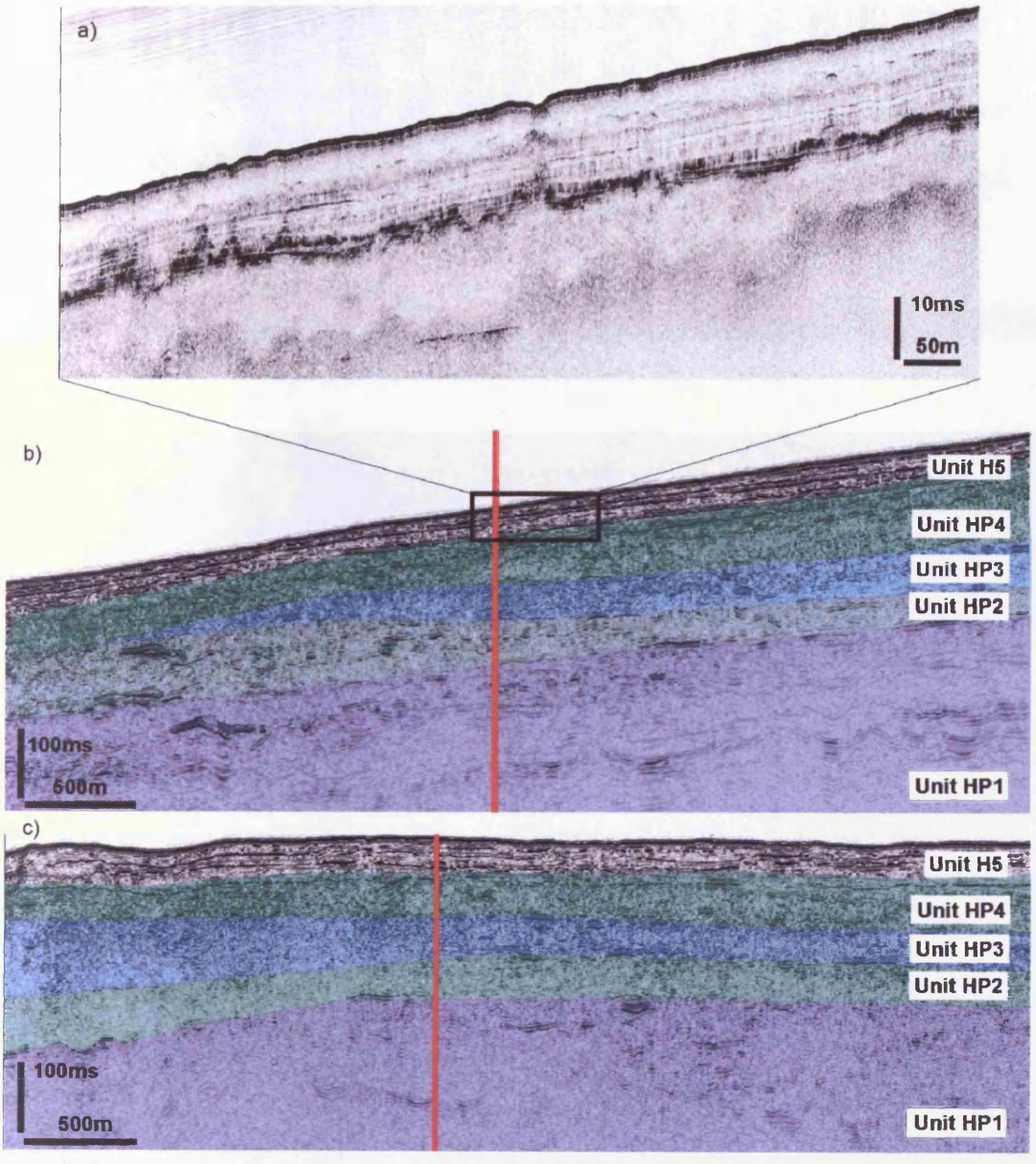

Figure 7.4 Seismic sequence stratigraphy. 2D UHR data in dip (b) and strike (c) directions and Chirp profiler (a) data shown. Mass Transport Deposit units Holocene-Pleistocene 1-4, drape package unit Holocene 5. Bottom simulating reflection in the UHR data (Unit H5) is a bubble pulse artefact.

7.5.1.1 Unit HP1

Unit HP1 is a predominantly low amplitude seismic facies of discontinuous and chaotic reflections with isolated pockets of high amplitude reflections (Fig. 7.4). The unit boundaries are difficult to distinguish but are marked by discontinuous, discordant, higher amplitude reflections. Unit HP1 is interpreted as a debris flow package with isolated pockets of coarser material (sand) which might contain gas.

7.5.1.2 Unit HP2

Unit HP2 is a predominantly low-medium amplitude seismic facies of discontinuous and chaotic reflections with large isolated pockets of high amplitude reflections (Fig. 7.4). The unit is of non-uniform thickness and locally thickens in a downslope direction before thinning. Unit boundaries are subtle discontinuous, non concordant, higher amplitude reflections and difficult to distinguish from the preceding and succeeding units. Unit HP2 is interpreted as a debris flow package with isolated pockets of coarser material (sand) which might contain gas.

7.5.1.3 Unit HP3

Unit HP3 is a predominantly high amplitude seismic facies of discontinuous and chaotic reflections with large zones of high amplitude reflections (Fig. 7.4). The unit is of near-uniform thickness but thins and pinches out in a downslope direction. Unit boundaries are discontinuous but concordant and horizontal in places, with the upper boundary erosionally truncated against Unit HP4. Unit HP3 is interpreted as a debris flow package which has been erosionally truncated at its distal end.

7.5.1.4 Unit HP4

Unit HP4 is a predominantly high amplitude seismic facies of discontinuous and chaotic reflections with isolated reflections of above background amplitude (Fig. 7.4). Unit boundaries are discontinuous in places but concordant and parallel to the

seabed. Internal reflections are highly chaotic but show evidence for minor faulting and thrusting propagating into Unit H5. Unit HP4 is interpreted as a debris flow package, the large number of the high amplitude reflections suggest the unit may contain numerous sandy or permeable bodies which could contain gas.

7.5.1.5 Unit H5

Unit H5 is a predominantly high amplitude seismic facies of finely layered, concordant, slope parallel, near continuous reflections (Fig. 7.4). Unit H5 is interpreted as a hemipelagic drape package.

7.5.2 Shallow gas on the Eastern Slope

The Chirp profiler data reveals evidence for acoustic wipeout at the base of the shallow sedimentary interval (uppermost < 40 ms). On average, the depth to the acoustic wipeout zone is ~20-40 ms below the seabed. The top of the acoustic wipeout zone is mapped on the basis of acoustic amplitude of wipeout (high amplitude) and the degree to which the wipeout obscures the stratified layering of Unit H5 (total obstruction). At the small scale, top of the acoustic wipeout zone is not concordant with strata but oscillates with a variable height difference of ~10-20 ms. The wipeout zone is interpreted as the top of a gas front (Floodgate and Judd, 1992; Naudts et al., 2009). Similar imaging of oscillating gas fronts have been observed by Iglesias and García-Gill (2007) and Naudts et al (2009).

The character of the gas front and its relationship with the background strata can be broadly categorised into three zones, proximal, central and distal (Fig. 7.5). The transition between zones is gradational in a downslope direction.

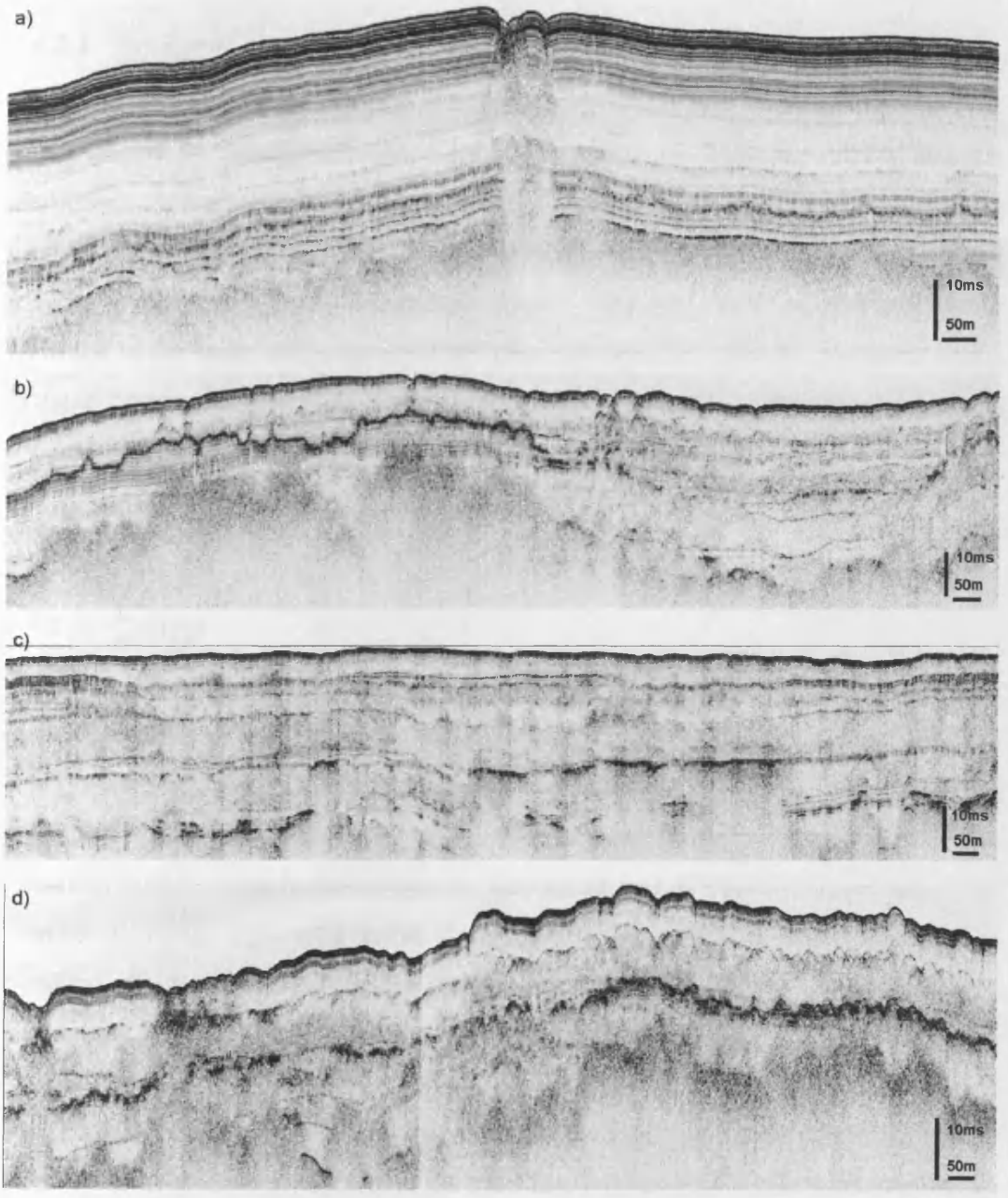

Figure 7.5 Position of the gas front on the Eastern Slope. a) Proximal, b) Central, c) Distal, d) Example of chaotic debris flow material in the near surface

7.5.2.1 Proximal

The proximal upper slope position is dominated by thinly bedded concordant seismic facies (Fig. 7.5). Where reflections are not disturbed by columnar vertical acoustic disruption, hereafter referred to as pipes (Løseth et al., 2009), reflections are continuous and seabed parallel. The uppermost ~40 ms of the shallow sedimentary interval is interpreted as hemipelagic drape. The gas front is stratigraphically confined to the base of the sequence and does not penetrate into the overlying strata. Isolated pockmarks and pipes transect the interval from the level of the gas front to the seabed. The proximal zone is upslope of the pockmark field.

7.5.2.2 Central

Thinly bedded, concordant, seabed parallel seismic facies, indicative of hemipelagic drape are visible in the uppermost ~20 ms of this mid-slope sequence (Fig. 7.5). The shallow sedimentary interval is obscured beneath this depth by semi-transparent acoustic disruption resulting in blanking of some areas of strata. Within the acoustic blanking, visible strata is discontinuous, discordant and of slightly higher amplitude than the blanking. It is not possible to map individual reflections due to the acoustic blanking effects, however I believe that these reflections represent localised shallow debris flow and/or debris slide units, hereafter simply referred to as debris flow units.

The Eastern Slope represents an accommodation zone for debris flow deposition from the large arcuate headscarp on the shelf break (Fig. 2.5). Material was probably deposited on the slope from 1) shelfal derived turbidite, debris flow and gully sources; 2) local instabilities in the headscarp and 3) reactivated shallow slope sliding in response to loading and fluid migration. Consequently, the seismic sequence stratigraphy is dominated by near-indistinguishable chaotic seismic facies which are difficult to separate into distinct seismic units.

The acoustic blanking of strata is visible from the ~400 m depth contour and deeper (Fig. 7.1). It is probable that the blanking is the result of gas seepage, or generation, in the debris flow units both within Unit H5 and/or deeper. It is difficult to

determine the top gas position, however the gas does appear to be trapped beneath the drape layer where present.

The pockmark field is located in this mid slope position (Fig. 7.1). There is an observational correlation between pockmarks and debris flow material (Fig. 7.5). Where the drape layer is absent, debris flow material is visible on the seabed and fewer pockmarks are observed. Localised high densities of pockmarks appear to bear an anti-correlation to surface debris flow material (this observation is further described in Fig 7.11).

7.5.2.3 Distal

The distal lower slope position is a complex interaction of semi-transparent acoustic blanking and visible discordant and concordant strata (Fig. 7.5). Similar to the Central zone, the distal seismic sequence stratigraphy shows evidence for thinly bedded, concordant, seabed parallel seismic facies, indicative of hemipelagic drape. Unlike, the central zone, this drape package is less spatially extensive and only visible with proximity to the former channel of the Rosetta Channel.

Discordant, non-seabed parallel, higher amplitude reflections, similar to the Central zone, are visible within the semi-transparent blanking. Equivalent to the Central zone, these reflections are interpreted as debris flow units. The units are more noticeable in this distal position and form more distinct packages.

The semi-transparent blanking in the distal zone is accompanied by regularly spaced vertical data collection artefacts. The gas front as described above is not evident in this zone. If present, the gas front is below the depth penetration of the Chirp profiler data (> 40 ms).

7.5.3 Seismic expression, interpretation and timing of unit pockmark formation in the pockmark field

Within the Rosetta Region > 25,300 pockmarks have been mapped (Fig. 7.6). The pockmark field contains > 13,800 unit pockmarks. An additional ~1,500 pockmarks are located on the Eastern Slope (totalling > 15,000 pockmarks) but are not considered to be within the pockmark field. Pockmark diameters within the field range between 5 – 41 m (average 17 m), with an average depth of 0.4-0.8 m. There is a positive correlation between pockmark diameter and depth. Their geometry is near circular with an average ellipticity ratio of 1:1.1 and 4-way dip slopes > 6 ° (measurements taken from the study area).

Pockmarks in the field are considered to be of average size for the Rosetta Region with slightly smaller pockmarks found in the MTC zone and larger pockmarks in the palaeochannel zone (Fig. 6.3 and 7.7). The pockmarks in the Rosetta Region are slightly larger than unit pockmarks (< 5 m) and smaller than normal pockmarks (50-100 m), as previously defined by Judd and Hovland (2007).

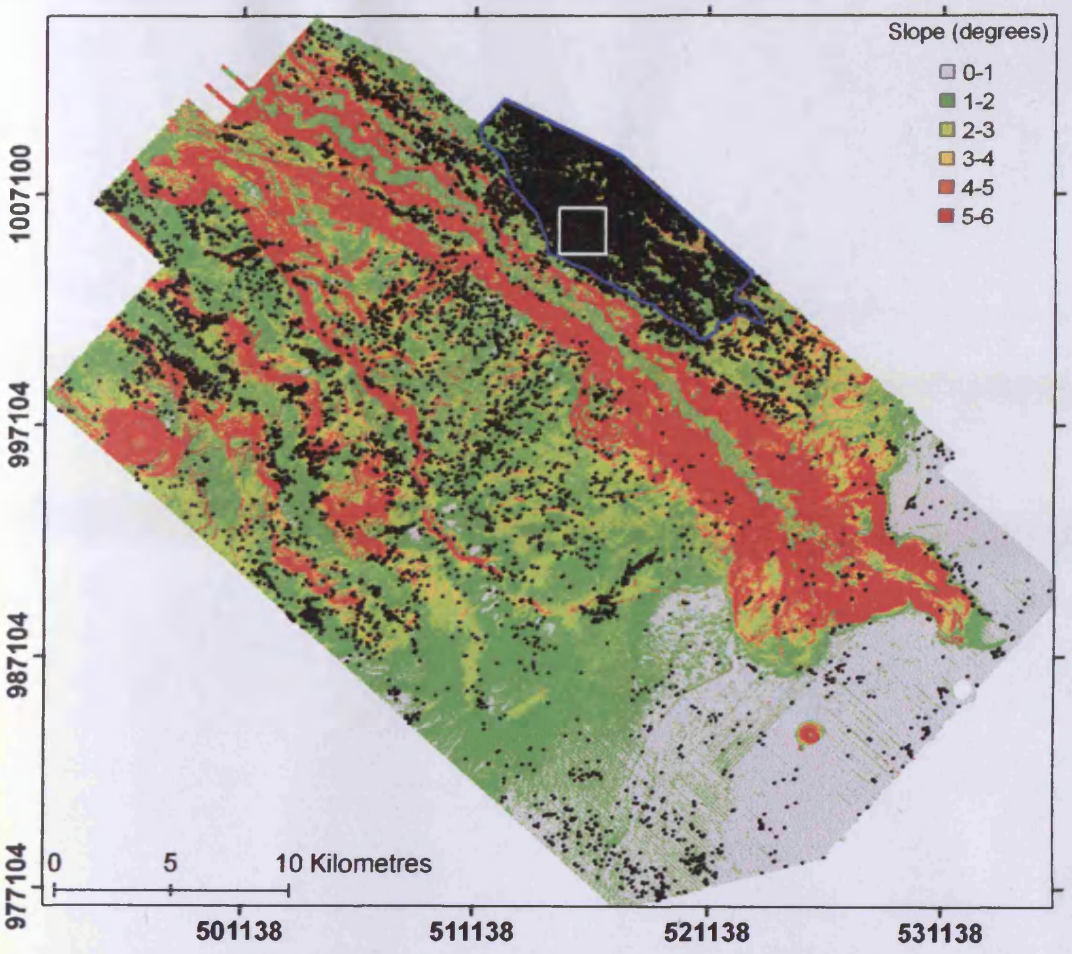

Figure 7.6 Distribution of >25,300 pockmarks within the Rosetta Region (black dots). Buried pockmarks are not mapped. Pockmark field is indicated by the blue outline. Seabed map is coloured according to slope (°). White box denotes the study area.

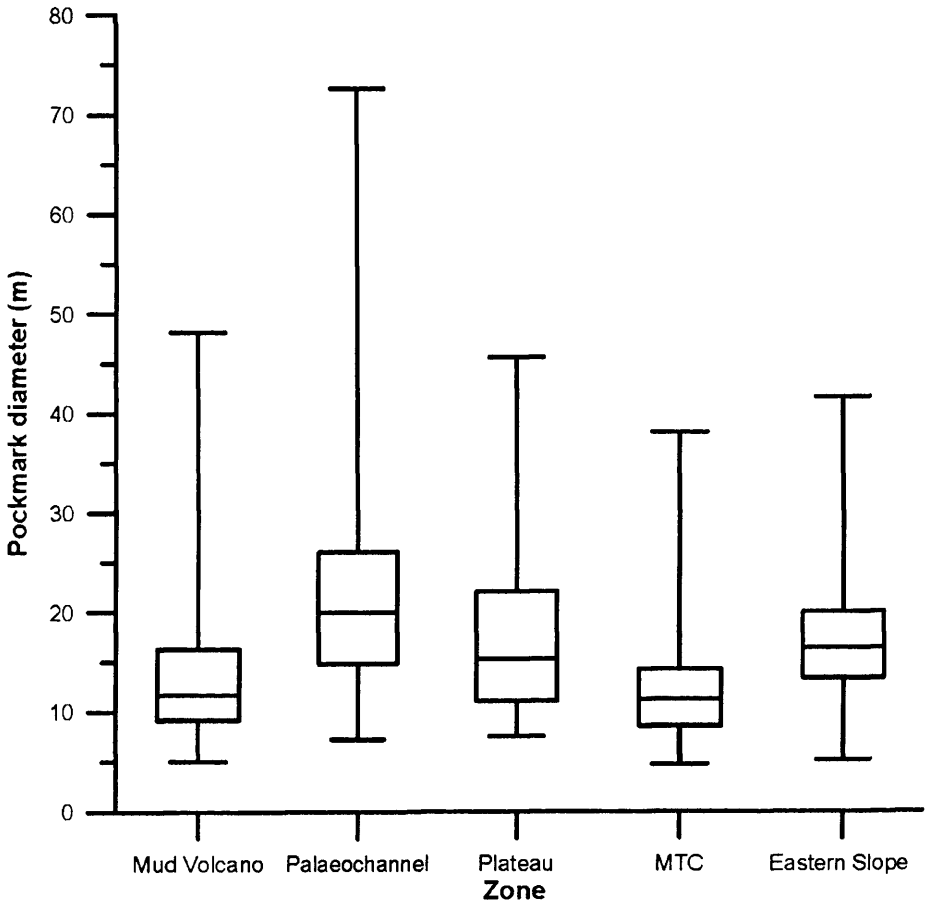

Figure 7.7 Pockmark diameter box plots. Comparison of surface pockmark sizes between the different geomorphological zones within the Rosetta Region (Fig. 6.3). Buried pockmarks are not included in the analysis.

The unit pockmarks in the pockmark field are imaged as v-shaped seabed depressions in the Chirp profiler data. The depressions transect the uppermost 2-3 reflections corresponding to < 5 ms beneath the seabed. Pockmarks are observed to either erosionally truncate the uppermost reflections or form short vertically stacked concave reflections 1-2 reflections high. The short stack of concave reflections is the same width as the pockmark and commonly dips into the centre of a bowtie artefact. Directly beneath the seabed depression, bowtie artefacts and other acoustic and amplitude anomalies are frequently observed e.g. chaotic inverted cone-shaped zones of high amplitudes or columnar vertical wipeout zones (Fig. 7.8). Both these artefacts are typically associated with the presence of gas within the sediments (Judd and Hovland, 2007).

Pockmarks are interpreted to have formed at the level of the deepest erosionally truncated reflection or deepest vertically stacked concave depression. This is predominantly at the A030 reflection for all the measured pockmarks within the field (Fig. 7.8) (I hereby recognise that this is a 2D dataset and despite closely spaced lines, it was not possible to sample all the pockmarks). It is feasible that the pockmarks may have formed either by hydraulic fracture or seepage of gas (and pore water) from a shallow reservoir. The erosional truncation of the reflections and the fine grained (clay) sediments suggest that hydraulic fracture may be the more likely scenario (Jain and Juanes, 2009) (Fig. 3.3).

Horizon A030 has been chronostratigraphically dated. The occurrence of pockmarks forming at this horizon places the timing of pockmark and pockmark field formation within the last 6,500 years. There is no evidence for buried pockmarks or fluid migration events before this time and continued fluid migration through these conduits is considered to be little to none given their recent formation.

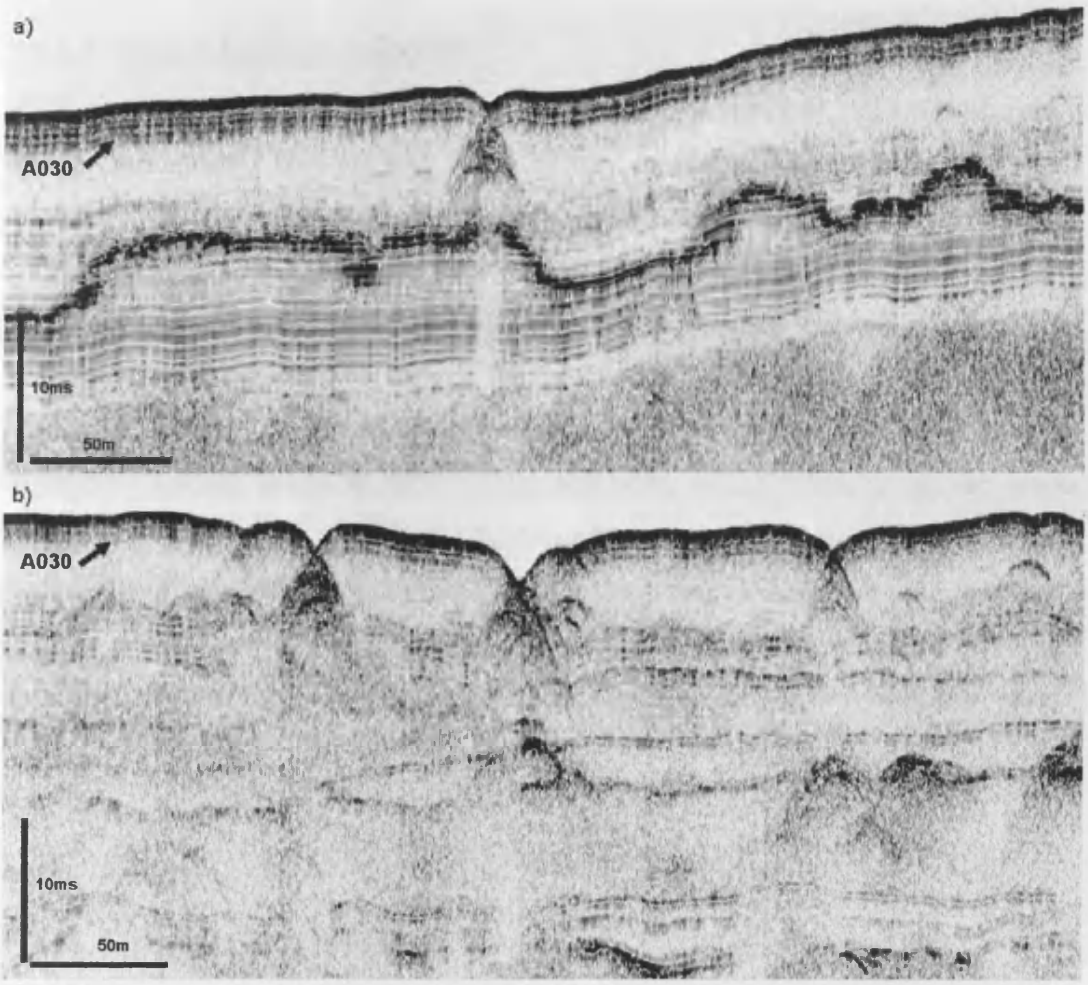

Figure 7.8 Unit pockmarks. Two contrasting examples of unit pockmarks within the field. a) series of stacked v-shaped depressions above a buried pockmark at the level of A030. High amplitude anomalies are present. b) erosional truncation of surrounding reflections to the level of A030

7.5.3.1 High amplitude reflections

High amplitude anomalies are detected in areas of well imaged, undisturbed, thinly bedded sedimentary layering (Fig. 7.8a). These anomalies are localised, short, high amplitude sections of reflections, that when viewed at the larger scale, appear to rise and fall in the sedimentary succession. The inability of the waveform to follow structural/sedimentary trends within the drape convinces me that this wave form is unrelated to geological processes. I tentatively suggest that these high amplitudes represent possible carbonate precipitates of (palaeo)biogenic microbial activity. Microbial activity produces CO^2 (biotic reaction), which when dissolved reacts chemically with Ca^{2+} to precipitate calcium carbonate in a chemical (abiotic) reaction (Libes, 1992). Without targeted drilling and sampling through this high amplitude seismic response, this interpretation must remain speculative. Similar high amplitude anomalies were also observed in the Rosetta Plateau pockmark arrays (Chapter 6, Fig. 6.8)

7.5.4 Spatial distribution

7.5.4.1 Qualitative observations from the pockmark field

Over 13,800 pockmarks have been identified in the pockmark field (~75 km^2) (Fig.7.6). The pockmarks are located in a complex stratigraphic setting comprising multiple interdigitated debris flow units, an oscillating gas front and high amplitude reflections interpreted as resulting from carbonate cement.

It has been observed that the location of the pockmark field is loosely related to the degree of gas seepage through Unit H5 afforded by the shallow interleaving debris flow packages. However, pockmarks are absent where debris material is observed on the seabed (Fig. 7.5d), and fewer pockmarks are present in the distal reaches of the Eastern Slope despite chaotic debris units.

At a more local scale, the position of individual pockmarks within the field is unrelated to the variable depth of the gas front or the high amplitude reflections (Fig.7.9).

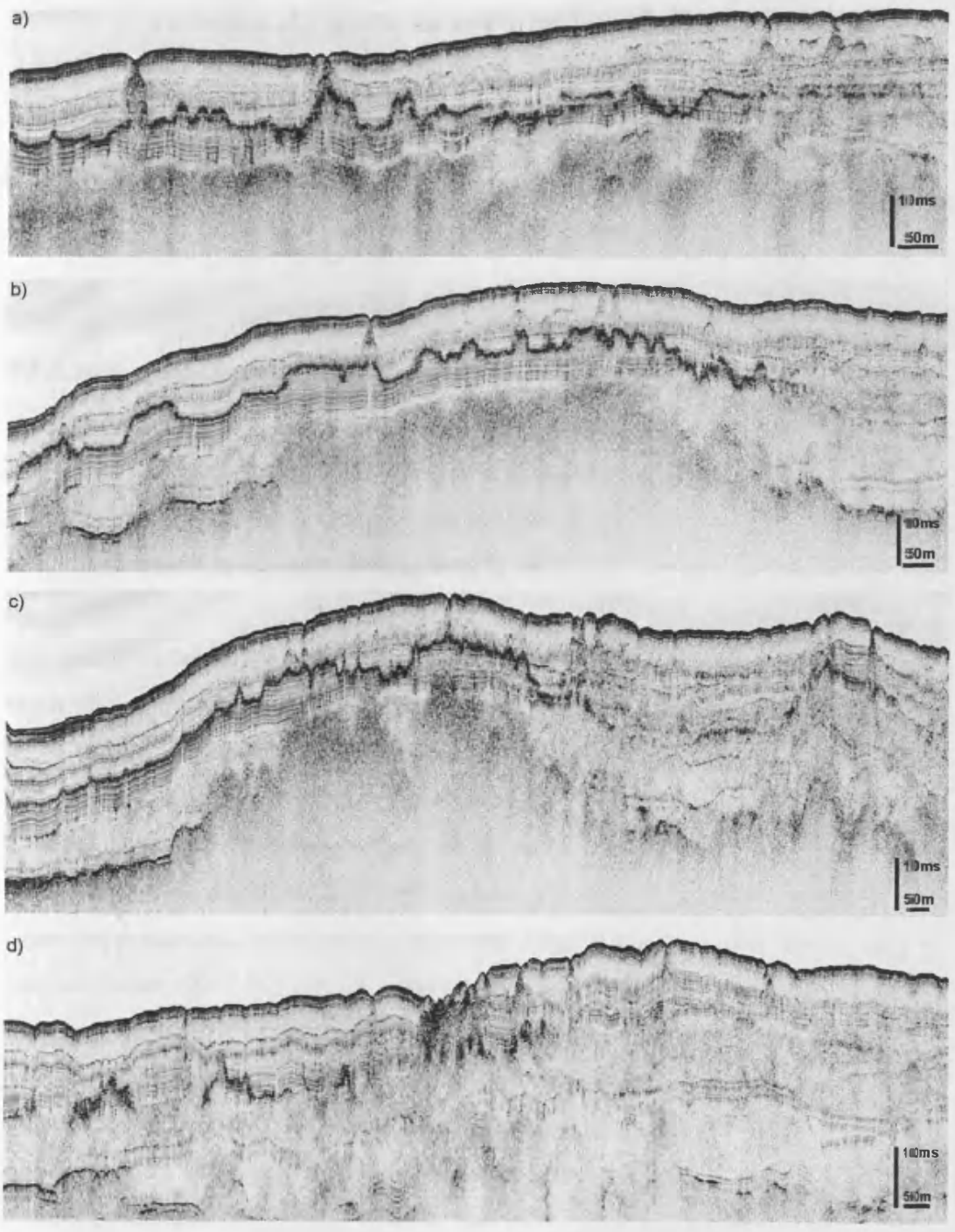

Figure 7.9 Gas front and high amplitude reflections. (a, b) Examples of oscillations in the high amplitude response and their relationship to the gas front. (c) Examples of oscillations in the top of the gas front. (d) High amplitude chaotic "plume" located beneath a densely (>600 pockmarks/km²) pockmarked area within the field.

Pockmarks are located above both the peaks and troughs of the gas front and high amplitude reflections. Additionally, there is no correlation between the size (diameter, depth) of the pockmark and its spatial position with relation to the depth of the gas front i.e. large pockmarks are not uniquely correlated to the peaks in the gas front.

7.5.4.2 Spatial statistics : Rosetta Region and pockmark field

Over 25,300 pockmarks have been identified and mapped across the entire Rosetta Region (~1000 km^2) (Fig. 7.6). The only exceptions are the central axis of the Rosetta Channel and the lower remobilised sections of the MTC zone where only a limited number of pockmarks are present (Fig. 6.3).

The spatial distribution of pockmarks within the Rosetta Region as a whole is the result of a combination of the complex heterogeneities in permeability (at all scales) in the subsurface combined with the structural and pressure history for the region. It is however noted that the spatial distribution of pockmarks east of the Rosetta Channel is markedly different to those on the west. First order characteristics of the statistical spatial distribution of pockmarks within the field have established that while the pockmark distribution is somewhat dispersed, the pattern may be due to random chance (*Rn* 1.02, *z* 1.22). Conversely, the spatial distribution of pockmarks west of the Rosetta Channel is clustered, and there is less than 1 % likelihood (critical value -2.58) that these clustered patterns could be the result of random chance. The palaeochannel pockmarks exhibit the greatest degree of clustering (*Rn* 0.35, *z* -54.55), followed by the mud volcano zone pockmarks (*Rn* 0.4, *z* -37.14), plateau pockmarks (*Rn* 0.42, *z* -48.79) and MTC zone (*Rn* 0.48, *z* -50.79). The pronounced difference between the spatial distribution of pockmarks within the field and the highly clustered nature of pockmarks west of the Rosetta suggests that the fluid source for the pockmark field is more spatially extensive than the focused migration associated with clusters.

The density map of the Rosetta Region has highlighted hot spots of pockmark occurrence (Fig. 7.10). The lateral margins of the pockmark field are broadly

delimited by densities in excess of 100 pockmarks/km^2 but densities in the centre of the field are in excess of 600 pockmarks/km^2. The detailed density map of the pockmark field reveals two hot spots of high density pockmark distributions within the field (Fig. 7.11). These hot spots are located in the centre of the field and are irregular in shape. Areas of low pockmark density within the field roughly correspond with areas of seabed debris flow deposition (Fig. 7.11).

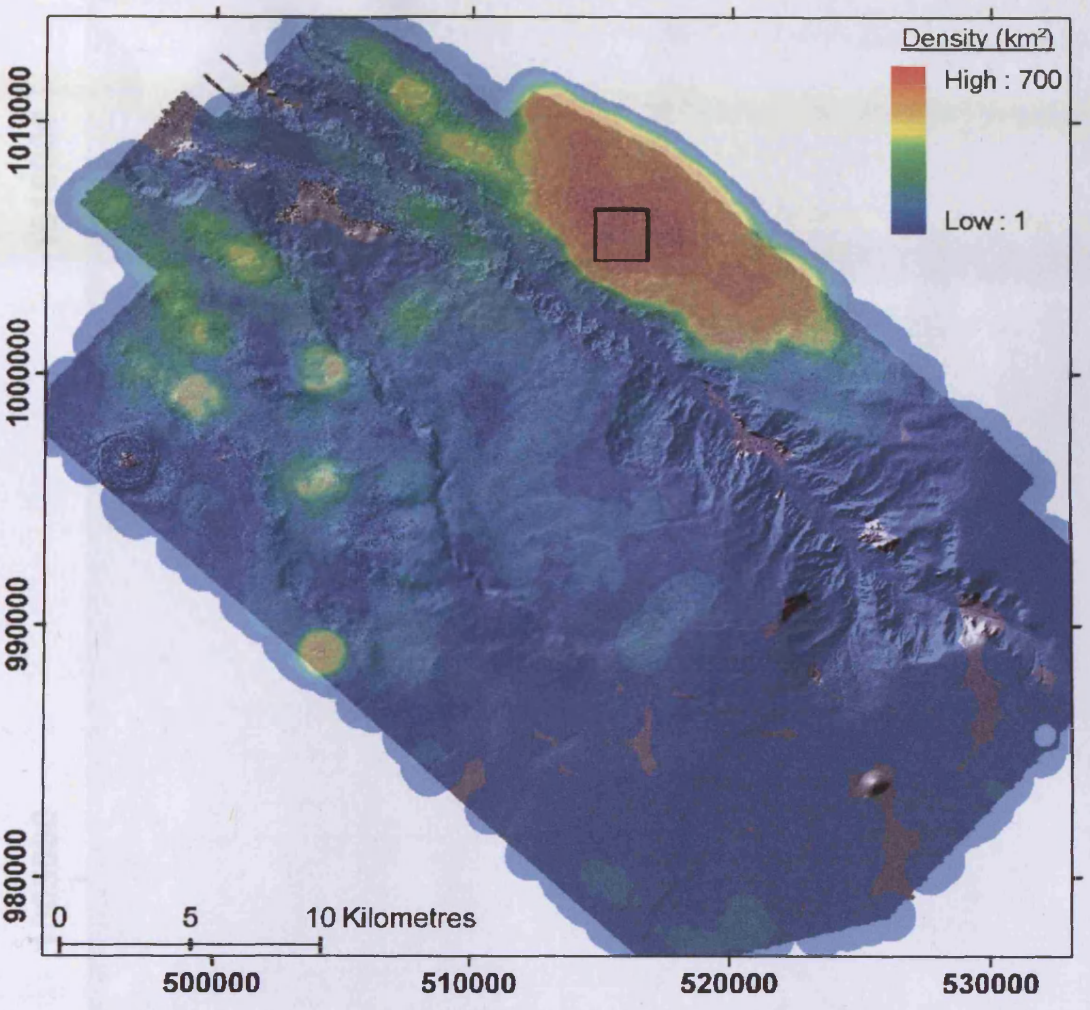

Figure 7.10 Density map. Density map of all surface pockmarks. Buried pockmarks are not included in the analysis. Density map shows average pockmark density per 1km². Study area utilised in spatial statistical analysis is shown.

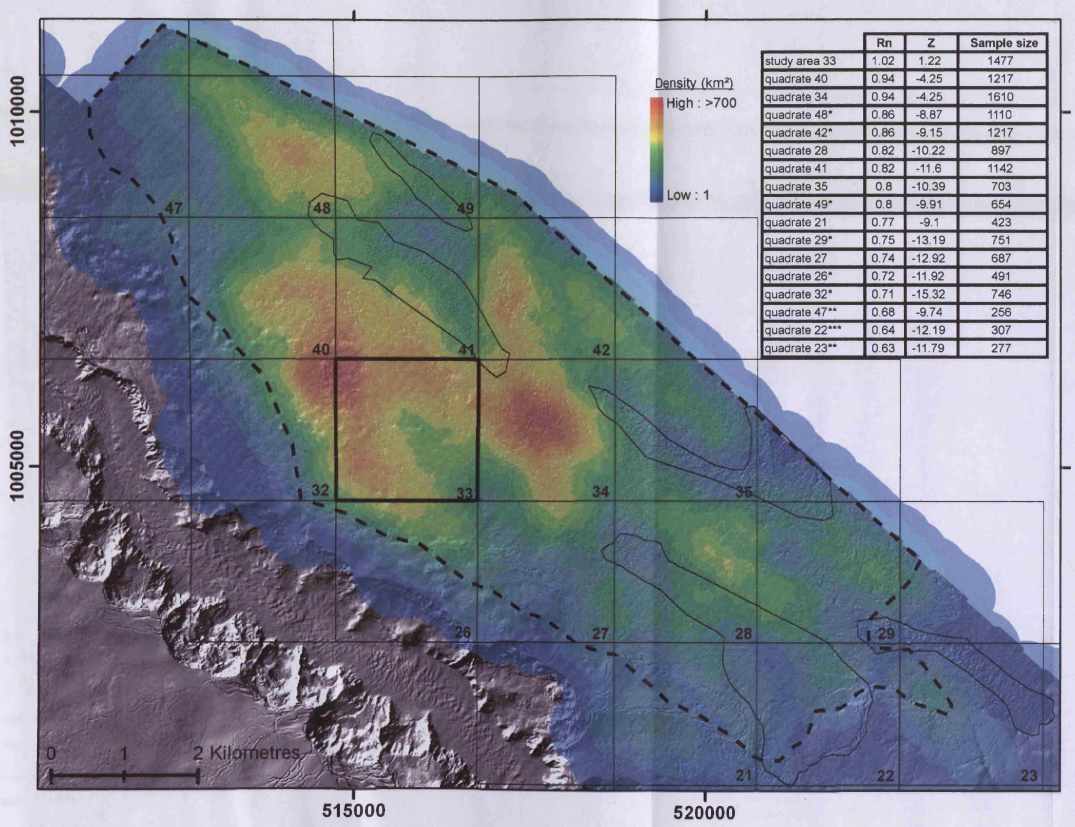

	Rn	Z	Sample size
study area 33	1.02	1.22	1477
quadrate 40	0.94	-4.25	1217
quadrate 34	0.94	-4.25	1610
quadrate 48*	0.86	-8.87	1110
quadrate 42*	0.86	-9.15	1217
quadrate 28	0.82	-10.22	897
quadrate 41	0.82	-11.6	1142
quadrate 35	0.8	-10.39	703
quadrate 49*	0.8	-9.91	654
quadrate 21	0.77	-9.1	423
quadrate 29*	0.75	-13.19	751
quadrate 27	0.74	-12.92	687
quadrate 26*	0.72	-11.92	491
quadrate 32*	0.71	-15.32	746
quadrate 47**	0.68	-9.74	256
quadrate 22***	0.64	-12.19	307
quadrate 23**	0.63	-11.79	277

Figure 7.11 Detailed density map of the pockmark field. Outline of pockmark field (dashed line), outline of surficial debris deposits (solid line), quadrates used in statistical analysis (wire frame), study area (black box) and Nearest Neighbour Index values for corresponding quadrates are shown. Given a critical value of -2.58 the null hypothesis that pockmarks are randomly distributed is rejected at the 99% level for all quadrates with the exception of study area 33.

The pockmark field was subdivided into 4 km^2 quadrates in order to analyse pockmark spatial distribution at a smaller scale. First order spatial statistical characteristics have established that all the quadrates show a tendency towards a random distribution (Fig 7.11). Nearest neighbour values range between *Rn* 0.64, *z* -12.19 to *Rn* 1.02, *z* 1.22 (Fig. 7.11). The lowest values i.e. those displaying a lower tenancy towards a random distribution are located on the edge of the pockmark field or associated with smaller pockmark populations (e.g. quadrates 22, 23 and 47). Greater tendancies towards a random distribution are associated with the centre of the pockmark field and higher pockmark populations (e.g. quadrates 33, 33, 40).

7.5.4.3 Spatial statistics : Study area

To facilitate more detailed statistical spatial analysis on such a large dataset I selected a 4 km^2 study area for analysis (quadrate 33, Fig 7.11). The study area contains 1,477 unit pockmarks at a maximum average density of > 650 pockmarks/km^2. The aim of the spatial analysis on the study area is to elicit any subtleties in the spatial distribution of pockmarks within a field.

First order statistical spatial analysis has established a tendency towards a random distribution within the study area. However first order characteristics only provide a general overview of a distribution based on average values within a single search radius. Second order characteristics look for patterns at multiple search radii (20m incremental buffering), providing a more robust assessment of spatial distributions. Ripley's K statistic (*L(d)*) has detected a tendency towards clustering between 20-1160 m, however this distribution is only statistically significant at the 99 % level for distances between 40-700 m. The pockmark distribution also shows a tendency towards dispersion between 1180-2000m however this distribution is not statistically significant at the 90 % level*. This tendency towards clustering refers to two subtle areas of localised clustering in the northeast and southwest of the study area.

* Graphical statistical output is provided in Appendix A5

Figure 7.12 Spatial analysis. a, b) normal distribution of pockmark diameters and map example. c,d) freq compared to a random population and map example showing the derived exclusion zone. g,h) ratio between

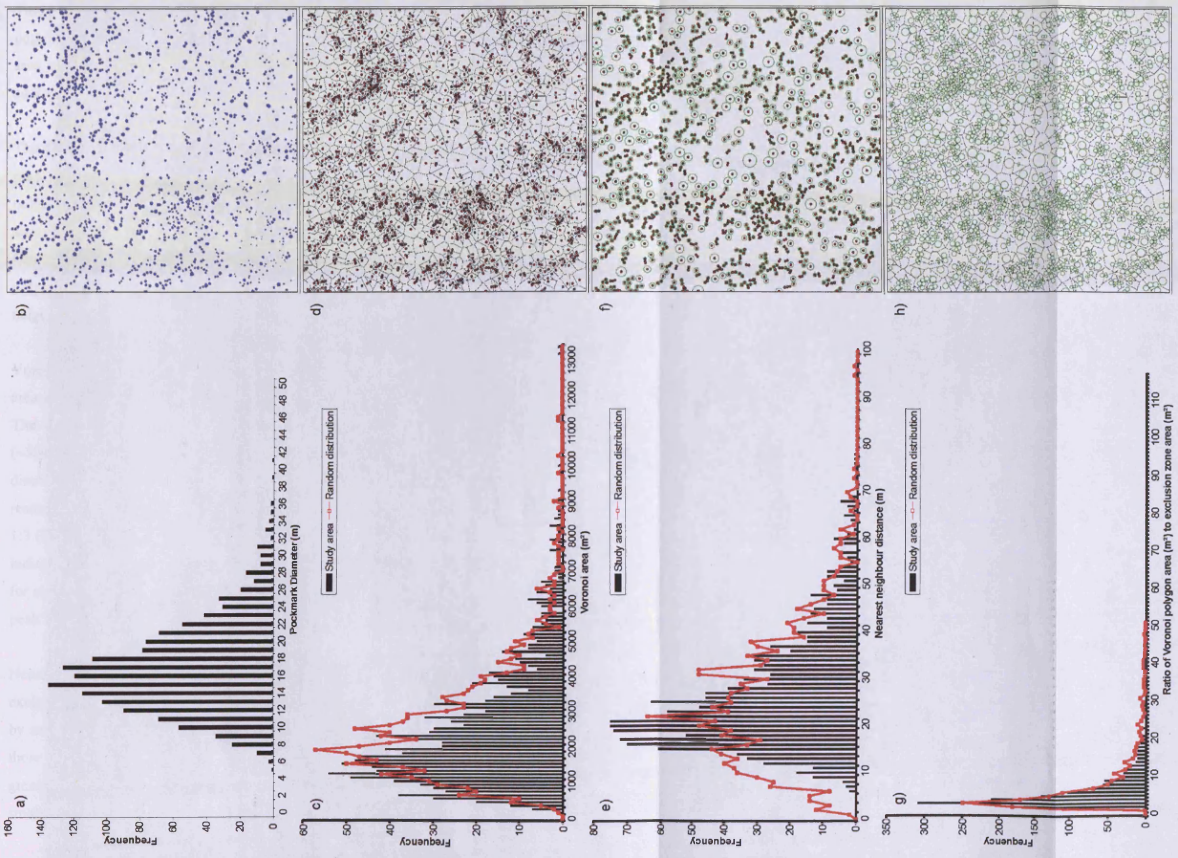

Figure 7.12 Spatial analysis. a, b) normal distribution of pockmark diameters and map example. c,d) frequency of Voronoi polygon areas compared to a random population and map example. e,f) nearest neighbour distances compared to a random population and map example showing the derived exclusion zone. g,h) ratio between Voronoi and exclusion zone area and map example

The graphs in Figure 7.12 compare measured frequencies with those for a random population. A random population of 1,477 data points within the 2km x 2km study area were generated by a random generator algorithm within the GIS and plotted against measured values to determine whether the values display an important trend.

The frequency histogram of pockmark diameters displays a normal distribution to pockmark sizes within the study area ranging between 5-41 m (Fig. 7.12). Voronoi polygon areas, nearest neighbour distances and the ratio between Voronoi polygon area and exclusion zone area (exclusion area radius generated from *nn* / 2) (see Chapter 2) show a positively skewed frequency distribution (Fig. 7.12). Voronoi polygon and exclusion zone areas are unrelated to pockmark diameter*. Nearest neighbour distances are unrelated to pockmark diameter*.

Voronoi polygon area, nearest neighbour distances and the ratio of Voronoi polygon area and exclusion zone area all show a slight deviation from a random distribution. The frequency distribution of Voronoi polygon area shows a slight positive skew (~500 m) towards smaller polygon areas, but essentially resembles a random distribution (Fig. 7.12). The ratio between Voronoi and exclusion zone area resembles a random distribution, with the exception of a frequency peak in ratios of 1:3 (Fig. 7.12). The ratio of exclusion zone area and Voronoi polygon area gives an indication of the relationship between available space and minimum required space for each pockmark in the field. When the ratio values are mapped, it is clear that this peak is not exclusively associated with the areas of clustering*.

Nearest neighbour distances (*nn*) range between < 10 m to > 60 m, creating unique exclusion zone areas around each pockmark, defining a minimal area not penetrated by any other pockmark. Nearest neighbour distance show a distinct deviation from those of random population. Frequencies of *nn* distances between 15-28 m are greater than a random distribution and, importantly, there is a distinct absence of smaller *nn* distances (< 15 m) when compared to the random population (Fig. 7.12).

* Graphs and maps shown in Appendix A5

The Minimal Spanning Tree (MST) measures shortest line distances (edges) between neighbouring points (Fig. 7.13) (see Chapter 2 and Appendix A7). The Minimal Spanning Tree records an absence of short edge lengths up to 12 m and an excess of edges 16-30 m in length when compared with a random population (Fig. 7.14).

To analyse the origins of the absence of short edge lengths, Minimal Spanning Tree statistic was re-run using parameters which define a hard core distribution and Self-Organised Criticality (SOC). A hard core distribution is a random distribution which is governed by a fixed exclusion zone around each point (Diggle, 1983, 2002). In test simulations, 14 m exclusion zone provided the closest match, mimicking the absence of short edges but fails to produce the peak ~15-25 m edges (Fig. 7.14). Self-Organised Criticality is a statistical law which describes the mechanism by which complexity arises in nature (Bak et al., 1987, 1988; Bak and Paczuski, 1995; Ball, 2004) (see Appendix A7). Self-Organised Criticality simulations run using 10m exclusion zones (collapse event) are shown (Fig.7.14). Both the absence of short edges and the peak in edge lengths is reproduced. These simulations have shown that the spatial distribution of pockmarks within the field do not reflect a hard core distribution but are more closely related to SOC.

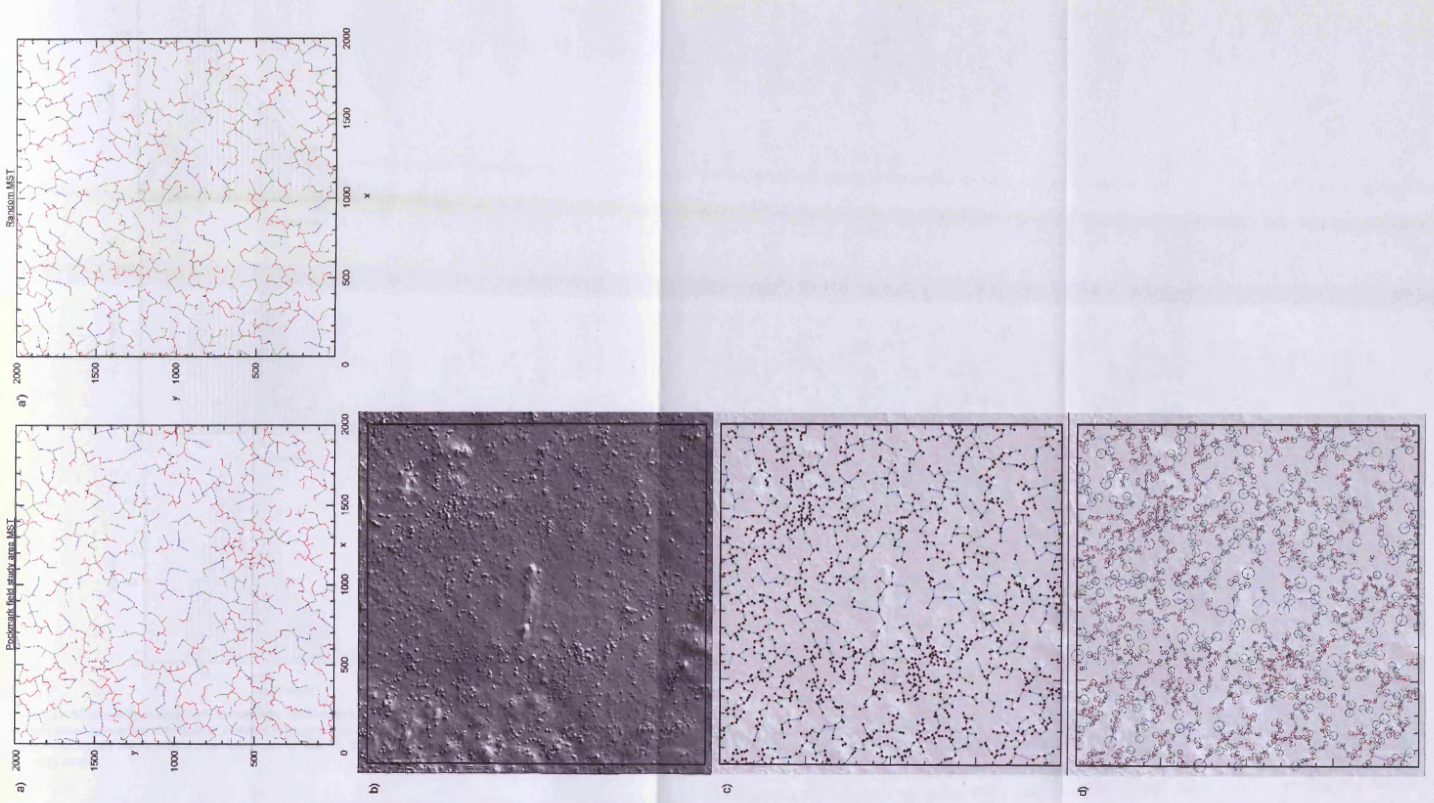

Figure 7.13 Minimal Spanning Tree examples. a) and a') MST model outputs, a) results from the study area, a') results from a randomly generated set of data points. Black lines are short edges, red lines are short-medium edges, green lines are medium-long edges, blue lines are long edges b) seabed dip map of the study area. c) and d) MST model integrated with GIS and side scan sonar data, c) location of pockmarks and their associated MST edge (faded dip map background), d) MST edge lengths and exclusion zone areas (faded dip map background).

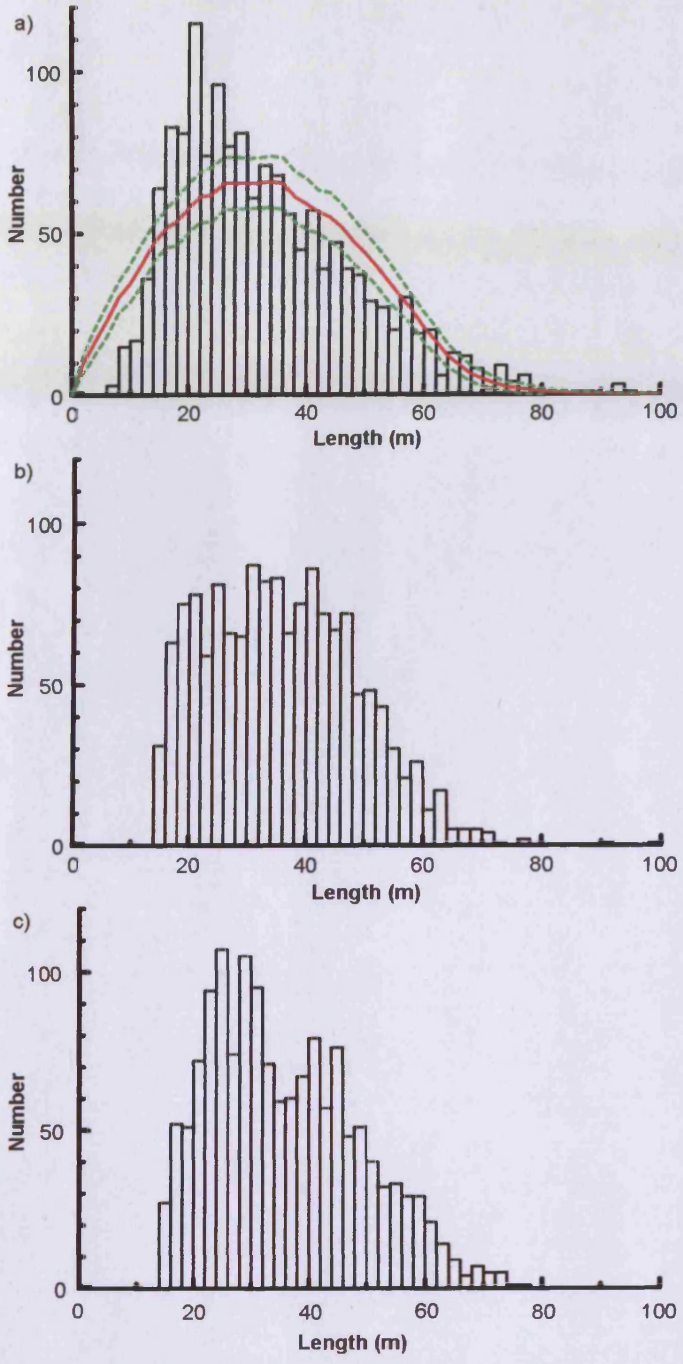

Figure 7.14 Minimal Spanning Tree histograms. a) Histogram of edge lengths, red line indicates mean values for 100 trials of random data, green dotted lines indicate the confidence envelope (95%). b) Histogram for the hard core model. c) Histogram for the Self Organised Criticality model.

7.5.5 Summary

Pockmark distributions are akin to a random distribution but show subtle deviations from "true" (statistically defined) Complete Spatial Randomness (CSR). This deviation from CSR may be a function of sub-clusters within the dataset (Ripley's K) or the pronounced lack of short nearest neighbour distances. The lack of close neighbouring pockmarks is an important, if somewhat subtle, point illuminated by the Minimal Spanning Tree. Assumptions of a variable exclusion zone surrounding pockmarks are confirmed by the MST's deviation from a hard core distribution with a fixed exclusion radius. Similarities between the pockmark distribution and Self-Organised Criticality emphasise an understated relationship between distribution, CSR and exclusion zone. The distribution of pockmarks within the field represents possible natural complexity in nature but within the complexity there is an underlying exclusion process dispersing pockmarks.

7.6 Discussion

7.6.1 Shallow gas : a fluid source for the pockmark field?

The Rosetta pockmark field is spatially extensive requiring a fluid source of similar proportions. Minimum requirements for the source layer are ~75 km^2 spatial coverage, hydrocarbon or biogenic fluid (gas) generation, a permeable reservoir unit and a sealing sequence. Additional consideration has to be given to the depth to the source layer.

Similar to previous studies, the acoustic distortion and wipeout at the maximum penetration of the Chirp profiler data is interpreted as a gas front resulting from gas migration (seepage) through the shallow sedimentary unit (Floodgate and Judd, 1992; Iglesias and García-Gil, 2007; Naudts et al., 2009). Both the gas front and the debris flow deposits are spatially comparable with the pockmark field. The gas front

and debris flow packages extend > 6 km north and south of the pockmark field (total coverage ~125 km^2, i.e. to the limit of Chirp profiler data on the Eastern Slope). The depth to the gas front is below the penetration limit of the Chirp profiler data (~40 ms) at the distal limit of the pockmark field, and shallow debris flow packages in the UHR and Chirp profiler data originate from the level of a small arcuate scar at the proximal limit of the pockmark field, suggesting that the interaction of these two factors may be important in determining the position of the field.

The gas front is commonly trapped beneath the hemipelagic drape sealing sequence (20-40 ms depth) (Fig. 7.15). In areas of complex debris flow packages, the drape sequence is destroyed at depth and the occurrence of acoustic disturbance is observed to climb in the sequence which is suggestive of gas seepage through these more permeable layers. Gas seepage through these more permeable layers is probably trapped by a shallower drape package (~20 ms depth) (Boudreau et al., 2005). In areas of surficial debris flow material identified on the side scan sonar, both the drape package and unit pockmarks are not present suggesting that either the debris flow has eradicated the sealing sequence and pockmarks are prevented from forming or that any pockmarks present on the seabed prior to the MTD have been buried by the debris flow deposits.

The observations presented above help to explain pockmark density variations within the field (Fig. 7.11). The highest densities are recorded where the sealing sequence is obscured by a high amplitude, chaotic zone of distortion (Fig. 7.7). This zone probably represents an area of intense fracture (possibly pre-existing fractures) or extreme overpressure resulting in a focused "plume" of fluids towards the seabed. The lowest densities are recorded where flow debris is found at or close to seabed (Fig. 7.5). Medium densities, like those in the study area, reflect the interaction between debris flow units at depth, the depth to the gas front and the thickness and position of the sealing unit in Unit H5.

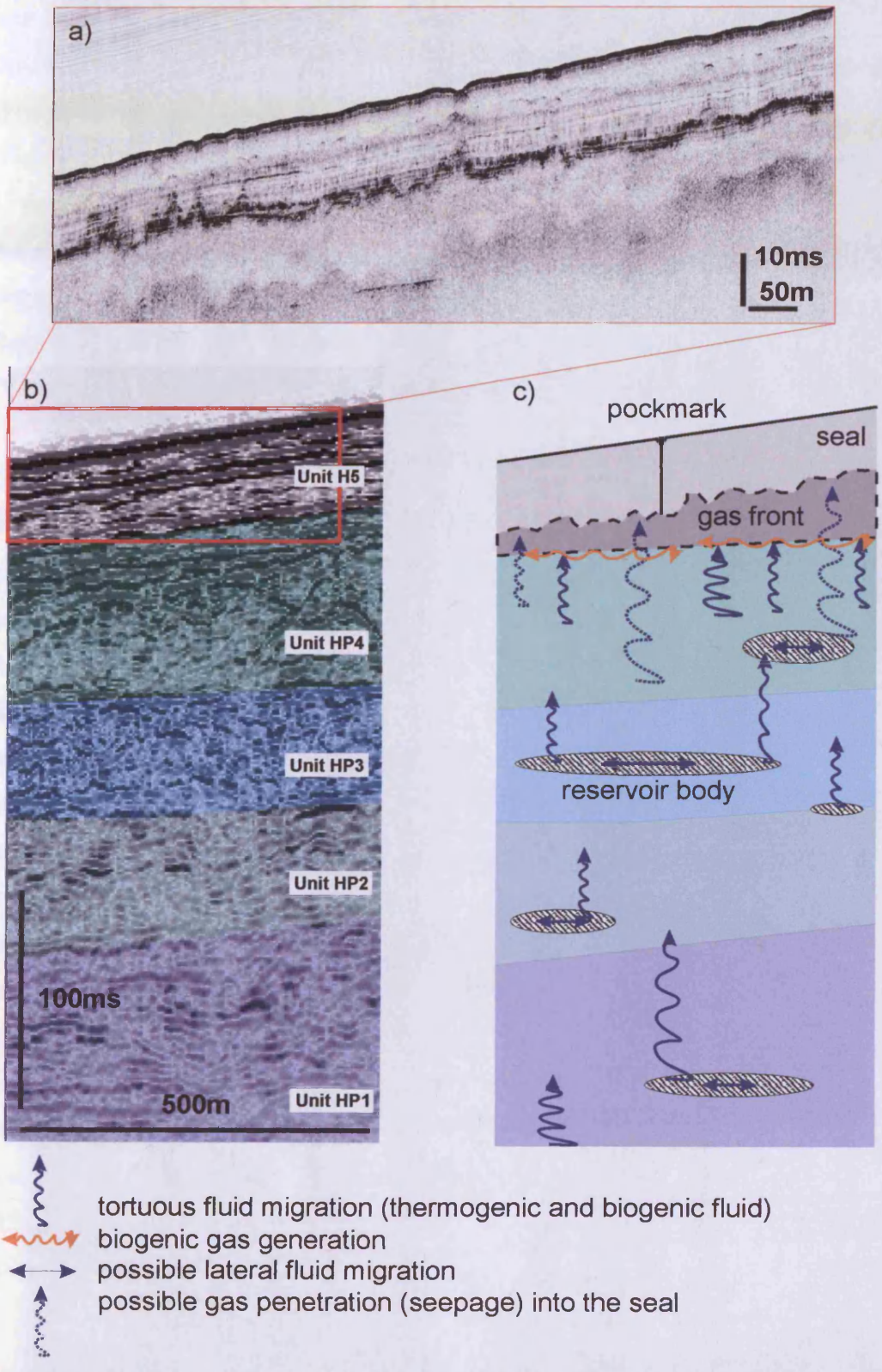

Figure 7.15 Plumbing system conceptual model. a) Chirp profiler data, b) UHR 2D data, c) conceptual model. Thermogenic and/or biogenic fluid (possibly methane) is anticipated to climb through the (heterogenic permeability) debris flow units (Unit HP1-4) and potentially mixes with biogenic (methane) generation at the level of Units HP4-H5. Fluid is trapped at the level Unit H5 except where surficial debris flow deposits are observed within Unit H5. With the support of shallow debris flow deposits within Unit H5, gas penetrates the seal by seepage creating the gas front. Seal breach at the level of the gas front results in pockmark formation.

The depth to the putative source layer is difficult to determine due to the acoustic distortion of the stratigraphy by the gas front. Pockmark feeder pipes, where visible (Fig. 7.8), can be traced to the gas front at the level the Unit HP4 – H5 unit boundary (Fig. 7.15). The origins of this gas front are unknown, but are likely to be related to 1) deep sourced thermogenic or biogenic fluid migrating towards the seabed (Abdel Aal et al., 2001; Samuel et al., 2003; Loncke and Mascle, 2004), 2) shallow sourced biogenic fluid (gas) generation (Gontharet et al., 2007), or 3) a combination of both thermogenic and biogenic fluid (microbial alteration of thermogenic methane) (Vandré et al., 2007).

Geochemical analysis of cores from Early Miocene to Pliocene reservoirs on the Western NDSF slope (1527-4480 m) have established the dominant generation pathway for fluid, identified as predominantly methane, is from both microbial and thermogenic origins (Vandré et al., 2007). Translating this research to the Rosetta Region study area, it is anticipated that any deep sourced thermogenic or biogenic fluid will migrate to the level of Unit HP4 where it is trapped beneath the sealing sequence in Unit H5. The vertical migration of fluids is likely to be tortuous, utilising isolated high amplitude pockets in the UHR data, interpreted as gas filled sand bodies, as temporary reservoirs. Following breach, buoyant fluids are thought to climb through the more permeable portions of debris flow units (HP1-4). At the small scale, I suggest fluids migrate across strata via bypass systems including small faults, and then migrate up-dip along relatively permeable strata along local structures where it is temporarily trapped by low permeability seals before migrating further up section via crestal breakout features. At shallower depths, it is possible that any terrigenous material transported onto the slope may have had a high organic content suitable for in-situ biogenic gas (methane) generation in Units HP4 and/or H5. The fluid source for the pockmark field is therefore most likely to be shallow (biogenic or thermogenic) gas (methane) and pore water trapped beneath the drape sequence in Unit H5.

7.6.2 Fluid source and its relationship to the timing of formative events

Pockmarks within the field are believed to have formed within a small time window in a spatially extensive fluid migration event, within the last ~6,500 years. Pockmarks within the field are observed to have formed at or above (< 2 ms) horizon H030 which has been chronostratigraphically dated at ~6,500 yrs BP.

In order to obtain widespread simultaneous pockmark formation, I argue the case for a shallow fluid source and a triggering event. Triggering events could be earthquakes, variations in hydrostatic pressure caused by the passage of waves and tides, changes in eustatic sea level, sediment loading and unloading and steam/hydrothermal fluid injection (Judd and Hovland, 2007). Due to the pockmark fields location in a non-igneous, deep water setting (> 400 m), and lack of recent (~6,500 year) large scale sliding events (Garziglia et al., 2008; Loncke et al., 2009) or substantial changes in sea level (Fig. 3.2), it is argued here that the effects of earthquake generated overpressure and release are the most likely trigger for widespread pockmark formation.

Prior to 6,500 yrs BP, the NDSF experienced a period of rapid sedimentation, wetter climate (pluvial period) and relatively lower sea levels (Stanley and Warne, 1993; Ducassou et al., 2008). These factors are believed to have pre-conditioned the Eastern Slope to the retention of pore waters, overpressure development and localised debris flow mobilisation. In the event of an earthquake sediments compact and decrease in volume. Retention of released pore fluids and buoyant gases by the seal (Unit H5) can potentially generate overpressures, which when released result in seal by-pass, "diapirism" and/or fluidisation and fluid escape (Gluyas and Swarbrick, 2004; Swarbrick et al., 2004; Cartwright et al., 2007). It is argued here that numerous pockmark formations during a small time window (~6,500 yrs) would require a single earthquake event of sufficient magnitude, or several earthquakes in quick succession, releasing fluid from a shallow source and instantaneous, non-interrupted vertical migration to the seabed via a short single pathway e.g. pipe (Fig. 7.15).

7.6.2.1 Unit pockmark formation

The two driving forces for fluid migration and pockmark formation are overpressure and buoyancy (Judd and Hovland, 2007; Cathles et al., 2010). Overpressures, where pore pressures are in excess of hydrostatic, are commonly attributed to tectonic compression (considered unimportant given the Egyptian passive margin), the sedimentation rate/rapid sediment loading (influencing the rate/degree of compaction and underconsolidation) and the generation of fluid (methane) at a rate faster than it can be expelled (Swarbrick and Osborne, 1998; Swarbrick et al., 2004). Buoyancy, as a function of a density inversion between the potentially underconsolidated unit where buoyant fluids (methane) are accumulating (Unit HP4), and the overlying normally consolidated sediment (Unit H5, drape), may force "diapirism" and/or fluidisation and fluid escape (Gluyas and Swarbrick, 2004; Swarbrick et al., 2004).

Following an earthquake overpressure and municipal fluid buoyancy beneath Unit H5 (considered a seal) can potentially contribute towards seal by-pass (Cartwright et al., 2007). Seal breach can be instigated by capillary invasion or hydrofracturing depending on the grain size of the seal (Jain and Juanes, 2009). Grain sizes measured from the margin of the pockmark field show Unit H5 grain sizes of < 2 μm (clay, minimum sieve size used) suggesting either mechanism is feasible. However at the shallow subseabed depths, substantial overpressure would be required to induce fracturing in relatively unlithified sediments (Jain and Juanes, 2009). Following seal breach, flow self organises into a columnar conduit (Novikov and Slobodskoy, 1979), eroding sediments during seabed fluid expulsion creating a pockmark (Judd and Hovland, 2007).

7.6.3 Conceptual Model

Consideration of pockmark formation focuses on the vertical migration of fluid. Here I consider whether the spatial positioning of pockmarks within a field can illuminate the lateral influence of these vertical processes.

7.6.3.1 Spatial statistics summary : emergence of a pockmark exclusion zone

The results presented here outline complexity within the pockmark field system which is not immediately apparent. First order characteristics produce baseline spatial statistics based on averages of the population. At this level, complexity is not apparent and the spatial distribution is merely described as random. Second order characteristics produce a more detailed level of analysis, searching for spatial patterns at variable scales. At this level of analysis, subtle clustering is observed and the distribution is no longer considered random. At the highest level of distribution analysis presented here, Complete Spatial Randomness (CSR), a statistically derived definition of random distribution, is rejected as complexities within the distribution are made apparent by the Minimal Spanning Tree. The pockmarks within the field are anti-clustered and an alternative explanation for their distribution is required.

Anti-clustering, or the decreased likelihood of finding neighbours within a close distance, suggests the pockmarks are separating or dispersing rather than grouping. Separation is captured by the nearest neighbour distance and the deviation from a Random Hardcore distribution (Diggle, 2002). The Hardcore or Diggle model (Diggle, 2002) produces a random distribution of points which is "buffered" by a fixed exclusion zone (14m radius) around each pockmark. Nearest neighbour distances record a variable exclusion zone around each pockmark, with a deficit of distances < 15 m compared to a random distribution. Exclusion zone distances are shown to be unique to each pockmark by the deviation from a Random Hardcore distribution. Pockmark distributions are shown to have more complexity than can be explained by a simple (Hardcore) exclusion zone policy.

Self-Organised Criticality (SOC) is considered to be one of the mechanisms by which complexity arises in nature. Following SOC discovery in statistical physics (Bak et al., 1987), Self-Organised Criticality is typically observed in slowly driven, non equilibrium systems where complexity could be generated as an emergent feature of extended systems with simple local interactions (Bak et al., 1987; Bak and Paczuski, 1995; Bak, 1996; Ball, 2004). Many examples of SOC have been identified in fields as diverse as ecology, evolutionary biology, astrophysics, astronomy, solar physics, geomorphology, natural hazards, neuroscience, economics

and sociology (Georgoulis and Vlahos, 1998; Dendy et al., 1999; Ray et al., 2000; Allen et al., 2001; Watkins et al., 2001; Ormerod, 2002; Andergasssen et al., 2003; Fonstad and Marcus, 2003; Pueyo, 2007; Suckling et al., 2008; Krenn and Hergarten, 2009) but to date there is no known set of general characteristics that guarantee a system will display SOC (Ball, 2004). The pockmark distribution displays certain characteristics of Self-Organized Criticality when modelled using the equivalent of a minimum 10 m radius exclusion zone (avalanche). To the author's knowledge, this is the first time that the possibility of self-organized criticality has been observed in seabed pockmarks.

It is evident from the spatial statistical analysis that a subtle, underlying phenomenon is influencing pockmark distribution within the field and preventing pockmarks from forming within close proximity of one another. I have been unable to prove precisely the nature of this phenomenon, but have shown statistical evidence for the possibility of an exclusion zone surrounding each pockmark producing anti-clustering tendencies and that there is a tendency for pockmarks to form just beyond the exclusion zone limit (Cartwright et al, submitted, Appendix A4). Below, I propose several conceptual models to explain this exclusion zone.

7.6.4 Conceptual model : Pockmark "drainage cell"

Pockmark formation comprises 3 key processes, overpressure generation, seal failure and vertical fluid (pipe) propagation. The spatial position of seal failure is commonly believed to be located at the point of maximum overpressure and focused by sub seismic heterogeneities in the seal e.g. small pre-existing fractures, localised small scale doming or minor permeability contrasts (Judd and Hovland, 2007).

It has been argued that a single, high magnitude, triggering event (possibly an earthquake) stimulated near-simultaneous overpressure generation and release in the Rosetta pockmark field. In a field setting with a spatially extensive, near uniform shallow depth fluid source with high lateral connectivity i.e. not faulted, overpressures need to be focused towards a single point location to form a pockmark.

It is assumed that failure to focus overpressures would result in widespread perforation of the seabed as fluid escapes by an immeasurable number of infinitesimal fracture or seepage pathways and bleeds into the water column. It is argued that this "focusing" of overpressure has a spatial component which has been elicited by the spatial statistics i.e. the exclusion zone. The conceptual models outlined below suggest that the exclusion zone surrounding individual pockmarks is a function of the processes inherent in pockmark formation and prevents pockmarks from forming in close proximity.

7.6.4.1 Sand bodies in Unit HP4

The spatial distribution of pockmarks within the field may relate to the position of isolated sand bodies within Unit HP4. A triggering event of sufficient magnitude could cause localised overpressure generation in sand bodies surrounded by lower permeability material, resulting in the formation of a single pipe and pockmark. The distribution of these bodies could explain the spatial distribution of pockmarks within the field.

The likelihood of > 13,000 isolated sand bodies, at a similar depth below seabed, all containing sufficient (pore)fluids for pockmark formation and located between the 400-800 m depth contour is considered to be fairly low.

7.6.4.2 Spatial ordering governed by the mode of seal failure

The spatial position of pockmarks may be determined at the level of the seal. Here it is considered whether the lateral influence of the mode of seal failure, hydrofracture or capillary invasion (Jain and Juanes, 2009), may produce an exclusion zone around a pockmark.

Capillary invasion involves the vertical migration of methane bubbles into the seal where the capillary entry pressure of the strata is exceeded (Jain and Juanes, 2009). It is envisaged that these bubbles will take various tortuous routes to the seabed as

determined by the gas pressure minus the water pressure, exceeding the capillary entry pressure of the pore throat (Jain and Juanes, 2009). It is proposed that further pockmark formation will be prohibited at any location within the lateral expanse of capillary invasion as a flow network to a single pockmark is already established. A density contrast may encourage pore water or methane advection, diffusion or dispersion into the flow network from the surrounding sediments thereby extending the lateral limits of the drainage cell.

Where the fracture pressure of the seal is exceeded hydrofractures open and propagate towards the seabed, forcibly moving sediment grains apart. This movement of sediment grains away from the opening void creates compression between grains on the margins of the fracture (Jain and Juanes, 2009). Compression between grains decreases the permeability of this zone, thereby reducing the likelihood for further hydrofracturing and pockmark formation. The spatial extent of this reduced permeability caused by a columnar conduit of interrelated, dendritic hydrofracture networks could potentially indicate the lateral limits of the exclusion zone.

Both these failure modes have been numerically modelled at the small (grain) scale (Cathles et al., 2009; Jain and Juanes, 2009). The arguments governing the prevention of further pockmark formation within the hydrofracture / capillary invasion zone generated by these modes of seal failure seem plausible. However it remains unclear whether these processes can be extended beyond the lateral limits of the conduit they form to the exclusion zone radii ~10 m.

7.6.4.3 Pockmark "Drainage Cell"

The spatial position of pockmarks may be determined within the fluid reservoir at the level of the seal. In hydrogeology and groundwater modelling, the "radius of well influence" for an extraction borehole in an aquifer can be modelled (Kresic, 2007). The radius of well influence in groundwater modelling is the maximum distance the effects of aquifer drawdown can be detected. In other words, the area drained by the well. The radius of well influence in an unconfined aquifer is a function of the well

pumping rate (discharge), hydraulic conductivity (permeability), the hydraulic head (pressure difference between the bottom and top of the well) and the aquifer thickness (Kresic, 2007). Here I tentatively suggest that the interaction of similar processes may govern the exclusion zone around a pockmark.

It is postulated that at the moment of seal breach, a hydraulic connection is established and built up overpressure is released. Overpressures are built up either uniformly throughout the fluid source or within localised pockets. The limits of these pockets or "cells" are determined by (sub)seismic changes in permeability, for example, the lateral boundaries between hemipelagic drape and debris flow deposits at a given depth within Unit H5. Once a seal breach has formed, fluid is "drawn" into the pipe by the pressure differential between fluid source and seabed. The fluid is "drawn" in from a radius around the breach which is unique to each pipe. I propose that this distance is determined by permeability. It is unclear how much fluid can be extracted from the reservoir at any given radii, but given the size of the pockmark (cf. Chapter 6) and by analogy with previous studies I assume that the total volume of fluid escaping through the pockmark will be quite low (Judd and Hovland, 2007).

Once the fluid has escaped and the pressure returned to hydrostatic, an area of fluid and/or pressure deficit surrounding the pockmark remains. Within this zone, further pockmark formation is prohibited by insufficient fluid and/or pressure build up (in the absence of a triggering mechanism fluid accumulation and overpressure generation are assumed to be related). I refer to either the area supplying a pockmark or drained by a pockmark as a pockmark drainage cell.

The drainage cell is a hypothetical concept which may only be applicable to certain well-layered pockmark fields, where 1) the fluid source is shallow and spatially extensive 2) any vertical fluctuations in the depth to the fluid source are minimal, 3) seabed gradients < 1 °, 4) there are no obvious structures, faults, migration pathways e.g. buried channels or changes in sediment characteristic which would affect permeability or overpressure, and 5) the timing of pockmark formation can be constrained to a relatively short time period. It is unlikely that a drainage cell would be circular as depicted here but form an irregular polygon, the 3D size and shape of

which is unique to each pockmark. It is conceivable that pressures (and possibly permeabilities), and therefore drainage cells, will vary with time, increasing the likelihood that drainage cells may overlap producing anomalously small exclusion zones when assessing pockmark fields based on a fixed point in time.

7.7 Summary and conclusions

A ~1,000 km^2 area in the Rosetta Channel region of the Western Nile Deep Sea Fan has been mapped using concurrent Ultra High Resolution 2D, Chirp profiler and side scan sonar data. Over 25,000 small circular seabed pockmarks were mapped, including > 13,800 pockmarks in a pockmark field, this subject of this chapter. The outcome of this mapping can be summarised as follows;

- Pockmarks have been mapped throughout the entire side scan sonar data coverage area known as the Rosetta Region (~1,000 km^2). This dataset is thought to span Holocene – Pleistocene period
- Pockmarks in the pockmark field on the Eastern Slope are of a similar size to those pockmarks located elsewhere in the dataset
- Pockmark density map of the Rosetta Region shows hot spots of pockmark formation in the palaeochannel and plateau zones, and distinctly defines the pockmark field which is unique in this dataset
- Pockmarks within the field have formed at (±1-2 ms) the same horizon, which has been chronostratigraphically date to ~6,500 yrs BP.
- A triggering event (possibly an earthquake) is envisaged to have caused the overpressure generation and near-simultaneous pockmark formation.
- The fluid source for the pockmark field is believed to be shallow biogenic / thermogenic gas accumulation / generation trapped beneath a drape sealing sequence in Holocene Unit H5
- Complex pockmark density contrasts within the field are shown to relate to areas of high amplitude gas "plumes" (high density) and surficial debris flow deposits (low density).

- Pockmarks within a 4 km^2 study area within the pockmark field were analysed for the statistical spatial distribution.
- Pockmark distribution is not random.
- Pockmarks are anti-clustering i.e. there is a decreased likelihood of finding neighbours within a close distance, suggesting the pockmarks are separating or dispersing rather than grouping
- An exclusion zone is identified around each pockmark, which is not penetrated by any other pockmark.
- The exclusion zone is shown to be variable and unique to each pockmark and not a fixed distance
- Pockmark distributions display Self-Organising Criticality tendencies. Self-Organised Criticality (SOC) is a mechanism by which complexities arises in nature. Similar complexities are observed in fractal patterns.

A conceptual model is proposed whereby the exclusion zone surrounding each pockmark is interpreted as a "drainage cell". A drainage cell represents an area "drained" by a pockmark. At the point of pockmark formation a radius of fluid is "drawn" into the cell based on the permeability's (and overpressures) of the host reservoir. Once formed, a fluid / pressure deficit exists around the pockmark preventing further pockmark formation within close proximity to the existing pockmark. I have termed this a drainage cell.

Chapter 8

8 SUMMARY AND DISCUSSION

8.1 Introduction

The aims of this chapter are 1) to summarise the observations and interpretations from Chapters 4, 5, 6, and 7; 2) to incorporate key results from Namibia and the Nile Deep Sea Fan into a single conceptual model; 3) to discuss the implications of this research; 4) to outline the limitations of this research; and 5) to suggest recommendations for further work

8.2 Summary

The 6 central themes of this research which dominate Chapters 4, 5, 6 and 7 are morphology and process, spatial and temporal distribution, and frequency and magnitude (Fig 1.5). These themes interact at the local and basinal scale interlinking the research presented in the preceding chapters through a common conceptual framework (Fig. 8.1).

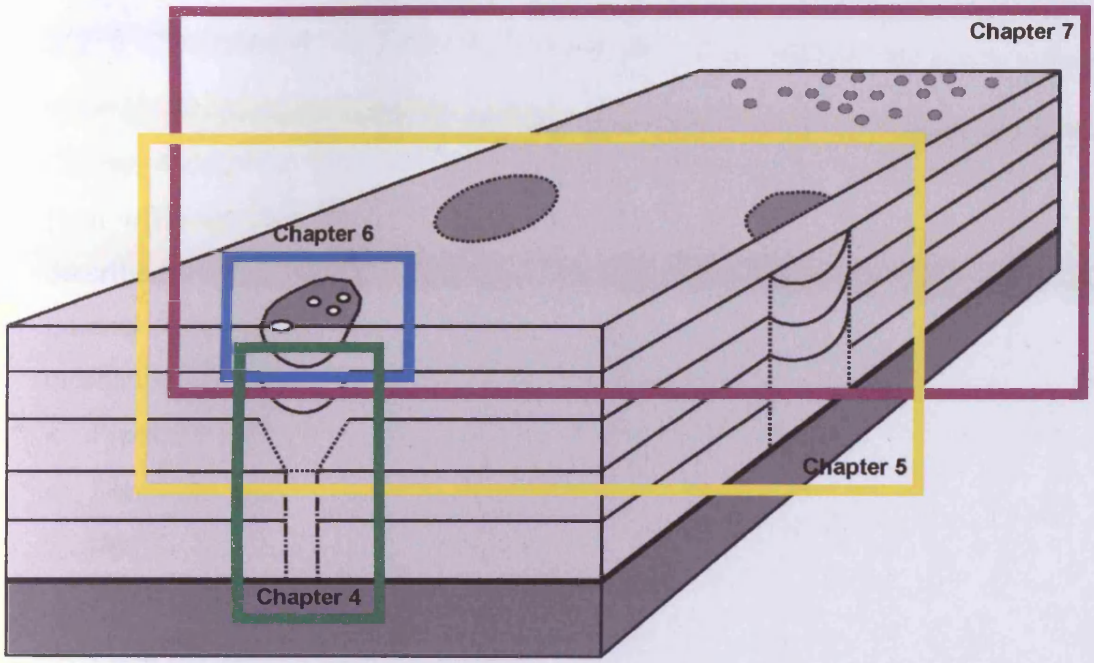

Figure 8.1 Schematic diagram representing a 3D pockmarked seabed. The themes covered in the previous four chapters of this thesis are placed within the context of this conceptual framework.

8.2.1 Chapter 4

Chapter 4 described a population of nearly 400 large kilometre scale blowout pipes from offshore Namibia. Blowout pipe seismic expression and geometry was described for wide and narrow pipes, followed by a discussion of the validity of the internal structure (geology or artefact), potential fluid sources and formation mechanism (blowout). The main findings can be summarised as follows;

- Pipes are elliptical, and their geometry changes with height
- Formation of the pipe involves disrupting the sedimentary layering to the extent that the reflections are disrupted. This implies a scale of disruption that is imaged by the seismic wavefront
- Pipes have been shown to form by blowout induced collapse
- There is a scaling relationship between pipe height and diameter. An increase in pipe height is correlated with an increase in pipe diameter. Pipe widening may be implicit in pipe re-use
- An erosional blowout crater is observed within the pipe structure
- Possible post formation fluid migration through the pipe is identified

8.2.2 Chapter 5

Chapter 5 extends this analysis by describing the spatial and temporal distribution of the Namibian pipes. The timing of pipe formation is shown to be intermittent yet persistent through time, the spatial position of which is governed by the inferred north-south migration of a basin scale fluid source and localised sporadic cluster and outlier formation. A conceptual model is proposed whereby pipe formation is the result of isolated pressure cells which are locally independent yet broadly controlled. At a local scale, multiple local factors interact producing a sporadic pipe formation distribution through an inferred system of individual, locally controlled, pressure cells, which generate overpressure and pipe formation. The main findings can be summarised as follows;

- Pipe formation is intermittent yet persistent through time
- Pipes with a common basal reflection do not form at the same time
- In a time sequence, sequential pipes do not form next to each other
- Pipes can form as clusters or outliers at the same time
- Pipes do not form at equidistance from existing pipes

8.2.3 Chapter 6

Chapter 6 tackles the theme of post formation fluid migration first proposed in Chapters 4 and 5. Utilising a higher resolution dataset from offshore Egypt, a group of large (100-700 m diameter) buried pockmarks were identified. Interpreted to have formed c. 50,000-80,000 yrs BP in response to eustatic sea level fall releasing fluids trapped beneath a shallow level Mass Transport Deposit, the large buried pockmarks have experienced high frequency, low magnitude post formation fluid migration resulting in the formation of seabed unit pockmarks. The main findings can be summarised as follows;

- Stacked concave reflections above the buried pockmarks are interpreted as pockmark arrays. Pockmark arrays represent a perpetuation of pockmark-like morphology of concave upwards reflections resulting from a purely drape-type deposition failing to infill the initial seabed crater, leaving vestigial relief.
- Longevity of fluid migration through pipes, buried pockmarks and pockmark arrays is identified
- There is a magnitude size difference between the flux of a normal pockmark and the flux of a unit pockmark
- Post formation fluid migration takes the form of clustered unit pockmarks above the original pipe/pockmark
- Post formation fluid migration on the NDSF plateau has been shown to last ~15,000-100,000 yrs

8.2.4 Chapter 7

Chapter 7 builds on the theme of pressure cells in pockmark formation. A pockmark field, offshore Egypt, containing over 13,000 small, circular, seabed pockmarks was analysed for their spatial distribution. A variable exclusion zone is identified surrounding each pockmark which is not penetrated by any other pockmark inducing anti-clustering tendencies within the field. The exclusion zone is interpreted as a pockmark "drainage cell". The main findings can be summarised as follows;

- Pockmark distribution within a field is not random
- A variable exclusion zone (minimum 10-15 m radius) exists around each pockmark in the field producing anti-clustering tendencies
- Pockmark distributions do not represent a hardcore distribution (Diggle, 1983, 2002)
- Spatial distribution of pockmarks within the Rosetta field holds an imprint of Self-Organised Criticality
- A conceptual model of a pockmark "drainage cell" is proposed to explain the exclusion zone in terms of a fluid/pressure deficit preventing further pockmark formation within the cell.

8.3 Discussion

The crux of this thesis has been to analyse the spatial and temporal distribution of pipe and pockmark formation. In this discussion I focus on a selection of comments and issues touched upon in previous chapters and expand the analysis as part of the implications of this research. The issues I have chosen to address are; 1) what are the implications of these results for seal risk analysis?, 2) what is the significance of pipe planform geometry (Chapters 4, 5 and 6)?, 3) what is the significance of overpressured cells (Chapters 5 and 7)?, 4) is it possible to predict the spatial location of pockmark formation within a shallow sourced field (Chapter 7)?, And 5) what are the implications of Self Organised Criticality for pockmark science (Chapter 7)?

I start the discussion with a conceptual model to illustrate how the findings of Chapters 4, 5, 6 and 7 relate to one another.

8.3.1 4D spatio-temporal conceptual model of pipe and pockmark formation

The 4D model conceptualises, in a sequence of arbitrary time-steps, the cross sectional growth of a pipe and pockmark and the spatial position of the pipe in relation to other new forming pipes (Fig. 8.2). The passage of time is marked by the addition of reflections. Erosional truncation of the host strata is symbolised by a v-shaped notch in the reflection geometry, and drape by a u-shape reflection depression (as seen in 3D seismic data, Chapter 4). This is a generalised / idealised conceptual model and does not relate to a specific basin or example.

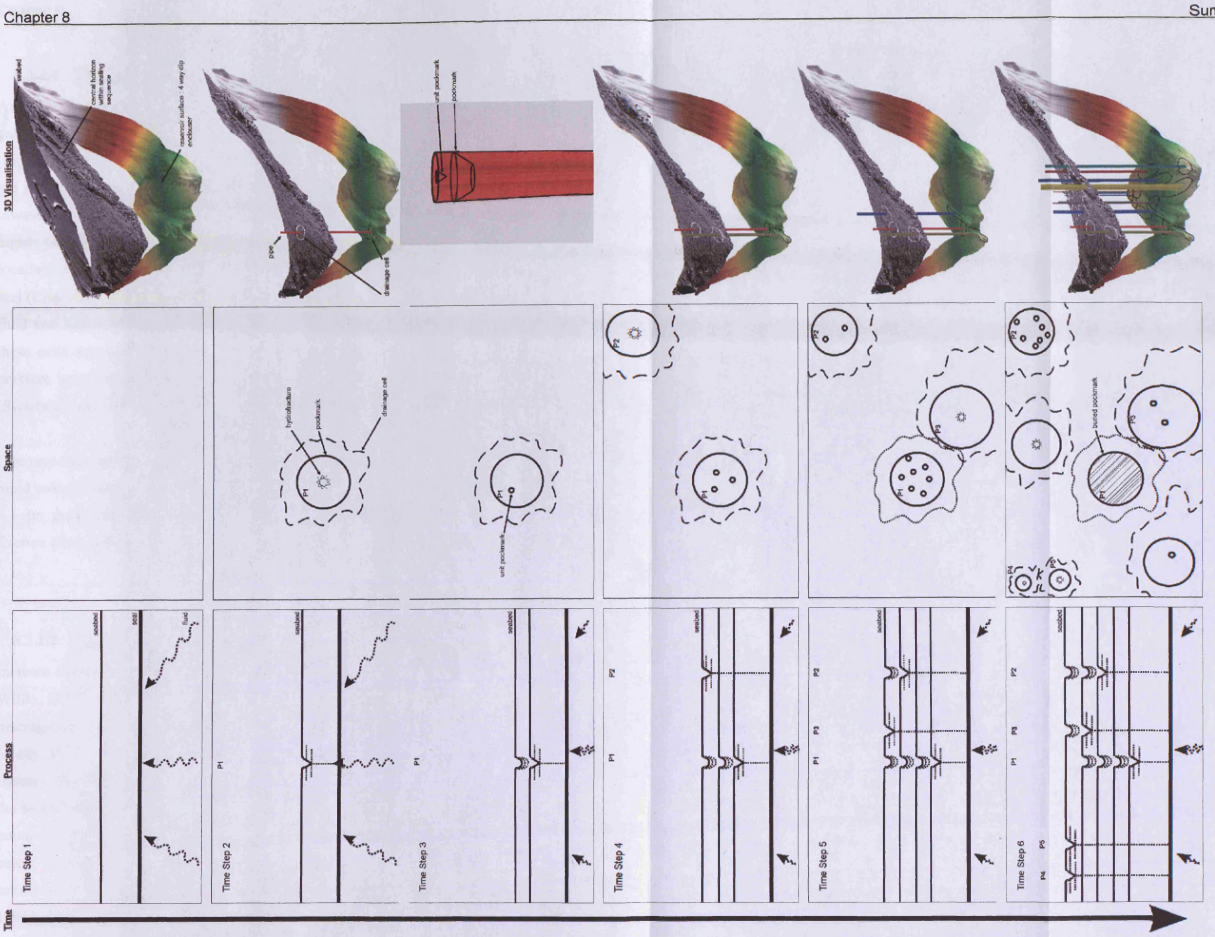

Figure 8.2 4D conceptual model of pipe and pockmark formation and evolution through time (arbitrary time scale). V-shaped reflections represent erosional truncation of the host strata, u-shaped reflections represent drape. The identification of these reflections can be used to identify the periods of fluid migration activity.

8.3.1.1 Time-step 1

A classic shallow (< 1 km depth) reservoir setting of fluid (thermogenic or biogenic gas) accumulation trapped beneath a fine grained, low permeability seal is implied (Fig.8.2). Density contrasts between the seal and reservoir encourage buoyancy in the immiscible fluids, promoting vertical migration of lower density fluids (gases) towards the seal (Gluyas and Swarbrick, 2004). Sub-seismic heterogeneities in the higher permeability reservoir stratigraphy and/or the sealing sequence help to define localised cells within the broader expanse of fluid accumulation trapped beneath the seal (Chapters 5 and 7). These cells may act as minor permeability barriers, focusing fluid and hence overpressure generation (Deming et al., 2002). It is probable that these cells are interconnected at the large scale, permitting "signals" of fluid and pressure level variations to be transmitted to other parts of the reservoir (Chapter 5) (Swarbrick and Osborne, 1996, 1998).

Overpressures are generated by fluid migration and accumulation in the trap and/or rapid sediment deposition. Pore pressures build exerting excess stress on the seal. In < 1 μm grain size environments, it envisaged that the seal will fail by hydraulic fracture (Jain and Juanes, 2009).

8.3.1.2 Time-step 2

Increase in pore pressures beneath the seal results in hydrofracturing (Hubbert and Willis, 1957) (Fig.8.2). The location of hydrofracturing is believed to be related to heterogeneities in the seal configuration, for example, locations where the seal locally domes (even if it is only by a matter of centimetres) or any natural small fissures. It is proposed that depending on the degree of pressure differential between the seabed and reservoir overpressure, the initiated (vertical) hydrofacture will either remain as a single fracture or bifurcate if the pressure and propagation velocity is below a threshold value (cf. Chapter 6). Hydrofracture propagation speeds are estimated to be 1000 m/yr (for hydrofractures of several meters length) (Nunn, 1996). The hydrofractures will propagate as flow self-organises, forcing grains apart. It is anticipated that the opening of the fracture moves grains on the edge of

the fracture closer together creating a halo of pore throat contraction and decreased relative permeability (Jain and Juanes, 2009).

A hydraulic connection is established when the hydrofractures reach the seabed resulting in "blowout". Flow velocities are anticipated to be quicker for consolidated than unconsolidated clay and silt (Lowe, 1975). If a minimum fluidisation velocity is reached the drag exerted by the moving pore fluids exceeds the buoyant weight of the grains, lifting sediment up the pipe to be expelled at the seabed. Fluidised sediment will be distributed on the seabed according to entrainment drop out theory, i.e. the heavier material falls out of suspension quicker and in closer proximity to the pockmark than the finer material which will travel a greater distance or may be lost to the water column. This is similar to channel-levee sediment entrainment, transport and deposition (Summerfield, 1991).

It has been shown that pipe diameter and height are positively correlated implying a scaling relationship between geometries (Chapter 4). It is therefore conceivable that pressure and pipe height are loosely related, as it is assumed that a greater overpressure and duration of this pressure is required to initiate and maintain more energetic fracture propagation and form taller pipes.

It is proposed that a "drainage cell" forms around the pipe and pockmark (Chapter 7). The drainage cell represents an exclusion zone around the pockmark which is not penetrated by the formation of another pockmark. Here the Namibian and NDSF conceptual models separate in their implications. At the basinal scale, it is inferred that the exclusion zone is temporary, lasting a minimum c. 100,000-200,000 yrs (estimated from the Namibian example, timescale may vary between basins), the time span represented by a single reflection (Chapter 5). Conjoined pipes support this supposition. At the field scale, spatial statistics and SOC imply that the exclusion zone is permanent, for at least up to 1,000 yrs (Chapter 7). It is proposed that the size, shape and boundary of the drainage cell is a function of permeability heterogeneities, overpressure build-up, release and re-charge patterns.

8.3.1.3 Time-step 3

Following formation of the initial pipe and pockmark, fluid migration continues through the conduit (Fig.8.2) (Chapter 5 and 6). Fluid flux is considered to be an order of magnitude smaller than the initial formative flux. Total blowout (high magnitude event, similar to the initial formation event) of the pipe is prevented by smaller scale overpressure and release episodes resulting in small unit pockmark formation (cf. Chapter 6). Post formation fluid migration may be either continuous or episodic. If continuous, it is likely that fluid is continuously migrating towards the pipe and seeping through the established conduit. Capillary infiltration may maintain seepage through the pipe if coarse material (sand) collapses into the conduit (Jain and Juanes, 2009). Continued migration prevents the settlement of hemiplegic drape above the pockmark thus maintaining the pockmark morphology (Pockmark array) through time.

Episodic migration is dictated by the timescale required for overpressure build up and release. Overpressure is built up by (re)forming a temporary seal within the pipe by either collapse of material into the pipe, sedimentation or MDAC build-up (Hovland, 2002). The shear strength of the temporary seal is not as strong as the original seal permitting failure at lower overpressures (cf. Chapter 6).

8.3.1.4 Time-step 4

Fluid continues to migrate through the pipe and pockmark, and the pockmark morphology perpetuates through time. Additional unit pockmarks may form above the pipe structure (Hovland et al., 2010). Multiple unit pockmarks may form above the pipe if the flow bifurcates in the pipe or if certain fractures or unit pockmarks become blocked. As fluid migration continues, the columnar seismic expression of the pipe grows with time and a slight increase in the width of the pipe is envisaged (cf. Chapter 4 and 5).

A new pipe (P2) forms, at a distance greater than the radius of the drainage cell of the existing pipe (P1) (Fig.8.2). As fluid is still migrating through P1, further pockmark formation is prevented within P1's drainage cell because fluid migration

pathways are already established and preventing overpressure generation sufficient to form a new pipe (cf. Chapter 7). The new pipe forms by hydraulic fracture, establishing its own unique drainage cell.

8.3.1.5 Time-step 5

Fluid migration through pipe and pockmark 1 has ceased and the pipe morphology has reached its penultimate stage. Post formation fluid migration continues through pipe and pockmark 2, creating additional unit pockmarks. A new pipe forms (P3). The spatial position of P3 is closer to P1 than P2 (Fig.8.2) (Chapter 5).

Pipe and pockmark 1 contains multiple unit pockmarks. It is likely that these pockmarks are in the order of 10-20 m diameter and are randomly distributed within the depression. An interesting component of Self-Organised Criticality (SOC) is the observation that the system displays Self-Similarity (SS). Self-Similarity is a form of scale invariance whereby the pattern is the same at all scales. Self-Organised Criticality was recognised within the Rosetta pockmark field, therefore, it is inferred that the pattern of random pockmark distributions incorporating an exclusion zone is present at both the basinal, field and within pockmark scale (this is a highly contentious issue and can not be resolved without further work) (Chapter 7).

The position at which P3 forms is likely to utilise the space between existing pipes and form closer to P1 than P2. Potentially, P3 could form as close to P1 as the boundary of the P1 drainage cell area. It is feasible that drainage area size and shape may change with time. Fluctuations in the drainage cell geometry may result from changes in 1) permeability e.g. from sedimentation or collapse within the pipe, 2) flux, 3) fluid migration into the pipe from depth, 4) degree and position of overpressure generation e.g. smaller amounts of overpressure is necessary to form the unit pockmarks and 5) contraction or closing of fractures e.g. cementation or hydrate formation.

8.3.1.6 Time-Step 6

Post formation fluid migration ceases through P1 (Fig.8.2). The pockmark is filled with hemiplegic drape and the depression is topographically healed (cf. Chapters 1 and 6). It is likely that fluid pressures within the drainage cell no longer exceed threshold values for capillary entry pressure or hydraulic fracture pressure. Reduced fluid pressures may be due to a decline in fluid generation or migration into the cell. The exclusion zone around P1 will remain until overpressures are sufficient to form a new pockmark within the drainage cell or migration continues through P1 (cf. Chapter 7). New pockmarks continue to form and post formation fluid migration is continuing through P2 and P3.

8.3.2 Implications

The 4D spatio-temporal conceptual model described above epitomises the research concept outlined in the introduction (Fig. 1.5). The implications outlined below were selected based on their close relationship to the research concept and the aims of this thesis, namely pipe / pockmark morphology and process, spatial and temporal distribution and magnitude and frequency.

This next section examines; 1) the implications for seal risk analysis; 2) the significance of pipe planform geometry; 3) the significance of overpressured cells; 4) predicting the spatial location of pockmark formation within a shallow sourced field; and 5) the implications of Self Organised Criticality.

8.3.2.1 Seal risk analysis

Seal risk analysis examines the possibility that a petroleum (or even CO_2 sequestration) reservoir seal has been (or could be) breached by a member of the Seal By-pass family (see Chapter 1) (Cartwright et al., 2007). Seal risk analysis is an important component of hydrocarbon play analysis (Gluyas and Swarbrick, 2004) and is invaluable in analysing the economic viability of a potential reservoir. As

noted in the thesis rationale (Chapter 1) seal risk analysis is one of the main applications of the science of focused fluid flow analysis using seismic data.

As members of the Seal By-pass System (SBS), cross stratal fluid migration through pipes is a component of seal risk analysis. The methodology adopted by this research (Chapters 3, 4, 5, 6 and 7) is generally applicable to analysing the spatial and temporal pattern of leakage from hydrocarbon reservoirs. Trap failure and seal by-pass can be identified, the position of failure within the trap determined i.e. anticline apex, and arbitrary chronostratigraphic dating of when leakage occurred and when / if it ceased. Leakage patterns can potentially be identified and included in geological models or play analysis, for example, directionality in seal failure or any cyclicity in overpressure and seal breach.

Similar assessments can be made when assessing the suitability of former hydrocarbon reservoirs for carbon capture and storage (CCS). By assessing any previous modes of trap failure it may be possible to suggest locations for potential future failure if supercritical CO2 is injected too fast or the fracture pressure is exceeded.

The scenarios described above could potentially relate to new emerging "reservoirs", for example, gas hydrates. Analysing spatio-temporal patterns of pipe formation from BSRs at the base of the gas hydrate stability field could potentially contribute towards an understanding of gas hydrates as a trap, overpressure mechanisms and patterns, episodicity/cyclicity of overpressure generation and migration triggering mechanisms e.g. hydrate dissociation.

8.3.2.2 Pipe morphology as a proxy for stress patterns

Stress and strain patterns are manifested by the change in shape of geological structures or sediments (Maltman, 1994). Understanding subsurface (and sub-seismic) strain patterns is important for numerous petroleum disciplines including basin analysis and modelling, geohazards analysis, well bore stability, field installation stability and fluid migration. In this section I discuss whether pipe

geometrical analysis may have implications for the analysis of stain patterns. This discussion is exemplified using the Namibian data presented in Chapter 4.

Hydraulic tensile fracturing (Hubbert and Willis, 1957) of low permeability top seals has been linked to pipe formation and the initiation of intrusive structures (Van Rensbergen et al., 1999; Dimitrov, 2002; Morley, 2003; Cartwright, 2010). Pressure-generated permeability is instigated when the pore fluid pressures exceed the minimal principal stress and tensile strength of the sediment (Hubbert and Willis, 1957; Secor, 1965; Luo and Vasseur, 2002; Hillis, 2003). Consequently hydrofractures develop perpendicular to the direction of minimum stress, which is often assumed to be horizontal (Bott, 1959). Under certain conditions, where horizontal and vertical stresses are equal, it is feasible that the sediment will fracture isotropically into a set of radial, geometrically complex, fractures (Jain and Juanes, 2009). It is anticipated that isotropical conditions would produce random fracture sets therefore making any stress / strain pattern analysis virtually impossible to detect, but this is not considered here.

Planform geometry of the Namibian pipes (Chapter 4) has been shown to be variable throughout the pipe height changing from unidirectional and elliptical at depth to multi-directional and circular towards the top (Fig. 8.3). This is commonly observed in many pipe, mud volcano and diatreme-like structures (Brown, 1990; Løseth et al., 2001; Davies and Stewart, 2005; Cartwright et al., 2007). In the Namibian example measured pipes are orientated in a NW-SE direction, crudely approximating the general slope strike (Chapter 4). This may represent the principle stress direction of the root zone stratigraphic unit. I suggest that the elliptical nature of the pipe root zone is related to the orientation of the seal hydrofracture which initiates the pipe or any pre-existing discontinuities near the root zone which may facilitate or direct focused flow e.g. faults (Hustoft et al., 2010).

Namibian pipes have been shown to be unrelated to polygonal faults in the base Miocene sequence (Fig. 8.4) suggesting orientations are related to deeper stratigraphic units or normal faults; however faults at depth have not been observed. Polygonal faults have no preferred orientation (assuming no stress bias during their formation (Hansen et al., 2005)) (Cartwright, 1994; Cartwright and Dewhurst, 1998),

therefore it can be assumed that pipes bleeding from polygonal faults may display various elliptical orientations, and not aligned in a single orientation as shown here (orientations shown here are possibly related to downslope stresses (Clausen et al., 1999)).

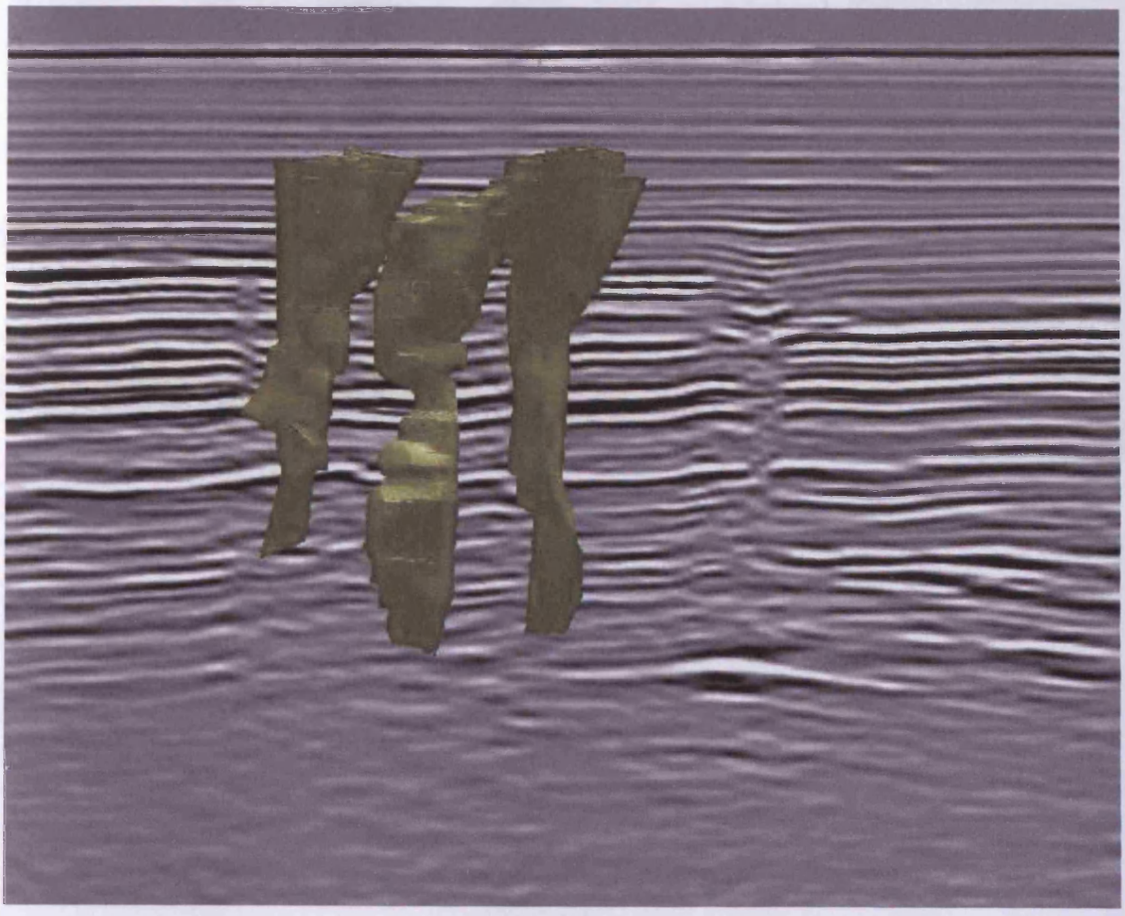

Figure 8.3 Pipes in 3D. Pipe geometry changes with height. Example from offshore Namibia.

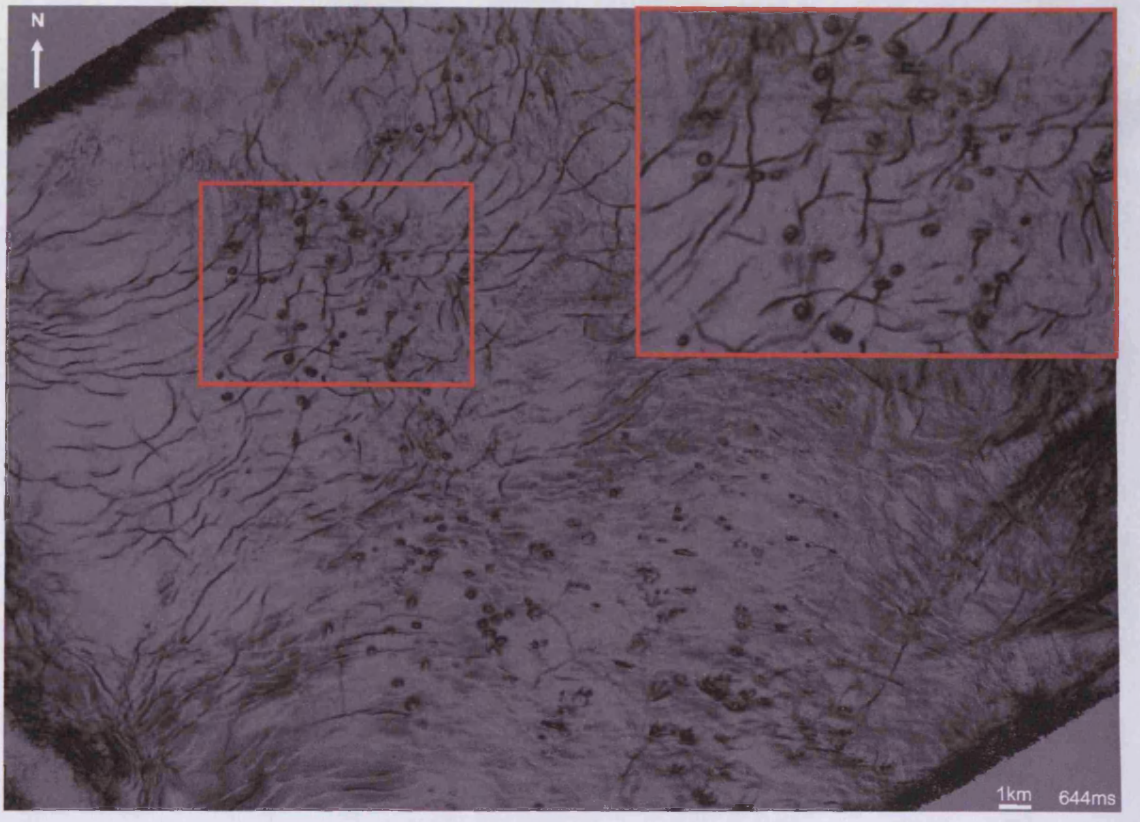

Figure 8.4 Coherency slice showing the co-existence between pipes and polygonal faults, offshore Namibia. Coherency slice taken 644ms below seabed (Post Rift 3).

Clear identification of the pipe root zone is of paramount importance if pipe orientation is to be used as a proxy for principle stress directions (cf. Chapter 4 and 5). It is acknowledged that pipe roots are difficult to constrain seismically because of 1) layer deformation or 2) anisotropic velocities within the pipes which may scatter the seismic energy and potentially produce migration artefacts and/or shadow zones below the pipes (Hustoft et al., 2010). Nevertheless it is important to measure true pipe base orientation or inaccuracies in stress direction may be introduced by the structural geometric changes observed with pipe height (Chapter 4).

In diatremes, it is suggested that this change in geometry from an elliptical root zone to circular top zone is a function of higher flow velocities within the central conduit (Novikov and Slobodskoy, 1979). It is assumed that a combination of upward increasing flow velocity (e.g. due to gas lift) and lower confining rock strength will increase the relative power of the fluid compared to that of the host rock, causing pipes to self organise as a cylindrical column during fluid ascent (all other factors being equal). High flow velocities can potentially be obtained in columnar structures through reduced wall friction between the upward flowing fluid and the surrounding host rock, altering the geometry as a function of process. A similar mechanism is therefore probable for pipes, and explains the geometrical variations with height observed (Chapter 4).

In summary, tensile fractures develop perpendicular to the direction of minimum horizontal stress (Bott, 1959), and this knowledge could potentially be used to analyse failure patterns (Price and Cosgrove, 1990). Here I suggest the genetic link between pipe formation and hydraulic fracturing could potentially help elucidate principle stress directions within certain stratigraphic units. Pipe root zone orientation as defined by hydraulic fracturing could be used as a proxy for principle stress directions. Caution is advised when using this proxy as hydraulic fracture orientations may be influenced by factors other than the direction of minimum stress, e.g. heterogeneities in strength.

8.3.2.3 Mapping overpressure and the significance of pipe diameter

In addition to utilising pipe root zone orientation as a proxy for principle stress directions, pipes represent loci for overpressure generation and release within a basin and are therefore ideal for locating previously overpressured cells (cf. Chapters 5 and 7). Seepage pipes are excluded from this discussion.

Mapping and modelling overpressure development is an important component in basin analysis. Numerical models are utilised to good effect for analysing the distribution of pressure within a petroleum reservoir, however these models require detailed numerical input and can only provide reliable results after extensive reservoir characterisation (Gluyas and Swarbrick, 2004). In this section I discuss whether pipe distribution and size (diameter) could potentially be used as a proxy for the relative distribution and amount of overpressure in a rapid, "first-pass", overpressure assessment prior to the main basin modelling. The Namibian pipes are utilised as a case study to exemplify this discussion (Chapters 4 and 5).

Pipe geometry alters with height (Chapter 5). Two different measurements of pipe diameter could potentially be used for this proxy; maximum pipe diameter and pipe base diameter.

Widest pipe diameters are commonly observed at the level of the blowout crater or several reflections immediately above. This marks the point of maximum flux which is subsequently modified by higher frequency, lower magnitude post formation fluid migration (Chapters 5 and 6). It is anticipated that initial seabed pockmark/crater formation is dependant on both the eruptive force and geotechnical properties of the seabed i.e. finer silty material may produce wider but shallower pockmarks when compared to stiffer clay-rich material (Van Rensbergen et al., 2007).

Pipe base diameters could not be measured within the Namibian dataset (Chapters 4 and 5). In the majority of examples, pipe minimum diameter was recorded at the deepest seismically resolvable point of the pipe, however small diameters have also been recorded from the very top of some pipes (cf. Chapter 4, Fig 4.8b). The base of a pipe is located at the point of maximum overpressure and hydrofracture

generation within a seal. Here I tentatively suggest that the diameter of the pipe base ellipse is roughly analogous to the fracture length at the time of blowout. It is acknowledged that flow through the hydrofracture will modify the original fracture geometry in terms of 2D size and shape i.e. width and possibly length; however analysing the degree of fracture propagation in response to fluid flow is beyond the scope of the discussion presented here.

Pipe diameter data previously analysed in this research (Fig. 4.2a) has been re-graphed in Figure 8.5 for the purposes of this discussion. Similar to Figure 5.5, a temporal frequency histogram has been constructed for the mean value of minimum, average and maximum pipe diameters. The histograms show that mean pipe diameters fluctuate with reflection (stratigraphic) depth or "time" (Fig 8.5) *. Mean minimum pipe diameters show no trend with time. Mean average and maximum diameters show a similar trend with time. Against a background fluctuation in diameter with time, mean diameters can be seen to broadly increase from R71 (base Miocene) to peak at R29, where there is a dramatic decrease in mean pipe diameters over a period of 1 reflection (R28), before mean pipe diameters steadily increase once again.

* Please refer to the digital appendix to view the spatial position of mean maximum pipe diameters displayed on an incremental reflection basis

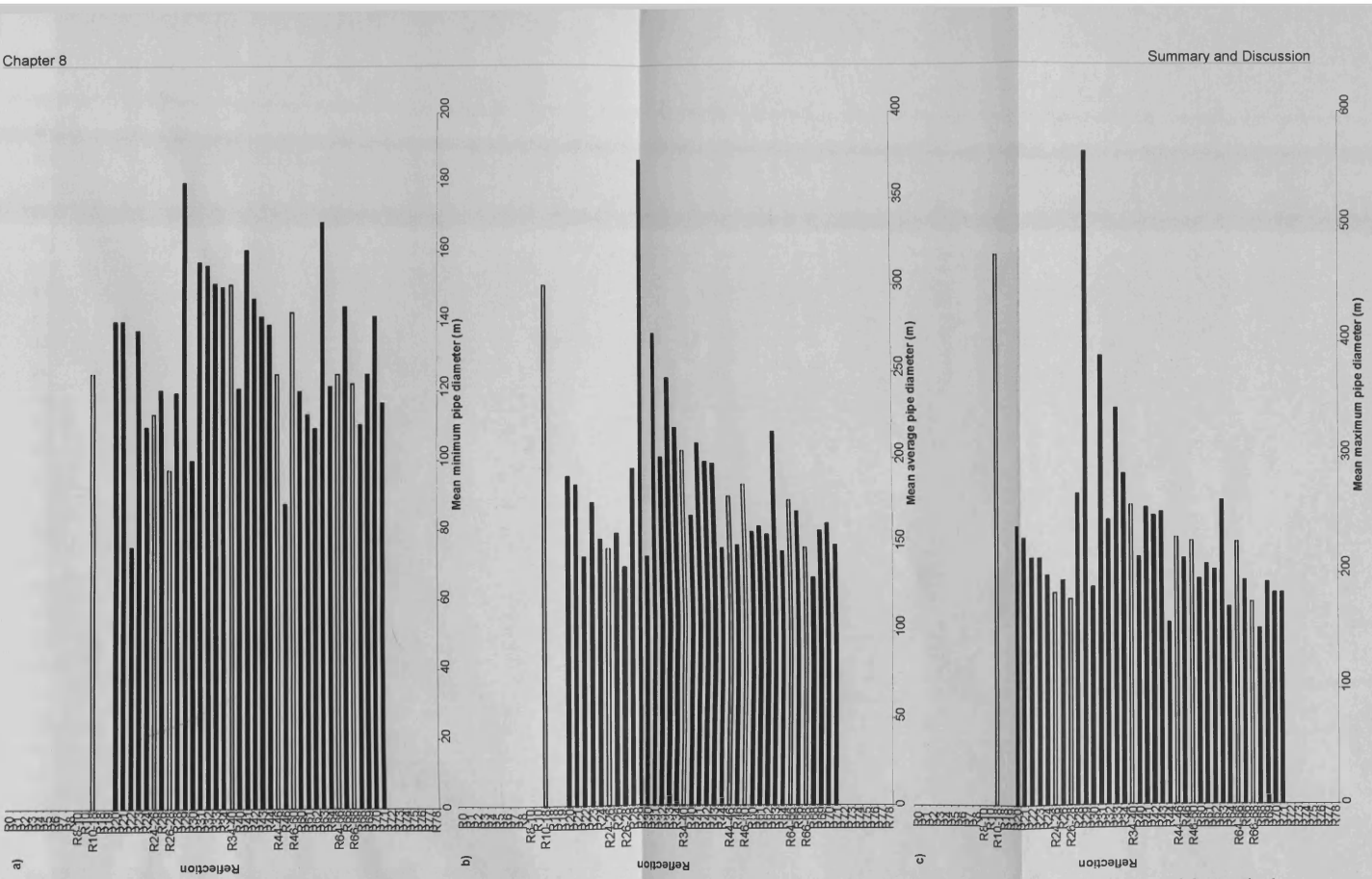

Figure 8.5 Temporal frequency histogram. a) Mean minimum pipe diameter (m), b) Mean average pipe diameter (m), c) Mean maximum pipe diameter (m). This graph is equivalent to maps showing pipe symbols proportional to maximum pipe diameter.

The interpretation of pipe diameter and its relationship to overpressure and release is of paramount importance when discussing the implications of pipe diameter for mapping overpressures. Pipe diameter can be interpreted in a variety of ways, 1) originating from the size of the hydrofracture, 2) as a function of pipe re-use (Chapters 5 and 6) and pipe height (Chapter 4), 3) as a function of geology and 4) as a function of acoustic anomalies (Løseth et al., 2009).

It is acknowledged that both geological heterogeneities and acoustic anomalies have a significant impact on pipe diameter. Acoustic anomalies may mask true pipe diameter (Chapter 4 and 5), producing erroneously large measurement values. Pipe geometry may alter as a function of geology, for example, if a pipe is focused through a channel-levee complex diameters may vary depending on the strength of the different materials within the complex. Both variables are independent of overpressure and constitute considerable limitations to using pipe diameter as a proxy for overpressure.

Pipe conduits are potential locations for repeated fluid migration flux (Chapter 5 and 6). If the volume of flux is sufficient it is possible that this fluid flow may erode the pipe walls by abrasion, widening the diameter of the pipe. This is supported by observations of a scaling relationship between pipe height and diameter (Chapter 4). This proposition makes certain assumptions about the type of pipe conduit. If narrow, hollow conduits are opened, Darcy flow could potentially abrade pipe walls, however if pipes are an interrelated, dendritic network of hydrofractures, abrasion would not be possible and any increase in pipe width is likely to be manifested in an extension of the hydrofracture network composing the pipe. It has also been suggested that this post formation fluid flow is of a higher frequency but lower magnitude than the flux associated with initial pipe formation (Chapter 6). Nonetheless, lower flux fluid migration may still influence pipe geometry.

Similar studies have been made on tropical soil pipes (Richards et al., 1996). Soil pipes are small (< 10 cm diameter), buried (< 30 cm below the surface) hollow pipes found mainly in humid tropical river catchments with clay-rich soils, which contribute a significant proportion of overland flow to rivers (14-16 %) (Walsh and Howells, 1988). Studies have shown that minor erosion of the soil pipe walls can

occur for both large and small rainfall (water) fluxes (Walsh, 1980; Walsh and Howells, 1988; Walsh, 1996; Sayer et al., 2004; Sayer et al., 2006).

Finally, pipe diameter may be a function of the degree of overpressure. It is conceivable that a greater degree of pressure may produce a larger seal hydrofracture once the initial subseismic fracture has formed (given an instantaneous blowout to seabed conceptual model). However fracture size may also be dependant upon seal geology i.e. fracture potential, sediment type/composition heterogeneities, permeability or contextual setting / dip. If these factors can be shown to be homogeneous, it could be assumed that degree of overpressure is related to hydrofracture size.

Taken together, these inferences suggest that pipe diameter may provide a relative proxy for overpressure. Minimum pipe diameters might represent a proxy for overpressure at the time of seal breach. Maximum pipe diameters may represent a proxy for both overpressure at the time of seal breach and any subsequent overpressure build up and release i.e. magnitude and frequency of flux. Applying this interpretation to the mean average and maximum pipe diameters Figure 8.5.b.c, implications are that within the Namib basin, broad scale overpressure has been slowly building since the Early Miocene to culminate in the Pliocene. Overpressures reached a critical limit (R29) and then dissipated to a level lower than recorded in R71. Following broad scale dissipation, pressures slowly build back up towards a critical limit in a possible large scale cyclic process. Mean minimum pipe diameters recorded here (Fig. 8.5.a) are not considered a proxy for hydrofracture size because clear identification of the pipe root zones was not possible. This may explain why the minimum diameter graph does not show a similar trend to average and maximum mean diameters.

It should be noted that the peak in overpressure (R29) does not coincide with the frequency peak in pipe formation (R34-40, TP1 scenario 1, Fig. 5.5). This may suggest that the degree of overpressure and the frequency of seal breach are unrelated or that the trend of overpressure with time is a function of conditions e.g. geological differences, other than overpressure. It has been noticed that the largest forming pipes are in the south of the study area and that these represent more recent pipe

formation*. The graph may therefore reflect geological conditions more suitable to large pockmark / crater formation in the south of the study area. However, geological variations (based on seismic stratigraphic observations) have not been noted in the south of the study area, and no confident correlations have been made between pipe timing, position and geometry and its relationship to the palaeochannels.

8.3.2.3.1 Implications for overpressured cells

I have suggested that the Namibian pipes are influenced by isolated pressure cells which are locally independent yet broadly controlled (Chapter 5). Pressure compartments or cells have previously been invoked to explain fluid movement and associated overpressure generation within petroleum basins (Bradley, 1975; Deming et al., 2002; Tingay et al., 2007). Overpressures have been shown to drive fluids within compartments (Bishop Stump and Flemings, 2000; Flemings et al., 2002) but the lateral connectivity or potential for overpressures to be redistributed or transferred to other pressure compartments over time is rarely discussed (Tingay et al., 2007). I believe that overpressure build up and dissipation with time shown in Figure 8.5 is another example in support my previous assumptions of pressure cells within the Namib Basin and also supports notions of connectivity between cells.

Overpressures are known to dissipate over time via fluid leakage (Borge, 2002), and consequently are thought to originate in close proximity to where they were generated (Swarbrick and Osborne, 1998). To approximate the two-scale model proposed here of localised over pressure and release (pipe formation) against a background of longer term, larger scale prolonged pressure build up and dissipation within the basin, I propose a conceptual model similar to Muggeridge et al (2004, 2005). The broad scale build up of basin wide anomalous pressure consists of groups of pressure compartments or cells (Bradley and Powley, 1994; Ortoleva, 1994; Ortoleva et al., 1995). These cells may be independent or may lay within larger cells forming "megacompartments" within the general "megacompartment complex" (Al-

* See digital Appendix on CD

Shaieb et al., 1994a, b; Muggeridge et al., 2004). Under this model the cells may have different degrees of overpressure (Muggeridge et al., 2004) but still retain connectivity to adjoining cells in the complex.

It has been suggested that the pressure gradient in a typical hydrocarbon reservoir compartment is anticipated to return to hydrostatic over timescales in the order of hours or days, but the rate of pressure dissipation from abnormally pressured compartments are likely to take periods of tens of thousands to hundreds of thousands of years (Muggeridge et al., 2005). The grouping of cells into "megacompartment complexes" may delay pressure dissipation for millions of years (Muggeridge et al., 2004). The time period (reflection) of a single interval recorded in the Namibian data is c. 100-200,000 years and the period between R71 and R29 may be as much as > 270,000 years. I therefore tentatively suggest that the Namibian data may display characteristics in common with the "megacompartment complexes" of Muggeridge et al (2004, 2005) and reinforce the view that the Namibian pipes are influenced by isolated pressure cells which are locally independent yet broadly controlled.

8.3.2.4 Prediction : Generalised predictive model

Predicting the location and timing of any future pockmark formation is a component of the geohazard and risk analysis for seabed petroleum installations (Hovland et al., 2002; Ligtenberg and Connolly, 2003; Orange et al., 2005). Geohazard and risk analysis is often concerned with potential events over the life of the field e.g. pockmark formation within the next 50 yrs. Though generally more applicable to pockmark fields, the research on pockmark exclusion zones presented here could be extrapolated to propose areas within a field that are likely and/or unlikely to be populated by new pockmark growth. Establishing the age of the existing pockmarks and any correlation to triggering mechanisms would help establish the likelihood for future pockmark growth within the life of the field.

A generalised, predictive, multi-layered model is proposed to broadly predict the location of new pockmarks within a pockmark field (Fig. 8.6). The model is outlined

below using a case study example from the Rosetta pockmark field (Chapter 7). The model relies on average values (as stated in this thesis) and spatial distribution analysis only.

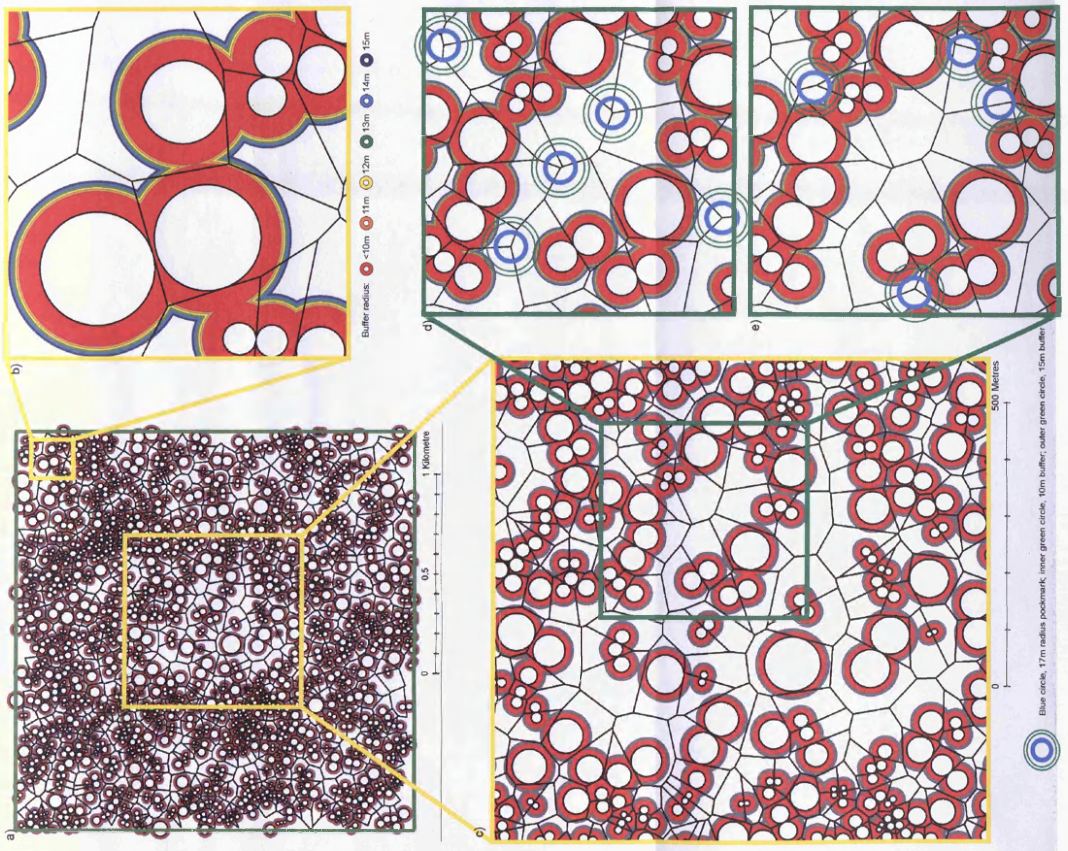

Figure 8.6 Generalised predictive model. a) existing pipe exclusion zone (white circles) for the total population of pockmarks within the Rosetta Region study area. b) buffered rings surrounding the exclusion zone providing minimum distances for the closest formation of new pockmarks to existing, c), possible positions for newly forming pockmarks at either d) maximum distance from existing pockmarks or e) close (clustering) distance from existing pockmarks.

Utilising the results of the Rosetta pockmark field analysis, a 10-15 m buffer was applied around the existing pockmark exclusion zone (assuming the exclusion zone is not penetrated by the formation of new pockmarks) (Fig. 8.6). This distance is based on a) the 10 m avalanche radius in SOC analysis, b) the deficit of Minimal Spanning Tree short edge lengths < 12 m, c) 14 m hardcore model and d) the deficit of nearest neighbour distances < 15 m (Fig. 7.9 and 7.11). This buffer simulates the anticipated exclusion zone surrounding any newly forming pockmarks. For simplicity in handling the large dataset, the buffer has been applied to the existing pockmark exclusion zone, delimiting the closest minimum distance a new pockmark could form to an existing pockmark. This distance also reflects the peak in MST edge lengths (above that for a random population) observed beyond the deficit of short edge lengths or exclusion zone distance (Fig. 7.13).

The model anticipates overpressure release to produce a pockmark 17 m in diameter (current average size for Rosetta field pockmarks, Fig. 7.9) (Fig. 8.6). New pockmark formation is predicted to occur in a minimal seabed area of c. 2730 m^2 (ratio of 3:1, Theissen polygon available space vs exclusion zone area, Fig. 7.9), thereby reducing the possible locations for new pockmark formation within the field. It is unclear, whether new pockmark formation will occur at maximum distance from, or cluster close to existing pockmarks (Fig. 8.6). Previous analysis from Namibia (Chapter 5) has shown that new pipes can form as both clusters and outliers at the same time, however the Rosetta pockmarks have shown a tendency towards clustering which may be favoured here (Chapter 7).

Complexity can be added to the basic model described here by incorporating aspects of Self-Organised Criticality in positioning the new pockmark(s) (spatial constraints included). Additional map layers pertaining to soil variability, permeability, pre existing fluid migration conduits e.g. faults or structures e.g. palaeochannels can be incorporated into this spatial model to restrict or group pockmark formation within a field.

Generalised predictive modelling as described above is only advisable once detailed spatial analysis has been conducted. Predictive models have to be site specific and tailored to the specific spatial requirements. For example the spatial distribution of

pockmarks within the Big Sur pockmark field, offshore California (Appendix A7), does not show any tendencies towards Self-Organised Criticality. Instead a linear density gradient has been observed which would need to be incorporated into any generalised predictive model.

This type of generalised spatial predictive model could be applied to pockmark fields above petroleum reservoirs. For example, multiple large petroleum accumulations have been discovered beneath pockmark fields, offshore Angola. Geohazard assessments and risk analysis to seabed installations in Angolan blocks may benefit from a general predictive approach.

8.3.2.5 Self-Organised Criticality and Self-Similar characteristics: implications for pockmark fields

A tendency towards Self-Organised Criticality (SOC) has been observed in the Rosetta pockmark field on the Nile Deep Sea Fan. Self-Organised Criticality is a relatively new approach to analysing complex systems, and is repeatedly claimed to be a new paradigm in universal theory of complex behaviour e.g. chaos theory (Frigg, 2003). To the author's knowledge, this is the first observation of SOC in pockmark distributions, but caution is advised when applying this universal theory to a new domain for the first time (Anderson, 1996; Frigg, 2003). The defining characteristic of SOC is self-similar characteristics in the magnitude of events (Bak et al., 1987; Bak, 1996; Ball, 2004; Cartwright et al., In press). The methodologies and results presented here have been unable to obtain definitive information on the "magnitude" of pockmark formative processes, however their spatial distribution has been shown to hold an "imprint" of SOC behaviour (Cartwright et al., In press). Here I discuss what information would be necessary to demonstrate SOC behaviour in pockmark formative processes and, if found, what the implication of this would be for pockmark science.

The basic message of Self-Organised Criticality is that large fluctuations are vital to the dynamics of large systems (Bak et al., 1987; Anderson, 1996). The premise was first displayed using a Sand Pile model (Bak et al., 1987, 1988). Grains are added

randomly to a slope composed of grains of sand. The additional grains cause the slope to become unstable and the slope fails (avalanche). The slope is maintained in a "critical state" at the angle of repose as grains are continuously added to the slope and the slope fails in response. In the model Bak et al (1987, 1988) found that a single grain can induce a slide of any magnitude. There is no characteristic scale to the system i.e. no there is no typical number of grains added to the slope which induce failure; it is scale-invariant or has self-similar characteristics. The probability of avalanche size is a power law or scaling law, describing the inverse relationship between avalanche size and the frequency of avalanches (f), commonly referred to as an $1/f$ law or $1/f$ behaviour (Ball, 2004). $1/f$ behaviour is unpredictable but clearly distinct from a purely random process (Ball, 2004). The system is self-organised because the pattern occurs spontaneously and minor perturbations (adding grains) can lead to effects (avalanches) of all sizes i.e. there is no outside "agent" affecting the system.

Components of SOC behaviour and scale invariance or self similar characteristics have been observed in a number of different situations within this research. Firstly, pockmark diameter and depth have been shown to be positively correlated at both the large and small scale for circular pockmarks (Chapters 6 and 7) (it is acknowledged that this may be a function of pockmark inner-slope stability). Secondly, in the hydrofractured mechanism for pockmark formation, a fracture is believed to initiate a near-circular pipe and resultant pockmark regardless of scale (the effects of imaging and acoustic artefacts are acknowledged) (Chapters 4 and 6). Finally, it is probable that the unit pockmarks above the buried pockmarks on the Rosetta Plateau hold an imprint of SOC in their spatial distribution despite their formation in a non-field environment (Chapter 6). Although not analysed, the unit pockmarks are small, circular, display a random distribution (according to first order characteristics) and have nearest neighbour values similar to the higher density regions of the pockmark field.

The formation of pockmarks by the non-linear failure of a sealing sequence once a critical [state] fluid pressure is reached suggests SOC behaviour is a possibility, however, classifying the "magnitude" of pockmark formation is problematic and one of the inherent weaknesses of SOC (Frigg, 2003). The magnitude of pockmark

formation could relate to 1) the size (height, depth, diameter) of the pockmark or pipe, 2) the degree of overpressure, 3) fluid flux (discharge rate, volume), 4) the geotechnical properties of the seal (composition, thickness), 5) depth to the fluid source or 6) permeability of the reservoir. Of the variables mentioned it has only been possible to measure pipe/pockmark size in this study. The frequency of Namibian pipe height and diameter (Chapters 4 and 5), Rosetta Plateau depression diameter (Chapter 6) and Rosetta field pockmark diameters (Chapter 7) do not show $1/f$ behaviour* and it is therefore probable that "size" is not a proxy for formation magnitude under a SOC system (given a population of < 400 measured variables).

In consideration of SOC behaviour, the sample size is critical. The spatial and temporal sample size needs to be sufficient to describe dissipative systems with extended degrees of freedom (Bak et al., 1987). It remains unclear whether the sample size utilised in this study is adequate.

In a Self-Organised Criticality model inferences can be made about the magnitude of the processes operating within the pockmark system, but not which processes are operating. If size is not a proxy for formation magnitude, I suggest additional proxies should be tested to explain the imprint of SOC in the Rosetta pockmark field. For example minor changes in methane generation or reservoir permeability may lead to overpressure generation at all magnitudes, and if overpressure demonstrates $1/f$ behaviour it may be possible that overpressure is the fundamental component which explains pockmark formation in a field environment.

Currently, SOC behaviour has been identified in the distances separating pockmarks, given a minimum avalanche size of 10 m. If this spatial behaviour proves to be an imprint of SOC behaviour in pockmark formation, it could have important implications for pockmark science. Self-Organised Criticality would suggest that, in principle, there is no difference between big and small pockmark formation, and that potentially, the frequency of the "magnitude" of formation could be "predicted" from the $1/f$ power law. In other words, SOC opens up new lines of enquiry by isolating and exaggerating components of the fluid flow system.

* see Appendix A6

The paradigm of Self-organised criticality is not without its drawbacks. Self-Organised Criticality and Self-Similar characteristics have been enthusiastically applied to many systems however not all systems fit the model as well as the original sand-pile model belonging to Bak et al 1987 (Anderson, 1996; Frigg, 2003). One example being turbulence in the field of hydrodynamics which displays a classic model for dissipative dynamics due to qualitative inhomogeneity of the system (Anderson, 1996). Rigorous testing of the application of SOC to pockmark formation is suggested before adopting this model.

8.3.3 Research limitations

The limitations of the research presented in the preceding chapters are as follows;

- Well calibration: both the Namibian and Nile Deep Sea Fan seismic data would have benefited from well calibration. Ideally multiple, deep boreholes in close proximity to the area under investigation would have helped to confirm the geology of different seismic stratigraphic units and provide chronostratigraphic age control. For example, age data and geotechnical characteristics of Mega Unit Post-Rift 2, offshore Namibia, would help to confirm the unit's role as a sealing sequence.
- High resolution data: the Namibian research would have benefited from a higher resolution seismic survey of Post-Rift 3. A high resolution seismic survey would help to more precisely define the pipes and therefore improve geometrical measurement accuracies (which currently stands at ~25 m by ~12 m)
- "Ground truthing" with ROV (Remotely Operated Vehicle) video footage and core sampling: the NDSF research would have benefited from either video footage or grab samples from within pockmarks to confirm methane seepage through the presence of MDAC, hard grounds, benthic communities or geochemical sampling.

8.3.4 Further work

Open questions remain regarding the validity of some of the assumptions made during this research. Further work is proposed to address these issues;

8.3.4.1 Additional datasets

Robust testing of the spatial analysis methodology is required. Application of the methodology to additional pockmark fields is necessary to determine whether tendencies towards Self-Organised Criticality is a general phenomena of pockmark fields or uniquely relates to the Rosetta Region (Chapter 7). Testing of the exclusion zone theory is paramount to the conclusions drawn here. If exclusion zones can be identified in other pockmark fields from around the world it strengthens the drainage cell hypothesis and suggests that, far from being random, pockmark formation adheres to some form of spatial positioning governed by the processes acting to form and maintain the focused fluid flow migration route (Chapter 7).

8.3.4.2 Pipe internal structure analysis

As mentioned in the introduction, the internal structure of pipes is very varied (Chapter 1). This may be a function of seismic imaging or processing etc or of genuine geology. Further research into the effects of imaging fluid escape structures with seismic data is required to resolve this issue.

8.3.4.3 Modelling

Modelling pipe and pockmark formation is a new paradigm within pockmark science (Cathles et al., 2009; Jain and Juanes, 2009). However, as noted in Chapter 7, these models are primarily concerned with 2D formation via vertical processes. Physical or numerical modelling which incorporated components to simulate the effects of

permeability, pressure, flow velocity etc in 3D or 4D (time) would help support some of the conclusions gained from spatial analysis.

8.3.4.4 Detailed interpretation of the drainage cell

The drainage cell is proposed here as a conceptual model to explain the anti-clustering observed in the spatial distribution of pockmarks (Chapter 7). The conceptual model requires robust testing (numerical modelling, physical modelling, geotechnical and geochemical sampling etc) to determine the influence of permeability, overpressure and fluid migration to the pockmark with distance (lateral). Additionally, other factors need to be addressed, for example whether a single process e.g. permeability, may have more of an influence on the size/shape of the drainage cell than other processes.

8.3.4.5 High amplitude reflection "waves"

A sampling campaign is required to fully analyse the high amplitude reflection "waves" observed in the Rosetta Region. Cores in excess of 50 m would be required to fully sample the stratigraphic sequence, both above and below the target. Cores (geomicrobiological and geotechnical) taken from the apex, syncline and shoulder of the "wave" could be analysed at regular intervals for pore water chemistry, in particular methane and sulphate, and relative elevated numbers of bacterial cell counts and activity. The "wave" could be sampled to test for calcium carbonate and the isotope composition of the calcium carbonate to determine if the precipitate is from biological or thermogenic sources e.g. δ13 C -80 ppm to δ13 C -50 ppm indicates biogenic sources and δ13 C -50 ppm to δ13 C -25 ppm indicates thermogenic sources (Horita and Berndt, 1999). The three samples could be carbon dated to determine when the high amplitude "wave" formed.

8.3.4.6 Self-Organised Criticality

Further analysis is required before claiming that pockmarks exhibit SOC behaviour. Firstly, identification of a pockmark formation process which exhibits a power law function between magnitude and frequency needs to be identified. Secondly, this process would need to show self-similar characteristics and third, testing of this theory would require a sufficiently large dataset. A large amount of multidisciplinary research is required before SOC behaviour can be endorsed.

Chapter 9

9 CONCLUSIONS

To the author's knowledge, this research represents the first published spatio-temporal analysis of pipe and pockmark formation of its kind (especially in the utilisation of quantitative statistical methods). The studies presented here illustrate how a spatio-temporal methodology can reveal valuable insights into process frequency and magnitude. These range from analysis at the basinal scale presented in Chapters 4 and 5 to the field scale presented in Chapters 6 and 7. The summary and discussions of Chapter 8, and the study specific conclusions drawn in Chapters 4, 5, 6 and 7, have provided observational, (semi)quantitative and interpretational conclusions. This section summaries the key findings and addresses the aims outlined in Chapter 1.

9.1 Extend the general descriptive base of Blowout pipes

- Chapter 4 has described a previously unknown group of pipes from offshore Namibia. The pipe family displays a great diversity and similarity in seismic characteristics. The pipes are clearly depicted in 3D seismic data from the recognition of systematic disruption and/or offset of the reflections within the pipe, augmented by observations of amplitude enhancement or dimming. Pipe bases are defined by a basal reflection that exhibits no disruption beneath the pipe and the upper terminus is defined by taking the first continuous reflection to cross above the pipe (this reflection often exhibits a fill morphology). Pipes range from < 100 m to > 300 m diameter and < 1100 m in height. Pipes are elliptical and their planform geometry changes with height. A scaling relationship between pipe height and diameter is observed. Wide pipes (> 100 m diameter) are characterised by an internal structure in which the majority of reflections are deflected downwards relative to the host stratigraphy (c. 10 to c. 60 m). In the

deeper part of the pipes, the 'sag' is abrupt and sharply delimits the lateral margins, whereas the depressions in the shallower portions of the pipe are more gently curving, and the pipe margins are less abruptly defined. I interpret these observations as indicative of a violent burst of escaping fluid/sediment at the seabed which induced subsequent collapse of the overburden (by volume loss due to fluidization at the base of the pipe) creating a blowout crater. Continued fluid migration through the conduit is a distinct possibility.

9.2 Investigate the spatial distribution of pipes and pockmarks

- Chapter 5 analysed the spatial distribution of a family of blowout pipes, using 3D seismic data from North Namibia. The pipes are not uniquely related to the up dip limit of structures or underlying stratigraphic units. They do not share a common basal reflection. The pipes are anti correlated with a mound apex (a potential structural trap) and are observed to form at the mound perimeter leaving the fold crest devoid of fluid flow features. Gross pipe distributions cluster in a horseshoe pattern around the central mound. On a smaller scale, pipe distributions display multiple patterns i.e. they can be clustered, dispersed or linear. Pipe formation colonises gaps between existing pipes and at large distance from the main group (outlier positions).

- Chapter 7 investigated the spatial distribution of pockmarks within a field using a case study from the Rosetta Region of the Nile Deep Sea Fan (NDSF). Pockmark distributions within the field are shown to be non-random. The pockmarks display anti-clustering tendencies i.e. there is a decreased likelihood of finding neighbours within a close distance. The exclusion zone between pockmarks does not fit a Hardcore distribution e.g. a regular lattice, and is shown to be highly variable between pockmarks. Pockmark distributions hold an imprint of Self-Organised Criticality.

9.3 Investigate the temporal distribution of pipes and pockmarks

- Chapter 5 analysed the sequential temporal distribution of blowout pipe formation in the Namib Basin, Namibia using an arbitrary chronostratigraphic timescale. Pipe formation is shown to be intermittent yet persistent through time. The pipes did not form at the same time, nor was their formation restricted to specific time intervals. The pipes are observed to form throughout a 5-10 My interval (Neogene) with 2 and 26 pipes forming during a single (or group) of reflections (approximately 100-200,000 years).

- Chapter 6 analysed the temporal formation pattern of buried pockmarks from the Rosetta Region of the NDSF and related their formation timings to potential triggering mechanisms. Buried pockmark formation has been shown to occur on 4 separate horizons chronostratigraphically dated at 15,000 yrs BP, 100,000 yrs BP and arbitrarily chronostratigraphically dated at c. 50,000-80,000 yrs BP. The majority of buried pockmarks formed during the c. 50,000-80,000 yrs BP time window. This time period coincides with a period of relatively low eustatic sea level which is believed to have triggered fluid migration.

9.4 Investigate the longevity of post formation fluid migration and make inferences about the frequency and magnitude of flux

- Chapter 4 discussed the interpretation of "stacked pockmarks" in 3D data. Stratigraphically positioned above the blowout crater, the Namibian pipes exhibited a stacked sequence of gently curving concave depressions. It is difficult to determine the precise origin of the stacked concavities using 3D data alone, however maintenance of successive generations of concavity over an

extended period of time and enhanced amplitude anomalies suggest fluid migration may be a component in their formation.

- Chapter 6 analysed and interpreted "stacked pockmarks" using high resolution 2D data from the NDSF. Using higher resolution data it is evident that the concave reflection geometry above buried pockmarks is the perpetuation of pockmark-like morphology through drape and not stacked pockmarks. I term these conduits pockmark arrays
- Chapter 6 identified and interpreted seismic reflection characteristics which typify post formation fluid migration. Within the pockmark arrays, clustered unit pockmarks are interpreted as evidence for continued migration through the conduit following formation of the buried pockmark. Due to their number and size, unit pockmarks are interpreted to result from a fluid migration flux which is of smaller magnitude but higher frequency when compared to the parent (buried) pockmark. The longevity of post formation fluid migration with the Rosetta Region of the Nile Deep Sea Fan is anticipated to be c. 15,000-100,000 yrs.

References

10 REFERENCES

Abdel Aal, A., El Barkooky, A., Gerrits, M., Meyer, H.J., Schwander, M., and Zaki, H., 2001, Tectonic evolution of the eastern Mediterranean basin and its significance for the hydrocarbon prospectivity of the Nile Delta deepwater area: GeoArabia, v. 6, p. 363-384.

Aiello, I.W., 2005, Fossil seep structures of the Monterey Bay region and tectonic/structural controls on fluid flow in an active transform margin: Palaeogeography, Palaeoclimatology, Palaeoecology, v. 227, p. 124-142.

Aizawa, M., Bluck, B., Cartwright, J., Milner, S., Swart, R., and Ward, J., 2000, Constraints on the geomorphological evolution of Namibia from the offshore stratigraphic record: Communications of the Geological Survey of Namibia, v. 12, p. 337-346.

Al-Shaieb, Z., Puckette, J., Abdalla, A.A., and Ely, P.B., 1994a, Megacompartment complex in the Anadarko Basin: A completely sealed overpressured phenomenon, in Basin Compartments and Seals, edited by P. J. Ortoleva: AAPG Memoir, v. 61, p. 55-68.

Al-Shaieb, Z., Puckette, J., Abdalla, A.A., and Ely, P.B., 1994b, Three levels of compartmentation within the overpressured interval of the Anadarko Basin, in Basin Compartments and Seals, edited by P. J. Ortoleva: AAPG Memoir, v. 61, p. 69-84.

Allen, A.P., Li, B.L., and Charnov, E.L., 2001, Population fluctuations, power laws and mixtures of lognormal distributions: Ecology Letters, v. 4, p. 1-3.

Andergasssen, R., Nijkamp, P., and Reggiani, A., 2003, Analysis of regional labour market dynamics: In search of indications for self-organised criticality: Journal of Geographical Systems, v. 5, p. 275-290.

Anderson, P.W., 1996, From the top down : A reivew of "How nature works, the science of self-organise criticality by P. Bak": Nature, v. 383, p. 772-773.

Andresen, K., Huuse, M., and Clausen, O.R., 2008, Morphology and distribution of Oligocene and Miocene pockmarks in the Danish North Sea - implications for bottom current activity and fluid migration: Basin Research.

Andresen, K.J., and Huuse, M., 2010, 'Bulls-eye' pockmarks and polygonal faulting in the Lower Congo Basin: Relative timing and implications for fluid expulsion during shallow burial: Marine Geology.

Anselin, L., 1995a, Local indicators of spatial association - LISA: Geographical Analysis, v. 27, p. 93-115.

Anselin, L., 1995b, Local indicators of spatial association – LISA: Geographical Analysis, v. 27, p. 93-115.

Antonioli, F., Bard, E., Potter, E.K., Silenzi, S., and Improta, S., 2004, 215-ka history of sea-level oscillations from marine and continental layers in Argentarola Cave speleothems (Italy): Global and Planetary Change, v. 43, p. 57-78.

Arntsen, B., Wensaas, L., Løseth, H., and Hermanrud, C., 2007, Seismic modeling of gas chimneys: Geophysics, v. 72, p. SM251-SM259.

Asuka, Y., Tomaru, N., Nisimura, N., Tsumura, Y., and Yamamoto, S., 2004, Heterogeneous genetic structure in a Fagus crenata population in an old-growth beech forest revealed by microsatellite markers: Molecular Ecology, v. 13, p. 1241-1250.

Austin Jr, J.A., and Uchupi, E., 1982, Continental- oceanic crustal transition off southwest Africa: American Association of Petroleum Geologists Bulletin, v. 66, p. 1328-1347.

Bagguley, J., and Prosser, S., 1999, The interpretation of passive margin depositional processes using seismic stratigraphy: examples from offshore Namibia, Geological Society Special Publication, Volume 153, p. 321-344.

Bailey, T.C., and Gatrell, A.C., 1995, Interactive spatial data analysis: Harlow, Longman Scientific & Technical, 413 p.

Bak, P., 1996, How nature works : the science of self-organized criticality: Oxford, Oxford University Press.

Bak, P., and Paczuski, M., 1995, Complexity, contingency, and criticality: Proceedings of the National Academy of Sciences of the United States of America, v. 92, p. 6689-6696.

Bak, P., Tang, C., and Wiesenfeld, K., 1987, Self-organized criticality: An explanation of the 1/f noise: Physical Review Letters, v. 59, p. 381-384.

Bak, P., Tang, C., and Wiesenfeld, K., 1988, Self-organized criticality: Physical Review A, v. 38, p. 364-374.

Ball, P., 2004, The self-made tapestry. Pattern formation in nature: Oxford, Oxford University Press, 287 p.

Baraza, J., and Ercilla, G., 1996, Gas-charged sediments and large pockmark-like features on the Gulf of Cadiz slope (SW Spain): Marine and Petroleum Geology, v. 13, p. 253-261.

Bayon, G., Loncke, L., Dupré, S., Caprais, J.C., Ducassou, E., Duperron, S., Etoubleau, J., Foucher, J.P., Fouquet, Y., Gontharet, S., Henderson, G.M., Huguen, C., Klaucke, I., Mascle, J., Migeon, S., Olu-Le Roy, K., Ondréas, H., Pierre, C., Sibuet, M., Stadnitskaia, A., and Woodside, J., 2009, Multi-disciplinary investigation of fluid seepage on an unstable margin: The case of the Central Nile deep sea fan: Marine Geology, v. 261, p. 92-104.

Berger, W.H., Lange, C.B., and Wefer, G., 2002, Upwelling History of the Benguela-Namibia System: A Synthesis of Leg 175 Results, *in* Wefer, G., Berger, W.H., and Richter, C., eds., Proceedings of the Ocean Drilling Program, Scientific Reports Vol 175, Volume 175, p. 1-103.

Berndt, C., 2005, Focused fluid flow in passive continental margins: Philosophical Transactions: Mathematical, Physical and Engineering Sciences (Series A), v. 363, p. 2855-2871.

Berndt, C., Bunz, S., and Mienert, J., 2003, Polygonal fault systems on the mid-Norwegian margin: A long-term source for fluid flow, in Van Rensbergen, P. et al., eds., Subsurface sediment mobilization., Geological Society Special Publication, Volume 216, p. 283-290.

Bertoni, C., and Cartwright, J.A., 2005, 3D seismic analysis of circular evaporite dissolution structures, Eastern Mediterranean: Journal of the Geological Society, v. 162, p. 909-926.

Bishop Stump, B., and Flemings, P.B., 2000, Overpressure and fluid flow in dipping structures of the offshore Gulf of Mexico (E.I. 330 field): Journal of Geochemical Exploration, v. 69-70, p. 23-28.

Bluck, B.J., Ward, J.D., Cartwright, J., and Swart, R., 2007, The Orange River, southern Africa: an extreme example of a wave-dominated sediment dispersal system in the South Atlantic Ocean Journal of the Geological Society v. 164, p. 341-351.

Bonadonna, C., and Houghton, B.F., 2005, Total grain-size distribution and volume of tephra-fall deposits: Bulletin of Volcanology, v. 67, p. 441-456.

Borge, H., 2002, Modelling generation and dissipation of overpressure in sedimentary basins: An example from the Halten Terrace, offshore Norway: Marine and Petroleum Geology, v. 19, p. 377-388.

Bott, M.H.P., 1959, The Mechanics of Oblique Slip Faulting: Geological Magazine, v. 96, p. 109-117.

Boudreau, B.P., Algar, C., Johnson, B.D., Croudace, I., Reed, A., Furukawa, Y., Dorgan, K.M., Jumars, P.A., Grader, A.S., and Gardiner, B.S., 2005, Bubble growth and rise in soft sediments: Geology, v. 33, p. 517-520.

Bouriak, S., Vanneste, M., and Saoutkine, A., 2000, Inferred gas hydrates and clay diapirs near the Storegga Slide on the southern edge of the Voring Plateau, offshore Norway: Marine Geology, v. 163, p. 125-148.

Bradley, J.S., 1975, Abnormal formation pressure: AAPG Bulletin, v. 59, p. 957-973.

Bradley, J.S., and Powley, D.E., 1994, Pressure compartments in sedimentary basins: A review, in Basin Compartments and Seals, edited by P. J. Ortoleva: AAPG Memoir, v. 61, p. 3-26.

Branney, M.J., 1995, Downsag and extension at calderas: new perspectives on collapse geometries from ice-melt, mining, and volcanic subsidence: Bulletin of Volcanology, v. 57, p. 303-318.

Brown, A.R., 2004, Interpretation of three-dimensional seismic data: Canada, AAPG Memoir 42 SEG Investigations in geophysics No 9, 541 p.

Brown, K.M., 1990, The nature and hydrogeologic significance of mud diapirs and diatremes for accretionary systems: Journal of Geophysical Research, v. 95, p. 8969-8982.

Bull, S., Cartwright, J., and Huuse, M., 2009, A subsurface evacuation model for submarine slope failure: Basin Research, v. 21, p. 433-443.

Bünz, S., and Mienert, J., 2004, Acoustic imaging of gas hydrate and free gas at the Storegga slide: Journal of Geophysical Research B: Solid Earth, v. 109, p. B04102.

Bünz, S., Mienert, J., and Berndt, C., 2003, Geological controls on the Storegga gas-hydrate system of the mid-Norwegian continental margin: Earth and Planetary Science Letters, v. 209, p. 291-307.

Bünz, S., Mienert, J., Bryn, P., and Berg, K., 2005, Fluid flow impact on slope failure from 3D seismic data: A case study in the Storegga Slide: Basin Research, v. 17, p. 109-122.

Cartwright, A., Moss, J.L., and Cartwright, J.A., In press, New statistical methods for investigating spatial point data in sedimentary basins applied to the analysis of pockmark distribution: Earth and Planetary Science Letters.

Cartwright, A., and Whitworth, A.P., 2004, The statistical analysis of star clusters: Monthly Notices of the Royal Astronomical Society, v. 348, p. 589-598.

Cartwright, J., 2007, The impact of 3D seismic data on the understanding of compaction, fluid flow and diagenesis in sedimentary basins: Journal of the Geological Society, v. 164, p. 881-893.

Cartwright, J., 2010, Regionally extensive emplacement of sandstone intrusions: a brief review: Basin Research, v. 22, p. 502-516.

Cartwright, J., and Huuse, M., 2005, 3D seismic technology: The geological 'Hubble': Basin Research, v. 17, p. 1-20.

Cartwright, J., Huuse, M., and Aplin, A., 2007, Seal bypass systems: American Association of Petroleum Geologists Bulletin, v. 91, p. 1141-1166.

Cartwright, J., Swart, R., Corner, B., Bluck, B., and Ward, J., 2008, Offshore stratigraphy of Namibia, *in* Mc G.Millar, R., ed., The Geology of Namibia, Volume 2, Namibian Geological Survey Memoirs, p. 59-72.

Cartwright, J., Wattrus, N., Rausch, D., and Bolton, A., 2004, Recognition of an early Holocene polygonal fault system in Lake Superior: Implications for the compaction of fine-grained sediments: Geology, v. 32, p. 253-256.

Cartwright, J.A., 1994, Episodic basin-wide fluid expulsion from geopressured shale sequences in the North Sea Basin: Geology, v. 22, p. 447-450.

Cartwright, J.A., and Dewhurst, D.N., 1998, Layer-bound compaction faults in fine-grained sediments: Bulletin of the Geological Society of America, v. 110, p. 1242-1257.

Cartwright, J.A., and Jackson, M.P.A., 2008, Initiation of gravitational collapse of an evaporite basin margin: The Messinian saline giant, Levant Basin, eastern Mediterranean: Bulletin of the Geological Society of America, v. 120, p. 399-413.

Cathles, L.M., Su, Z., and Chen, D., 2009, The physics of gas chimney and pockmark formation, with implications for assessment of seafloor hazards and gas sequestration: Marine and Petroleum Geology.

Cathles, L.M., Su, Z., and Chen, D., 2010, The physics of gas chimney and pockmark formation, with implications for assessment of seafloor hazards and gas sequestration: Marine and Petroleum Geology, v. 27, p. 82-91.

Chand, S., Rise, L., Ottesen, D., Dolan, M.F.J., Bellec, V., and Bøe, R., 2009, Pockmark-like depressions near the Goliat hydrocarbon field, Barents Sea: Morphology and genesis: Marine and Petroleum Geology, v. 26, p. 1035-1042.

Chapron, E., Van Rensbergen, P., De Batist, M., Beck, C., and Henriet, J.P., 2004, Fluid-escape features as a precursor of a large sublacustrine sediment slide in Lake Le Bourget, NW Alps, France: Terra Nova, v. 16, p. 305-311.

Choi, H.W., Park, J.M., Kim, H.W., and Kim, Y.O., 2007, Identifying spatial distribution pattern of water quality in Masan Bay using spatial autocorrelation index and Pearson's r: Ocean and Polar Research, v. 29, p. 391-400.

Christodoulou, D., Papatheodorou, G., Ferentinos, G., and Masson, M., 2003, Active seepage in two contrasting pockmark fields in the Patras and Corinth gulfs, Greece: Geo-Marine Letters, v. 23, p. 194-199.

Çifçi, G., Dondurur, D., and Ergün, M., 2003, Deep and shallow structures of large pockmarks in the Turkish shelf, Eastern Black Sea: Geo-Marine Letters, v. 23, p. 311-322.

Clari, P., Cavagna, S., Martire, L., and Hunziker, J., 2004, A Miocene mud volcano and its plumbing system: A chaotic complex revisited (Monferrato, NW Italy): Journal of Sedimentary Research, v. 74, p. 662-676.

Clari, P., Dela Pierre, F., Martire, L., and Cavagna, S., 2009, The Cenozoic CH4-derived carbonates of Monferrato (NW Italy): A solid evidence of fluid circulation in the sedimentary column: Marine Geology, v. 265, p. 167-184.

Clark, P.J., and Barber, G.M., 1954, Distance to nearest neighbor as a measure of spatial relationships in populations: Ecology, v. 35, p. 445-53.

Clark, P.J., and Evans, F.C., 1954, Distance to nearest neighbor as a measure of spatial relationships in populations: Ecology, v. 35, p. 445-453.

Clausen, J.A., Gabrielsen, R.H., Reksnes, P.A., and Nysæther, E., 1999, Development of intraformational (Oligocene-Miocene) faults in the northern

North Sea: Influence of remote stresses and doming of Fennoscandia: Journal of Structural Geology, v. 21, p. 1457-1475.

Clemson, J., Cartwright, J., and Booth, J., 1997, Structural segmentation and the influence of basement structure on the Namibian passive margin: Journal of the Geological Society, v. 154, p. 477-482.

Clemson, J., Cartwright, J., and Swart, R., 1999, The Namib Rift: a rift system of possible Karoo age, offshore Namibia, Geological Society Special Publication, Volume 153, p. 381-402.

Cobbold, P.R., Clarke, B.J., and Løseth, H., 2009, Structural consequences of fluid overpressure and seepage forces in the outer thrust belt of the Niger Delta: Petroleum Geoscience, v. 15, p. 3-15.

Cole, D., Stewart, S.A., and Cartwright, J.A., 2000, Giant irregular pockmark craters in the Palaeogene of the outer Moray Firth Basin, UK North Sea: Marine and Petroleum Geology, v. 17, p. 563-577.

Cooper, A.H., 1986, Subsidence and foundering of strata caused by the dissolution of Permian gypsum in the Ripon and Bedale areas, North Yorkshire (England): The English Zechstein and related topics, p. 127-139.

Corner, B., Cartwright, J., and Swart, R., 2002, Volcanic passive margin of Namibia: A potential fields perspective: The Geological Society of America Special Publication, v. 362, p. 203–220

Courtillot, V., Armijo, R., and Tapponnier, P., 1987, The Sinai triple junction revisited: Tectonophysics, v. 141, p. 181-190.

Cowley, R., and O'Brien, G.W., 2000, Identification and interpretation of leaking hydrocarbons using seismic data: Australian Petroleum Production and Exploration Association Journal, v. 40, p. 121-150.

Cunningham, G.A., and Shannon, P.M., 1997, The Erris Ridge: A major geological feature in the NW Irish Offshore Basins: Journal of the Geological Society, v. 154, p. 503-508.

Cunningham, R., and Lindholm, R.M., 2000, Seismic evidence for widespread gas hydrate formation, Offshore West Africa: Petroleum systems of South Atlantic margins, v. 73, p. 93-105.

Dangerfield, J.A., 1992, Ekofisk field development: Making images of a gas obscured reservoir, *in* Sheriff, R.E., ed., Reservoir geophysics SEG, p. 98–109.

Davies, R., Bell, B.R., Cartwright, J.A., and Shoulders, S., 2002, Three-dimensional seismic imaging of Paleogene dike-fed submarine volcanoes from the northeast Atlantic margin: Geology, v. 30, p. 223-226.

Davies, R.J., 2003, Kilometer-scale fluidization structures formed during early burial of a deep-water slope channel on the Niger Delta: Geology, v. 31, p. 949-952.

Davies, R.J., Goulty, N.R., and Meadows, D., 2008, Fluid flow due to the advance of basin-scale silica reaction zones: Bulletin of the Geological Society of America, v. 120, p. 195-206.

Davies, R.J., and Stewart, S.A., 2005, Emplacement of giant mud volcanoes in the South Caspian Basin: 3D seismic reflection imaging of their root zones: Journal of the Geological Society, v. 162, p. 1-4.

De Boever, E., Birgel, D., Thiel, V., Muchez, P., Peckmann, J., Dimitrov, L., and Swennen, R., 2009a, The formation of giant tubular concretions triggered by anaerobic oxidation of methane as revealed by archaeal molecular fossils (Lower Eocene, Varna, Bulgaria): Palaeogeography, Palaeoclimatology, Palaeoecology, v. 280, p. 23-36.

De Boever, E., Huysmans, M., Muchez, P., Dimitrov, L., and Swennen, R., 2009b, Controlling factors on the morphology and spatial distribution of methane-related tubular concretions - Case study of an Early Eocene seep system: Marine and Petroleum Geology, v. 26, p. 1580-1591.

De Boever, E., Swennen, R., and Dimitrov, L., 2006a, Lower Eocene carbonate-cemented "chimney" structures (Varna, Bulgaria) - Control of seepage rates on their formation and stable isotopic signature: Journal of Geochemical Exploration, v. 89, p. 78-82.

De Boever, E., Swennen, R., and Dimitrov, L., 2006b, Lower Eocene carbonate cemented chimneys (Varna, NE Bulgaria): Formation mechanisms and the (a)biological mediation of chimney growth?: Sedimentary Geology, v. 185, p. 159-173.

Deming, D., Cranganu, C., and Lee, Y., 2002, Self-sealing in sedimentary basins: Journal of Geophysical Research B: Solid Earth, v. 107.

Dendy, R.O., Helander, P., and Tagger, M., 1999, Self-Organised Criticality in Astrophysical Accretion Systems: Physica Scripta T, v. 82, p. 133-136.

Diggle, P.J., 1983, Statistical analysis of spatial point patterns London, Academic Press, 148 p.

Diggle, P.J., 2002, Statistical analysis of spatial point patterns: London, Hodder Arnold, 159 p.

Dimitrov, L.I., 2002, Mud volcanoes-the most important pathway for degassing deeply buried sediments: Earth-Science Reviews, v. 59, p. 49-76.

Dirichlet, G.L., 1850, Über die Reduktion der positiven quadratischen Formen mit drei unbestimmten ganzen Zahlen: J. reine angew. Math, v. 40, p. 209-227.

Downey, M.W., 1984, Evaluating seals for hydrocarbon accumulation: AAPG Bulletin, v. 68, p. 1752-1763.

Ducassou, E., Capotondi, L., Murat, A., Bernasconi, S.M., Mulder, T., Gonthier, E., Migeon, S., Duprat, J., Giraudeau, J., and Mascle, J., 2007, Multiproxy Late Quaternary stratigraphy of the Nile deep-sea turbidite system - Towards a chronology of deep-sea terrigeneous systems: Sedimentary Geology, v. 200, p. 1-13.

Ducassou, E., Mulder, T., Migeon, S., Gonthier, E., Murat, A., Revel, M., Capotondi, L., Bernasconi, S.M., Mascle, J., and Zaragosi, S., 2008, Nile floods recorded in deep Mediterranean sediments: Quaternary Research, v. 70, p. 382-391.

Duck, R.W., and Herbert, R.A., 2006, High-resolution shallow seismic identification of gas escape features in the sediments of Loch Tay, Scotland: Tectonic and microbiological associations: Sedimentology, v. 53, p. 481-493.

Dupré, S., Woodside, J., Foucher, J.P., de Lange, G., Mascle, J., Boetius, A., Mastalerz, V., Stadnitskaia, A., Ondréas, H., Huguen, C., Harmégnies, F., Gontharet, S., Loncke, L., Deville, E., Niemann, H., Omoregie, E., Olu-Le Roy, K., Fiala-Medioni, A., Dählmann, A., Caprais, J.C., Prinzhofer, A., Sibuet, M., Pierre, C., and Damsté, J.S., 2007, Seafloor geological studies above active gas chimneys off Egypt (Central Nile Deep Sea Fan): Deep-Sea Research Part I: Oceanographic Research Papers, v. 54, p. 1146-1172.

Dussert, C., Rasigni, G., and Llebaria, A., 1988, Quantization of directional properties in biological structures using the minimal spanning tree: Journal of Theoretical Biology, v. 135, p. 295-302.

Dussert, C., Rasigni, G., Rasigni, M., Palmari, J., and Llebaria, A., 1986, Minimal spanning tree: A new approach for studying order and disorder: Physical Review B, v. 34, p. 3528-3531.

Dussert, C., Rasigni, G., Rasigni, M., Palmari, J., and Llebaria, A., 1989, Minimal spanning tree analysis of regular, random and cluster structures: Zeitschrift für Physik D Atoms, Molecules and Clusters, v. 12, p. 41-44.

Dussert, C., Rasigni, M., and Palmari, J., 1987, Minimal spanning tree analysis of biological structures: Journal of Theoretical Biology, v. 125, p. 317-323.

Ebdon, D., 1985, Statistics in geography: Oxford, Blackwell, 232 p.

El-Sayed, A., Korrat, I., and Hussein, H.M., 2004, Seismicity and seismic hazard in Alexandria (Egypt) and its surroundings: Pure and Applied Geophysics, v. 161, p. 1003-1019.

El-Sayed, A., Wahlströ, m, R., and Kulhánek, O., 1994, Seismic hazard of Egypt: Natural Hazards, v. 10, p. 247-259.

Elenean, K.M.A., Mohamed, A.M.E., and Hussein, H.M., 2010, Source parameters and ground motion of the Suez-Cairo shear zone earthquakes, Eastern Desert, Egypt: Natural Hazards, v. 52, p. 431-451.

England, P.C., 1987, Diffuse continental deformation: length scales, rates and metamorphic evolution: Philosophical Transactions of the Royal Society of London, v. A321, p. 1557-1567.

Evans, B.J., 1997, A handbook for seismic data acquisition in exploration: SEG Geophysical Monograph Series: Tulsa, Society of Exploration Geophysicists, 305 p.

Flemings, P.B., Liu, X., and Winters, W.J., 2003, Critical pressure and multiphase flow in Blake Ridge gas hydrates Geology, v. 31, p. 1057-1060.

Flemings, P.B., Stump, B.B., Finkbeiner, T., and Zoback, M., 2002, Flow focusing in overpressured sandstones: Theory, observations, and applications: American Journal of Science, v. 302, p. 827-855.

Floodgate, G.D., and Judd, A.G., 1992, The origins of shallow gas: Continental Shelf Research, v. 12, p. 1145-1156.

Fonstad, M., and Marcus, W.A., 2003, Self-organized criticality in riverbank systems: Annals of the Association of American Geographers, v. 93, p. 281-296.

Frey-Martínez, J., Cartwright, J., and James, D., 2006, Frontally confined versus frontally emergent submarine landslides: A 3D seismic characterisation: Marine and Petroleum Geology, v. 23, p. 585-604.

Frigg, R., 2003, Self-organised criticality - What it is and what it isn't: Studies in History and Philosophy of Science Part C, v. 34, p. 613-632.

Galéron, J., Menot, L., Renaud, N., Crassous, P., Khripounoff, A., Treignier, C., and Sibuet, M., 2009, Spatial and temporal patterns of benthic macrofaunal communities on the deep continental margin in the Gulf of Guinea: Deep-Sea Research Part II: Topical Studies in Oceanography, v. 56, p. 2299-2312.

Gallo, F., and Woods, A.W., 2004, On steady homogeneous sand-water flows in a vertical conduit: Sedimentology, v. 51, p. 195-210.

García-García, A., Orange, D.L., Maher, N.M., Heffernan, A.S., Fortier, G.S., and Malone, A., 2004, Geophysical evidence for gas geohazards off Iskenderun Bay, SE Turkey: Marine and Petroleum Geology, v. 21, p. 1255-1264.

García-Gil, S., Vilas, F., and García-García, A., 2002, Shallow gas features in incised-valley fills (Ría de Vigo, NW Spain): A case study: Continental Shelf Research, v. 22, p. 2303-2315.

Garziglia, S., Migeon, S., Ducassou, E., Loncke, L., and Mascle, J., 2008, Mass-transport deposits on the Rosetta province (NW Nile deep-sea turbidite

system, Egyptian margin): Characteristics, distribution, and potential causal processes: Marine Geology, v. 250, p. 180-198.

Gaullier, V., Mart, Y., Bellaiche, G., Mascle, J., Vendeville, B.C., Zitter, T., Benkhelil, J., Buffet, G., Droz, L., Ergun, M., Huguen, C., Kopf, A., Levy, R., Limonov, A., Shaked, Y., Volkonskaia, A., and Woodside, J., 2000, Salt tectonics in and around the Nile deep-sea fan: Insights from the PRISMED II cruise, Geological Society Special Publication, p. 111-129.

Gay, A., and Berndt, C., 2007, Cessation/reactivation of polygonal faulting and effects on fluid flow in the Vøring Basin, Norwegian Margin: Journal of the Geological Society, v. 164, p. 129-141.

Gay, A., Lopez, M., Berndt, C., and Séranne, M., 2007a, Geological controls on focused fluid flow associated with seafloor seeps in the Lower Congo Basin: Marine Geology, v. 244, p. 68-92.

Gay, A., Lopez, M., Berndt, C., Seranne, M., Flemings, P., Behrmann, J.H., and John, C.M., 2007b, Sea level fall and rise controlling cyclic fluid expulsion: comparison between pockmarks in the Congo Basin and mud volcanoes in the Gulf of Mexico: Geophysical Research Abstracts, v. 9, p. 1-2.

Gay, A., Lopez, M., Cochonat, P., Levaché, D., Sermondadaz, G., and Seranne, M., 2006a, Evidences of early to late fluid migration from an upper Miocene turbiditic channel revealed by 3D seismic coupled to geochemical sampling within seafloor pockmarks, Lower Congo Basin: Marine and Petroleum Geology, v. 23, p. 387-399.

Gay, A., Lopez, M., Cochonat, P., Séranne, M., Levaché, D., and Sermondadaz, G., 2006b, Isolated seafloor pockmarks linked to BSRs, fluid chimneys, polygonal faults and stacked Oligocene-Miocene turbiditic palaeochannels in the Lower Congo Basin: Marine Geology, v. 226, p. 25-40.

Gay, A., Lopez, M., Cochonat, P., Sultan, N., Cauquil, E., and Brigaud, F., 2003, Sinuous pockmark belt as indicator of a shallow buried turbiditic channel on the lower slope of the Congo basin, West African margin, in Van Rensbergen, P. et al., eds., Subsurface sediment mobilization., Geological Society Special Publication, Volume 216, p. 173-189.

Geletti, R., Del Ben, A., Busetti, M., Ramella, R., and Volpi, V., 2008, Gas seeps linked to salt structures in the central adriatic sea: Basin Research, v. 20, p. 473-487.

Georgoulis, M.K., and Vlahos, L., 1998, Variability of the occurrence frequency of solar flares and the statistical flare: Astronomy and Astrophysics, v. 336, p. 721-734.

Gibson, R.E., 1958, The progress of consolidation in a clay layer increasing in thickness with time: Geotechnique, v. 8, p. 171-182.

Gladczenko, T.P., Skogseid, J., and Eldhom, O., 1998, Namibia volcanic margin: Marine Geophysical Researches, v. 20, p. 313-341.

Gluyas, J., and Swarbrick, R., 2004, Petroleum Geoscience: Oxford, Blackwell, 359 p.

Gontharet, S., Pierre, C., Blanc-Valleron, M.M., Rouchy, J.M., Fouquet, Y., Bayon, G., Foucher, J.P., Woodside, J., and Mascle, J., 2007, Nature and origin of diagenetic carbonate crusts and concretions from mud volcanoes and pockmarks of the Nile deep-sea fan (eastern Mediterranean Sea): Deep-Sea Research Part II: Topical Studies in Oceanography, v. 54, p. 1292-1311.

Gorman, A.R., Holbrook, W.S., Hornbach, M.J., Hackwith, K.L., Lizarralde, D., and Pecher, I., 2002, Migration of methane gas through the hydrate stability zone in a low-flux hydrate province: Geology, v. 30, p. 327-330.

Goudie, A.S., 2005, The drainage of Africa since the Cretaceous: Geomorphology, v. 67, p. 437-456.

Gower, J.C., and Ross, G.J.S., 1969, Minimum spanning trees and single-linkage cluster analysis: Applied Statistics, v. 18, p. 54-64.

Granli, J.R., Arntsen, B., Sollid, A., and Hilde, E., 1999, Imaging through gas-filled sediments using marine shear-wave data: Geophysics, v. 64, p. 668-677.

Guiraud, R., and Maurin, J.C., 1992, Early Cretaceous rifts of Western and Central Africa: an overview: Tectonophysics, v. 213, p. 153-168.

Haacke, R.R., Hyndman, R.D., Park, K.P., Yoo, D.G., Stoian, I., and Schmidt, U., 2009, Migration and venting of deep gases into the ocean through hydrate-choked chimneys offshore Korea: Geology, v. 37, p. 531-534.

Hammer, O., 2009, New statistical methods for detecting point alignments: Computers and Geosciences, v. 35, p. 659-666.

Hanken, N., Rønholt, G., and Hovland, M., 1999, Dannelsen av "Blow-out pipes" basert på studier av Plio-Pleistocene sedimenter på Rhodos (Abstract in Norwegian), Norwegian Geological Union, Vintermøte, Conference Proceedings: Stavanger, Norway, Jan. 6-8, p. 52.

Hanken, N.M., Bromley, R.G., and Miller, J., 1996, Plio-Pleistocene sedimentation in coastal grabens, north-east Rhodes, Greece: Geological Journal, v. 31, p. 393-418.

Hansen, D.M., 2006, The morphology of intrusion-related vent structures and their implications for constraining the timing of intrusive events along the NE Atlantic margin: Journal of the Geological Society, v. 163, p. 789-800.

Hansen, J.P.V., Cartwright, J.A., Huuse, M., and Clausen, O.R., 2005, 3D seismic expression of fluid migration and mud remobilization on the Gjallar Ridge, offshore mid-Norway: Basin Research, v. 17, p. 123-139.

Hasiotis, T., Papatheodorou, G., Kastanos, N., and Ferentinos, G., 1996, A pockmark field in the Patras Gulf (Greece) and its activation during the 14/7/93 seismic event: Marine Geology, v. 130, p. 333-344.

Haskell, N., Nissen, S., Hughes, M., Grindhaug, J., Dhanani, S., Heath, R., Kantorowicz, J., Antrim, L., Cubanski, M., Nataraj, R., Schilly, M., and Wigger, S., 1999, Delineation of geologic drilling hazards using 3-D seismic attributes: Leading Edge (Tulsa, OK), v. 18.

Heggland, R., 1998, Gas seepage as an indicator of deeper prospective reservoirs. A study based on exploration 3D seismic data: Marine and Petroleum Geology, v. 15, p. 1-9.

Heggland, R., 2004, Definition of geohazards in exploration 3-D seismic data using attributes and neural-network analysis: American Association of Petroleum Geologists Bulletin, v. 88, p. 857-868.

Hillis, R.R., 2003, Pore pressure/stress coupling and its implications for rock failure : Geological Society Special Publication v. 216, p. 359-368.

Hirsch, F., Flexer, A., Rosenfeld, A., and Yellin-Dror, A., 1995, Palinspastic and crustal setting of the eastern Mediterranean: Journal of Petroleum Geology, v. 18, p. 149-170.

Hjelstuen, B.O., Haflidason, H., Sejrup, H.P., and Nygård, A., 2009, Sedimentary and structural control on pockmark development-evidence from the Nyegga pockmark field, NW European margin: Geo-Marine Letters, p. 1-10.

Holm, N.G., and Charlou, J.L., 2001, Initial indications of abiotic formation of hydrocarbons in the Rainbow ultramafic hydrothermal system, Mid-Atlantic Ridge: Earth and Planetary Science Letters, v. 191, p. 1-8.

Holtar, E., and Forsberg, A.W., 2000, Postrift development of the Walvis Basin, Namibia: Results from the exploration campaign in Quadrant 1911: AAPG Memoir, v. 73, p. 429-446.

Hopkins, A.E., 2006, Seismic stratigraphic interpretation of contourite systems, Namibian continental margin Cardiff, University of Cardiff, Thesis.

Horita, J., and Berndt, M.E., 1999, Abiogenic methane formation and isotopic fractionation under hydrothermal conditions: Science, v. 285, p. 1055-1057.

Hovland, M., 2002, On the self-sealing nature of marine seeps: Continental Shelf Research, v. 22, p. 2387-2394.

Hovland, M., Gardner, J.V., and Judd, A.G., 2002, The significance of pockmarks to understanding fluid flow processes and geohazards: Geofluids, v. 2, p. 127-136.

Hovland, M., Heggland, R., De Vries, M.H., and Tjelta, T.I., 2010, Unit-pockmarks and their potential significance for predicting fluid flow: Marine and Petroleum Geology, v. doi:10.1016/j.marpetgeo.2010.02.005.

Hovland, M., and Judd, A.G., 1988, Seabed pockmarks and seepages: impact on geology, biology and the marine environment: London, Graham and Trotman.

Hovland, M., and Svensen, H., 2006, Submarine pingoes: Indicators of shallow gas hydrates in a pockmark at Nyegga, Norwegian Sea: Marine Geology, v. 228, p. 15-23.

Hovland, M., Svensen, H., Forsberg, C.F., Johansen, H., Fichler, C., Fossa, J.H., Jonsson, R., and Rueslåtten, H., 2005, Complex pockmarks with carbonate-ridges off mid-Norway: Products of sediment degassing: Marine Geology, v. 218, p. 191-206.

Hubbert, M., K, and Willis, D.G.W., 1957, Mechanics of hydraulic fracturing: Transactions of the American Institue of Mineral Engineering, v. 210, p. 153-168.

Hunt, J.M., 1990, Generation and migration of petroleum from abnormally pressured fluid compartments: American Association of Petroleum Geologists Bulletin, v. 74, p. 1-12.

Hustoft, S., Bünz, S., and Mienert, J., 2010, Three-dimensional seismic analysis of the morphology and spatial distribution of chimneys beneath the Nyegga pockmark field, offshore mid-Norway: Basin Research, v. 22, p. 465-480.

Hustoft, S., Bünz, S., Mienert, J., and Chand, S., 2009a, Gas hydrate reservoir and active methane-venting province in sediments on < 20 Ma young oceanic crust in the Fram Strait, offshore NW-Svalbard: Earth and Planetary Science Letters, v. 284, p. 12-24.

Hustoft, S., Dugan, B., and Mienert, J., 2009b, Effects of rapid sedimentation on developing the Nyegga pockmark field: Constraints from hydrological modeling and 3-D seismic data, offshore mid-Norway: Geochemistry, Geophysics, Geosystems, v. 10, p. doi:10.1029/2009GC002409.

Hustoft, S., Mienert, J., Bünz, S., and Nouze, H., 2007, High-resolution 3D-seismic data indicate focussed fluid migration pathways above polygonal fault systems of the mid-Norwegian margin: Marine Geology, v. 245, p. 89-106.

Iglesias, J., and García-Gil, S., 2007, High-resolution mapping of shallow gas accumulations and gas seeps in San Simo?n Bay (Ri?a de Vigo, NW Spain). Some quantitative data: Geo-Marine Letters, v. 27, p. 103-114.

Iglesias, J., and García-Gil, S., 2007, High-resolution mapping of shallow gas accumulations and gas seeps in San Simón Bay (Ría de Vigo, NW Spain). Some quantitative data: Geo-Marine Letters, v. 27, p. 103-114.

Ingram, G.M., Chisholm, T.J., Grant, C.J., Hedlund, C.A., Stuart-Smith, P., and Teasdale, J., 2004, Deepwater North West Borneo: Hydrocarbon accumulation in an active fold and thrust belt: Marine and Petroleum Geology, v. 21, p. 879-887.

Jain, A.K., and Juanes, R., 2009, Preferential mode of gas invasion in sediments: Grain-scale mechanistic model of coupled multiphase fluid flow and sediment mechanics: Journal of Geophysical Research B: Solid Earth, v. 114, p. B08101 doi:10.1029/2008JB006002.

Judd, A.G., 1981, Evaluating the hazard potential of pockmarks, Oceans Conference Record (IEEE), Volume 1, p. 694-698.

Judd, A.G., and Hovland, M., 2007, Seabed fluid flow: The impact on geology, biology and the marine environment: Cambridge, Cambridge University Press.

Judd, A.G., and Hovland, M., 2008, The role of chemosynthesis in supporting fish stocks in the North Sea: Journal of Fish Biology, p. 329-330.

Karner, G.D., Driscoll, N.W., and Barker, D.H.N., 2003, Syn-rift regional subsidence across the West African continental margin: The role of lower plate ductile extension, Geological Society Special Publication, p. 105-129.

Kearey, P., Brooks, M., and Hill, I., 2002, An introduction to geophysical exploration: Oxford, Blackwell Publishing.

Keller, E.A., Duffy, M., Kennett, J.P., and Hill, T., 2007, Tectonic geomorphology and hydrocarbon induced topography of the Mid-Channel Anticline, Santa Barbara Basin, California: Geomorphology, v. 89, p. 274-286.

Kelley, J.T., Dickson, S.M., Belknap, D.F., Barnhardt, W.A., and Henderson, M., 1994, Giant sea-bed pockmarks: evidence for gas escape from Belfast Bay, Maine: Geology, v. 22, p. 59-62.

Kieft, T.L., McCuddy, S.M., Onstott, T.C., Davidson, M., Lin, L.H., Mislowack, B., Pratt, L., Boice, E., Lollar, B.S., Lippmann-Pipke, J., Pfiffner, S.M., Phelps, T.J., Gihring, T., Moser, D., and van Heerden, A., 2005, Geochemically generated, energy-rich substrates and indigenous microorganisms in deep, ancient groundwater: Geomicrobiology Journal, v. 22, p. 325-335.

King, L.H., and MacLean, B., 1970, Pockmarks on the Scotian Shelf: Geological Society of America Bulletin, v. 81, p. 3141-3148.

Krenn, R., and Hergarten, S., 2009, Cellular automaton modelling of lightning-induced and man made forest fires: Natural Hazards and Earth System Science, v. 9, p. 1743-1748.

Kresic, N., 2007, Hydrogeology and Groundwater Modeling: London, CRC Press, 807 p.

Lastras, G., Canals, M., Urgeles, R., Hughes-Clarke, J.E., and Acosta, J., 2004, Shallow slides and pockmark swarms in the Eivissa Channel, western Mediterranean Sea: Sedimentology, v. 51, p. 837-850.

Le Pichon, X., Chamot-Rooke, N., Lallemant, S., Noomen, R., and Veis, G., 1995, Geodetic determination of the kinematics of central Greece with respect to

Europe: implications for eastern Mediterranean tectonics: Journal of Geophysical Research, v. 100, p. 12,675-12,690.

León, R., Somoza, L., Medialdea, T., Hernández-Molina, F.J., Vázquez, J.T., Díaz-del-Rio, V., and González, F.J., 2010, Pockmarks, collapses and blind valleys in the Gulf of Cádiz: Geo-Marine Letters, v. 30, p. 231-247.

Li, Y.L., Peacock, A.D., White, D.C., Geyer, R., and Zhang, C.L., 2007, Spatial patterns of bacterial signature biomarkers in marine sediments of the Gulf of Mexico: Chemical Geology, v. 238, p. 168-179.

Libes, S.M., 1992, An introduction to marine biogeochemistry: Chichester, Wiley, 734 p.

Light, M.P.R., Maslanyj, M.P., and Banks, N.L., 1992, New geophysical evidence for extensional tectonics on the divergent margin offshore Namibia : Magmatism and the causes of continental break-up: Geological Society, London; Special Publication, v. 68, p. 257-270.

Light, M.P.R., Maslanyj, M.P., Greenwood, R.J., and Banks, N.L., 1993, Seismic sequence stratigraphy and tectonics offshore Namibia : Tectonics and seismic sequence stratigraphy: Geological Society Special Publication, v. 71, p. 163-191.

Ligtenberg, J.H., 2005, Detection of Fluid migration pathways in seismic data: Implications for fault seal analysis: Basin Research, v. 17, p. 141-153.

Ligtenberg, J.H., and Connolly, D., 2003, Chimney detection and interpretation, revealing sealing quality of faults, geohazards, charge of and leakage from reservoirs: Journal of Geochemical Exploration, v. 78-79, p. 385-387.

Lollar, B.S., Lacrampe-Couloume, G., Slater, G.F., Ward, J., Moser, D.P., Gihring, T.M., Lin, L.H., and Onstott, T.C., 2006, Unravelling abiogenic and biogenic sources of methane in the Earth's deep subsurface: Chemical Geology, v. 226, p. 328-339.

Loncke, L., Gaullier, V., Bellaiche, G., and Mascle, J., 2002, Recent depositional patterns of the Nile deep-sea fan from echo-character mapping: American Association of Petroleum Geologists Bulletin, v. 86, p. 1165-1186.

Loncke, L., Gaullier, V., Droz, L., Ducassou, E., Migeon, S., and Mascle, J., 2009, Multi-scale slope instabilities along the Nile deep-sea fan, Egyptian margin: A general overview: Marine and Petroleum Geology, v. 26, p. 633-646.

Loncke, L., Gaullier, V., Mascle, J., Vendeville, B., and Camera, L., 2006, The Nile deep-sea fan: An example of interacting sedimentation, salt tectonics, and inherited subsalt paleotopographic features: Marine and Petroleum Geology, v. 23, p. 297-315.

Loncke, L., and Mascle, J., 2004, Mud volcanoes, gas chimneys, pockmarks and mounds in the Nile deep-sea fan (Eastern Mediterranean): Geophysical evidences: Marine and Petroleum Geology, v. 21, p. 669-689.

Long, D., 1992, Devensian late-glacial gas escape in the central North Sea: Continental Shelf Research, v. 12, p. 1097-1110.

Løseth, H., Gading, M., and Wensaas, L., 2009, Hydrocarbon leakage interpreted on seismic data: Marine and Petroleum Geology, v. 26, p. 1304-1319.

Løseth, H., Wensaas, L., Arntsen, B., Hanken, N., Basire, C., and Graue, K., 2001, 1000m long gas blow out pipes: 63rd EAGE Conference and Exhibition, Extended Abstratcts, p. 524.

Løseth, H., Wensaas, L., Arntsen, B., and Hovland, M., 2003, Gas and fluid injection triggering shallow mud mobilization in the Hordaland Group, North Sea. In.

Van Rensbergen, P. et al (eds.) Subsurface sediment mobilization.: Geological Society Special Publication, p. 139-157.

Løvlie, R., and Hanken, N.M., 2002, Conglomerate test of non-lithified Plio-Pleistocene marine sediments and rock magnetic constrains suggests pDRM type remagnetisation: Physics and Chemistry of the Earth, v. 27, p. 1121-1130.

Lowe, D.R., 1975, Water escape structures in coarsegrained sediments: Sedimentology, v. 22, p. 157-204.

Luo, X., and Vasseur, G., 2002, Natural hydraulic cracking: Numerical model and sensitivity study: Earth and Planetary Science Letters, v. 201, p. 431-446.

Maldonado, A., and Stanley, D.J., 1976, The Nile Cone: Submarine fan development by cyclic sedimentation: Marine Geology, v. 20, p. 27-35,39-40.

Maldonado, A., and Stanley, D.J., 1979, Depositional patterns and Late Quaternary evolution of two Mediterranean submarine fans: A comparison: Marine Geology, v. 31, p. 215-250.

Maltman, A., 1994, The Geological Deformation of Sediments: Glasgow, Chapman and Hall, p. 362.

Mascle, J., Benkhelil, J., Bellaiche, G., Zitter, T., Woodside, J., and Loncke, L., 2000, Marine geologic evidence for a Levantine-Sinai plate, a new piece of the Mediterranean puzzle: Geology, v. 28, p. 779-782.

Maslanyj, M.P., Light, M.P.R., Greenwood, R.J., and Banks, N.L., 1992, Extension tectonics offshore Namibia and evidence for passive rifting in the South Atlantic: Marine and Petroleum Geology, v. 9, p. 590-601.

Mazzotti, L., Segantini, S., Tramontana, M., and Wezel, F.C., 1987, Characteristics of pockmarks on the Jabuka Trough floor (central Adriatic Sea): Bollettino di Oceanologia Teorica ed Applicata, v. 5, p. 237-250.

McCallum, M.E., 1985, Experimental evidence for fluidization processes in Breccia pipe formation: Economic Geology, v. 80, p. 1523-1543.

McClusky, S., Balassanian, S., Barka, A., Demir, C., Ergintav, S., Georgiev, I., Gurkan, O., Hamburger, M., Hurst, K., Kahle, H., Kastens, K., Kekelidze, G., King, R., Kotzev, V., Lenk, O., Mahmoud, S., Mishin, A., Nadariya, M., Ouzounis, A., Paradissis, D., Peter, Y., Prilepin, M., Reilinger, R., Sanli, I., Seeger, H., Tealeb, A., Toksöz, M.N., and Veis, G., 2000, Global Positioning System constraints on plate kinematics and dynamics in the eastern Mediterranean and Caucasus: Journal of Geophysical Research B: Solid Earth, v. 105, p. 5695-5719.

McDonnell, A., Loucks, R.G., and Dooley, T., 2007, Quantifying the origin and geometry of circular sag structures in northern Fort Worth Basin, Texas: Paleocave collapse, pull-apart fault systems, or hydrothermal alteration?: American Association of Petroleum Geologists Bulletin, v. 91, p. 1295-1318.

McKenzie, D.P., 1970, Plate tectonics of the mediterranean region: Nature, v. 226, p. 239-243.

Michaud, F., Chabert, A., Collot, J.Y., Sallarès, V., Flueh, E.R., Charvis, P., Graindorge, D., Gustcher, M.A., and Bialas, J., 2005, Fields of multi-kilometer scale sub-circular depressions in the Carnegie Ridge sedimentary blanket: Effect of underwater carbonate dissolution?: Marine Geology, v. 216, p. 205-219.

Mienert, J., and Posewang, J., 1999, Evidence of shallow- and deep-water gas hydrate destabilizations in North Atlantic polar continental margin sediments: Geo-Marine Letters, v. 19, p. 143-149.

Mienert, J., Posewang, J., and Baumann, M., 1998, Gas hydrates along the northeastern Atlantic margin: possible hydrate- bound margin instabilities and possible release of methane, Geological Society Special Publication, Volume 137, p. 275-291.

Mitchell, A., 2005, The ESRI guide to GIS analysis. Volume 2: Spatial measurements and statistics: California, ESRI Press, 238 p.

Morelli, C., 1978, Eastern Mediterranean: Geophysical results and implications: Tectonophysics, v. 46, p. 333-346.

Morley, C.K., 2003, Mobile shale related deformation in large deltas developed on passive and active margins, Geological Society Special Publication, p. 335-357.

Morley, C.K., and Guerin, G., 1996, Comparison of gravity-driven deformation styles and behavior associated with mobile shales and salt: Tectonics, v. 15, p. 1154-1170.

Muggeridge, A., Abacioglu, Y., England, W., and Smalley, C., 2004, Dissipation of anomalous pressures in the subsurface: Journal of Geophysical Research B: Solid Earth, v. 109, p. 1-16.

Muggeridge, A., Abacioglu, Y., England, W., and Smalley, C., 2005, The rate of pressure dissipation from abnormally pressured compartments: American Association of Petroleum Geologists Bulletin, v. 89, p. 61-80.

Naudts, L., de Batist, M., Greinert, J., and Artemov, Y., 2009, Geo- and hydro-acoustic manifestations of shallow gas and gas seeps in the Dnepr paleodelta, northwestern Black Sea: Leading Edge (Tulsa, OK), v. 28, p. 1030-1040.

Naudts, L., Greinert, J., Artemov, Y., Staelens, P., Poort, J., Van Rensbergen, P., and De Batist, M., 2006, Geological and morphological setting of 2778 methane seeps in the Dnepr paleo-delta, northwestern Black Sea: Marine Geology, v. 227, p. 177-199.

Naudts, L., Greinert, J., Poort, J., Belza, J., Vangampelaere, E., Boone, D., Linke, P., Henriet, J.P., and De Batist, M., 2010, Active venting sites on the gas-hydrate-bearing Hikurangi Margin, off New Zealand: Diffusive- versus bubble-released methane: Marine Geology, v. 272, p. 233-250.

Nicholson, T., Sambridge, M., and Gudmundsson, Ã., 2000, On entropy and clustering in earthquake hypocentre distributions: Geophysical Journal International, v. 142, p. 37-51.

Novikov, L.A., and Slobodskoy, R.M., 1979, Mechanisms of formation of Diatremes: International Geological Review, v. 21, p. 1131-1139.

Nunn, J.A., 1996, Buoyancy-driven propagation of isolated fuild-filled fractures: Journal of Geophysical Research, v. 101, p. 2963-2970.

Nürnberg, D., and Müller, R.D., 1991, The tectonic evolution of the South Atlantic from Late Jurassic to present: Tectonophysics, v. 191, p. 27-53.

Nyman, S.L., Nelson, C.S., and Campbell, K.A., 2009, Miocene tubular concretions in East Coast Basin, New Zealand: Analogue for the subsurface plumbing of cold seeps: Marine Geology.

O'Brien, J., 2004, Seismic amplitudes from low gas saturation sands: Leading Edge (Tulsa, OK), v. 23, p. 1236-1243.

Okabe, A., Boots, B., Sugihara, K., and Chiu, S.N., 2000, Spatial tessellations : concepts and applications of Voronoi diagrams Chichester, Wiley, 671 p.

Olu-Le Roy, K., Caprais, J.C., Fifis, A., Fabri, M.C., Galéron, J., Budzinsky, H., Le Ménach, K., Khripounoff, A., Ondréas, H., and Sibuet, M., 2007, Cold-seep

assemblages on a giant pockmark off West Africa: Spatial patterns and environmental control: Marine Ecology, v. 28, p. 115-130.

Orange, D.L., García-García, A., McConnell, D., Lorenson, T., Fortier, G., Trincardi, F., and Can, E., 2005, High-resolution surveys for geohazards and shallow gas: NW Adriatic (Italy) and Iskenderun Bay (Turkey): Marine Geophysical Researches, v. 26, p. 247-266.

Ormerod, P., 2002, The US business cycle: Power law scaling for interacting units with complex internal structure: Physica A: Statistical Mechanics and its Applications, v. 314, p. 774-785.

Ortoleva, P.J., 1994, Basin compartmentation: Definitions and mechanisms, in Basin Compartments and Seals, edited by P. J. Ortoleva: AAPG Memoir, v. 61, p. 39-52.

Ortoleva, P.J., Al-Shaieb, Z., and Puckette, J., 1995, Genesis and dynamics of basin compartments and seals: American Journal of Science, v. 295, p. 345-427.

Osborne, M.J., and Swarbrick, R.E., 1997, Mechanisms for generating overpressure in sedimentary basins: A reevaluation: American Association of Petroleum Geologists Bulletin, v. 81, p. 1023-1041.

Parkes, R.J., Cragg, B.A., and Wellsbury, P., 2000, Recent studies on bacterial populations and processes in subseafloor sediments: A review: Hydrogeology Journal, v. 8, p. 11-28.

Paull, C., Ussler Iii, W., Maher, N., Greene, H.G., Rehder, G., Lorenson, T., and Lee, H., 2002, Pockmarks off Big Sur, California: Marine Geology, v. 181, p. 323-335.

Paull, C.K., Ussler Iii, W., Holbrook, W.S., Hill, T.M., Keaten, R., Mienert, J., Haflidason, H., Johnson, J.E., Winters, W.J., and Lorenson, T.D., 2008, Origin of pockmarks and chimney structures on the flanks of the Storegga Slide, offshore Norway: Geo-Marine Letters, v. 28, p. 43-51.

Pecher, I.A., Kukowski, N., Huebscher, C., Greinert, J., and Bialas, J., 2001, The link between bottom-simulating reflections and methane flux into the gas hydrate stability zone - New evidence from Lima Basin, Peru Margin: Earth and Planetary Science Letters, v. 185, p. 343-354.

Perez-Garcia, C., Feseker, T., Mienert, J., and Berndt, C., 2009, The Håkon Mosby mud volcano: 330 000 years of focused fluid flow activity at the SW Barents Sea slope: Marine Geology, v. 262, p. 105-115.

Pilcher, R., and Argent, J., 2007, Mega-pockmarks and linear pockmark trains on the West African continental margin: Marine Geology, v. 244, p. 15-32.

Pimenov, N.V., Ulyanova, M.O., Kanapatsky, T.A., Veslopolova, E.F., Sigalevich, P.A., and Sivkov, V.V., 2010, Microbially mediated methane and sulfur cycling in pockmark sediments of the Gdansk Basin, Baltic Sea: Geo-Marine Letters, p. 1-10.

Pinet, N., Duchesne, M., and Lavoie, D., 2009, Linking a linear pockmark train with a buried Palaeozoic structure: a case study from the St. Lawrence Estuary: Geo-Marine Letters, p. 1-6.

Pinet, N., Duchesne, M., Lavoie, D., Bolduc, A., and Long, B., 2008, Surface and subsurface signatures of gas seepage in the St. Lawrence Estuary (Canada): Significance to hydrocarbon exploration: Marine and Petroleum Geology, v. 25, p. 271-288.

Plaza-Faverola, A., Bünz, S., and Mienert, J., 2010, Fluid distributions inferred from P-wave velocity and reflection seismic amplitude anomalies beneath the

Nyegga pockmark field of the mid-Norwegian margin: Marine and Petroleum Geology, v. 27, p. 46-60.

Price, N.J., and Cosgrove, J.W., 1990, Analysis of Geological Structures: Cambridge, Cambridge University Press.

Pueyo, S., 2007, Self-organised criticality and the response of wildland fires to climate change: Climatic Change, v. 82, p. 131-161.

Rabinowitz, P.D., and Labrecque, J., 1979, The Mesozoic South Atlantic ocean and evolution of its continental margins: Journal of Geophysical Research, v. 84, p. 5973-6002.

Ray, T.S., Moseley, L., and Jan, N., 2000, Self-organised criticality in a genetic model of species-species interaction: Theory in Biosciences, v. 119, p. 132-138.

Richards, P.W., Walsh, R.P.D., Baillie, I.C., and Greg-Smith, P., 1996, The tropical rain forest: an ecological study. Second edition.

Riedel, M., Novosel, I., Spence, G.D., Hyndman, R.D., Chapman, R.N., Solem, R.C., and Lewis, T., 2006, Geophysical and geochemical signatures associated with gas hydrate-related venting in the northern Cascadia margin: Bulletin of the Geological Society of America, v. 118, p. 23-38.

Ripley, B.D., 1976, The Second-Order Analysis of Stationary Point Processes: Journal of Applied Probability, v. 13, p. 255-266.

Ripley, B.D., 1977, Modelling Spatial Patterns: Journal of the Royal Statistical Society B, v. 39, p. 172-212.

Ripley, B.D., 1979, Tests of randomness for spatial point patterns: Journal of the Royal Statistical Society B, v. 4, p. 3.

Rise, L., Sættem, J., Fanavoll, S., Thorsnes, T., Ottesen, D., and Bøe, R., 1999, Sea-bed pockmarks related to fluid migration from Mesozoic bedrock strata in the Skagerrak offshore Norway: Marine and Petroleum Geology, v. 16, p. 619-631.

Roberts, K.S., Davies, R.J., and Stewart, S.A., 2010, Structure of exhumed mud volcano feeder complexes, Azerbaijan: Basin Research, v. 22, p. 439-451.

Rogers, J.N., Kelley, J.T., Belknap, D.F., Gontz, A., and Barnhardt, W.A., 2006, Shallow-water pockmark formation in temperate estuaries: A consideration of origins in the western gulf of Maine with special focus on Belfast Bay: Marine Geology, v. 225, p. 45-62.

Rollet, N., Logan, G.A., Ryan, G., Judd, A.G., Totterdell, J.M., Glenn, K., Jones, A.T., Kroh, F., Struckmeyer, H.I.M., Kennard, J.M., and Earl, K.L., 2009, Shallow gas and fluid migration in the northern Arafura Sea (offshore Northern Australia): Marine and Petroleum Geology, v. 26, p. 129-147.

Ross, D.A., and Uchupi, E., 1977, Structure and sedimentary history of Southeastern Mediterranean Sea - Nile Cone area: AAPG Bulletin (American Association of Petroleum Geologists), v. 61, p. 872-902.

Roussel, E.G., Bonavita, M.A.C., Querellou, J., Cragg, B.A., Webster, G., Prieur, D., and Parkes, R.J., 2008, Extending the sub-sea-floor biosphere: Science, v. 320, p. 1046.

Rozas, V., Zas, R., and Solla, A., 2009, Spatial structure of deciduous forest stands with contrasting human influence in northwest Spain: European Journal of Forest Research, v. 128, p. 273-285.

Rubey, W.W., and Hubbert, M., K, 1959, Role of fluid pressure in mechanics of overthrust faulting: II. Overthrust belt in geosynclinal area of western

Wyoming in light of fluidpressure hypothesis: Gelololigcal Society of America Bulletin, v. 70, p. 167-205.

Ryan, W.B.F., 1978, Messinian badlands on the southeastern margin of the Mediterranean Sea: Marine Geology, v. 27, p. 349-363.

Sahling, H., Bohrmann, G., Spiess, V., Bialas, J., Breitzke, M., Ivanov, M., Kasten, S., Krastel, S., and Schneider, R., 2008, Pockmarks in the Northern Congo Fan area, SW Africa: Complex seafloor features shaped by fluid flow: Marine Geology.

Salem, R., 1976, Evolution of Eocene-Miocene sedimentation patterns in parts of Northern Egypt: AAPG Bulletin (American Association of Petroleum Geologists), v. 60, p. 34-64.

Samuel, A., Kneller, B., Raslan, S., Sharp, A., and Parsons, C., 2003, Prolific deep-marine slope channels of the Nile Delta, Egypt: American Association of Petroleum Geologists Bulletin, v. 87, p. 541-560.

Sayer, A.M.. Walsh, R.P.D., and Bidin, K., 2006, Pipeflow suspended sediment dynamics and their contribution to stream sediment budgets in small rainforest catchments, Sabah, Malaysia: Forest Ecology and Management, v. 224, p. 119-130.

Sayer, A.M., Walsh, R.P.D., Clarke, M.A., and Bidin, K., 2004, The role of pipe erosion and slopewash in sediment redistribution in small rainforest catchments, Sabah, Malaysia: IAHS-AISH Publication, p. 29-36.

Scanlon, K.M., and Knebel, H.J., 1989, Pockmarks in the floor of Penobscot Bay, Maine: Geo-Marine Letters, v. 9, p. 53-58.

Secor, D.T., 1965, Role of fluid pressure in jointing: American Journal of Science, v. 263, p. 633-646.

Shackleton, N.J., 1987, Oxygen isotopes, ice volume and sea level: Quaternary Science Reviews, v. 6, p. 183-190.

Sheriff, R.E., and Geldart, L.P., 1995, Exploration seismology Cambridge, Cambridge University Press, 590 p.

Sibson, R.H., 1995, Selective fault reactivation during basin inversion: potential for fluid redistribution through fault-valve action: Geological Society Special Publication, v. 88, p. 3-19.

Siede, R., and Büchler, R., 2006, Spatial distribution patterns of Acute Bee Paralysis Virus, Black Queen Cell Virus and Sacbrood Virus in Hesse, Germany: Wiener Tierarztliche Monatsschrift, v. 93, p. 90-93.

Sleep, N.H., Meibom, A., Fridriksson, T., Coleman, R.G., and Bird, D.K., 2004, H2-rich fluids from serpentinization: Geochemical and biotic implications: Proceedings of the National Academy of Sciences of the United States of America, v. 101, p. 12818-12823.

Stanley, D.J., and Warne, A.G., 1993, Sea level and initiation of Predynastic culture in the Nile delta: Nature, v. 363, p. 435-438.

Stanton, R.J., 1966, The solution brecciation process: Geological Society of America Bulletin, v. 77, p. 843-848.

Su, Z., Cathles, L.M., Chen, D.F., and Wu, N.Y., 2010, Computation on free gas seepage and associated seabed pockmark formation, AIP Concerence Proceedings, Volume 1207, p. 1030-1035.

Suckling, J., Wink, A.M., Bernard, F.A., Barnes, A., and Bullmore, E., 2008, Endogenous multifractal brain dynamics are modulated by age, cholinergic blockade and cognitive performance: Journal of Neuroscience Methods, v. 174, p. 292-300.

Suess, E., Bohrmann, G., Von Huene, R., Linke, P., Wallmann, K., Lammers, S., Sahling, H., Winckler, G., Lutz, R.A., and Orange, D., 1998, Fluid venting in the eastern Aleutian subduction zone: Journal of Geophysical Research B: Solid Earth, v. 103, p. 2597-2614.

Summerfield, M.A., 1991, Global geomorphology : an introduction to the study of landforms: New York, Longman Scientific & Technical.

Svensen, H., Planke, S., Jamtveit, B., and Pedersen, T., 2003, Seep carbonate formation controlled by hydrothermal vent complexes: A case study from the Vøring Basin, the Norwegian Sea: Geo-Marine Letters, v. 23, p. 351-358.

Swarbrick, R.E., and Osborne, M.J., 1996, The nature and diversity of pressure transition zones: Petroleum Geoscience, v. 2, p. 111-116.

Swarbrick, R.E., and Osborne, M.J., 1998, Mechanisms that generate abnormal pressures: An overview: AAPG Memoir, p. 13-34.

Swarbrick, R.E., Osborne, M.J., and Yardley, G.S., 2004, Comparison of overpressure magnitude resulting from the main generating mechanisms: AAPG Memoir, p. 1-12.

Swart, R., 2009, Hydrate occurrences in the Namibe Basin, offshore Namibia, Geological Society Special Publication, Volume 319, p. 73-80.

Thorsen, C.E., 1963, Age of growth faulting in the southeast Louisiana: Transactions of the Gulf Coast Association of Geological Societies v. 13, p. 103–110.

Tingay, M.R.P., Hillis, R.R., Swarbrick, R.E., Morley, C.K., and Damit, A.R., 2007, 'Vertically transferred' overpressures in Brunei: Evidence for a new mechanism for the formation of high-magnitude overpressure: Geology, v. 35, p. 1023-1026.

Tréhu, A.M., Flemings, P.B., Bangs, N.L., Chevallier, J., Gràcia, E., Johnson, J.E., Liu, C.-S., Liu, X., Riedel, M., and Torres, M.E., 2004, Feeding methane vents and gas hydrate deposits at south Hydrate Ridge: Geophysical Research Letters, v. 31, p. 1-4.

Tréhu, A.M., Long, P.E., Torres, M.E., Bohrmann, G., Rack, F.R., Collett, T.S., Goldberg, D.S., Milkov, A.V., Riedel, M., Schultheiss, P., Bangs, N.L., Barr, S.R., Borowski, W.S., Claypool, G.E., Delwiche, M.E., Dickens, G.R., Gracia, E., Guerin, G., Holland, M., Johnson, J.E., Lee, Y.J., Liu, C.S., Su, X., Teichert, B., Tomaru, H., Vanneste, M., Watanabe, M., and Weinberger, J.L., 2004, Three-dimensional distribution of gas hydrate beneath southern Hydrate Ridge: Constraints from ODP Leg 204: Earth and Planetary Science Letters, v. 222, p. 845-862.

Trincardi, F., Cattaneo, A., Correggiari, A., and Ridente, D., 2004, Evidence of soft sediment deformation, fluid escape, sediment failure and regional weak layers within the late Quaternary mud deposits of the Adriatic Sea: Marine Geology, v. 213, p. 91-119.

Trude, J., Cartwright, J., Davies, R.J., and Smallwood, J., 2003, New technique for dating igneous sills: Geology, v. 31, p. 813-816.

Ussler III, W., Paull, C.K., Boucher, J., Friederich, G.E., and Thomas, D.J., 2003, Submarine pockmarks: A case study from Belfast Bay, Maine: Marine Geology, v. 202, p. 175-192.

Van Rensbergen, P., De Batist, M., Klerkx, J., Hus, R., Poort, J., Vanneste, M., Granin, N., Khlystov, O., and Krinitsky, P., 2002, Sublacustrine mud volcanoes and methane seeps caused by dissociation of gas hydrates in Lake Baikal: Geology, v. 30, p. 631-634.

Van Rensbergen, P., Morley, C.K., Ang, D.W., Hoan, T.Q., and Lam, N.T., 1999, Structural evolution of shale diapirs from reactive rise to mud volcanism: 3D seismic data from the Baram delta, offshore Brunei Darussalam: Journal of the Geological Society, v. 156, p. 633-650.

Van Rensbergen, P., Rabaute, A., Colpaert, A., Ghislain, T.S., Mathijs, M., and Bruggeman, A., 2007, Fluid migration and fluid seepage in the Connemara field, porcupine basin interpreted from industrial 3D seismic and well data combined with high-resolution site survey data: International Journal of Earth Sciences, v. 96, p. 185-197.

Vandré, C., Cramer, B., Gerling, P., and Winsemann, J., 2007, Natural gas formation in the western Nile delta (Eastern Mediterranean): Thermogenic versus microbial: Organic Geochemistry, v. 38, p. 523-539.

Voronoi, G., 1907, Nouvelles applications des paramètres continus à la théorie des formes quadratiques: Journal für die Reine und Angewandte Mathematik, v. 133, p. 97-178.

Voronoi, G., 1908, Recherches sur les paralléloèdres Primitives: J. reine angew. Math, v. 134, p. 198-287.

Walsh, R.P.D., 1980, Runoff processes and models in the humid tropics: Zeitschfrift fur Geomorphologie, Supplementband, v. 36, p. 176-202.

Walsh, R.P.D., 1996, Drainage density and network evolution in the humid tropics: Evidence from the Seychelles and the Windward Islands: Zeitschrift fur Geomorphologie, Supplementband, v. 103, p. 1-23.

Walsh, R.P.D., and Howells, K.A., 1988, Soil pipes and their role in runoff generation and chemical denudation in a humid tropical catchment in Dominica: Earth Surface Processes & Landforms, v. 13, p. 9-17.

Watkins, N.W., Freeman, M.P., Chapman, S.C., and Dendy, R.O., 2001, Testing the SOC hypothesis for the magnetosphere: Journal of Atmospheric and Solar-Terrestrial Physics, v. 63, p. 1435-1445.

Watts, N.L., 1987, Theoretical aspects of cap-rock and fault seals for single- and two-phase hydrocarbon columns: Marine and Petroleum Geology, v. 4, p. 274-307.

Webb, K.E., Hammer, Ø., Lepland, A., and Gray, J.S., 2009, Pockmarks in the inner Oslofjord, Norway: Geo-Marine Letters, v. 29, p. 111-124.

Westbrook, G.K., Chand, S., Rossi, G., Long, C., BÃ¼nz, S., Camerlenghi, A., Carcione, J.M., Dean, S., Foucher, J.P., Flueh, E., Gei, D., Haacke, R.R., Madrussani, G., Mienert, J., Minshull, T.A., NouzÃ©, H., Peacock, S., Reston, T.J., Vanneste, M., and Zillmer, M., 2008a, Estimation of gas hydrate concentration from multi-component seismic data at sites on the continental margins of NW Svalbard and the Storegga region of Norway: Marine and Petroleum Geology, v. 25, p. 744-758.

Westbrook, G.K., Exley, R., Minshull, T.A., Nouze, H., Gailler, A., Jose, T., Ker, S., and Plaza, A., 2008b, High-resolution 3D seismic investigations of hydrate-bearing fluid-escape chimneys in the Nyegga region of the Voring Plateau, Norway: Vancouver BC, Canada, International Conference on Gas Hydrates, paper 5597.

Whiticar, M.J., 1999, Carbon and hydrogen isotope systematics of bacterial formation and oxidation of methane: Chemical Geology, v. 161, p. 291-314.

Xie, X., Li, S., He, H., and Liu, X., 2003, Seismic evidence for fluid migration pathways from an overpressured system in the South China Sea: Geofluids, v. 3, p. 245-253.

Appendices

11 APPENDICES ON CD

Chapter 11 : Appendix A1

- Additional data in support of Chapter 1
- Non-extensive database of published pockmark geometries and geological setting.

Chapter 12 : Appendix A2

- Additional data in support of Chapters 4
- Seabed dip map showing pipe locations
- Pipe base reflection frequency
- Top pipe relief graphs
- Base Miocene map showing pipe locations (pipe names)
- Raw data : basic measurements
- Raw data : RMS amplitude measurements

Chapter 13 : Appendix A3

- Additional data in support of Chapter 5
- Root zone frequency
- Correlation between structural and isopach maps and Post Rift 1, Post Rift 2 and the Syn Rift
- Map showing the spatial distribution of TP2 values (scenario 2)
- Map showing the spatial distribution of TP1 values (scenario 3)
- Correlation between the timing of pipe formation and the
    - depth (m)
    - slope (°)
    - aspect (°)
    - thickness (m)

of the Post Rift 2 and the Syn-Rift sequences

- Correlation between the timing of pipe formation TP1 and TP2
- the depth of the pipe base
- the reflection value assigned to the pipe base
- Individual time points (PowerPoint presentation, see attached CD)
- Pipes forming in sequence movie (see attached CD). Please note, no significance should be attached to the time taken between each set of pipes appearing
- Incremental time points (PowerPoint presentation, see attached CD)
- Incremental Voronoi polygon analysis (PowerPoint presentation, see attached CD)

Chapter 14 : Appendix A4

- Additional data in support of Chapter 6
- Stacked and buried pockmarks
- Frequency histograms of unit pockmark and depression a-axis diameters (m)
- Geometrical relationships : various graphical relationships between pockmark area, depth, diameter and depression area, diameter, depth and number of unit pockmarks
- Relationship between the temporal point of buried pockmark formation and depression area, diameter, depth and number of unit pockmarks
- Raw data table : Rosetta plateau pockmarks
- Raw data table : Rosetta plateau buried pockmarks

Chapter 15 : Appendix A5

- Additional data in support of Chapter 7
- Ripley's K spatial statistic – statistic graphical output
- Relationship between exclusion zone and Voronoi polygon area, and pockmark diameter
- Relationship between Nearest Neighbour distance and pockmark diameter
- Raw data table : Rosetta pockmark field study area

Chapter 16 : Appendix A6

- Additional data in support of Chapter 8
- SOC magnitude log : log plots

Chapter 17 : Appendix A7

New Statistical Methods (paper)

- This chapter has been submitted for publication as Cartwright, A., Moss. J. L. and Cartwright, J. (in review) New Statistical Methods for Investigating Submarine Pockmarks in Computers and Geoscience.